Charles University in Prague, Faculty of Science

Institute of Petrology and Structural Geology

Study program: Geology

Mgr. Petr Brož

Small-scale volcanoes on Mars: image analysis, numerical modeling, and comparison with terrestrial analogs

Malé sopky na Marsu: obrazová analýza, numerické modelování a srovnání s pozemskými analogy

Ph.D. thesis

Supervisor:

doc. Mgr. David Dolejš, Ph.D.

Prague, 2015

Declaration

Author declares that the presented Ph.D.'s thesis is an original work which is result of research carried out by author in cooperation with coauthors fully acknowledged in section "Contribution by the author" or listed as authors in individual chapters of this thesis. This thesis contains no material published elsewhere or extracted in whole or in part from a thesis by which I have qualified for or been awarded another degree or diploma. No other person's work has been used without due acknowledgment in the main text of the thesis. All the relevant literature and used sources had been cited properly.

Prohlášení

Prohlašuji, že jsem závěrečnou práci zpracoval samostatně a že jsem uvedl všechny použité informační zdroje a literaturu. Tato práce ani její podstatná část nebyla předložena k získání jiného nebo stejného akademického titulu.

Praha, 11. června 2015

……………………….

Mgr. Petr Brož

Preface

The goal of this doctoral thesis is to extend our knowledge of small-scale volcanoes on Mars. This planet was volcanically active in the past, and as the most common volcanoes on Earth are small monogenetic volcanoes, it is logical to expect their existence on Mars and to search for their evidence. When I started to be interested in this field of volcanology, I searched through scientific literature and found out that these structures had not been investigated in detail so far. This was partly due to image resolution that was still insufficient to allow detection and investigation of small-scale edifices, but also because martian small volcanic landforms were neglected by researchers for a long time. Many volcanologists focused their attention to the famous large shield volcanoes situated within the well-known volcanic provinces. Small-scale volcanoes were mentioned only rarely, mostly as story sidelines accompanying studies of larger volcanoes. This discrepancy in our knowledge motivated me to spend a part of my scientific career by searching for 'tiny' martian volcanoes in an attempt to prove their existence. In the end, I found a great pleasure in my work; investigating this rich and diverse family of small volcanic structures. I could spend dozens of hours 'flying' above the martian surface via GoogleEarth™ with the feeling that I might discover volcano in another world. A volcano which has never been seen and which I should now investigate.

Here I summarize my knowledge and contributions to small-scale volcanoes that I have gained during the last few years with a collaborative help of my colleagues. I am sure that our understanding is not final and complete. It may be extended and/or overcome in the future as new planetary probes will stream back to Earth new data leading to new scientific breakouts in this field. We can only hardly estimate where our knowledge will stand after next several decades. I hope that my research will serve as essential background for future studies and that our results will become an integral part of the flow of knowledge.

This Ph.D. thesis is based on the results summarized in the following papers, where I am the senior and corresponding author. These papers were reprinted with permission from the respective journal and are used here for degree-granting purposes in compliance with the license agreements between the author and the publishing houses:

1. **Brož**, P., Hauber, E., 2012. *A unique volcanic field in Tharsis, Mars: Pyroclastic cones as evidence for explosive eruptions*, Icarus, 218(1), 88–99, doi: 10.1016/j.icarus.2011.11.030.
2. **Brož**, P., Hauber, E., 2013. *Hydrovolcanic tuff rings and cones as indicators for phreatomagmatic explosive eruptions on Mars*, Journal of Geophysical Research: Planets, 118, 1656–1675, doi: 10.1002/jgre.20120.
3. **Brož**, P., Čadek, O., Hauber, E., Rossi, A. P., 2014. *Shape of scoria cones on Mars: insights from numerical modeling of ballistic pathways,* Earth and Planetary Science Letters, 406, 14–23, doi: 10.1016/j.epsl.2014.09.002.
4. **Brož**, P., Hauber, E., Platz, T., Balme, M., 2015. *Evidence for Amazonian highly viscous lavas in southern highlands on Mars*, Earth and Planetary Science Letters, 415, 200–212, doi: 10.1016/j.epsl.2015.01.033.
5. **Brož**, P., Čadek, O., Hauber, E., Rossi, A. P., (submitted). *Scoria cones on Mars: detailed investigation of morphometry based on HiRISE and CTX DEMs,* submitted to Journal of Geophysical Research: Planets.

Contribution by the author and co-authors

All five articles (Brož and Hauber, 2012; 2013; Brož et al., 2014, 2015, submitted) have been produced in collaboration with Dipl.-Geol. Ernst Hauber from the Institut für Planetenforschung, Deutsches Zentrum für Luft- und Raumfahrt (DLR) in Berlin (Germany). The three publications have additional co-authors: Dr. Thomas Platz from the Freie Universität in Berlin (Germany), Dr. Matt Balme from the Open University in the Milton Keynes (United Kingdom), doc. Ondřej Čadek from the Faculty of Mathematics and Physics of the Charles University in Prague (Czech Republic), and Dr. Angelo Pio Rossi from the Jacobs University in Bremen (Germany). I am the senior and corresponding author of all publications presented here, and I was responsible for formulating and definition the initial ideas and methodological approach, review of the current state of knowledge, analysis and interpretation of data, and writing and coordinating the completion of the manuscripts. The co-authors contributed by critically evaluating and discussing the early steps of manuscript preparation and through editorial revisions. Ernst Hauber contributed to the organization of all presented manuscripts, and kindly advised me during data processing and manuscript preparation. He also provided valuable insights, inspiring ideas and consultation time. Thomas Platz helped me with a crater-counting technique, presented partly in Brož and Hauber (2012), and in more detail in Brož et al. (2015), and he provided valuable insight into the mechanism of evolved magma formation in the current martian crust. Matt Balme critically improved the quality and accuracy of the final text in Brož et al. (2015). Ondřej Čadek contributed with essential skills and knowledge of numerical modeling used in Brož et al. (2014), the design of the numerical model reflects his substantial involvement. He was also responsible for the data management and processing in Brož et al. (submitted). Angelo Pio Rossi participated in generation of Digital Elevation Models (DEM) from stereo-images used in the studies of Brož et al. (2014) and Brož et al. (submitted).

Acknowledgements

Since every good story has its beginning, also my story has one. It all began several years ago when the most significant event in my scientific life happened. Martin Pauer sent me on a virtual trajectory outside this planet. At that time none of us knew where I would land. Martin helped me arrange my first internship at the Deutsches Zentrum für Luft- und Raumfahrt in Berlin where I met Ernst Hauber, a person who became my steady guide through the exploration of volcanic landforms on Mars. Therefore, I am grateful to Martin because without him I would have never worked on such an amazing topic and I would probably quit an academic career soon after my master's degree.

Very close second, I have to thank Ernst Hauber for all his help, time and hospitality. I could write dozens of pages by describing how Ernst fundamentally affected me and how much I owe him for my scientific growth and development. This would still not cover all aspects. Therefore, I will write it short: thanks, Ernst, for everything! Your critical view and comments forced me to think about my work from new perspectives while sharpening final ideas.

There is a number of people which I would like to thank as well because this thesis would have never been done without them. I am thankful to Aleš Špičák who allowed me to work at the Institute of Geophysics of the Czech Academy of Science from the beginning of my career; to Prokop Závada who provided me his help in these hard beginnings, to Matěj Machek who always had time to answer my general questions about geology, to Václav Kuna for his interest to discuss some crazy ideas about Mars (which later surprisingly proved to be valuable scientific contributions!), and also to other members of our department. I would also thanks to Thomas Platz and Thomas Kneissl for their help with crater-counting technique and with the program 'CraterTool' for ArcGIS software respectively, to Matt Balme who provided me the opportunity to join his research team at the Open University in Milton Keynes (UK) during my fellowship, and to Angelo Pio Rossi for his valuable help with the generation of digital elevation models from stereo-images. I cannot forget to mention Ondřej Čadek who decided to transform my general geological ideas into solid numerical models enabling us more in-depth research, and to David Dolejš who oversaw the 4 years of my Ph.D. study. And of course, there are many more to whom I owe my thanks. I really appreciate your hints, valuable comments, ideas, help or just simple advices. And I hope it will continue to be so…

I gratefully acknowledge the Grant Agency of the Charles University for funding through the project 'Distribution of pyroclastic cones on Mars: analogue modeling and comparison with terrestrial analogues' (#580313) during the years 2013-2015 and the grant program KONTAKT of the Ministry of Education of the Czech Republic (ME09011).

And of course, I wish to thank my family and friends. To my parents which supported me all the time and to my wife Tereza who tolerated (and hopefully will continue so) my frequent overtimes spent on Mars, my scientific travels and stays, and 'suffered' on our holidays spent in volcanic regions over the globe.

Abstract

Small-scale volcanoes represent diverse group of landforms which vary in morphology, morphometry, and mechanisms of their formation. They are the most common volcanic form on Earth, and their existence and basic characteristics were also predicted for Mars. Availability of high-resolution image data now allows to search, identify and interpret such small volcanic features on the martian surface. This thesis extends our knowledge about the small-scale volcanoes with the following objectives: (a) to document the existence of martian analogues to some of the terrestrial volcanoes, in particular scoria cones, tuff cones, tuff rings and lava domes; (b) to establish their morphological and morphometrical parameters; and (c) to examine the effect of environmental factors, which differ on Earth and Mars, on the mechanisms of formation of the scoria cones.

Interpretation of remote sensing images and digital elevation models reveals that scoria cones, tuff rings and cones, and lava domes exist on different parts of the martian surface and, in some cases, far away from previously well-known volcanic provinces. Scoria cones have been identified in the volcanic field Ulysses Colles situated within the Tharsis volcanic province; tuff cones and tuff rings have been found in the Nephenthes/Amenthes region at the southern margin of the ancient impact basin Utopia, north of Isidis Planitia in the Arena Colles region and within an impact crater Lederberg in Xanthe Terra, and lava domes were located within an unnamed depression in Terra Sirenum. These findings document volcanic processes responsible for such diversity: the scoria cones prove the presence of explosive basaltic volcanic activity on Mars and formed in response to variations in magma volatile content over the geological history; the tuff rings and tuff cones provide evidence for the presence of (sub)surface water and/or water ice in the martian history; the lava domes record much larger variations in magma viscosity than previously interpreted.

In addition, the shapes of small-scale explosive volcanoes (scoria cones, tuff cones and tuff rings) reveal the effect of environmental setting such as the gravity field and atmospheric pressure as a significant factor affecting the physics of volcanic eruptions and causing the differences from their terrestrial analogues. Most of the scoria cones show larger volumes of ejected material, larger heights, and lower average slopes (rarely exceeding 30°) than their terrestrial counterparts. This is due to the lower gravity and atmospheric pressure on Mars which allow the ejected particles to be spread over a larger area than on Earth. As the volumes of erupted material are typically low, flank slopes do not reach the angle of repose – a common situation on Earth. This suggests only a minor role of avalanche redistribution during growth of martian scoria cones and permits their growth to be numerically tracked by modelling the ballistic trajectories and recording the cumulative deposition of repeatedly ejected particles. The ejected particles are about twenty times finer (about 2 mm) and ejected by a factor of two faster (~92 m/s) than on Earth.

The results indicate that small-scale volcanoes on Mars have wide spatial extent and diverse shapes. This extends our knowledge on the volcanological diversity of Mars and underlines the differences driven by local physical and environmental factors.

Abstrakt

Malé sopky představují různorodou skupinu povrchových těles, které se od sebe liší morfologií, morfometrií, ale i mechanismem svého vzniku. Na Zemi představují tyto malé sopky nejrozšířenější druh sopečných těles a jejich existence byla předpovězena i pro Mars. Dostupnost snímků ve vysokém rozlišení nyní umožňuje tyto malé sopky hledat, identifikovat a interpretovat jejich přítomnost na povrchu této planety. Tato dizertace se právě na tato malá sopečná tělesa zaměřuje a to ve snaze a) zdokumentovat existenci některých druhů malých sopek na povrchu Marsu, konkrétně sypaných kuželů, tufových kuželů, tufových prstenců a lávových dómů; b) určit jejich základní morfologické a morfometrické parametry a c) prozkoumat vliv rozdílného prostředí panujícího na povrchu Marsu a Země na příkladu mechanismu vzniku a vývoje sypaných kuželů.

Interpretace satelitních snímků a topografických dat odhalila, že se na povrchu Marsu vyskytují sypané kužele, tufové kužele, tufové prstence a lávové dómy – v některých případech ležících daleko od dobře známých sopečných provincií. Sypané kužele byly popsány v rámci sopečného pole Ulysses Colles ležícího v Tharsis; tufové kužele a tufové prstence byly objeveny v oblasti Nephenthes/Amenthes, která se rozkládá na jižním okraji prastaré impaktní pánve Utopia. Dále byly popsány v oblasti Arena Colles ležící severně od impaktní pánve Isidis Basin, ale i uvnitř impaktního kráteru Lederberg v oblasti Xanthe Terra, lávové dómy pak byly objeveny uvnitř nepojmenované deprese ležící v oblasti Terra Sirenum. Přítomnost těchto sopek na povrchu Marsu tak dokumentuje řadu různorodých sopečných procesů: sypané kužele například dokládají existenci explozivního bazaltového vulkanismu a přítomnost a změnu zastoupení sopečných plynů v magmatu v průběhu geologické historie planety, tufové kužele a tufové prstence pro změnu dokládají výskyt (pod)povrchové vody a/či vodního ledu v marsovské historii a lávové dómy pak zaznamenávají doklady o mnohem větší variaci ve viskozitě magmatu, než se dříve myslelo.

Tvary malých explozivních sopečných těles (konkrétně sypaných kuželů, tufových kuželů a tufových prstenců) navíc odhalily, že vliv prostředí představuje významný faktor ovlivňující nejenom průběh samotné sopečné erupce, ale způsobuje i rozdíly ve vzhledu jednotlivých typů sopek při srovnání s jejich pozemskými obdobami. Například většina marsovských sypaných kuželů je vyšší než jejich pozemské obdoby, vykazují větší objemy vyvrženého materiálu, ale i přes to mají pozvolnější svahy (jen zřídka dosahující hodnoty 30°). To je způsobeno právě vlivem nižší gravitačního zrychlení a atmosférického tlaku. Nižší hodnoty těchto dvou parametrů umožňují vyvrženým částicím, aby byly distribuovány do větších vzdáleností od místa erupce, a tedy i na větší plochu, než v případě Země. Jelikož množství vyvrženého materiálu je obvykle malé, sklony svahů vznikajících kuželů nedosáhnou sypného úhlu strusky, což je na naproti tomu obvyklé pro pozemské sypané kužele. Redistribuce vyvrženého materiálu vlivem svahových procesů tak hraje během formování marsovských sypaných kuželů jen okrajovou roli. Tento rozdíl v mechanismu ukládání strusky na svazích kuželů tak umožňuje rekonstruovat růst marsovských kuželů za pomoci numerického modelování letu balistických trajektorií a zaznamenávání jejich kumulativního ukládání v místě dopadu, a tak určit inverzní úlohou parametry charakterizující samotnou sopečnou erupci. Řešení této úlohy pak naznačuje, že na Marsu jsou vyvržené částice přibližně dvacetkrát menší (okolo 2 mm) a vyvrženy přibližně dvakrát rychleji (okolo 92 m/s) než v případě Země.

Výsledky této práce tak dokládají, že malé sopky představují na povrchu Marsu globálně rozšířený fenomén s bohatým množstvím tvarů. Toto zjištění rozšiřuje naše znalosti o sopečné různorodosti Marsu a současně podtrhává význam rozdílného prostředí, které panuje na povrchu planety, na výsledný tvar sopečných těles.

Table of contents

1. Introduction

Volcanic activity is a characteristic feature of all terrestrial planets (Mercury, Venus, Earth and Mars), some moons (Earth's Moon, Jupiter's moon Io), and some large asteroids (Vesta) (Platz et al., 2015). Volcanic edifices vary in shapes as do local environmental conditions, mainly gravitational acceleration, atmospheric pressure and chemical composition on individual cosmic bodies. These observations imply that the Solar system hosts an astonishing array of volcanic phenomena that are sometimes very different from the known terrestrial analogs. Their morphology as well as styles of formation are both likely to exceed the variability that has been known on Earth.

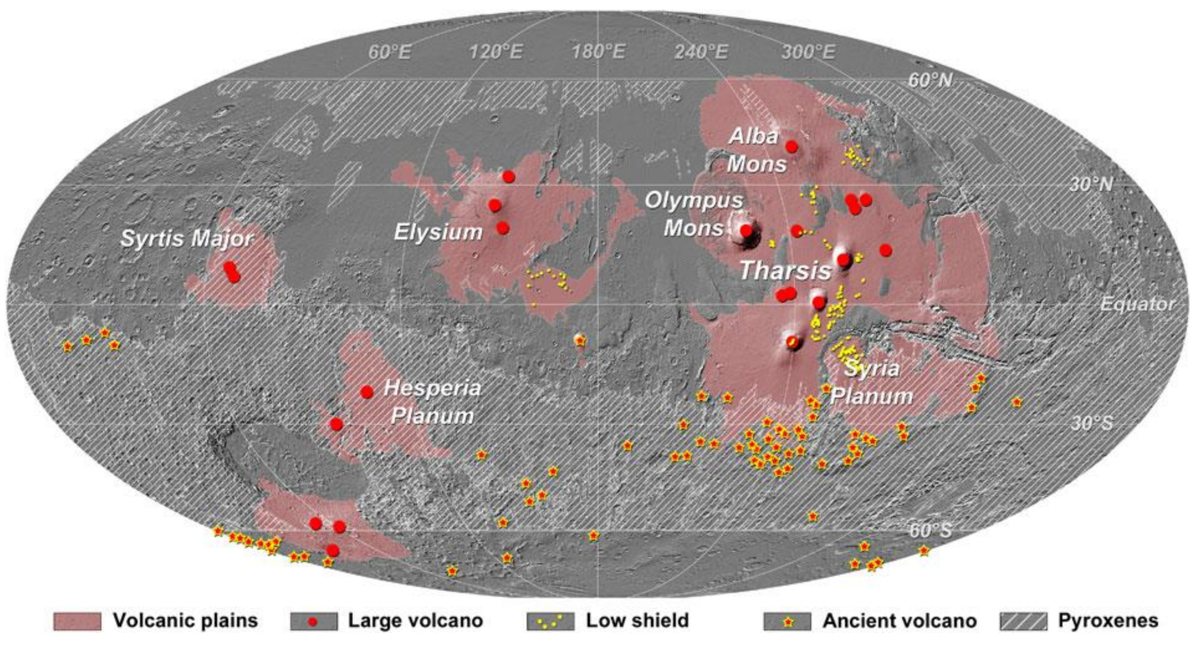

Figure 1.1. Map of volcanic landforms on Mars on the basis of morphological observations, based on MOLA DEM in Mollweide projection. Visible volcanic activity on Mars is spread globally, however, localized into several main volcanic provinces (Grott et al., 2013).

1.1. General background and definition of the subject

The first evidence for extensive volcanic products on the martian surface comes from imaging during flybys of the American planetary probes Mariner 4, 6, 7 and 9, Viking I and II, which successfully entered into an orbit of Mars. The martian landscape is dominated by mountains dozens kilometers high with summit craters – later interpreted as large shield volcanoes with multiple calderas – and by lava flows extending over hundreds of kilometers of the planetary surface (McCauley et al., 1972; Greeley and Spudis, 1981; Grott et al., 2013 and references therein). Main attention was initially paid to the large volcanic edifices, e.g., Olympus, Arsia, Pavonis, Ascraeus, and Elysium Mons. These volcanoes are associated with extensive volcanic plains, together forming two prominent volcanic provinces – Tharsis and Elysium – but other volcanic centers exist as well (Grott et al., 2013 and references therein; Fig. 1.1). The morphological, morphometric and spectroscopic data revealed that the Tharsis and Elysium centers, and the Syrtis Major volcanic complex, represent prominent large-scale volcanic effusions of low-viscous basaltic lavas (e.g., Mouginis-Mark et al., 1992; Zimbelman, 2000; Hauber et al., 2011). By contrast, the volcanoes associated with the Hellas Basin vary in morphologies from those known in Tharsis and Elysium, and they may represent relics of ancient explosive volcanism (Williams et al., 2007, 2008). Both groups were extensively studied and their formation, timing and evolution were reviewed (e.g., Grott et al., 2013; Platz et al., 2015).

By contrast, little attention was paid to small-scale volcanic landforms, only several kilometers large, due to inadequate spatial resolution of the cameras orbiting Mars. The cameras onboard Viking orbiters allow observing most of martian surface with a resolution of about 200 m/pixel, locally between 50 and 200 m/pixel and a very small fraction of Mars with a resolution of about 10 m/pixel. Such resolutions were in some areas sufficient for observations of structures, which might prove to be small-scale volcanoes

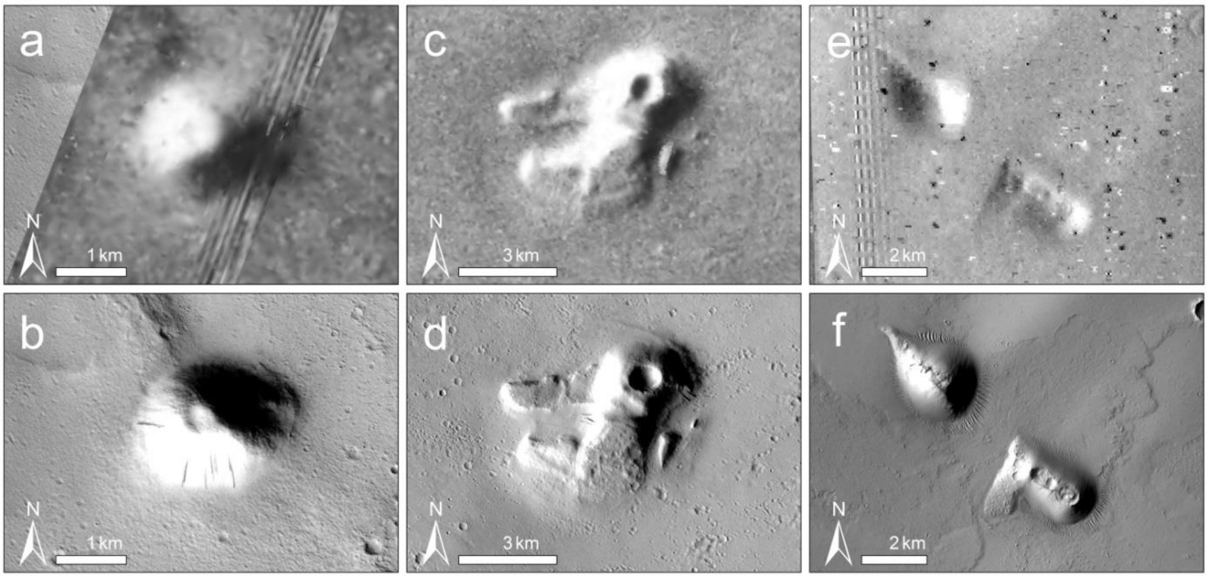

Figure 1.2. Comparison of images available in the post-Viking and post-CTX era interpreting potential volcanic edifices (a-d) of Hodges and Moore (1994) and an unrecognized group of two small-scale volcanoes (e-f). Stream of CTX images permits observation of necessary details to confirm or reject their volcanic origin. (a) Viking image 691A44 and (b) CTX image B11_013894_1959_XI_15N171W centered at 15.46°N 188.87°E. (c) Viking image 691A43 and (d) CTX image P04_002673_1959_XI_15N170W centered at 15.80°N, 189.20°E. (e) Viking image 931A02 and (f) CTX image B02_010318_1799_XI_00S098W centered at 0.07°S, 261.20°E.

(Hodges and Moore, 1994), however without the required accuracy to verify these suggestions (Fig. 1.2). A new generation of images from the fleet of probes orbiting Mars since 1997 offered a possibility to investigate great spatial details of the martian surface and, as a result, revealed existence of volcanic edifices on kilometer scale.

The existence of low shield volcanoes (e.g. Hauber et al., 2009a; Vaucher et al., 2009a), scoria cones (Keszthelyi et al., 2008; Mouginis-Mark and Christensen, 2005; Meresse et al., 2008; Hauber et al., 2009a; Lanz et al., 2010), lava domes (Rampey et al., 2006), tuyas (Hodges and Moore, 1979; Keszthelyi et al., 2010 and references therein), spatter cones (Cattermole; 1986; Head et al., 2005; Hauber et al., 2009a), and rootless cones (Greeley and Theilig, 1978; Keszthelyi et al., 2010 and references therein) was suggested and/or subsequently confirmed. Only some of these volcanic groups, in particular the low shield volcanoes, tuyas and rootless cones, were subjects of detailed research (e.g., Hauber et al., 2009aa Vaucher et al., 2009a; Hodges and Moore, 1979; Greeley and Theilig, 1978; Keszthelyi et al., 2010), whereas physical volcanology and comparative studies with terrestrial analogs remain poorly constrained.

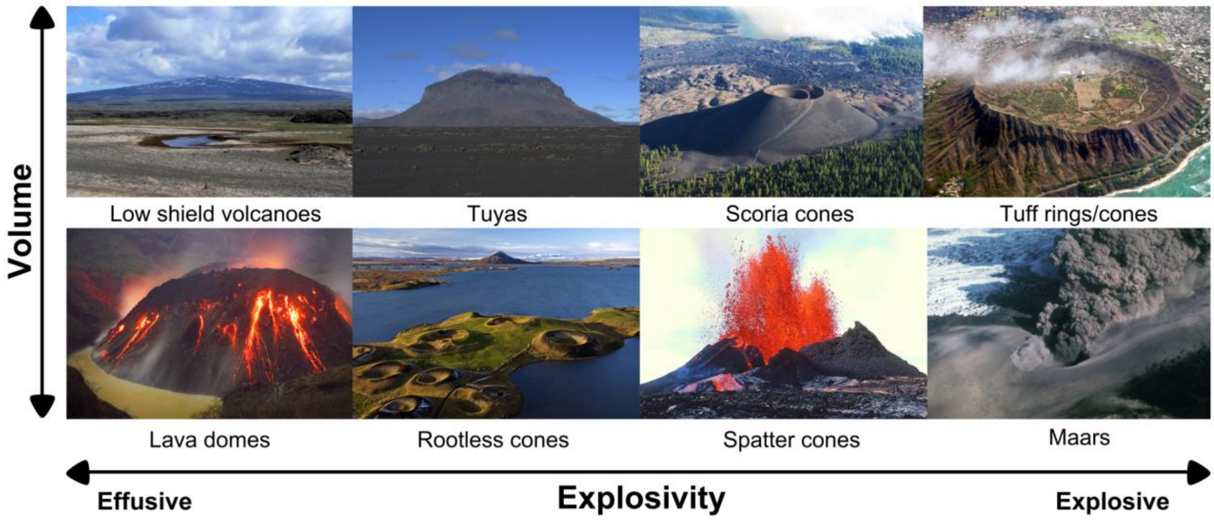

Figure 1.3. Examples of small-scale volcanoes on Earth resulting from effusive and explosive activity. Low shield volcanoes: Skjaldbreiður, Iceland, photographed by Christian Bickel (Creative Commons BY-SA 2.0 DE[1]); tuyas: Herðubreið Mt., Iceland, photographed by Icemuon (Creative Common BY-SA 3.0[2]); scoria cones: Lassen Volcanic National Park, California, photographed by the National Park Service; tuff rings/cones: Diamond Head Crater, Hawaii, photographed by Charles W. Carrigan; lava domes: Kelud volcano, East Java, Indonesia, photographed by Tom Pfeiffer; rootless cones: Mývatn, Iceland, photographed by Jonas Bendiksen, National Geographic; spatter cone: Pu`u `O`o, Kilauea, Hawaii, photographed by J.D. Griggs (USGS); maars: East Maar of Ukinrek Maars, Alaska, photographed by Juergen Kienle (USGS).

[1] https://creativecommons.org/licenses/by-sa/2.0/de/deed.cs.
[2] https://creativecommons.org/licenses/by-sa/3.0/deed.cs.

1.2. Previous work

On Earth, small-scale volcanoes represent a wide group of volcanic landforms which vary in shapes and mechanism of their formation (Fig. 1.3), and similar characteristics should be valid for Mars. A common aspect of these edifices on Mars is a low magma volume with a representative maximum of 2×10^2 km^3 (Hauber et al., 2009a). This is particularly well illustrated by comparison with the shield volcanoes in Tharsis and Elysium that are several orders of magnitude larger. The small-scale volcanoes are formed by effusive or explosive volcanic eruptions in a direct response to magma fragmentation (Sheridan and Wohletz, 1983; Parfitt and Wilson, 2008). For the effusive volcanic edifices (extrusion as homogeneous liquid without mechanical disruption) to form, the rising magma must be bubble-free or -poor to prevent its disaggregation (Parfitt and Wilson, 2008). By contrast, the explosive eruptions are characterized by ejection of magma fragments of various sizes. They represent more complex phenomena as fragmentation may be caused by magma degassing and/or water-magma interaction (Sheridan and Wohletz, 1983).

1.2.1. Small-scale effusive volcanoes

1.2.1.1. Low-shield volcanoes

The small-scale volcanoes formed by the effusive activity mainly include low shield volcanoes (Hauber et al., 2009a; Vaucher et al., 2009a; Platz and Michael, 2011). The low shield volcanoes were discovered on Mars from images obtained by Viking I and II (Hodges, 1979, 1980; Hodges and Moore, 1994 and references therein) and were studied in detail in the post-Viking era (e.g., Hauber et al., 2009a; Vaucher et al., 2009a; Platz and Michael, 2011). The low shield volcanoes on Mars are believed to represent analogs to terrestrial volcanoes formed by plain-style volcanism, a well-known phenomenon from Snake River Plain in Idaho, USA or Iceland (Greeley, 1982). A typical martian low shield volcano has a diameter of less than 50 km and a relatively low topographic profile of approximately few hundred meters and extremely shallow flank slopes of less than 0.5° (Hauber et al., 2009a). This suggests that they were formed from low viscous basaltic lavas (Hauber et al., 2009a, 2011). Their occurrences are mainly concentrated into two areas, Tharsis and Elysium. In Tharsis they constitute several individual clusters containing many edifices overlapping each other and masking the older surface of wide plains extending between the large volcanoes (Hauber et al., 2009a). Their dating reveals that they were formed in a time range of dozens to hundreds of millions years ago (Hauber et al., 2011). Nowadays, they represent the stratigraphically youngest observational unit in a large part of Tharsis, and suggest a significant volcanic activity in recent geological history.

1.2.1.2. Lava domes

On Earth, lava domes are small volcanic landforms formed by highly viscous lavas (Fink and Griffiths, 1998). Such a magma may result from extensive crystallization or from chemical differentiation generating the silica-rich composition. On Mars, a small group of domical structures located in the eastern Arcadia Planitia were identified as lava domes based on similarities in the height-to-basal diameter with the felsic lava domes of Mono Craters in California (Hodges, 1980). Similar edifices – individual hills, clusters, and chains – were more recently discovered in another part of Arcadia Planitia – the Tyndall Dome field (Rampey et al., 2006). These hills often have a central core surrounded by annuli that are well visible on thermal images. The cores vary from 620 to 3090 m in size (mean value of 1550 m) and are from 30 to 400 meters high (mean value of 160 m; Rampey et al., 2006). They may represent analogs to terrestrial felsic and mafic lava domes and/or cryptodomes (Rampey et al., 2006). However, their spectral absorption characteristics are consistent with the presence of olivine and a high-Ca pyroxene, commonly augite, suggesting a basaltic composition; a more silica-rich composition (basaltic–andesitic or andesite) has not yet been ruled out (Farrand et al., 2011).

1.2.1.3. Tuyas

Tuyas are edifices formed by the effusive activity resulting from pressure of overburden ice, even though some of their parts may be associated with the explosive activity. On Earth, the tuyas are flat-topped and steep-sided volcanic edifices, 1 to 10 km large and up to 1000 m high, formed by subglacial eruptions (Martínez-Alonso et al., 2011). However, when the amount of lava is sufficient to completely melt the overburden ice, an explosive activity may occur. The tuyas were widely postulated to occur on Mars (Hodges and Moore, 1979; Keszthelyi et al., 2010) in order to explain the abundant and enigmatic mesas spread over the martian surface. The most characteristic edifices are situated in Chryse and Acidalia Planitiae (Martínez-Alonso et al., 2011). However, direct confirmation of their existence by observations of pillow lavas and columnar jointing is missing (Keszthelyi et al., 2010). Hence existence of the tuyas on Mars still remains questionable.

1.2.2. Small-scale explosive volcanoes

Small-scale volcanoes formed by explosive volcanic activity are a result of magma fragmentation during ascent and its subsequent spreading around the vent; the product is generally a small and conical edifice of pyroclastic material. In general, the fragmentation can be caused by two main processes: by magma degassing resulting in the growth of scoria cones or spatter cones (Parfitt and Wilson, 2008), or by water-magma interaction leading to the formation of tuff rings, tuff cones, maars and rootless cones (Sheridan and Wohletz, 1983). These processes depend on the amount of water available to drive the magma fragmentation (Sheridan and Wohletz, 1983; Cashman et al., 2000). Small-scale explosive volcanoes are very common on Earth and may be found in all tectonic regimes. The most common types on Earth are scoria cones, followed by tuff rings, tuff cones, and maars (Vespermann and Schmincke, 2000). Despite these numerous occurrences on Earth, their existence on Mars is much less known.

1.2.2.1. Scoria cones

Presence of scoria cones was suggested in several regions of Mars by the Viking data (Carr et al., 1977; Frey and Jarosewich, 1982; Edgett, 1990; Hodges and Moore 1994; Plescia, 1994), however with no unambiguous confirmation due to the low resolution of images available. More recent high-resolution images allow recognition of the martian scoria cones as parasitic cones on flanks of larger volcanoes, e.g., Pavonis Mons (Bleacher et al., 2007; Keszthelyi et al., 2008) or Tharsis Tholus (Platz et al., 2013), as clusters in volcanic fields, e.g., Hydraotes Colles in the chaotic terrains (Meresse et al., 2008), on the floor of Coprates Chasma (Harrison and Chapman, 2008), in the northern lowlands (Lanz et al., 2010) or as individual cones in volcanic provinces in Tharsis (Keszthelyi et al., 2008; Hauber et al., 2009a). Frequently, they are only described as a subordinate feature accompanying other principal processes (Meresse et al., 2008; Hauber et al., 2009a; Lanz et al., 2010), or they were proposed as one of several alternative explanations, for instance, to mud volcanism (e.g., Skinner and Tanaka, 2007; Harrison and Chapman, 2008). The basic characteristics of their morphometry are provided by Meresse et al. (2008); the cones are small, 0.5 to 1.5 km in diameter, with heights between 180 and 230 m, and with a mean slope from 15 to 31°. Relatively little is still known about the shapes of the martian scoria cones despite previous theoretical studies (Wood, 1979; Dehn and Sheridan, 1990; Wilson and Head, 1994; Fagents and Wilson, 1996; Parfitt and Wilson, 2008).

1.2.2.2. Spatter cones

Explosive volcanic events characterized by very low eruption energies, mainly due to the magma degassing, produce spatter cones where the volcanic ejecta are deposited only in the closest vicinity of the vent. On Earth, the spatter cones are generally less than several meters wide, up to 5 meters high, and have steep flanks exceeding the angle of repose of the fragmental material because of spattering of the ejected particles. They are among common features on terrestrial basaltic volcanoes (e.g., Blackburn et al., 1976), and this may also apply to Mars. Occurrence of the spatter cones was suggested at the flanks of Alba Patera (Cattermole, 1986), Arsia Mons (Head et al., 2005), and as edifices accompanying the low shield volcanoes (Keszthelyi et al., 2008; Hauber et al., 2009). However, their small size usually prevents detailed interpretation of their particulate material – the spatter particles, fine tephra or some other fragmented material (Hauber et al., 2009).

1.2.2.3. Hydrovolcanism

Hydrovolcanism is a general term for water-magma interaction during eruption and cooling. Given the abundance of the volcanic activity and ground ice on Mars (Baker, 2001; Feldman et al., 2004; Smith et al., 2009), the existence of explosive interactions triggered by water and producing typical edifices such as tuff rings, tuff cones, and maars, is expectable, although credible identification is still lacking (Keszthelyi et al., 2010). Untypical cratered cones situated near the northern pole of Mars were initially interpreted as tuff cones (Hodges and Moore, 1979), but this hypothesis was later considered as unconfirmed (Keszthelyi et al., 2010).

1.2.2.4. Rootless cones (pseudocraters)

Rootless cones belong to the best described and highly controversial potential explosive edifices on Mars. On Earth, they are formed by magma-water interaction when a lava interacts with groundwater or wet sediments and produces pyroclastic material, which is then deposited on the surface of a lava flow (e.g., Fagents and Thordarson, 2007). The resulting edifices are mainly between few tens up to hundreds meter in diameter, up to 60 m high, and often with a well-developed central crater. They were extensively described from the martian northern lowlands (see Keszthelyi et al., 2010 for review). However, similar image data were also interpreted as landforms of non-volcanic origin, formed by the action of ice or mud (cf. Tanaka et al., 2003a; Farrand et al., 2005), and the debate about their origin is not still settled.

1.3. Objectives of the thesis

For several types of small-scale volcanoes the mechanisms of their formation remain poorly understood or controversial. I have therefore defined the following thesis objectives:

1. To document the presence of poorly described or unknown small-scale volcanic edifices on the martian surface by image analyses in the visible light range; to use topographic data to compare edifice shapes with possible terrestrial analogs in an attempt to extend current knowledge about the variety of volcanoes on Mars and to provide principal morphometric properties of their shapes.

2. To investigate the morphometric shape of one particular type of edifice in detail, for instance the scoria cones, in order to evaluate their variations from terrestrial analogs and provide genetic explanation.

3. To develop a numerical model for the formation of martian scoria cones and to investigate the effects of the initial eruption parameters on the nature of Strombolian eruptions. I expect to explain the causal reasons for differences in the cone shapes on Mars and, in addition, to address the source of their variations with respect to their terrestrial analogs.

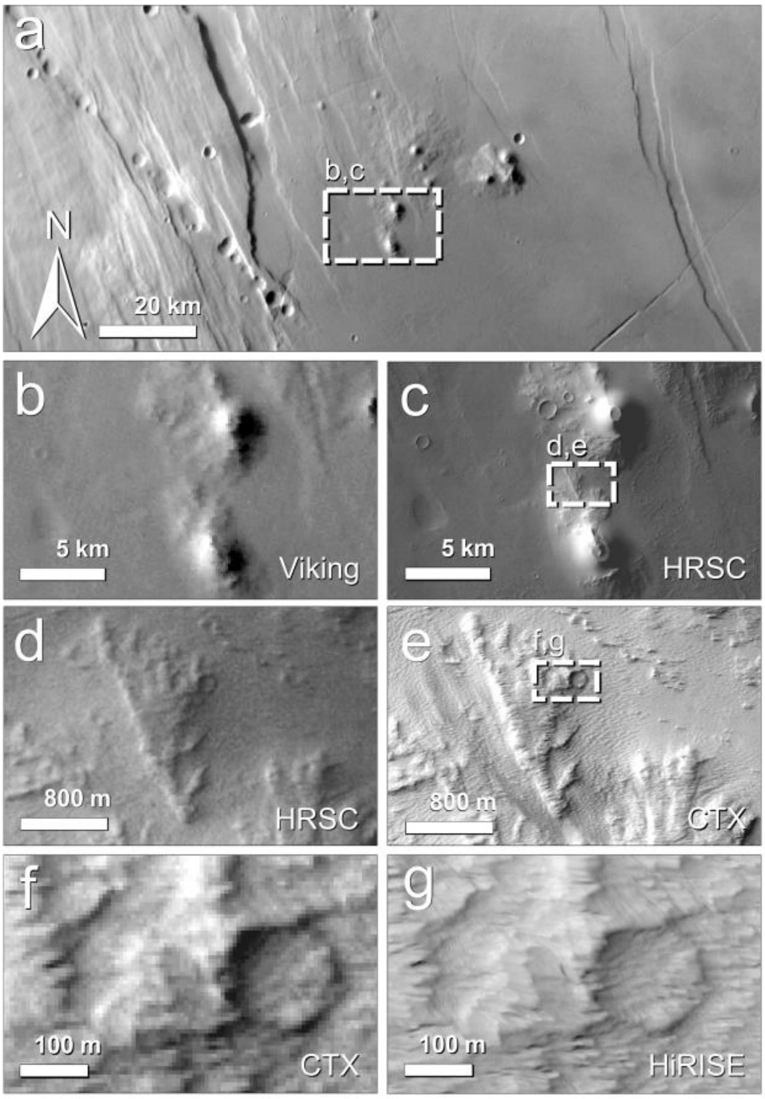

Figure 1.4. Images of the Ulysses Colles region in Tharsis captured by several cameras with different resolution: (a) general overview, with the southern part of the field and an old fractured crust. The image is based on a Viking mosaic of images 044B49, 049B67, 049B68 and 049B69, centered at 6.04°N, 236.89°E; (b) maximum resolution obtained from the Viking images. No details of the investigated cones are visible; (c) an HRSC image (h1023_0000) permits detection of associated flows; (d) zoom of the previous image. No additional details of the lava flows can be seen; (e) a CTX image (P19_008262_1862_XN_06N123W) permit observation of details larger than 20 meters; (f) a maximum resolution of previous image; irregular surface of lava flow is visible (g) a high-resolution HiRISE image (PSP_008262_1855) permit observation of thick dust cover hiding the real surface of lava flow.

1.4. Methodology

Morphological features of Mars cannot be analyzed by terrestrial telescopes due to the insufficient spatial resolution. However, images resulting from planetary probes capturing meter-scale aspects of the martian surface are now available (Fig. 1.4.) as are detailed elevation models. Several types of image data acquired in visible light by Context camera (CTX; 5–6 m/pixel; Malin et al., 2007) and during High Resolution and Imaging Science Experiment (HiRISE; ~30 cm/pixel; McEwen et al., 2007), both onboard Mars Reconnaissance Orbiter and by High Resolution Stereo Camera (HRSC; 10-20 m/pixel; Jaumann et al., 2007) onboard Mars Express were used as well as the thermal data taken by Thermal Emission Imaging System (THEMIS-IR day and night; ∼100m/pixel; Christensen et al., 2004) onboard Mars Odyssey Mission. These data were browsed via GoogleEarth™ (Google Inc., 2011[3]) to search for objects of interest. Once such objects were discovered, freely available raw data were downloaded from the Mars Space Flight Facility 'Image Explorer' database[4] and processed with the USGS software ISIS3[5] ('Integrated Software for Imagers and Spectrometers') for calibration and projection. The projection was chosen with the respect to latitude where objects of interest were situated. This procedure minimizes any possible distortion of final shapes of the investigated edifices; the Mercator projection was used for equatorial areas and the sinusoidal projection for mid-latitudes. Images processing in ISIS3 returned the proper orientation and position of the images on the martian surface. The projected images were uploaded to the ESRI ArcGIS 10[6] software together with the topographic data from global datasets – by Mars Orbiter Laser Altimeter (MOLA; Zuber et al., 1992; Smith et al., 2001) placed onboard Mars Global Surveyor, from the HRSC stereo

[3] GoogleEarth™ version 7.1.2.2041.
[4] Available on http://viewer.mars.asu.edu.
[5] ISIS3 version 3.4.8, available at http://isis.astrogeology.usgs.gov.
[6] ESRI ArcGIS version 10.2.1. for Desktop.

images onboard Mars Express (Jaumann et al., 2007), and from stereo-pairs of HiRISE and CTX images following the methods described, for instance, by Moratto et al. (2010).

The resolution of these datasets generally varies due to the different methods of their generation. The MOLA data have vertical accuracy on the order of several meters, depending on a signal quality and a terrain roughness. Horizontal spacing between individual spots is near ~300 m in the south-north direction (Smith et al., 2001), whereas the east-west spacing depends on the latitude; it is lower in polar regions but may reach several kilometers near the equator. The HRSC DEM is derived from stereo-images where the topographic model has been interpolated from 3D points on a regular grid spaced 50 to 100 m with an average intersection error of 12.6 m (Gwinner et al., 2010). The HRSC DEM data provide a good vertical and horizontal resolution even in the equatorial regions. These HiRISE and CTX DEM data reach a spatial resolution of ~1 or ~10 m/pixel, respectively, and the vertical accuracy of the stereo-derived DEM data can be estimated to be a few meters.

The visible-light and topographic data were merged in the ArcGIS 10 software, the objects of interest were mapped, and their morphological and morphometrical properties were interpreted using the 3D analyst tool in the ArcGIS 10 environment. The same procedure of image analysis was applied to several terrestrial regions in order to locate and compare analogous volcanic phenomena, and match their shape characteristics. The terrestrial data were obtained from the GoogleEarth™ software. GoogleEarth™ uses the DEM data collected by the NASA Shuttle Radar Topography Mission (Farr et al., 2007) with a cell size of 10 to 30 m for the USA, and ~90 m for the rest of the world. The vertical error of these DEM is reported to be less than 16 m (Jarvis et al., 2008).

In addition, spatial connection between individual cones was investigated by a 2-point azimuth technique described by Cebriá et al. (2011). Absolute model ages were determined from the crater size-frequency distributions utilizing the software tool CraterTools[7] (Kneissl et al., 2011), which ensures a distortion-free measurement of crater diameters independent of map projection. The age data were interpreted using the impact-cratering chronology model with the software Craterstats[8] (Michael and Neukum, 2010), which applies the production function of Ivanov (2001).

[7] CraterTools version 2.1.
[8] Craterstats version 2.0.

2. A unique volcanic field in Tharsis, Mars: Pyroclastic cones as evidence for explosive eruptions

Petr Brož[1,2] and Ernst Hauber[3]

[1]*Institute of Geophysics ASCR, v.v.i., Prague, Czech Republic*
[2]*Institute of Petrology and Structural Geology, Faculty of Science, Charles University, Prague, Czech Republic*
[3]*Institute of Planetary Research, DLR, Berlin, Germany*

Status: Published in Icarus 218(1), doi: 10.1016/j.icarus.2011.11.030.

2.0. Abstract

Based on theoretical grounds, explosive basaltic volcanism should be common on Mars, yet the available morphological evidence is sparse. We test this hypothesis by investigating a unique unnamed volcanic field north of the shield volcanoes Biblis Patera and Ulysses Patera on Mars, where we observe several small conical edifices and associated lava flows. Twenty-nine volcanic cones are identified and the morphometry of many of these edifices is determined using established morphometric parameters such as basal width, crater width, height, slope, and their respective ratios. Their morphology, morphometry, and a comparison to terrestrial analogs suggest that they are martian equivalents of terrestrial pyroclastic cones, the most common volcanoes on Earth. The cones are tentatively interpreted as monogenetic volcanoes. According to absolute model age determinations, they formed in the Amazonian period. Our results indicate that these pyroclastic cones were formed by explosive activity. The cone field is superposed on an old, elevated window of fractured crust which survived flooding by younger lava flows. It seems possible that a more explosive eruption style was common in the past, and that wide-spread effusive plain-style volcanism in the Late Amazonian has buried much of its morphological evidence in Tharsis.

2.1. Introduction and background

Most volcanoes on Mars that have been studied so far seem to be basaltic shield volcanoes (e.g., Mouginis-Mark et al., 1992; Zimbelman, 2000), which can be very large with diameters of hundreds of kilometers (Plescia, 2004) or much smaller with diameters of several kilometers only (Hauber et al., 2009a). The eruptive style of the large shields, at least in the later part of martian history, was early interpreted to be predominantly effusive (Greeley, 1973; Carr et al., 1977; Greeley and Spudis, 1981), although theoretical considerations predict that basaltic explosive volcanism should be common on Mars (Wilson and Head, 1994). Unequivocal evidence for explosive volcanism on Mars is rare and mainly restricted to ancient terrains. Some of the old highland paterae (e.g., Hadriaca, Tyrrhena, and Apollinaris Paterae; >3.5 Ga) display easily erodible and very shallow flanks that were interpreted to be composed of airfall and pyroclastic flow deposits (Greeley and Crown, 1990; Crown and Greeley, 1993; Gregg and Williams, 1996; Gregg and Farley, 2006; Williams et al., 2007, 2008). Widespread layered deposits in the equatorial regions of Mars, e.g., the Medusae Fossae Formation, were interpreted to be pyroclastic deposits (Chapman, 2002; Hynek et al., 2003; Mandt et al., 2008; Kerber et al., 2010), but their nature and timing are not well understood.

Pyroclastic cones, defined in this study as scoria, cinder, or tephra cones (Vespermann and Schmincke, 2000), are the most common type of terrestrial volcanoes (Wood, 1979a,b) and were suggested by several authors already decades ago to exist on Mars (e.g., Wood, 1979b; Dehn and Sheridan, 1990). However, only few Viking Orbiter-based studies reported their possible existence near the caldera of Pavonis Mons, on the flanks of Alba Patera, in the caldera of Ulysses Patera, and in the Cydonia and Acidalia regions (Carr et al., 1977; Wood, 1979a,b; Frey and Jarosewich, 1982; Edgett, 1990; Hodges and Moore, 1994; Plescia, 1994). It was recognized that this might have been an observational effect caused

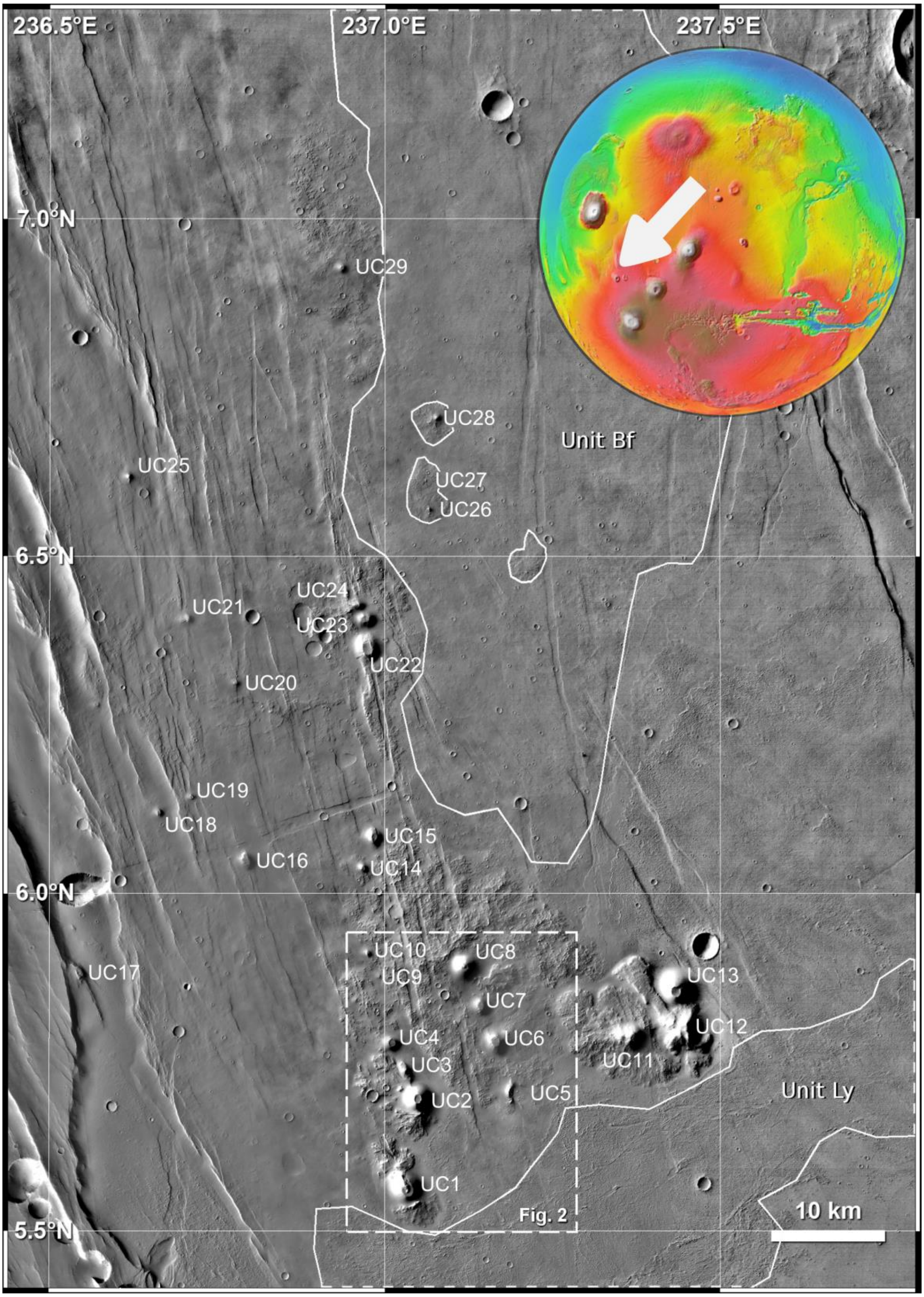

Figure 2.1. Mosaic of CTX and HRSC images showing all investigated cones. Cone IDs are the same as used in Tab. 2.2 (CTX images B17_016134_1842, P19_008262_1862, P22_009554_1858 and image HRSC h8396_0009). Dashed line shows location of Fig. 2.2. Cf and Ly represent areas for crater counting. See text for more details.

by the relatively low image resolution of the Viking Orbiter cameras (typically 60-100 m/pixel), and Zimbelman (2000) presumed that many small domes on Mars might have a volcanic origin. It was indeed only the advent of higher-resolution data that led to the interpretation of previously unknown edifices as rootless cones (Fagents and Thordarson, 2007; Keszthelyi et al., 2010) or scoria cones (Bleacher et al., 2007, Keszthelyi et al., 2008; Lanz et al., 2010), but without in-depth analyses of their origin. A volcanic cone in the caldera of Nili Patera, part of the Syrtis Major volcanic complex, is associated with a lava flow and silica deposits that might be the result of hydrothermal activity (Skok et al., 2010). Ground-based observations by the Mars Exploration Rover, Spirit, revealed further morphologic evidence (‘bomb sags’) for explosive volcanic activity (Squyres et al., 2008).

Pyroclastic cones have not yet been described and measured in detail on the martian surface. Previous studies were mostly based on low-resolution Viking data that did not allow the description of individual cones, or high-resolution studies that discussed only isolated features. Only Lanz et al. (2010) were able to provide quantitative analyses of multiple cones in a high-resolution study of a possible volcanic rift zone in SW Utopia Planitia. They investigated an area exhibiting scoria cones and associated lava flows, and measured the crater and basal diameters of putative scoria cones, which they compared with other cones surrounding their study area.

The identification of pyroclastic cones can constrain the nature of associated eruption processes and, indirectly, improve our understanding of the nature of parent magmas (e.g., volatile content; Roggensack et al., 1997). Moreover, the morphometry and spatial distribution of pyroclastic cones can reveal tectonic stress orientations (Nakamura, 1977; Tibaldi, 1995) and the geometry of underlying feeder dikes (Corazzato and Tibaldi, 2006). Hence, pyroclastic cones on Mars are therefore potentially interesting study objects, and the increasing amount of high-resolution data enables their detailed analysis. We test

Table 2.1. Table of image scenes used for this study (pixel resolution, imaging time, and illumination geometry). †HiRISE resolutions are given for map-projected images.

Image ID	Ground pixel resolution	Acquisition time	Solar elevation above horizon	Solar azimuth (for map projected image)
h1012_0000	11.8 m pixel^{-1}	02 Nov 2004	36°	295.0
h1023_0000	11.5 m pixel^{-1}	05 Nov 2004	37°	295.1
P19_008262_1862	5.51 m pixel^{-1}	01 May 2008	41°	277.03°
P21_009198_1858	5.42 m pixel^{-1}	13 Jul 2008	38°	277.12°
P21_009409_1858	5.53 m pixel^{-1}	29 Jul 2008	37°	277.05°
P22_009554_1858	5.53 m pixel^{-1}	09 Aug 2008	38°	277.21°
B17_016134_1842	5.35 m pixel^{-1}	04 Jan 2010	48°	277.09°
B12_014156_1857	5.46 m pixel^{-1}	03 Aug 2009	49°	277.12°
PSP_008262_1855†	50 cm pixel^{-1}	01 May 2008	41°	277°
PSP_009198_1860†	50 cm pixel^{-1}	13 Jul 2008	38°	277.12°
PSP_009409_1860†	50 cm pixel^{-1}	29 Jul 2008	37°	277.05°
PSP_009554_1860†	25 cm pixel^{-1}	09 Aug 2008	38°	277.21°

the hypothesis that explosive basaltic volcanism should be common on Mars and report on our investigation of a unique unnamed cluster of possible volcanic cones situated north of Biblis Patera in the Tharsis region (Fig. 2.1). To our knowledge, this is the first ever study of this unique volcanic field.

2.2. Data and methods

This study uses imaging data from several cameras, i.e. ConTeXt Camera (CTX; Malin et al., 2007), High Resolution Stereo Camera (HRSC; Jaumann et al., 2007), and High Resolution Imaging Science Experiment (HiRISE; McEwen et al., 2007) (Tab. 2.1). CTX images have sufficient resolution (5-6 meters/pixel) to identify possible scoria cones, associated lava flows and their relationships to the geological context. On the other hand, HiRISE data were used to investigate small details of cones in very high spatial resolution. Topographic information (e.g., heights and slope angles) were determined from single shots of the Mars Orbiter Laser Altimeter (MOLA; Zuber et al., 1992; Smith et al., 2001) in a GIS environment, and from stereo images (HRSC, CTX) and derived gridded digital elevation models (DEM). An anaglyph image made from two HiRISE observations provided qualitative topographic information.

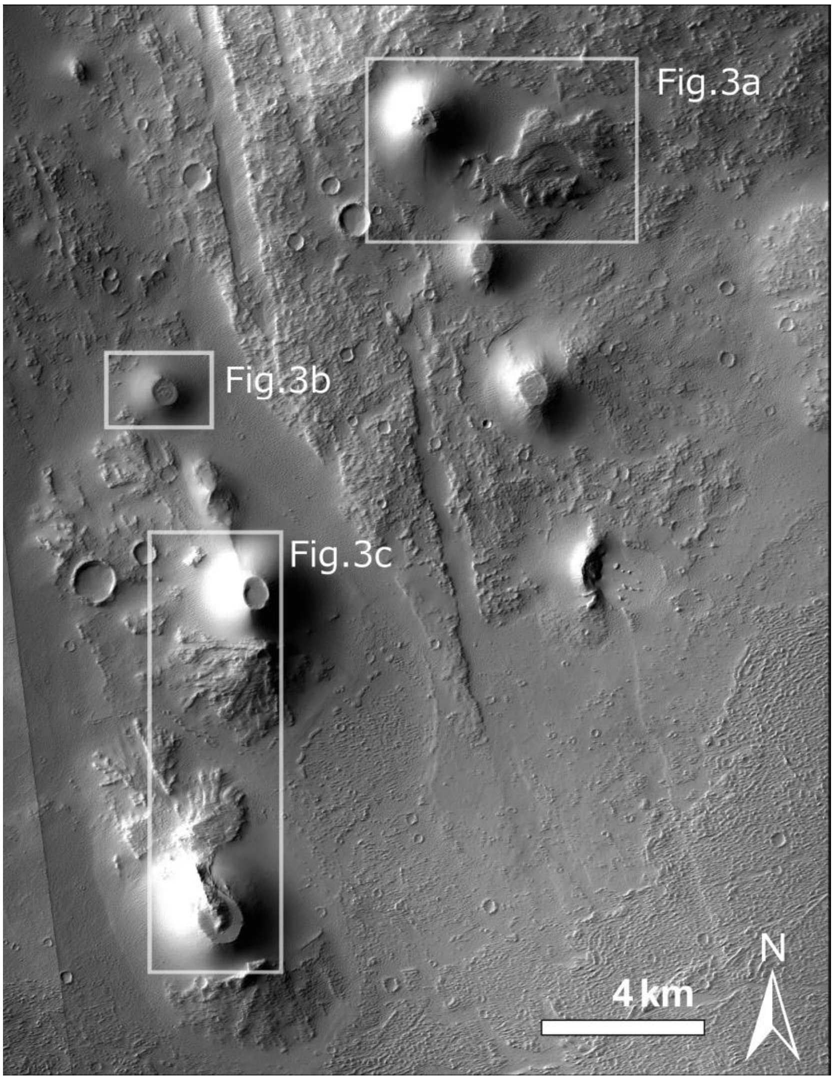

Figure 2.2. Selected cones and associated flows emanating from the cones in the study area. The distribution of cones is controlled by NW-trending extensional fault systems (CTX image P19_008262_1862, image center at 5.75°N/237.1°E; see Fig. 2.1 for location).

2.3. Regional setting

The study area is situated within the Tharsis volcanic province, the largest known volcano-tectonic province on Mars (Fig. 2.1). It is located at the southeastern margin of the several hundred kilometer-long fault system, Ulysses Fossae, and north of two

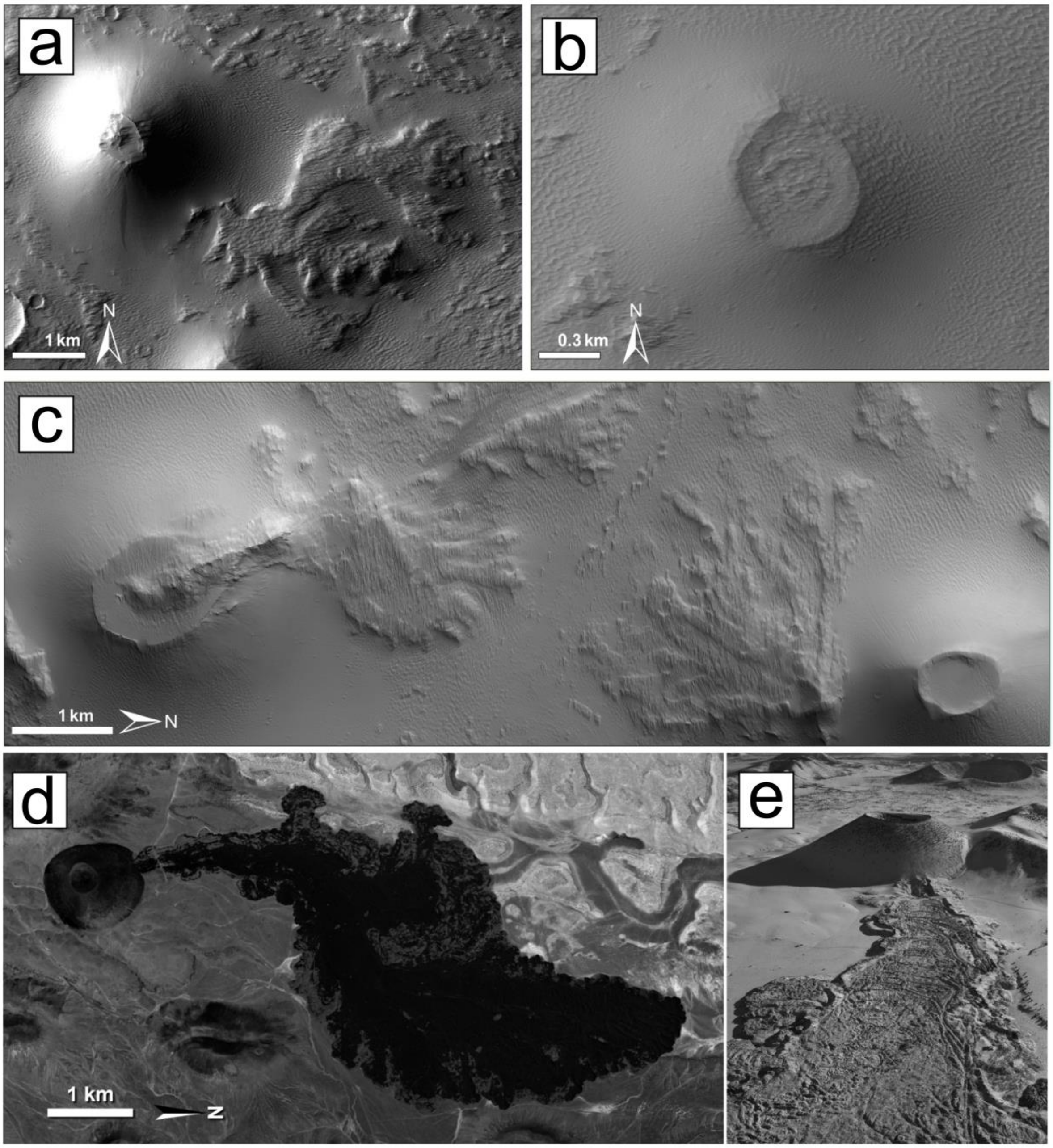

Figure 2.3. (a) Detail of lobate flow-like deposit starting at the base of a cone (detail of CTX P22_009554_1858, centered at 5.87°N/237.15°E). (b) Summit crater of cone with well-developed rim and flat summital plateau (detail of HiRISE PSP_008262_1855, centered at 5.78°N/237.01°E). (c) Flow-like deposits with branching morphology. One flow originates from a fissure-like source cutting a cone (right), another flow originates at the lower flank of a cone (lower left). Note that the transition between the flows and the surrounding terrain is partly obscured by a thick dust layer (detail of HiRISE PSP_008262_1855, centered at 5.65°N/237.02°E). (d) Terrestrial cinder cone with associated lava flow in plan view (SP Mountain, Arizona, USA; image: NASA). (e) Oblique aerial view of the same cinder cone with detail of lava flow in the foreground (image: Michael Collier).

large volcanoes, Biblis and Ulysses Paterae. The Ulysses Fossae itself represent a window of older crust, probably of early Hesperian age (Anderson et al., 2001), which survived later resurfacing of large younger lava flows (Scott and Tanaka, 1986). The investigated area seems to be part of this older crust, which is partly embayed by younger lava material.

The study area is structurally characterized by extensive N- to NNW-trending normal faults, which often form grabens that dissect especially the northern and western part of it (Scott and Dohm, 1990). The southern and eastern parts are covered by younger lava flows that had their origin towards the southeast. Most of the topographic edifices are observed close to the transition between the younger lava flows and the older heavily fractured crust. The spatial arrangement of the edifices is obviously controlled by the fault trend, and single edifices appear aligned along faults, building small clusters (Fig. 2.1 and 2.2). Several cones grew on older deposits with a rough texture that partly buries the underlying faults. Parts of these rough deposits are disrupted by faults, however, suggesting a later reactivation of faulting (Fig. 2.1 and 2.2). Close inspection of HiRISE images suggests that the entire area is thickly mantled by dust.

2.4. Morphology

A total of 29 possible volcanic edifices were identified. These cones are spread over an area of about 50 × 80 kilometers, with the main clustering of edifices in the south and several widely spread cones in the north (see Fig. 2.1 for the detailed spatial distribution of cones). All the measured dimensions of the cones increase from North to South. The more southern edifices are also better preserved, with well-developed morphologies of truncated cones and uniform flank slopes. In contrast, the northern cones are smaller and appear degraded without preserved visible craters on their top. In plan view, the cone morphology is characterized by circular to elongated outlines (Fig. 2.3a and 2.3b), relatively steep-appearing

Table 2.2. All measured values of investigated volcanic cones. Positions are drawn in Fig. 2.1 for each cone.

ID	W_{CO} average [m]	W_{CR} average [m]	H_{CO} [m]	W_{CR}/W_{CO}	H_{CO}/W_{CO}	Slope [°]	Volume [km^3]
A1	3909	1185	539	0.30	0.14	21.60	3.01
A2	3219	721	651	0.22	0.20	27.53	2.25
A3	-	-	-	-	-	-	-
A4	1785	606	130	0.34	0.07	12.43	0.16
A5	-	-	-	-	-	-	-
A6	2891	779	314	0.27	0.11	16.56	0.92
A7	2258	638	-	0.28	-	-	-
A8	3311	637	422	0.19	0.13	17.51	1.49
A9	-	-	-	-	-	-	-
A10	-	-	88	-	-	-	-
A11	2968	732	519	0.25	0.17	24.90	1.56
A12	-	-	-	-	-	-	-
A13	3694	883	-	0.24	-	-	-
A14	1092	401	120	0.37	0.11	19.15	0.06
A15	1715	665	180	0.39	0.10	18.92	0.21
A16	1964	795	164	0.40	0.08	15.68	0.26
A17	-	598	-	-	-	-	-
A18	-	365	82	-	-	-	-
A19	-	304	83	-	-	-	-
A20	-	-	112	-	-	-	-
A21	1507	390	-	0.26	-	-	-
A22	2904	1147	292	0.39	0.10	18.38	1.00
A23	2150	609	250	0.28	0.12	17.97	0.41
A24	1325	454	129	0.34	0.10	16.49	0.09
A25	-	-	125	-	-	-	-
A26	-	-	64	-	-	-	-
A27	-	-	-	-	-	-	-
A28	980	183	150	0.19	0.15	20.62	0.05
A29	1452	281	180	0.19	0.12	17.08	0.38

flanks, and summit craters or plateaus (Fig. 2.3b). Some cones are associated with lobate and sometimes branching deposits, which emanate from the summit craters or from some points at or very near the flanks (Fig. 2.3a and 2.3c). The outline of these features in plan view resembles that of lobate flows. The flow-like features appear to be rather short and thick, as compared to most lava flows in Tharsis and Elysium. A thick dust cover, which is typical for Tharsis and hinders the full exploitation of the very high spatial resolution of HiRISE (Keszthelyi et al., 2008), prevents the identification of meter-scale textural details of the cones and the associated lobate flows. Both cones and associated flows are superposed on terrain with a rough texture that forms local topographic bulges.

The cones and flows are much better preserved than recently detected cones and flows in Utopia (Lanz et al., 2010). The association of cones with lobate flows distinguishes these cones from other cone fields on Mars, which were mostly interpreted as clusters of rootless cones (Frey and Jarosewich, 1982; Fagents and Thordarson, 2007; Lanagan et al., 2001). Interestingly, however, none of the craters on top of the cones is breached by a lava flow, which is a common situation for terrestrial pyroclastic cones (Wood, 1980a; Head and Wilson, 1989). Pyroclastic cones observed by Bleacher et al. (2007) and Keszthelyi et al. (2008) are breached, but no associated flows could be identified. Our observations reveal that at least three cones are associated with flows starting at the base of cones or on their flanks.

2.5. Morphometry

Our investigation is based on measurements of basic morphologic properties of identified cones, which were previously used for terrestrial pyroclastic cones and other types of volcanic edifices (e.g., Porter, 1972; Settle, 1979; Wood, 1979a, Hasenaka and Carmichael, 1985b; for a review of previous studies on volcano morphometry see Grosse et al., 2012). Cone diameter (W_{CO}) and crater diameter (W_{CR}) were determined by averaging four measurements in different directions. Cone height (H_{CO}) was obtained from MOLA single tracks or from HRSC DEM. These basic parameters were used to calculate two basic ratios, W_{CR}/W_{CO} and H_{CO}/W_{CO}, and the slope angle (Porter, 1972; and references therein).

The volume was calculated via the equation for a truncated cone, also used by Hasenaka and Carmichael (1985a):

$$V = (\pi H_{CO} / 3) (R_{CR}^2 + R_{CR} R_{CO} + R_{CO}^2) \quad (2.1)$$

where the radii, R_{CR} and R_{CO}, are 0.5 W_{CR} and 0.5 W_{CO}, respectively. It was possible to measure the morphometric properties for almost half of the 29 cones (Tab. 2.2). Burial of the lower parts of cones by later lava flows would imply that we only measured the apparent basal diameter after embayment and a correspondingly smaller height, but based

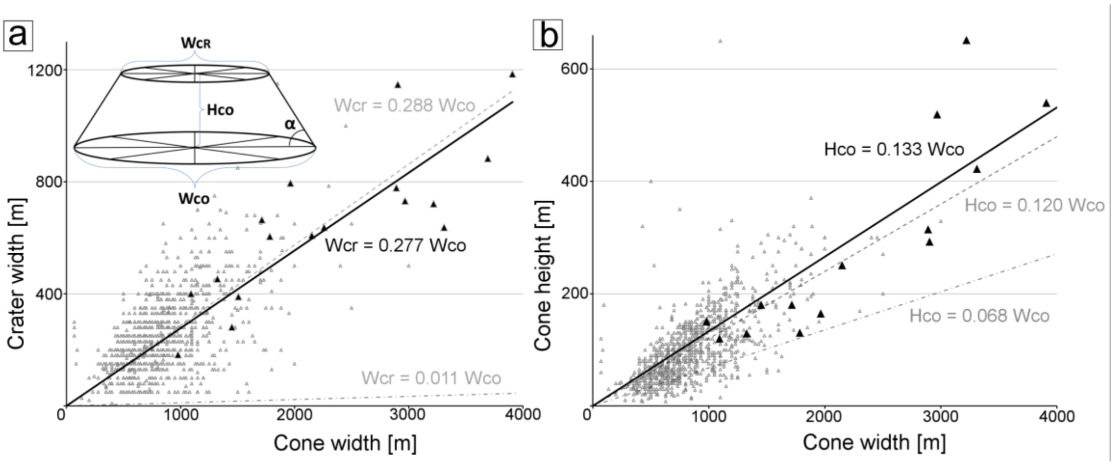

Figure 2.4. Morphometry of investigated cinder cones in comparison with terrestrial cinder cones and stratovolcanoes with summit craters. Full triangles correspond to investigated Martian cones; empty triangles to terrestrial cinder cones (~1060 edifices from Hasenaka and Carmichael, 1985a; Inbar and Risso, 2001; Pike, 1978). The inset in A illustrates the morphometric parameters used in this study. W_{CO} is basal width of cone, H_{CO} cone height, W_{CR} represents the basal crater diameter, and α is the slope angle. (a) Plot of summit crater width (W_{CR}) versus basal cones width (W_{CO}) of cones. The solid line represents the best fit (linear regression) for Martian cones with a value W_{CR}/W_{CO} = 0.277. Terrestrial cinder cones are represented by dashed line (W_{CR}/W_{CO} = 0.288), and for comparison the dotted-and-dashed line represents terrestrial stratovolcanoes with summit craters (W_{CR}/W_{CO} = 0.011). (b) Plot of cone height (H_{CO}) versus basal width of cone. Lines represent the same edifices as in plot a. Both plots demonstrate the morphometrical similarity between Martian cones and terrestrial cinder cones.

on the visual appearance of the cones we consider this possible effect to be insignificant. The morphometry of terrestrial monogenetic volcanic landforms was previously determined (e.g., Wood, 1979a or Tab. 2.3). In particular, Wood (1980a) reports the morphometry of 910 scoria cones from different volcanic fields. Scoria cones on Earth have a mean basal diameter of 900 m, but can range widely in dimension (Wood; 1980a). The ratio between crater diameter and basal diameter has an average value of 0.4 (Wood, 1980a; Porter, 1972),

Table 2.3. Comparison of morphometric data (mean values) of pyroclastic cones on Earth and Mars. *N*-number of cones, W_{CO}-width of cone, W_{CR}-width of crater, H_{CO}-height of cone.

Volcanic field or region	**N**	W_{CO} **[m]**	W_{CR} **[m]**	H_{CO} **[m]**	W_{CR}/W_{CO}	H_{CO}/W_{CO}	**Volume [km^3]**	**Source(1)**
Mauna Kea (Hawaii)	-	-	115(2)	-	0.4	0.18	-	[1]
Michoacán-Guanajuato (Mexico)	901	830	240	100	-	-	0.038	[2]
Michoacán-Guanajuato (Mexico)	11	950	308	170	0.32	0.17	0.07	[3]
Xalapa (Mexico)	57	698	214	90	0.3	0.14	0.13	[4]
Payun Matru (Argentina)	120	1,100	306	127	0.32(3)	0.13	-	[5]
Kamtchatka (Russia)	9	795	n.a.	149	-	0.18	0.07	[6]
Lamongan (Indonesia)	36	760	77(4)	94	0.19(4)	0.13(5)	0.039	[7]
Ulysses Fossae (Mars)	29	2,300	620	230	0.28	0.13	0.85	this study

(1) [1] Porter (1972). [2] Hasenaka and Carmichael (1985a). [3] Hasenaka and Carmichael (1985b). [4] Rodriguez et al., 2010. [5] Inbar and Risso (2001). [6] Inbar et al. (2011). [7] Carn (2000).
(2) measured for 218 cones (see Fig. 3 of Porter, 1972).
(3) only determined for 76 cones for which a crater diameter is given by Risso and Inbar (2001).
(4) determined for 14 cones.
(5) determined for 27 cones

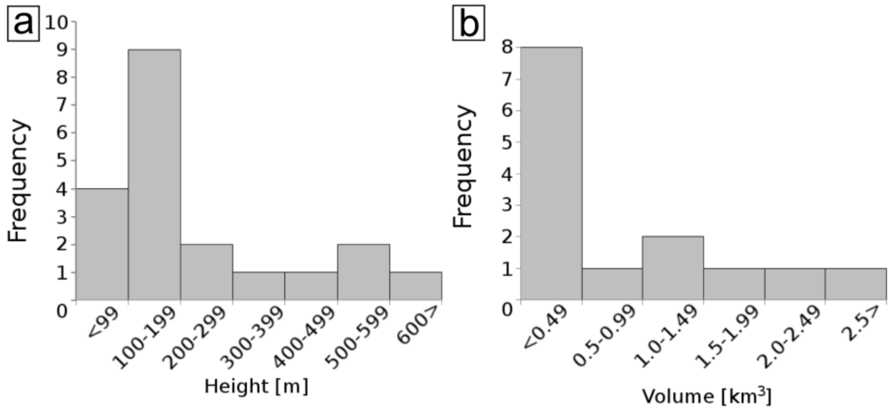

Figure 2.5. a) Histogram of cones heights. (b) Histogram of cone volumes.

but other studies including scoria cones in different stages of erosion show a lower value for this ratio (see Fig. 2.4a, black dashed line). The height of fresh scoria cones on Earth is equivalent to 0.18 W_{CO} (Porter, 1972; Wood, 1980a), but the height distribution has a wide range towards lower values.

Our measurements suggest that the cones in the study area have a mean basal diameter of 2300 m, with a range from ~1000 to ~3900 m. This is about ~2.6 times larger than the basal diameter of terrestrial pyroclastic cones and also larger than the scoria cones reported by Lanz et al. (2010) in Utopia Planitia (~280 to 1000 m). The crater diameter for the cones studied here ranges from ~185 to ~1185 m, with an average of 650 m, which is about ~2.5 times larger than terrestrial pyroclastic cones (average ~257 m). It is also larger than that of the scoria cones reported by Lanz et al. (2010) (110 to 450 m). The W_{CR}/W_{CO} ratio of the investigated cones has a mean value of 0.277. The edifices are also higher (from 64 to 651 m; Fig. 2.5a) than terrestrial pyroclastic cones (average height: 105 m, based on measurements of 1063 edifices, data from Hasenaka and Carmichael, 1985b; Inbar and Risso, 2001; and Pike, 1978; for additional morphometric measurements of terrestrial pyroclastic cones see Rodriguez et al., 2010). The H_{CO}/W_{CO} ratio is 0.133 (Fig. 2.4b), which is less than that of pristine terrestrial pyroclastic cones with a ratio of 0.18. The slope distribution of cone flanks is between 12° and 27.5° (the steepest sections reach >30°), with higher values for well-preserved cones with associated flow-like features and lower values corresponding to more degraded edifices. These values are in agreement with slope angles for terrestrial pyroclastic cones in different stages of erosion, with older and more eroded cones exhibiting progressively lower slope angles (Hooper and Sheridan, 1998). The volume is ranging from 0.05 to 3.01 km^3 (Fig. 2.5b), while the average terrestrial value is 0.046 km^3 (determined from 986 edifices, data from Pike, 1978; Hasenaka and Carmichael, 1985b). The volume of the cones in the study area is mostly one to two orders of magnitude higher than that of pyroclastic cones on Earth.

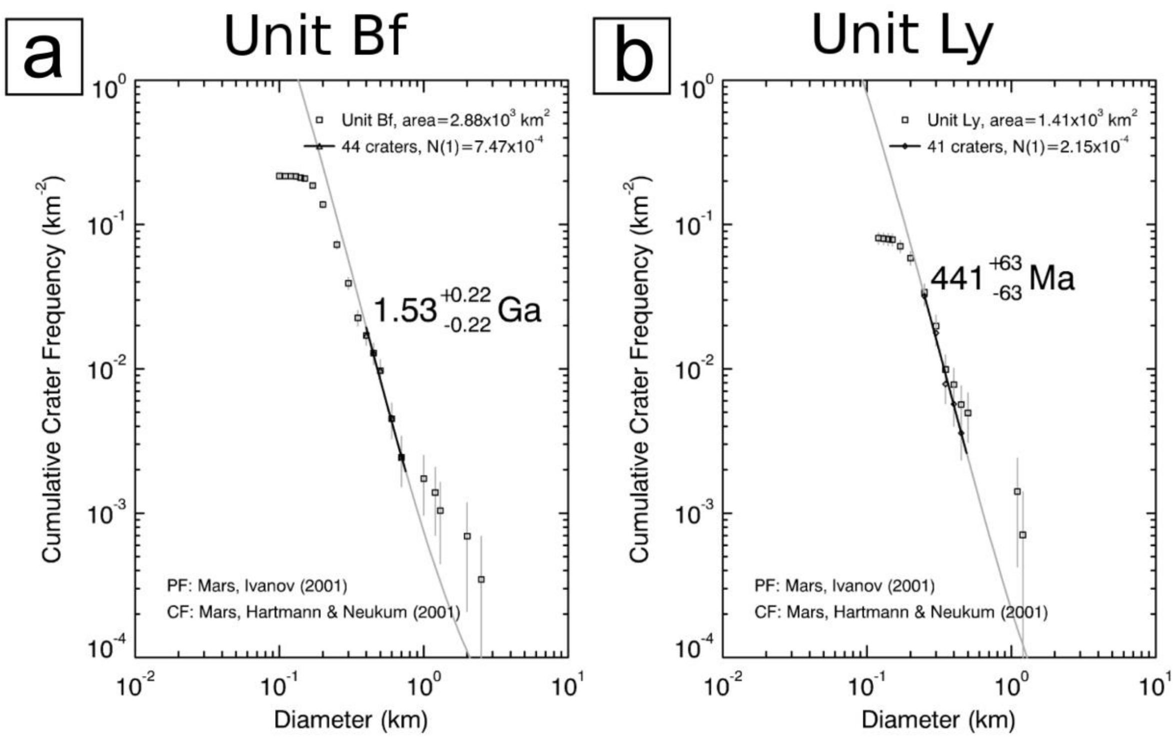

Figure 2.6: Absolute model ages for two surface units which are interpreted to be older and younger than the volcanic cones, thereby bracketing the age of volcanic activity. (a) Crater size-frequency distribution of the fractured basement (Unit Bf) on which the volcanic field was emplaced. The cumulative crater curve indicates an absolute model age of ~1.5 Ga. (b) Same for the lava flows (unit Ly) that embay the volcanic field in the southeast. The absolute model age is about 440 Ma. See Fig. 2.1 for location of units Bf and Ly.

2.6. Age

The absolute model age determination of planetary surfaces uses the crater size-frequency distribution as measured on images (Crater Analysis Techniques Working Group, 1979). The small size of, and the thick dust cover on the cones prevent the counting of small craters on the cones themselves. Moreover, their shape with slope angles of up to 30° renders them useless for crater counting, since gravitational movements on the slopes would cause distortions of the original geometry of impact craters. Instead, we dated two areas (*cf*. Fig. 2.1) which we consider to be older and younger than the cones, thus bracketing their formation age. One of these areas is the faulted basement, which by definition is older than the faulting and, therefore, older than the cones. The other area represents the lava flows in the southeast, which embay the topographic high and are assumed to be younger than the cones. Representative surface areas for age determinations were mapped and craters counted on CTX images utilizing the software tool 'cratertools' (Kneissl et al., 2011). Absolute crater model ages were derived with the software tool 'craterstats' (Michael and Neukum, 2010) by analysis of crater-size frequency distributions applying the production function coefficients of Ivanov (2001) and the impact-cratering chronology model coefficients of Hartmann and Neukum (2001). We determined absolute model ages of ~1.5 Ga and ~0.44 Ga for the older and the younger area, respectively, thus the formation of the cones probably occurred within this time interval (Fig. 2.6). This method of absolute age range determination can not reveal any age differences between individual cones (see below), since no degradational sequence can be inferred from the observed unit relationships.

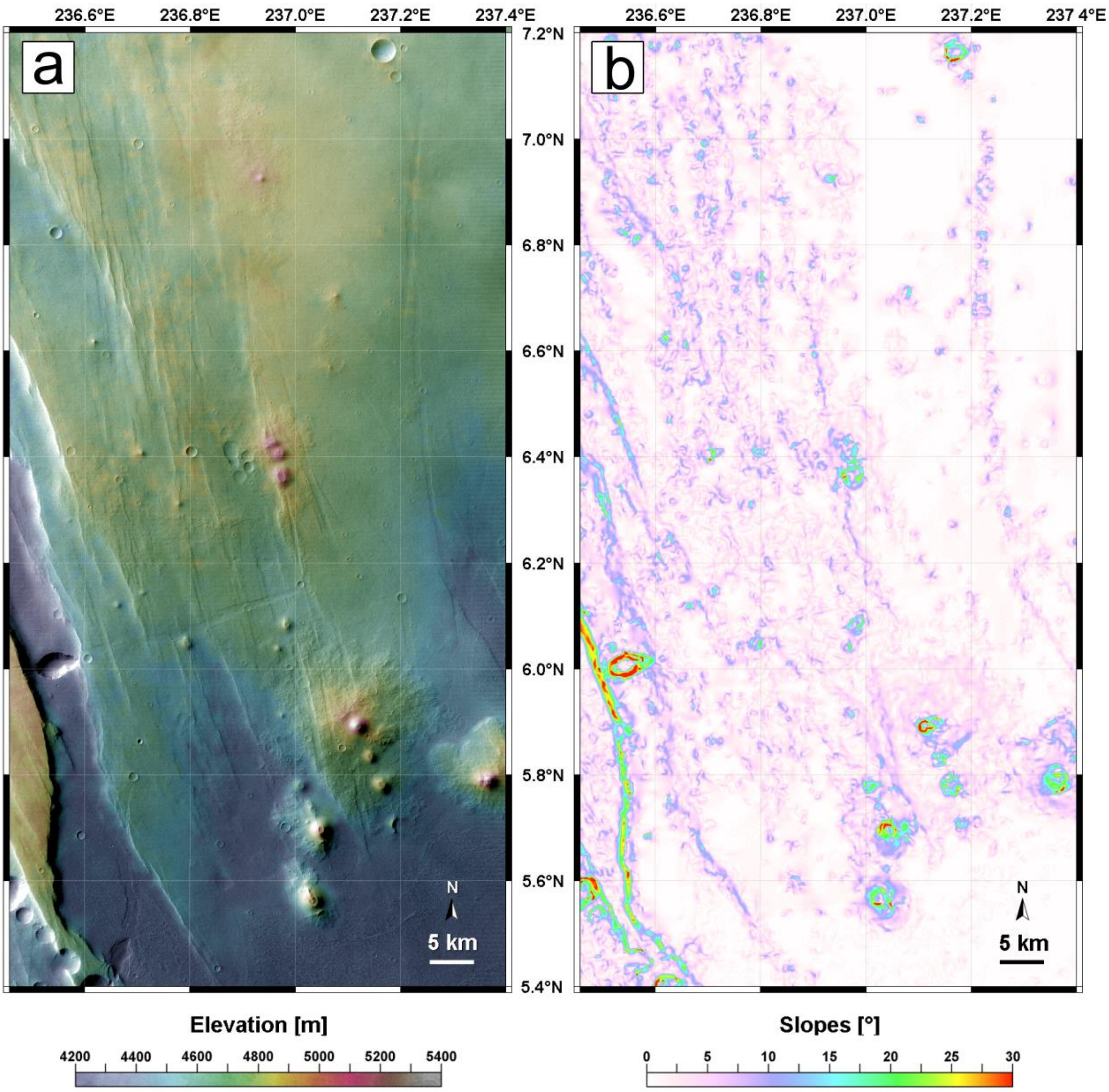

Figure 2.7: (a) Topographic map of western part of the study area. (b) Slope map. Note that the substrate on which the cones are superposed has very low slope angles, and therefore does not affect the morphometry of the cones (cf. Tibaldi, 1995, who noted that substrate slopes >9° can affect cone morphometry). Both maps were derived from HRSC image sequence h1023_0000.

2.7. Discussion

Some morphological and morphometrical characteristics of the cones in the study area suggest an origin as pyroclastic cones. Their appearance as truncated cones with smooth flanks of more or less uniform slope angles, summit craters or plateaus, and associated flows is analogous to terrestrial scoria or cinder cones associated with lava flows (Fig. 2.3). The most striking morphometric similarity between the martian cones and terrestrial scoria cones is the W_{CR}/W_{CO} ratio (Fig. 2.5a). It is clearly distinguished from that of terrestrial stratovolcanoes, which has typically values of ~0.027 (McKnight and Williams, 1997). The influence of preexisting topography on cone morphology is negligible. Tibaldi (1995) reports that substrate slopes <9° do not affect cone shapes. Topographic and slope maps of the study area (Fig. 2.7) show that the substrate has slopes <9° throughout the study area. Other morphometric parameters of the studied cones, however, are different from terrestrial pyroclastic cones, e.g., the basal diameter and the height. Theoretical considerations predict considerable differences between pyroclastic (scoria) cones on Earth and Mars (for a given magma volume and volatile content), due to the specific surface environment on both planets, in particular gravity and atmospheric pressure (Wilson and Head, 1994). Pyroclastic cones on Mars should have larger basal diameters and lower heights (Wilson and Head, 1994; Fagents and Wilson, 1996; Parfitt and Wilson, 2008), and the W_{CR}/W_{CO} ratio should be larger (Wilson and Head, 1994). However, Wood (1979b) assumed that this ratio is independent of gravity and atmospheric pressure, because the wider dispersal of ejecta material would affect crater width and basal diameter in the same way. Therefore, W_{CR}/W_{CO} should be the same for pyroclastic cones on Earth, Mars or others bodies. Dehn and Sheridan (1990) theoretically modeled pyroclastic cones on different terrestrial bodies, and they predicted that basal diameters of pyroclastic cones on Mars should be 2 to 3 times larger than those of terrestrial pyroclastic cones. The same authors also suggest that the cones should be >100 m high and display well-developed deep central craters. Our measurements show cone basal diameters ~2.6 times larger than for typical terrestrial scoria cones, fitting

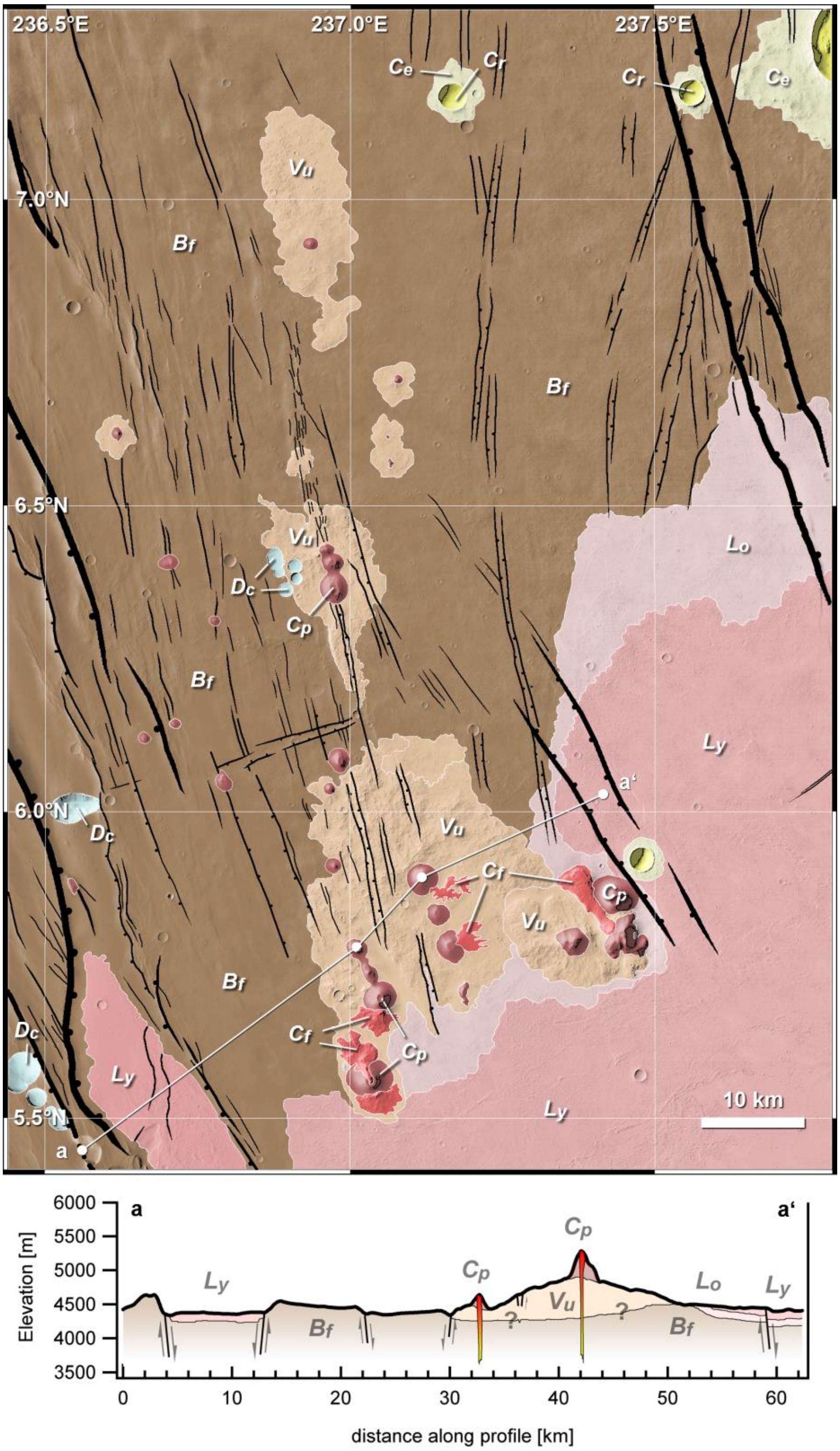

Figure 2.8: Schematic geological and structural map. Units: *Cp*-pyroclastic cone; *Cf*-Lava flows associated with pyroclastic cones; *Vu*-volcanic deposits (unclassified); *Dc*-collapse depressions, *Lo*-older lava flows; *Ly*-younger lava flows; Bf-fractured basement; *Cr*-large crater; *Ce*-crater ejecta. Black lines with hatches on one side: grabens, dipping toward hatched side; other black lines: fractures (mostly normal faults).

numerically to previously established values. However, the cones in our study area are several hundred meters high, which is in disagreement with previously established theoretical considerations (Wood, 1979b; Wilson and Head, 1994).

Several types of monogenetic volcanoes on Earth (spatter cones, rootless cones and scoria/cinder cones) have a similar W_{CR}/W_{CO} ratio of ~0.4 (Wood, 1979a). It is impossible, therefore, to classify an investigated edifice as scoria or cinder cone only from the W_{CR}/W_{CO} ratio alone. Generally, different types of volcanic cones cannot be separated from each other by using a single morphometric factor such as cone basal diameter or cone height (Wood, 1979a). Moreover, climatic conditions and the grain size distribution might have an influence on morphometry (Wood, 1980b; Riedel et al., 2003; Rodriguez et al., 2010) and morphometric ratios are an indication of the average shape and construct structure, but do not relate to a typical cone-forming process (Kervyn et al., 2012). Independent information on the geological context is required to further distinguish between different cone types. Our observations show that flow-like features are associated with several cones (Fig. 2.3a and 2.3c). We interpret these lobate deposits as lava flows, similar to terrestrial lava flows associated with scoria cones (Fig. 2.3d and 2.3e). The association of cones with lava flows, typical for terrestrial scoria cones (Pioli et al., 2009) or spatter cones, strongly supports an origin of the cones as pyroclastic cones. This interpretation excludes an origin of the cones as rootless cones, because these are rootless edifices without any connection to deeper magma sources. Moreover, the dimensions of rootless cones are several times smaller than those of the investigated cones. Spatter cones are another alternative, but Wood (1979a) points out that, in general, all morphometric parameters have lower values for spatter cones as compared to scoria or cinder cones. For example, the *mean* cone basal diameter of spatter cones on Earth is one order of magnitude smaller than that of scoria or cinder cones, and the volume range is typically smaller by two orders of magnitude. These differences might suggest that spatter emplacement was not the dominant mode of formation for these cones as opposed to scoria emplacement.

The larger basal diameters and heights of the cones in our study area as compared to pyroclastic cones on Earth could be accounted for by larger erupted magma volumes than for terrestrial pyroclastic cones. The basically identical W_{CR}/W_{CO} ratio is not in agreement with theoretical predictions by Wilson and Head (1994), however, it is consistent with the results of Wood (1979b). Based on the morphological and morphometrical arguments presented above and the association of cones with lava flows, we interpret the cones as pyroclastic (scoria) cones. The cones and the associated lava flows are superposed on a material with rough texture, which is again superposed on the fractured basement. We interpret the rough material as a mixture of distal pyroclastic deposits and lava flows. Our interpretation of the geologic context of the volcanic field is shown in Fig. 2.8. Although it is not possible to determine the duration of the formation of single cones, the similarity to monogenetic volcanic fields on Earth tentatively suggests that the martian cones might be monogenetic volcanoes as well.

The spatial arrangement of the cones is obviously controlled by the grabens of Ulysses Fossae (Fig. 2.1, 2.2, 2.7, 2.8), an extensional fracture zone that is characterized by several sets of normal faults that commonly form grabens (Scott and Dohm, 1990). The orientation of the faults is generally NW, N, and NNE, but a few faults also trend roughly WSW-ENE. The cones are aligned along fractures trending NNW (Fig. 2.2), and an eruptive fissure (Fig. 2.3c) is also parallel to this fault trend. Cone alignment on Earth is commonly controlled by regional and local tectonic patterns such as defined by fault and rift zones (e.g., Connor and Conway, 2000; Bonali et al., 2011). It seems possible that the cone-related volcanic activity was directly related to the extensional stress in the martian lithosphere. Analogies are well known from the Earth, where rifting will typically start as a broad zone of extension, but will eventually transition towards a narrow zone of focused magmatic intrusion (e.g., Rooney et al., 2011). Magma can ascend via dikes to produce surface volcanism, which can be manifested as aligned scoria cones as it is observed, e.g., in the Main Ethiopian Rift (Rooney et al., 2011). In this case, the magmatism would be contemporaneous to the rifting and be an integral part of the rifting itself (magma-assisted rifting; e.g., Kendall et al., 2005). Alternatively, the distribution of vents in monogenetic volcanic fields may be controlled by the reactivation of older structures that enable a more favorable magma ascent (e.g., Cebriá et al., 2011), a mechanism which was also suggested for Mars (Bleacher et al., 2009). Currently it is not possible to decide which of the two options applies to the study area. Detailed age dating would be a way to solve this question, but this appears difficult due to the inherent problems in dating small-scale features with a thick dust cover.

Terrestrial pyroclastic cones are formed by scoria clasts and are susceptible to erosion. Several of the cones in the study area, mainly in its southern part, are relatively well preserved. This observation, together with the well-developed associated lava flows, suggests that there was no significant erosion since their emplacement. Cones in the northern part of the study area appear more degraded, and no associated lava flows can be identified. On Earth, the degradational evolution of pyroclastic cones is correlated with the amount of time they have been exposed to erosion (Hooper and Sheridan, 1998), and the H_{CO}/W_{CO} ratio as well as the maximum and average slope angles of their flanks decrease with time (e.g., Dohrenwend et al., 1986; but note the limitations of this method to estimate relative cone age by Favalli et al., 2009a). Indeed, the H_{CO}/W_{CO} ratio of cones in the study area is generally increasing from north to south (Tab. 2.2). By analogy, we conclude that the cones in the north part of the study area are older than those in the southern part. The northern cones appear much more degraded (see also Tab. 2.2), and since erosion rates on Mars are very low after the Noachian (Golombek et al., 2006), this suggests that the formation of the cones in the entire study area spans an extended period of time. The relatively small number of cones does not seem to be in disagreement with this notion. Firstly, the original number of cones might have been larger, but most of them have been eroded beyond identification. Secondly, the number of cones in a volcanic field does not correspond with its longevity (Connor and Conway, 2000), so even a field with a small number of vents might have been long-lived.

Pyroclastic cones are typically formed by Hawaiian and/or Strombolian eruptions (e.g., Head and Wilson, 1989; Vergniolle and Mangan, 2000). Strombolian explosive eruptions are characterized by the more or less intermittent formation and bursting of a gas bubble close to the surface (e.g., Blackburn et al., 1976; Wilson, 1980). Different models exist to describe the mechanisms of Hawaiian-style lava fountaining (e.g., Wilson, 1980; Wilson and Head, 1981; Jaupart and Vergniolle, 1988; see review by Parfitt, 2004). It is not possible to distinguish between the two eruptive styles on Mars on the basis of cone morphology in our study area. Moreover, there is a continuum between these two styles of volcanism, and it is common that one type of activity changes to the other one during an eruption (Parfitt and Wilson, 1995; Vergniolle and Mangan, 2000). The observation of lava flows and eruptive fissures (Fig. 2.3) suggests that at least some stages in the eruptions might have been dominated by fire fountaining, leading to the formation of a pyroclastic cone, lava flows and rootless flows according to the scheme discussed by Head and Wilson (1989; see their Fig. 7). Nevertheless, some possible aspects of the eruptions responsible for cone formation in the Ulysses Fossae regions can be discussed.

The observed style of eruptive activity in the study area differs markedly from that of younger plain-style volcanism in Tharsis and Elysium, which is predominantly effusive (Hauber et al., 2009a; Vaucher et al., 2009b). In general, the explosivity of a basaltic eruption is controlled by various parameters, such as the volatile content of the magma, magma viscosity and magma rise speed, and interaction of magma with ground water or ground ice (e.g., Wilson, 1980; Roggensack et al., 1997; Pioli et al., 2009). Materials forming pyroclastic cones can originate by explosive fragmentation from ascending magma by two main processes. Firstly, material is forming from rapid exsolution and decompression of magmatic volatiles, and secondly by interaction of groundwater with magma, or by a combination of these two styles (Vespermann and Schmincke, 2000). The first mechanism was theoretically discussed by Wilson and Head (1994), and the lower atmospheric pressure on Mars would promote the explosivity of martian eruptions under current atmospheric conditions. The same authors, however, predict that the higher ejection velocities of the fragmented particles would lead to a wider dispersal of eruption products, thus making the identification of deposits difficult (Francis and Wood 1982; Wilson and Head, 2007). The observed morphology of the cones in our study area, with readily identified pyroclastic material, does not agree with these predictions. Partly this might be due to a thicker atmosphere at the time of cone formation (perhaps higher CO_2 contents from polar cap sublimation caused by astronomical forcing of climate changes; Phillips et al., 2011), but it is not clear if plausible increases in atmospheric pressure would be a sufficient explanation.

The difference between the eruptive style in the study area and in the younger volcanic plains is obvious, but there is no straightforward explanation. Volcanic fields with morphologies similar to the study area might have been more widespread in the past, but might now be buried under younger lava plains. Magma viscosity might have been different, but due to the thick dust cover there are no compositional data from orbiting spectrometers. The morphology of the lava flows might be an indirect indicator of more viscous magma (which would promote explosive activity), since the flows are relatively short and appear to have steep flow fronts. This lava morphology is distinct from that typically observed in most young plain-style regions of Tharsis and Elysium, where lavas seem to have low viscosities (e.g., Vaucher et al., 2009b; Hauber et al., 2011). Large and long-lived magma chambers beneath the study area might have allowed magma to differentiate to more silicic compositions, and stratification together with volatile differentiation would potentially have favor explosive activity at least in the initial stages of an eruption (Mitchell and Wilson, 2001). Without additional evidence, however, this explanation is very speculative.

2.8. Conclusions

1) Based on morphological and morphometrical analyses, we interpret an assemblage of landforms in Tharsis as a volcanic field with pyroclastic cones and associated lava flows. This result is consistent with the hypothesis that explosive basaltic volcanism should be common on Mars. It is surprising that this is the only well-preserved field of this kind seen so far on Mars, given the fact that pyroclastic cones are the most common volcanoes on Earth (Wood, 1980a; Valentine and Gregg, 2008). A possible explanation is that similar volcanic fields existed in the past, but were subsequently buried by younger volcanic deposits. If true, this might imply a gradual change in eruption style in Tharsis, from more explosive towards more effusive volcanism.

2) The spatial distribution of cones is controlled by regional tectonic trends, and cones are aligned along NNW-trending normal faults and grabens. It is not clear whether the volcanic activity was contemporaneous with the faulting, or whether the magmatism postdated the tectonism, with dikes ascending along pre-existing lines of structural weakness. Faulted volcanic substrate beneath the cones suggests that at least some of the faulting was post-volcanic.

3) The observed evidence for physiological diversity of martian volcanism is still growing (see also Lanz et al., 2010). The morphologic detection of volcanic centres in dust-free areas might enable the detection of further hydrothermal deposits (Skok et al., 2010).

Acknowledgements

Discussions with Thomas Platz helped to improve the manuscript. We appreciate two detailed and constructive reviews by Jacob Bleacher and Julia Lanz. We thank to Felix Jagert for his help with ArcGIS and Thomas Kneissl for help with CraterTool. This study was partly supported by the Helmholtz Alliance 'Planetary Evolution and Life' and by grant ME09011 of the program KONTAKT of the Ministry of Education of the Czech Republic.

3. Hydrovolcanic tuff rings and cones as indicators for phreato-magmatic explosive eruptions on Mars

Petr Brož[1,2] and Ernst Hauber[3]

[1]Institute of Geophysics ASCR, v.v.i., Prague, Czech Republic
[2]Institute of Petrology and Structural Geology, Faculty of Science, Charles University, Prague, Czech Republic
[3]Institute of Planetary Research, DLR, Berlin, Germany

Status: Published in Journal of Geophysical Research: Planets 118,

doi: 10.1002/jgre.20120.

3.0. Abstract

Hydrovolcanism is a common natural phenomenon on Earth, and should be common on Mars, too, since its surface shows widespread evidence for volcanism and near-surface water. We investigate fields of pitted cones in the Nephentes/Amenthes region at the southern margin of the ancient impact basin, Utopia, which were previously interpreted as mud volcanoes. The cone fields contain pitted and breached cones with associated outgoing flow-like landforms. Based on stratigraphic relations, we determined a Hesperian or younger model age. We test the hypothesis of a (hydro)volcanic origin. Based on a detailed morphological and morphometrical analysis and an analysis of the regional context, an igneous volcanic origin of these cones as hydrovolcanic edifices produced by phreatomagmatic eruptions is plausible. Several lines of evidence suggest the existence of subsurface water ice. The pitted cones display well-developed wide central craters with floor elevations below the pre-eruptive surface. Their morphometry and the overall appearance are analogous to terrestrial tuff cones and tuff rings. Mounds that are also observed in the same region resemble terrestrial lava domes. The hydrovolcanic interaction between ascending magma and

subsurface water and/or water ice may explain the formation of the pitted cones, although other scenarios such as mud volcanism cannot be ruled out. Together with the mounds, the cones might represent effusive and explosive edifices of a monogenetic volcanic field composed of lava domes, tuff rings, tuff cones, and possibly maars.

3.1. Introduction and background

Mars was volcanically active throughout most, if not all, of its history (e.g., Werner, 2009; Hauber et al., 2011; Robbins et al., 2011; Xiao et al., 2012), and volcanism played a significant role in the formation of its surface. Most volcanoes on Mars have been interpreted to be formed predominantly by effusive eruptions (Greeley, 1973; Carr et al., 1977; Greeley and Spudis, 1981). Another significant factor modifying the martian surface is water, both in liquid and frozen state, and at and beneath the surface (e.g., Baker, 2001; Feldman et al., 2004; Smith et al., 2009). Therefore, interactions of magma with water and/or ice should be common on Mars. On Earth, such interactions are known to trigger hydrovolcanism (Sheridan and Wohletz, 1983), the natural phenomenon of magma or magmatic heat interacting with an external water source (Sheridan and Wohletz, 1983). This interaction might lead to explosive, phreatomagmatic eruptions (Lorenz, 1987; Morrissey et al., 1999). Hydrovolcanism is a common phenomenon occurring on Earth in all volcanic settings (Sheridan and Wohletz, 1983).

The relative importance of explosive volcanism on Mars was predicted based on theoretical considerations (e.g., Wilson and Head, 1994, 2004). Basically, there are two possibilities how explosive eruptions originate and how magma might be fragmented. One can be considered as a ‘dry’ process, in which the eruption is driven solely by gases originally dissolved in the magma. It occurs when magma ascends rapidly and is accompanied by rapid decompression (Cashman et al., 2000). The second possibility involves ‘wet’

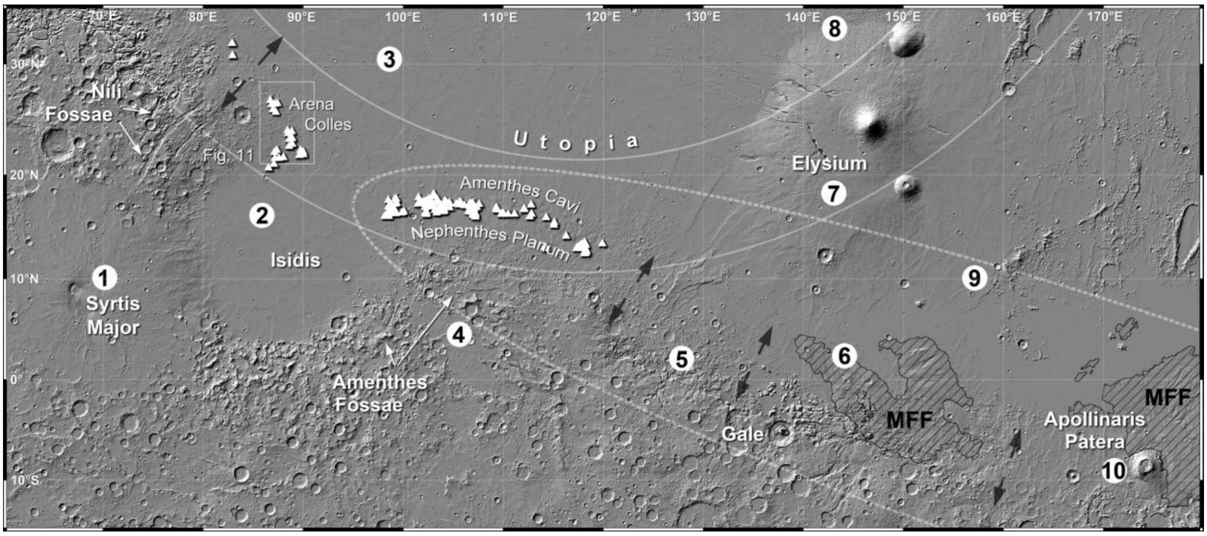

Figure 3.1: Study area (with pitted cones marked as white symbols) in regional context with most significant features highlighted. Large circles drawn with white lines mark perimeters of Utopia rings following Skinner and Tanaka (2007). White box marks location of Fig. 3.11, black arrows mark extension as reported by Watters (2003). White ellipse (dashed line) shows hypothetical dispersal of volcanic ash from the NAC cone field, indicating a possible contribution to the Medusae Fossae Formation. 1 - Low-relief shield volcano Syrtis Major, 2 – Pseudocraters in Isidis Planitia (Ghent et al., 2012), 3 –Rift zone volcanism (Lanz et al., 2010), 4 – Volcanic flooding (Erkeling et al., 2011), 5 – Possible subglacial volcanoes (de Pablo and Caprarelli, 2010), 6 - Cone fields with hydrothermal activity (Lanz and Saric, 2009), 7 - Elysium bulge, 8 – Phreatomagmatic eruptions (Wilson and Mouginis-Mark, 2003a), 9 – Cerberus Fossae and Athabasca Valles (e.g., Plescia, 2003) and 10 - Apollinaris Patera.

(phreatomagmatic) eruptions and occurs when magma of all types is mixed with an external water source, e.g., groundwater, ground ice Cashman et al., 2000), or a surficial body of water (Sheridan and Wohletz, 1983). The basic principle of this interaction is rapid heat transport from magma to water, leading to water vaporization, steam expansion and pressure build-up, and fragmentation and explosion (Basaltic Volcanism Study Project, 1981, p. 729). These types of eruptions are characterized by the production of steam and fragmented magma ejected from the central vent in a series of eruptive pulses (Sheridan and Wohletz, 1983).

Recently, several studies reported evidence of explosive volcanism forming small pyroclastic cones on Mars (Bleacher et al., 2007; Keszthelyi et al., 2008; Brož and Hauber, 2012), but these edifices were observed in relatively ‘dry’ environments (i.e. in Tharsis, for example at Pavonis Mons, Mareotis Tholus, Ulysses Fossae), and hence the explosive eruptions were probably driven by magma degassing. Only Meresse et al. (2008) and Lanz et al. (2010) investigated areas with pyroclastic cones that might have experienced a higher abundance of water/water ice. Meresse et al. (2008) focused on Hydraotes Chaos, a region thought to have formed by volcanic interaction with a subsurface layer enriched in water ice. Meresse et al. (2008) proposed that the formation of volcanic sills caused melting of the ice and the release of the water at the surface. On the other hand, Lanz et al. (2010) investigated pyroclastic cones associated with a rift-like structure in Utopia Planitia, an area that was may have been enriched in water ice, too (Erkeling et al., 2012). It is now clear that water ice is common in the shallow martian subsurface at a wide range of latitudes (e.g., Feldman et al., 2004; Smith et al., 2009; Byrne et al., 2009; Vincendon et al., 2010). Thus it is reasonable to expect that phreatomagmatic explosions left some observable evidence (Carruthers and McGill, 1998). Indeed, several in-situ observations made by rovers suggest the past action of hydrovolcanic explosions (e.g., Rice et al., 2006; Schmidt et al., 2006; Ennis et al., 2007; Keszthelyi et al., 2010) and other studies based on remote sensing data suggested phreatomagmatic activity (e.g., Wilson and Mouginis-Mark, 2003a, 2003b; Wilson and Head, 2004). Despite the growing evidence of martian volcanic diversity, the most abundant hydrovolcanic landforms on Earth, i.e. tuff rings, tuff cones and maars (Sheridan and Wohletz, 1983), were not yet reported in detail from Mars (Keszthelyi et al., 2010).

Here we present our observations of a large field of pitted cones along the dichotomy boundary in the Nephentes Planum and Amenthes Cavi region (Fig. 3.1), previously interpreted by Skinner and Tanaka (2007) as mud volcanoes. In the following, we refer to these cones as the Nephentes-Amenthes Cones (NAC). For the first time, we also report observations of another cone field north of Isidis Planitia in the Arena Colles region, which was previously unknown. This field is located in an almost identical geotectonic context, at a topographic bench along the margin of Utopia. Previous studies of the NAC are sparse. They were briefly mentioned by Erkeling et al. (2011), who referred to them as ‘volcano-like landforms’ without further explanation. To our knowledge, the only in-depth study is that of Skinner and Tanaka (2007), who interpreted these cones as mud volcanoes. This conclusion was based on the morphological analysis of an assemblage of landforms which consists of four elements: (1) fractured rises, (2) mounds, (3) isolated and coalesced depressions, and (4) the pitted cones which are the main subject of our study. Skinner and Tanaka (2007) considered the tectonic and sedimentary setting of the NAC and compared the landforms to possible terrestrial analogs. They developed a consistent scenario of mud volcanism that considers the local morphology as well as the regional tectonic context. According to their hypothesis, the giant Utopia impact formed a multi-ring basin (e.g., Spudis, 1993). Deposits filled and loaded the central part of the basin, whereas parts of the periphery were partly eroded and relaxed, producing an overall gently sloping basin surface. Skinner and Tanaka (2007) hypothesized that volatile-rich components were sedimented in annular ring grabens. These buried regions of weekly consolidated material enabled the formation of weaker zones beneath surface, which serve as a source reservoir for sedimentary diapirism. Material could have been mobilized through processes such as density inversion, seismicity, or contractional tectonism as implied by wrinkle ridges. Each mobilization would have led to resurfacing by mud effusion forming pitted cones, mud flows and mounds. As a result of mud volcanism, in which fine-grained material from deeper crustal levels would have moved upward to the surface, the Amenthes Cavi were then formed by subsidence in response to the source region depletion.

It is not our objective to disprove the mud volcano hypothesis of Skinner and Tanaka (2007), which offers a self-consistent scenario for landscape modification of the NAC region in the Hesperian. Instead, our aim is to test the alternative hypothesis of an igneous volcanic origin of the pitted cones and mounds. We compare the NAC with terrestrial analogs, both of igneous and mud volcanic origin, and discuss the most significant discrepancies and consistencies. We show that morphologically analogous structure may be found elsewhere on Mars, suggesting that the NAC may not be unique on Mars and, therefore, may not require a unique geologic context for their formation. Finally, we explore scenarios that may explain igneous volcanism at the study area.

3.2. Data and methods

3.2.1. Images and topography

For morphological analyses, we used different image data sets acquired by several cameras, i.e., Context Camera (CTX; Malin et al., 2007), High Resolution Stereo Camera (HRSC; Jaumann et al., 2007), and High Resolution Imaging Science Experiment (HiRISE; McEwen et al., 2007), with typical resolutions of 5–6 m/pixel, 10-20 m/pixel, and ~30 cm/pixel, respectively. CTX and HRSC image data were processed by the USGS Astrogeology image processing software, Integrated System for Imagers and Spectrometers (ISIS3), and Video Imaging Communication and Retrieval (VICAR), respectively.

Topographic information (e.g., elevations and slope angles) was derived from gridded Digital Elevation Models (DEM) derived from stereo images (HRSC). HRSC DEM are interpolated from 3D points with an average intersection error of 12.6 m and have a regular grid spacing of 50 to 100 m (Scholten et al., 2005; Gwinner et al., 2010). Although is well known that the quantification of various morphometric parameters depends on DEM resolution (e.g., Kienzle, 2004; Guth, 2006), even coarse DEM with a resolution equal or lower than HRSC DEM (e.g., DEM derived from Shuttle Radar Topography Mission (SRTM) with a grid size of typically 90 m) can be used for reliable measurements of volcano topography (Wright et al., 2006; Gilichinsky et al., 2010). Importantly, the size of the investigated feature should be several times larger than the spatial DEM cell size (Kervyn et al., 2007). The investigated NAC cones have typical basal diameters of >5 km and are, therefore, about two orders of magnitude larger than HRSC DEM grid sizes. Hence, the main results of our topographic analyses should be robust, although it cannot be excluded that flank slopes derived from HRSC DEM somewhat underestimate the true maximum flank slopes.

For comparative analyses, terrestrial data were obtained from Google Earth software (Google Inc., 2011). Google Earth uses DEM data collected by NASA's Shuttle Radar Topography Mission (Farr et al., 2007) with a cell size of 10 to 30 meters for the USA, and around 90 meters for the rest of the world (the case of Azerbaijan). The vertical error of these DEM is reported to be less than 16 meters (Jarvis et al., 2008). It has to be noted, however, that using this data may raise some problems. These are caused by the 90 m SRTM DEM, which is not ideal for small-scale (500 m) and/or steep topographic features (Kervyn et al., 2008), because it might lead to some measurement uncertainties. On the other hand, similar uncertainties are possibly associated with data from Mars used for morphometric comparison.

3.2.2. Cluster analysis: Nearest neighbour and two-point azimuthal analysis

To analyze the spatial distribution of cones within the field of NAC, we used Average Nearest Neighbor, part of Spatial Statistics tool in ArcGIS 10. This tool enables determination of clustering or dispersing behavior of investigated features by measuring the distance from every point (i.e. surface feature) to its nearest neighbor. The method is based on testing the randomness in spatial distribution by calculating the ratio between the observed mean distance and the expected mean distance for a random point distribution. If the ratio is <1, the points are clustered; the closer to zero, the more clustered (Clark and Evans, 1954).

The two-point azimuth technique developed by Lutz (1986) can been used to identify structurally controlled trends within a volcanic field. It tests if there is a preferential alignment of points along certain orientations (Cebriá et al., 2011). This method is based on a quantitative analysis of the azimuth angles of lines connecting each vent with all other vents, thus connecting all possible pairs of points in the investigated area (for N points, the total number of lines is N(N-1)/2). A vent is represented by a discrete point (Cebriá et al., 2011) and can therefore be used for this technique. The method was tested in different terrestrial and martian volcanic fields (e.g., Wadge and Cross, 1988; Connor, 1990, Lutz and Gutmann, 1995; Bleacher et al., 2009; Richardson et al., 2013). A modification of the two-point azimuth technique was developed by Cebriá et al. (2011), who defined a minimum significant distance between vents (Equation 3.1) to eliminate potential problems with a preferential alignment of points caused by the shape of the investigated area.

$$d \leq \frac{(x-1\sigma)}{3} \tag{3.1}$$

where *d* is the minimum significant distance, x is the mean of all distances between vents, and σ is the standard deviation of the mean distance between vents. This minimum significant distance should be able to filter out any large amount of non-significant data corresponding to the most likely orientation caused by the shape of the investigated area (Cebriá et al., 2011). For example, a field in the shape of a narrow ellipse will lead to a preferred orientation in the direction of the semi-major axis of the ellipse. This is exactly the case of the NAC field, which is elongated in an east-west direction. A histogram of azimuth values (from 0° = north, 90° = east, 180° = south) was produced, with bins of 15°. Following earlier authors (Lutz, 1986; Bleacher et al., 2009; Cebriá et al., 2011) we expect that bins containing an anomalously high number of lines connecting vents are evidence for a structural relationship or alignment between vents in the field.

To get information about morphological parameters and distinguish between different classes of volcanic edifices, we used three main morphometrical parameters already widely used by several authors in a range of terrestrial and martian volcanic fields (e.g., Porter, 1972; Wood, 1980a; Brož and Hauber, 2012; Kervyn et al., 2012). Specifically, cone diameter (W_{CO}) and crater diameter (W_{CR}) were determined by averaging two measurements in different directions. Cone height (H_{CO}) and crater depth (D_{CR}) were obtained from HRSC DEM. These basic parameters were used to calculate three basic ratios, W_{CR}/W_{CO}, H_{CO}/W_{CO} and H_{CO}/W_{CR}. To enable comparison of data from different sources, we used crater depth (D_{CR}) as the difference between the mean crater rim elevation and the lowest observed elevation inside the crater as used by Kervyn et al. (2012).

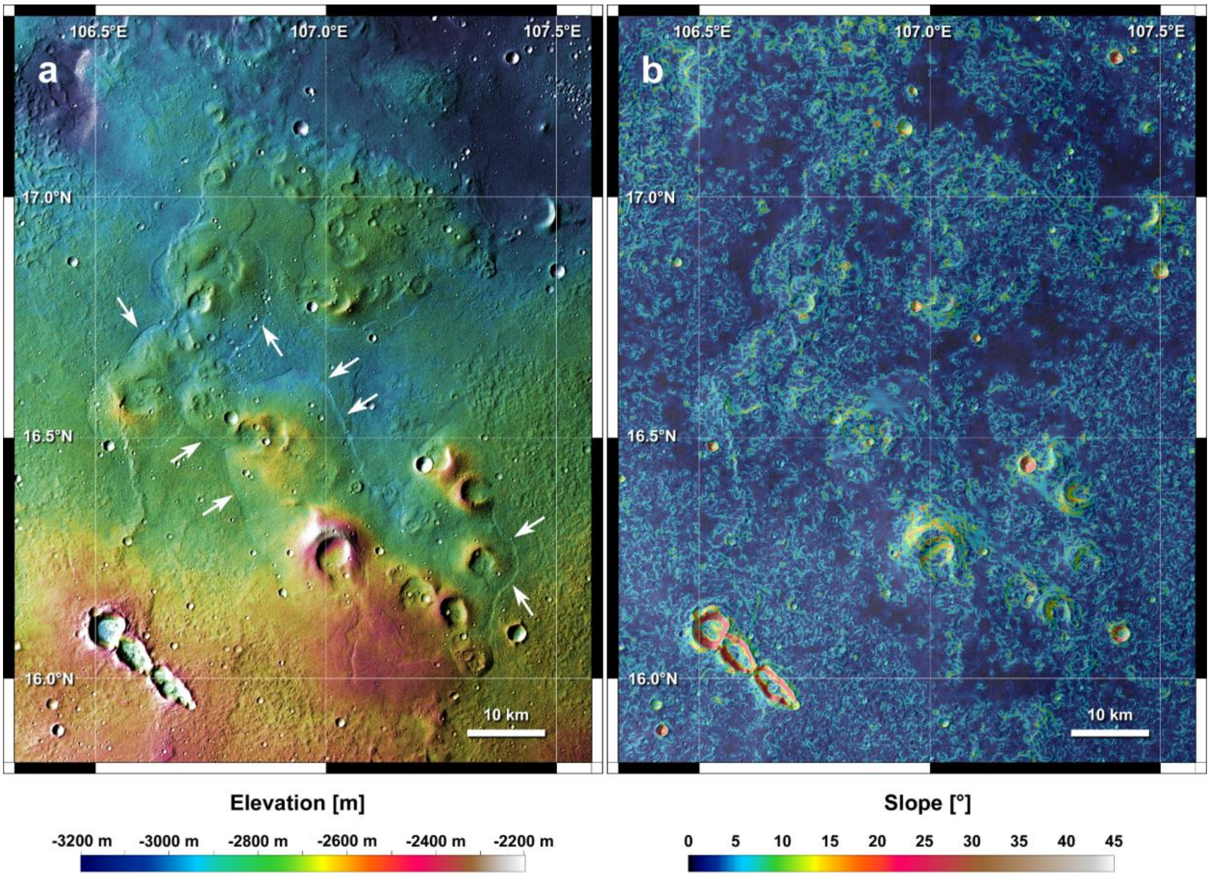

Figure 3.2: Pitted cones in the NAC field. (a) Topographic image map. Note the clustered distribution and the fact that several of the cones are breached in different directions. Smooth lobate material embays the cones (arrows). Detail of HRSC imaging sequence h3032_0000, orthoimage overlain by color-coded DEM derived from stereo images. (b) Slope map derived from HRSC DEM. Slopes were measured over a baselength of 50 m, corresponding to the cell size of the HRSC DEM.

3.2.3. Ages

The absolute cratering model age determination of planetary surfaces uses the crater size–frequency distribution as measured on images (Crater Analysis Techniques Working Group, 1979). Representative surface areas for age determinations are mapped on the basis of morphology (stratigraphy), and craters were counted on CTX images utilizing the software 'cratertools' (Kneissl et al., 2011). Absolute cratering model ages were derived with the software tool 'craterstats' (Michael and Neukum, 2010) by analysis of the crater-size frequency distributions applying the production function coefficients of Ivanov (2001) and the impact cratering chronology model coefficients of Hartmann and Neukum (2001).

3.3. Regional setting

The study area lies close to the dichotomy boundary, between cratered highlands of Tyrrhena Terra in the south and smoother appearing plains of Utopia Planitia in the north (Fig. 3.1). It is located on a topographic bench termed Nephentes Planum and also contains part of the Amenthes Cavi region (10°N to 20°N and 95°E to 125°E). The regional context was described by Tanaka et al. (2003, 2005), Skinner and Tanaka (2007) and mentioned by Erkeling et al. (2011). The whole NAC region is covered by dust, which complicates identifying surface details. Utopia Planitia probably formed by a giant impact during the pre-Noachian period around 4.5-4.1 Ga (e.g., McGill, 1989; Tanaka et al., 2005; Carr and Head, 2010). In an extension of McGill's original basin interpretation for Utopia (McGill, 1989), Skinner and Tanaka (2007) proposed the existence of annular ring basins that would have acted as locations of sediment accumulation in southern Utopia Planitia. Another relatively close basin is Isidis Planitia (e.g., Schultz and Frey, 1990), lying west of the Nephentes/Amenthes region and contributing to the history of the western part of the study area (Erkeling et al., 2011). Close to the rim of Isidis Planitia, near the southern part of the investigated area, a series of NNE-trending tectonic grabens, Amenthes Fossae, indicate extensional tectonics associated with the Isidis impact (Erkeling et al., 2011), analogous to the morphologically similar graben system, Nili Fossae, to the NW of Isidis.

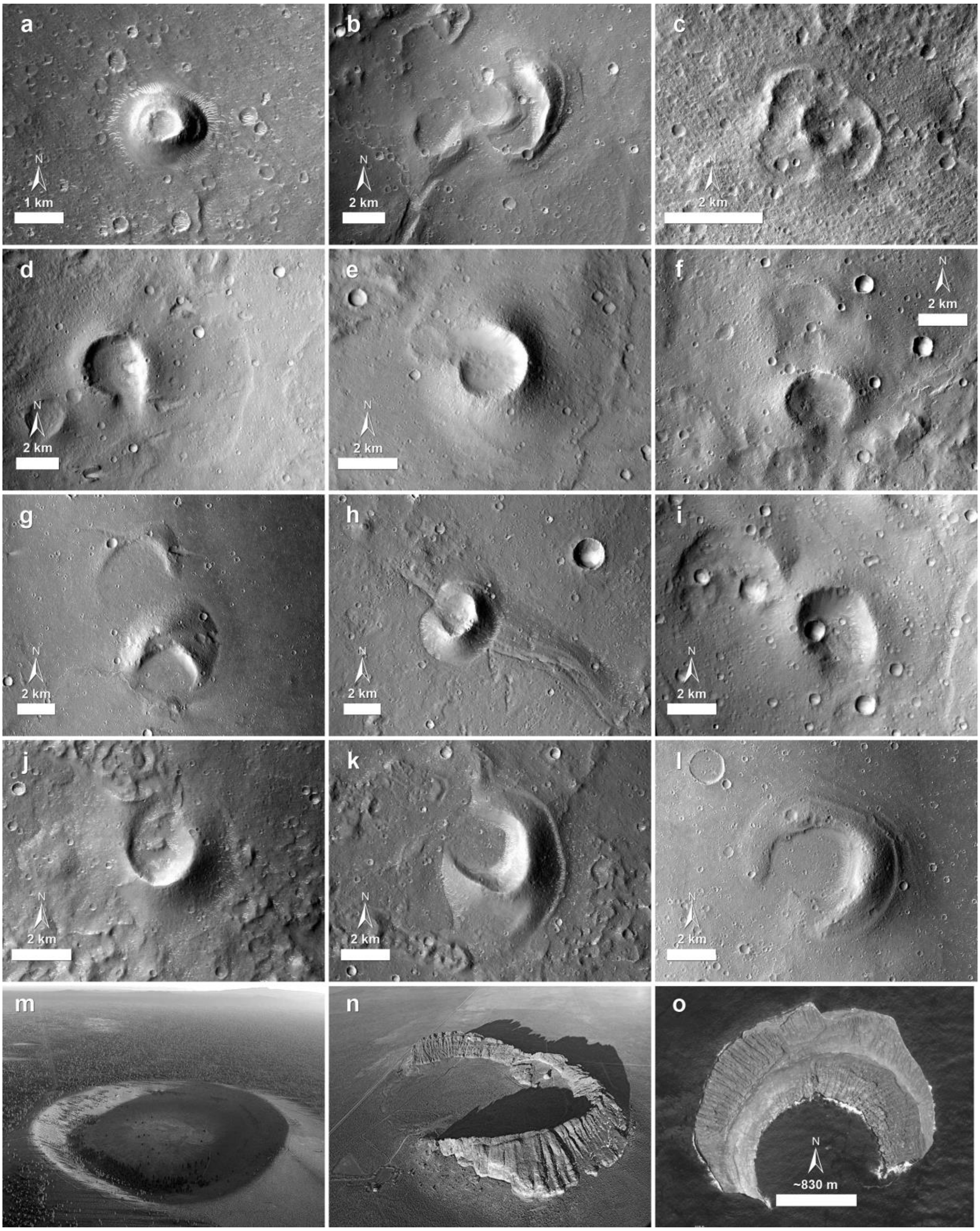

Figure 3.3 (opposite page): Examples of pitted cones in the NAC field (a to l) and examples of terrestrial tuff rings for comparison (*m* to *o*). (a) Cone at 16°N/114.56°E. This cone is unusual in that its crater rim is not breached (detail of CTX G01_018657_1961). (b) Nested cones near 16.97°N/112.30°E; detail of CTX P22_009519_1969. (c) Cone with nested craters at 17.6°N/104.57°E; detail of CTX B19_017075_1974. (d) Two cones near 16.5°N/102.37°E; detail of CTX P17_007489_1967. (e) Cone at 16.62°N/103.33°E; detail of CTX P04_002452_1969. (f) Cone at 16.67°N/104.13°E; detail of CTX G01_018776_1974. (g) Two cones, one of them only with a remaining small segment, near 18.31°N/103.11°E; detail of CTX P04_002452_1969. (h) Cone aligned along and split by a fissure, centered at 16.49°N/111.31°E; detail of CTX G04_019857_1964. (i) Two cones at 16.16°N/107.25°E (detail of CTX G01_018499_1961). (j) Cone at 16.05°N/112.86°E; detail of CTX P21_009308_1962. (k) Prominent cone at 16.48°N/113.07°E; detail of CTX B03_010653_1966. Note the morphological similarity to the terrestrial tuff ring, Fort Rock (Oregon, USA), in panel (n). (l) Cone at 17.06°N/104.19°E; CTX mosaic of B19_017075_1974 and G01_018776_1974. Note the morphological similarity to the tuff ring on the Galápagos Islands (Ecuador) in panel (o). (m) Maar 'Hole-in-the-Ground' (Oregon, USA; rim-to-rim diameter ~1500 m; oblique view towards NW; image: Q. Myers). Note similarity to (d), (e), (f), and (j). (n) Tuff ring 'Fort Rock' (Oregon, USA; diameter ~1300 m, oblique view toward WSW; image: Q. Myers). Note similarity to (k). (o) Tuff ring on the Galápagos Islands (Ecuador; image: DigitalGlobe, GoogleEarth™). Note similarity to (l).

Isidis was formed later than Utopia (Tanaka et al., 2005). Ivanov et al. (2012) interpreted the area of Isidis Planitia as a volcanic center which was mainly active at ~3.8-3.5 Ga. Later, the area experienced fluvial/glacial activity (early Hesperian-early Amazonian, ~3.5-2.8 Ga), and the associated processes may have left wet deposits on the floor of Isidis (Ivanov et al., 2012).

The region hosting the NAC is bordered to the East by the Elysium bulge and Elysium Planitia, previously recognized as significant volcanic centres (Malin, 1977; Plescia, 1990). The spatially closer regional context displays several lines of evidence for subsurface water ice (rampart craters, pseudo-craters, and the Hephaestus and Hebrus Fossae channels). Recently, several studies reported volcanic activity at various locations in a broad area around the NAC region (de Pablo and Pacifici, 2008; de Pablo and Caprarelli, 2010; Lanz et al., 2010; Ghent et al., 2012), suggesting focused locations of potential volcanic activity in the regional context.

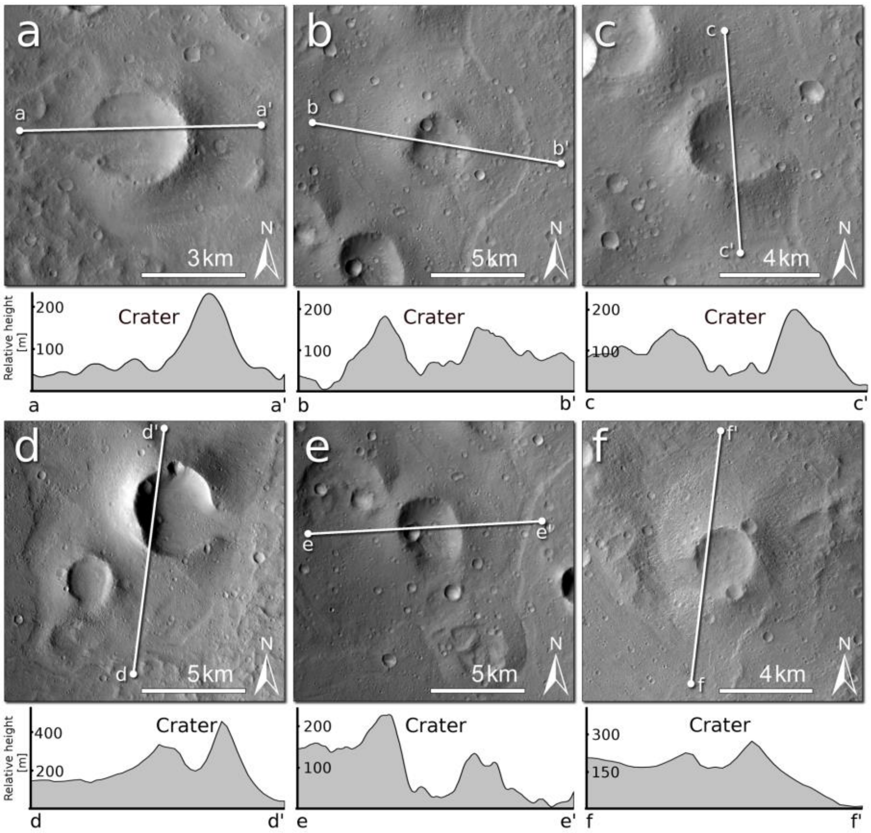

Figure 3.4: Details of several investigated cones in the NAC field. Note the wide central craters with floor elevations sometimes below surrounding surface level (image a = cone B15, CTX P17_007489_1967; image b = cone C28, CTX G01_018499_1961; image c = cone C27, CTX G01_018499_1961; d = cone B35, CTX P04_002452_1969; e = cone C30, CTX G01_018499_1961; f = cone B68, CTX B19_017075_1974). For locations see Tab A.1. in the Appendix.

3.4. Observations

3.4.1. Morphology

3.4.1.1. Cones

The study area containing the NAC displays ~170 pitted cones (on the basis of fewer and lower resolution images, Skinner and Tanaka (2007) had already identified ~85 cones) that are widely spread throughout the area of interest. Cones often coalesce and/or overlap each other and form chaotic clusters (Fig. 3.2a). They display texturally smooth flanks and typically wide central craters (Fig. 3.3). In many cases, the rims of the central craters are

Table 3.1. Measurement of mud volcanoes in Azerbaijan used as terrestrial analogues by Skinner and Tanaka (2007). Measurements based on Google Earth software (Google, 2011; Jarvis et al., 2008). Most mud volcanoes in Azerbaijan do not show any evidence of a deep crater on their top.

ID	**Location**	W_{CO} **[m]**	W_{CR} **[m]**	***Hco*** **[m]**	**Depth of crater [m]**	W_{CR}/W_{CO}	H_{CO}/W_{CR}	H_{CO}/W_{CO}
1	40.32°N, 49.43°E	2782	950	130	non	0.34	0.14	0.05
2	40.32°N, 49.31°E	3050	610	127	non	0.20	0.21	0.04
3	40.27°N, 49.30°E	1880	250	119	non	0.13	0.48	0.06
4	40.26°N, 49.31°E	2540	180	138	non	0.07	0.77	0.05
5	40.22°N, 49.35°E	3300	260	142	non	0.08	0.55	0.04
6	40.16°N, 49.30°E	4980	580	280	non	0.12	0.48	0.06
7	40.14°N, 49.38°E	4600	450	380	non	0.10	0.84	0.08
8	40.24°N, 49.51°E	6200	815	291	non	0.13	0.36	0.05
9	40.38°N, 49.61°E	3350	380	228	non	0.11	0.60	0.07
10	40.02°N, 49.37°E	3300	400	160	non	0.12	0.40	0.05
11	39.97°N, 49.36°E,	3170	210	198	non	0.07	0.94	0.06
12	39.92°N, 49.26°E	4450	750	200	non	0.17	0.27	0.04
13	40.11°N, 49.34°E	6030	430	233	non	0.07	0.54	0.04
14	40.01°N, 49.36°E	2020	438	52	19	0.22	0.12	0.03
15	40.15°N, 49.18°E	2200	336	165	non	0.15	0.49	0.08
17	40.01°N, 49.25°E	5250	320	281	non	0.06	0.88	0.05
Average	Location	3694	460	195	non	0.13	0.50	0.05

breached, and only segments of a full cone can be observed (Fig. 3.4). In several cases, lobate flows seem to have emanated from breached cones and moved gravitationally downslope (see Fig. 3.2a, marked with white arrows). Flank slopes of cones are mainly concave-upwards, but can turn to convex near the crater rims. High-resolution HRSC DEMs show that flank slopes are typically below 10°, but can reach up to about 20° in the steepest parts close to the crater rim (see Fig 3.2b). Crater floors may have elevations above or, interestingly, below the surrounding plains (Fig. 3.4; see Tab A.1. in the Appendix for cone heights and crater depths).

The study area is not fully covered by HRSC DEM, limiting the amount of cones suitable for morphometric study to a subset of ~50 cones. Based on detailed morphological measurements, the investigated cones are ~3 to 15 km wide (mean 7.8 km; based on measurements of 92 edifices) and ~30 to ~370 m high (mean ~120 m; based on measurements of 53 edifices), resulting in an average H_{CO}/W_{CO} ratio of 0.016 (based on measurements of 52 edifices). Many cones have well-developed central deep and wide craters (average depth 80 m; based on 52 edifices; average width 3.1 km, based on measurements of 92 edifices), resulting in a large W_{CR}/W_{CO} ratio of 0.42 (for more details about all measurements see Tab A.1. in the Appendix). These values differ in some aspects slightly from those obtained by Skinner and Tanaka (2007). They reported basal cone diameters in the range of 4 to 8 km (mean 6.4 km), with heights below 300 m (mean 230 m), cone slopes between 2° to 9° (mean ~6°). However, it is not clear how many cones were measured by Skinner and Tanaka (2007) and which cones were selected for detailed investigations. Therefore, no direct comparison with our data was possible.

Skinner and Tanaka (2007) used mud volcanoes in Azerbaijan as terrestrial analogs to the cones in the NAC region, but without details on their morphometry. Therefore, we also measured basic morphological parameters of cones in Azerbaijan (Tab. 3.1). The mud volcanoes have average basal widths and heights of ~4 km and ~200 m, respectively. They possess craters with an average diameter of 460 m, but since the crater depth could not be resolved in the available data, it is thought to be commonly less than 10 m. The W_{CR}/W_{CO} ratio is on average 0.13; the W_{CO}/W_{CR} and H_{CO}/W_{CO} ratios are 0.5 and 0.05, respectively. In comparison to the NAC, the mud volcanoes in Azerbaijan have a significantly lower W_{CR}/W_{CO} ratio (0.13 as compared to 0.42) and a higher H_{CO}/W_{CO} ratio (0.05 vs. 0.016). In relation to their diameters, therefore, they have smaller craters and larger heights than the NAC.

Table 3.2. Morphometric comparison of terrestrial and Martian landforms that resemble tuff cones and tuff rings.

Volcanic field or region	Type	N	W_{CO} [m]	W_{CR} [m]	H_{CO} [m]	Depth of crater [m]	W_{CR}/W_{CO}	H_{CO}/W_{CR}	H_{CO}/W_{CO}	Source
Azerbaijan	mud volcanoes	16	3694	460	195	none	0.13	0.50	0.05	This study[a]
Xalapa (Mexico)	scoria cones	57	698	214	90	none	0.32	0.42	0.13	Rodriguez et al., 2010
Ulysses Colles (Mars)	scoria cones	29	2300	620	230	none	0.28	0.37	0.13	Brož and Hauber, 2012
La Caldera de Montana Blanca (Lanzarote)	tuff cone	1	1555	1106	109	191	0.71	0.10	0.07	Kervyn et al., 2012
Crater Elegante (Mexico)	tuff ring	1	3350[a]	1600	50	200	0.48	0.03	0.01	Wohletz and Sheridan, 1983
Kilbourne Hole (New Mexico)	tuff ring	1	5600[a]	2500	50	80	0.45	0.02	0.01	Wohletz and Sheridan, 1983
Cone B39, Amenthes Region (Mars)	tuff ring (?)	1	7675	3185	227	220	0.41	0.07	0.03	This study[b]

[a]Based on Google Earth, this study.

[b]Based on HRSC DEM and CTX image.

In addition, we collected morphometric measurements of volcanic edifices on Mars and Earth published in earlier studies (Pike, 1978; Hasenaka and Carmichael, 1985b; Inbar and Risso, 2001; Hauber et al., 2009a; Brož and Hauber, 2012) and compared them to the corresponding results obtained for the NAC (Tab. 3.2). The underlying substrate

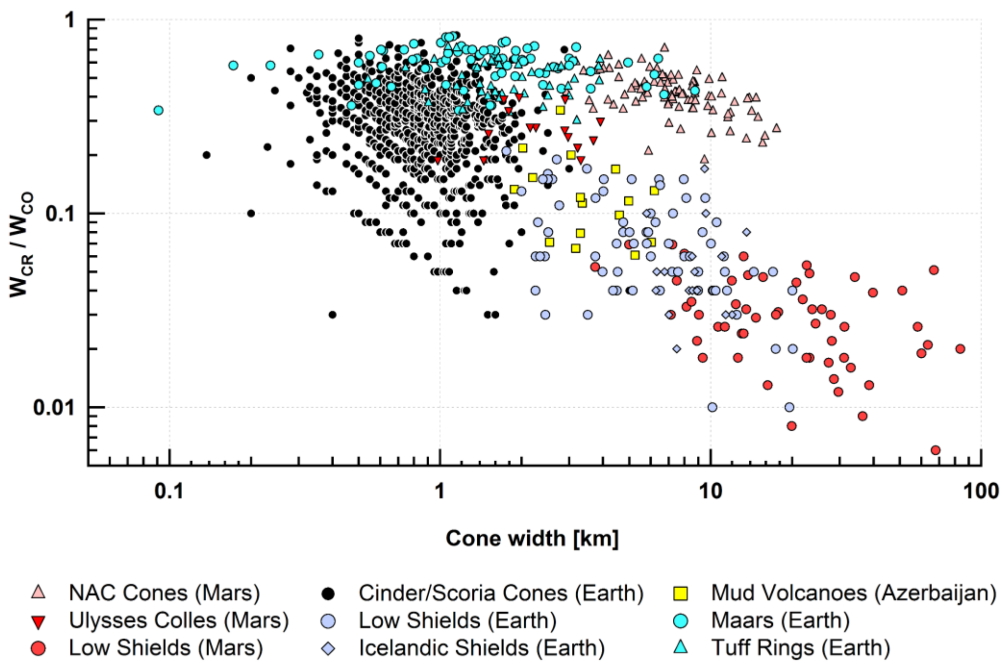

Figure 3.5: Morphology of pitted cones in Amenthes region in comparison with several other types of terrestrial and martian volcanic cones displayed in plot of the ratio W_{CR}/W_{CO} versus the basal width (W_{CO}). Data for investigated cones in Amenthes are from Tab A.1. in the Appendix, for terrestrial mud volcanoes in Azerbaijan from Table 3.1 based on Google Earth observations, values for martian low shield volcanoes from Hauber et al. (2009b), for martian scoria cones (Ulysses Colles) from Brož and Hauber (2012), for tuff rings and maars from Pike (1979) and for terrestrial scoria cones from Hasenaka and Carmichael (1985), Pike (1978) and Inbar and Risso (2001). Note the difference in position and therefore W_{CR}/W_{CO} ratio between the NAC pitted cones and mud volcanoes that were offered as analogues by Skinner and Tanaka (2007).

consists of plains material with a very low regional slope, and therefore the results should not be affected by slope effects (Tibaldi, 1995). A graphical representation of the W_{CR}/W_{CO} versus W_{CO} ratio, commonly used in remote sensing-based attempts to classify volcanic edifices (e.g., Pike, 1978; Hasenaka and Carmichael, 1985b; Inbar and Risso, 2001; Hauber et al., 2009a; Brož and Hauber, 2012), reveals that the NAC are clearly distinguished from other igneous volcanic edifices on Earth and Mars as well as from the mud volcanoes in Azerbaijan (Fig. 3.5). Specifically, the NAC have a larger cone width than terrestrial tuff rings and maars, although the W_{CR}/W_{CO} ratio is identical. Similarly, terrestrial scoria cones are smaller in their basal diameters, with a larger spread in their W_{CR}/W_{CO} ratios. Martian scoria cones (Brož and Hauber, 2012) are also smaller in diameter than the NAC. On the other hand, low volcanic shields built by effusive volcanism (i.e. lava flows) have comparable basal diameters, but are distinguished from the NAC by a significantly higher W_{CR}/W_{CO} ratio. Finally, the mud volcanoes in Azerbaijan are both smaller in diameter and have lower W_{CR}/W_{CO} ratios.

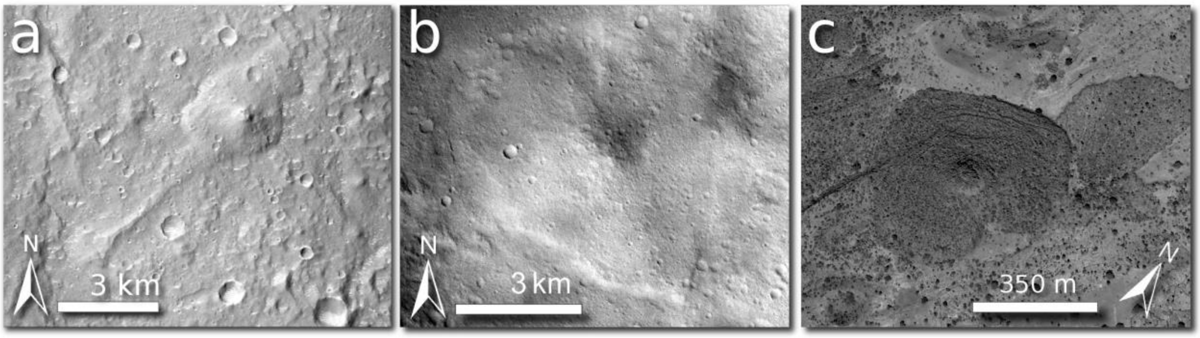

Figure 3.6: (a) Mound aligned along a NE-trending structural feature (at 16.5°N/112.79°E; detail of CTX image P21_009308_1962). (b) Example of mound in NAC field with small central hill surrounded by outgoing material (image centered at 16.85°N/103.52°E; detail of CTX image B11_013963_1975). (c) Morphologically analogous lava dome (e.g., Buisson and Merle, 2002). The image shows coulées in a volcanic field on the northern side of Tullu Moje in Ethiopia (image: GeoEye, obtained via GoogleEarth^{TM}).

3.4.1.2. Mounds

Another type of positive topographic landform in the NAC area is represented by small mounds with sub-circular to elliptical plan-form shapes. These features were also already described by Skinner and Tanaka (2007), who identified around 80 edifices predominantly distributed in the central and eastern part of the NAC study area, forming their own clusters independently of pitted cones. Some of them, however, are situated within the clusters of pitted cones. According to Skinner and Tanaka (2007), the basal diameters

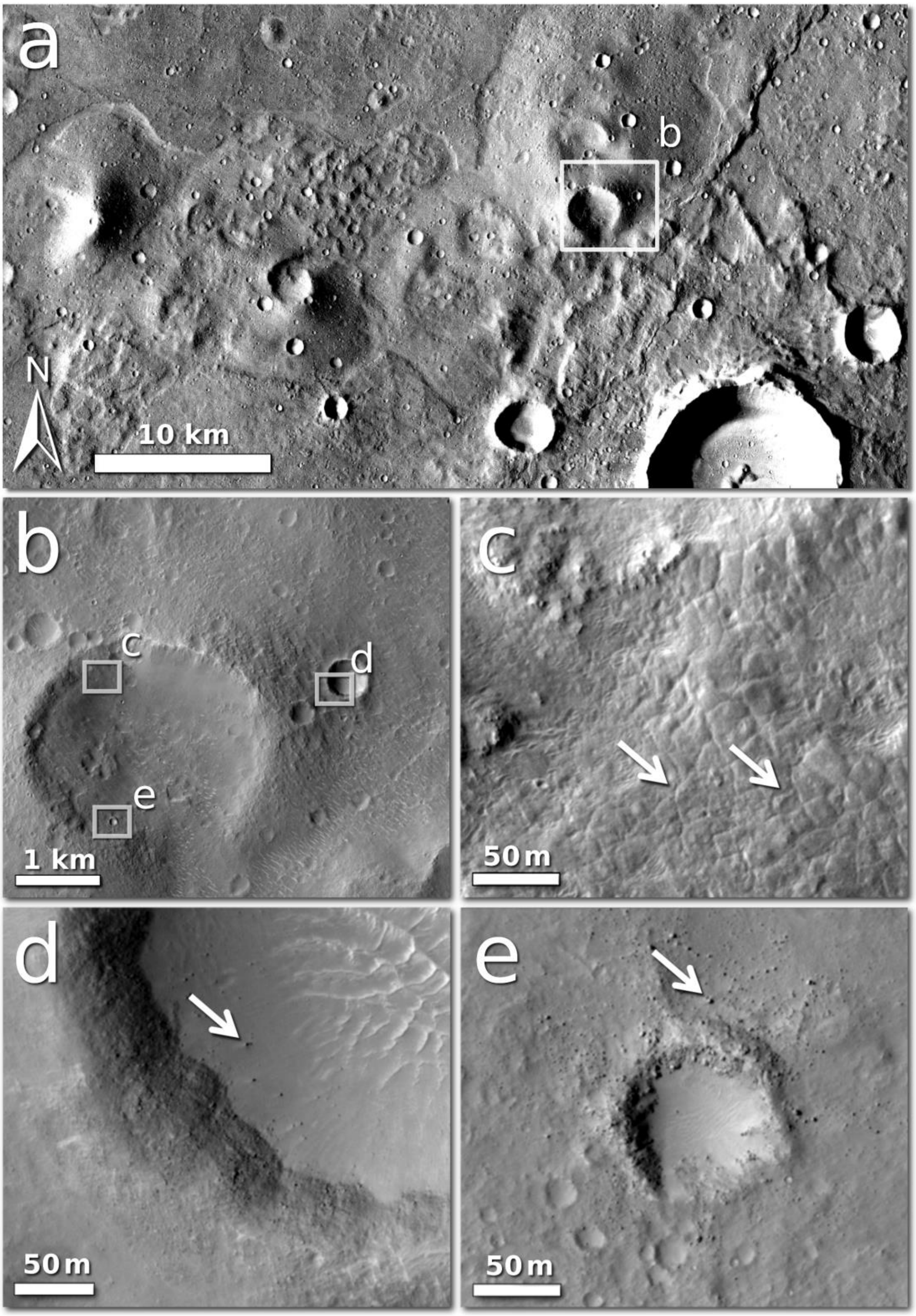

Figure 3.7: (a) Detail of one of the cluster of investigated NAC cones (16.59°N/104°E) (b) Pitted cone in the NAC field with well-developed central crater and steep inner flanks (detail of HiRISE image ESP_018776_1970; 16.65°N/104.15°E). (c) Detail of polygon-like pattern visible in some locations on the inner flank of the cone. (d and e) Large boulders associated with two impact craters, suggesting that the cone consists of consolidated material with some cohesive strength. The polygonal patterns may be related to a smooth mantling deposit, possibly suggesting a younger age than the main cone.

of these mounds range from 2 to 12 km (mean 4 km), with heights between 10 to 200 m (where measurable). Many mounds have small summit cones or pits a few hundred meters across near their centres. Mounds can be aligned along structural lineaments (Fig. 3.6a). As for the cones, it is not clear which mounds were selected by Skinner and Tanaka (2007) for measurements and where they are situated. Skinner and Tanaka (2007) also noted that mounds are often situated proximal or on top of wrinkle ridges or large arches. Our observations confirm the reports of Skinner and Tanaka (2007) on the distribution and general properties of these mounds, especially the existence of the small central hills (see Fig. 3.6b).

3.4.1.3. Other morphological features

In several cases we observed flow-like features emanating from the central vents of cones, which had already been identified and described by Skinner and Tanaka (2007). Elsewhere, small-scale morphological details (Fig. 3.7a) revealed by the inspection of HiRISE images do not provide unambiguous evidence for one or the other formation mechanism. The flanks of one pitted cone (Fig. 3.7b) are cut by fractures arranged in a polygonal pattern (Fig. 3.7c), which resembles desiccation cracks and would be consistent with tensional stresses acting on a drying mud surface (e.g., Konrad and Ayad, 1987). The fractured material may have formed much later as a mantling deposit, and may not be directly associated with the origin of the cone. On the other hand, small-scale impacts into the flanks of this cone excavated boulders with sizes of several meters from the fractured material (Figs. 3.7d and 3.7e). This may suggest a material with considerable cohesive strength, because it did not break apart during ejection and landing. The required strength may be easier explained by igneous volcanic material than by compacted mud.

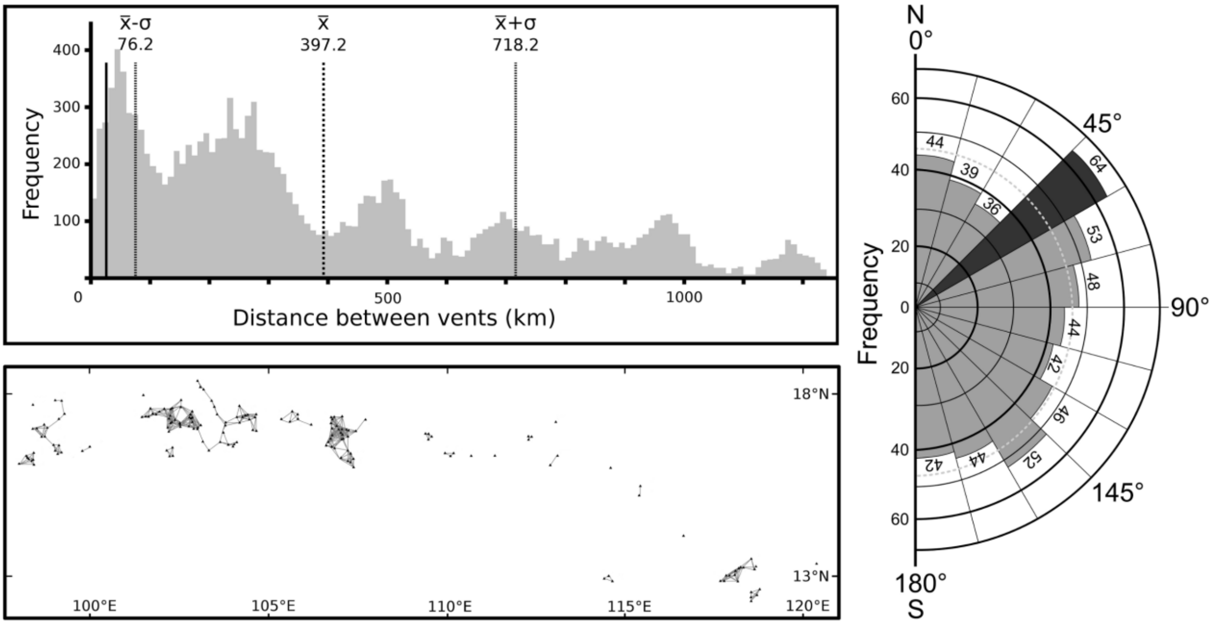

Figure 3.8: Results of the two-point azimuth technique. The upper left panel shows a frequency histogram of the lengths of lines connecting the NAC cones. Several peaks are visible due to the clustering of cones in the area of interest. The lower left panel shows the mapped distribution of lines with lengths ≤25.4 km, corresponding to the minimum significant distance (i.e., (x-1σ)/3) as defined by Cebriá et al. [2011]). Some NE-directed orientation of lineaments can be observed. The right part of the figure represents a rose diagram with 15°bin intervals, containing the numbers of lines per bin for lines ≤25.4 km long. The dotted line represents the arithmetic mean of frequency per bin (46.2, standard deviation 7.1), and the dark grey color marks the bin where frequency is higher than one standard deviation above the mean. This predominant orientation is in agreement with the lineaments observable in the mapped distribution.

3.4.1.4. Spatial alignment

We investigated the spatial alignment of cones in the study area to test if there is some structural control within the field which might explain its origin. We also tested if the cones are clustered by using the Average Nearest Neighbor tool in ArcGIS 10. If the ratio is <1, the points are statistically clustered; the closer to zero, the more clustered (Clark and Evans, 1954). Our results reveal a Nearest Neighbor Ratio of 0.44, which indicates clustering. Clustering of vents is a well-known characteristic for terrestrial fields of monogenetic volcanoes (e.g., Connor and Conway, 2000). However, clustering may also be a common characteristic of other landforms with similar topographic appearance (Burr et al., 2009a). For example, rootless cones on Mars can be clustered when certain conditions of lava emplacement are met (Hamilton et al., 2011), and clustering is common for vent populations inside the crater of mud volcanoes (Roberts et al., 2011) and even for mud volcanoes itself (Burr et al., 2009a).

The application of the two-point azimuth technique (Fig. 3.8) did not reveal any dominant trend (see the rose diagram in Fig. 3.8 for details) which would indicate significant structural control. However, a weak peak in orientation is visible between 45°N to 60°N. This is quite different from the trend of the Amenthes Fossae, which are oriented between 15°N

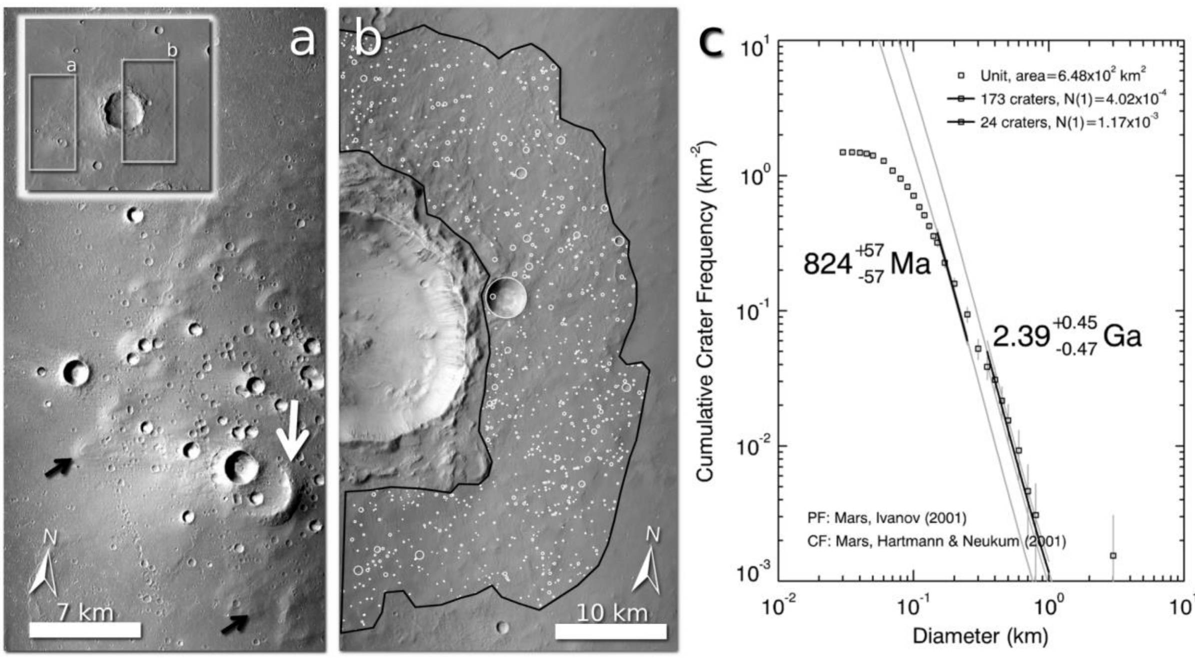

Figure 3.9: Absolute model age for ejecta of rampart crater embaying one of the NAC cones. See small inserted image for detail position. (a) Fluidized ejecta of this crater (marked by black arrows) are partly overlapping a small cluster of pitted cones (white arrow), suggesting that the crater is younger than these cones (detail of CTX image B19 016917 1976; centered at 17.84°N/99.09°E). Water ice had to be present in the subsurface at the time of rampart crater formation, and hence was likely present at the time of cones formation, too. (b) Selected area for crater counting with marked craters (detail of CTX image P18_008056_1980; centered at 18.12°N/99.79°E). (c) Crater size-frequency distribution of ejecta. The cumulative crater frequency curve indicates an absolute model age of ~2.39 Ga.

and 30°N. Therefore, we discard the possibility that the cone orientation would be controlled by a now hidden fracture set with the same orientation as the Amenthes Fossae. We were also not able to detect any link to the formation of Elysium Planitia.

The NAC area contains numerous wrinkle ridges, which are contractional tectonic features with positive relief, commonly interpreted as thrust-propagation folds (Mueller and Golombek, 2004). Most of them have an orientation between 10°N to 20°N in the area of pitted cones and mounds (Head et al., 2002). There is no obvious correlation between the results of the two-point azimuth technique and the dominant wrinkle ridge trend.

3.4.2. Chronology

Small clusters of pitted cones do not represent suitable areas for the determination crater size–frequency distributions because they are small, relatively steep (specifically in the crater areas) and typically heavily affected by secondary craters. All these factors would lead to considerable uncertainties of absolute model ages. Instead, we made use of the relative stratigraphy between the ejecta blankets of rampart craters and pitted cones. In some cases, rampart ejecta are partly overlapping or embaying pitted cones, indicating that at least some of these cones must be older than the associated impact. We choose one representative case where the stratigraphic relation is obvious and where the ejecta blanket does not exhibit clusters of secondary craters. We determined an absolute model age of ~2.4 Ga (see Fig. 3.9 for more details), which implies that at least some of the activity producing the pitted cones has to be older than that. The maximum age of the landforms is poorly constrained. We estimate a Hesperian or younger age for the modification of the plains that host the cones, an age that would be consistent with Skinner and Tanaka`s (2007) age estimate. The relatively smooth flanks of the cones, which do not show evidence of fluvial dissection, also point to a formation time after the main period of fluvial activity on Mars (Fassett and Head, 2008).

3.5. Discussion

3.5.1. Evaluation of arguments against igneous volcanism

In this section, we discuss the individual arguments used by Skinner and Tanaka (2007) to reject igneous volcanism. Skinner and Tanaka (2007) considered an igneous volcanic origin of the NAC unlikely because of (1) the large distance to known volcanic vents, (2) a lack of obvious structural control of dike-related eruptions, (3) the confinement to a specific latitude and elevation range, (4) the setting in a compressional tectonic regime, and (5) the pitted cones being part of a broader assemblage of landforms. We explore these arguments now to evaluate if they indeed disfavor an igneous origin. The distance to known volcanic vents may be smaller than previously thought, since localized spots of volcanism around the NAC region have by now being suggested by several subsequent studies (Lanz and Saric, 2009; Lanz et al., 2010; de Pablo and Pacifici, 2008; de Pablo and Caprarelli, 2010; Ghent et al., 2012). A lack of obvious structural control of dike-related eruptions, first qualitatively assumed by Skinner and Tanaka (2007), can now be confirmed quantitatively by our test applying the two-point azimuth method (Fig. 3.8). At least one mound (Fig. 3.6a) appears to be associated with a fissure that may represent an underlying dike, but this is not sufficient evidence for a general structural control. This lack of structural control, however, is not necessarily arguing in favor of mud volcanism, since mud volcanoes are themselves known to be controlled by tectonic structures (Roberts et al., 2011; Bonini, 2012). The lack of structural control, therefore, does not seem to put constraints on either of the two possible formation hypotheses, igneous volcanism or mud volcanism. The confinement to a specific latitude and elevation range might be explained by the location along the dichotomy boundary (see below).

The location of the cones in an area characterized by a compressional tectonic regime is not a strong argument against igneous volcanism, either. Although it has been widely held that volcanism can occur only in extensional tectonic regimes, favoring magma ascent along (sub)vertical fractures trending perpendicular to the least principal stress (σ_3), this axiom has been challenged. Based on an in situ investigation of El Reventador volcano in Ecuador, Tibaldi (2005) demonstrated that volcanism can also occur in compressional settings (the greatest principal stress σ_1 acting horizontally). He argued that magma can move upward in a compressional regime along vertical or subvertical planes which are oriented perpendicular to σ_2 (the direction of intermediate principal stress) and are related to reverse faulting associated to vertical σ_3. The assemblage of landforms is probably the strongest line of evidence provided by Skinner and Tanaka (2007) to support a formation of the NAC as mud volcanoes. However, at least one more of the landscape elements, the mounds, can also be explained by igneous volcanism (as it was done for mound-like structures elsewhere on Mars, cf., Rampey et al. [2007]). Morphologically analogous features are well known from terrestrial volcanic fields, whether basaltic or more silica-rich in composition. These structures are a type of lava domes called *coulées* (Fink and Anderson, 2000). They form by more viscous magma, effusively erupted onto the planetary surface and laterally spreading outwards. Once the rate of the supplying magma decreases, the gravitational acceleration causes the outer parts to further flow outward, even without sufficient lava supplies. The flow thickens into a dome-like shape at the periphery, but a low amount of ascending magma is still able to build a small hill above the vent (Hale et al., 2007). The result is a structure looking similar to the mounds in the Nephentes/Amenthes region (see Fig. 3.6c for comparison). Similar structures, termed 'festoon flows', were also observed on Venus (Head et al., 1992; Moore et al., 1992), where igneous volcanism is the only plausible explanation. We suggest, therefore, that the mounds can be interpreted as igneous volcanic mounds and are not unambiguous evidence for mud volcanism. This notion is further supported by the morphology of salt domes (e.g., see Fig. 1c in Neish et al., 2008), which can be more or less identical and suggests that there is a type of landforms that are all produced by the surface extrusion of relatively high-viscous material, prohibiting unambiguous interpretation. The steep-sided depressions with irregular outlines in plan view named Amenthes Cavi, attributed to collapse following mud reservoir depletion at depth by Skinner and Tanaka (2007), are not easily explained by the igneous volcanic scenario. They may be related to maars, and indeed maars such as Kilboune Hole and Hunt's Hole (New Mexico, USA) can display irregular shapes (cf., Ollier, 1967), but we are not able to further substantiate this hypothesis.

The flow-like features emanating from the central vents of some cones might be explained by an insufficient source of subsurface water to fully fragment the ascending magma, so lava could leak out effusively from the central crater and produce a lava flow (Basaltic Volcanism Study Project, 1981; Lorenz, 1986). However, the thick dust cover in the NAC region prevents identifying any surface flow structure of these hypothesized flows and distinguishing characteristic patterns of basaltic lava flows.

3.5.2. Morphometric comparison with terrestrial analogs

For comparison between different types of volcanoes, including mud volcanoes in Azerbaijan, we quantitatively measured parameters commonly used in the morphometric analyses of volcanic edifices (Tab. 3.2). A morphometric comparison of the cones in the study area with volcanic cones on Mars and Earth reveals that the NAC form a quite distinct group of edifices in a plot of W_{CR}/W_{CO} over W_{CO} (Fig. 3.5). As compared to terrestrial pyroclastic edifices (scoria cones, tuff cones, maars), the NAC have larger basal diameters, but their W_{CR}/W_{CO} ratio is basically identical. As compared to terrestrial effusive edifices (low basaltic lava shields), the NAC have a similar range of basal diameters, but a distinctly higher W_{CR}/W_{CO} ratio. Moreover, low shields produced by effusive eruptions have larger basal diameters on Mars than on Earth, but very similar W_{CR}/W_{CO} ratios. The same observation

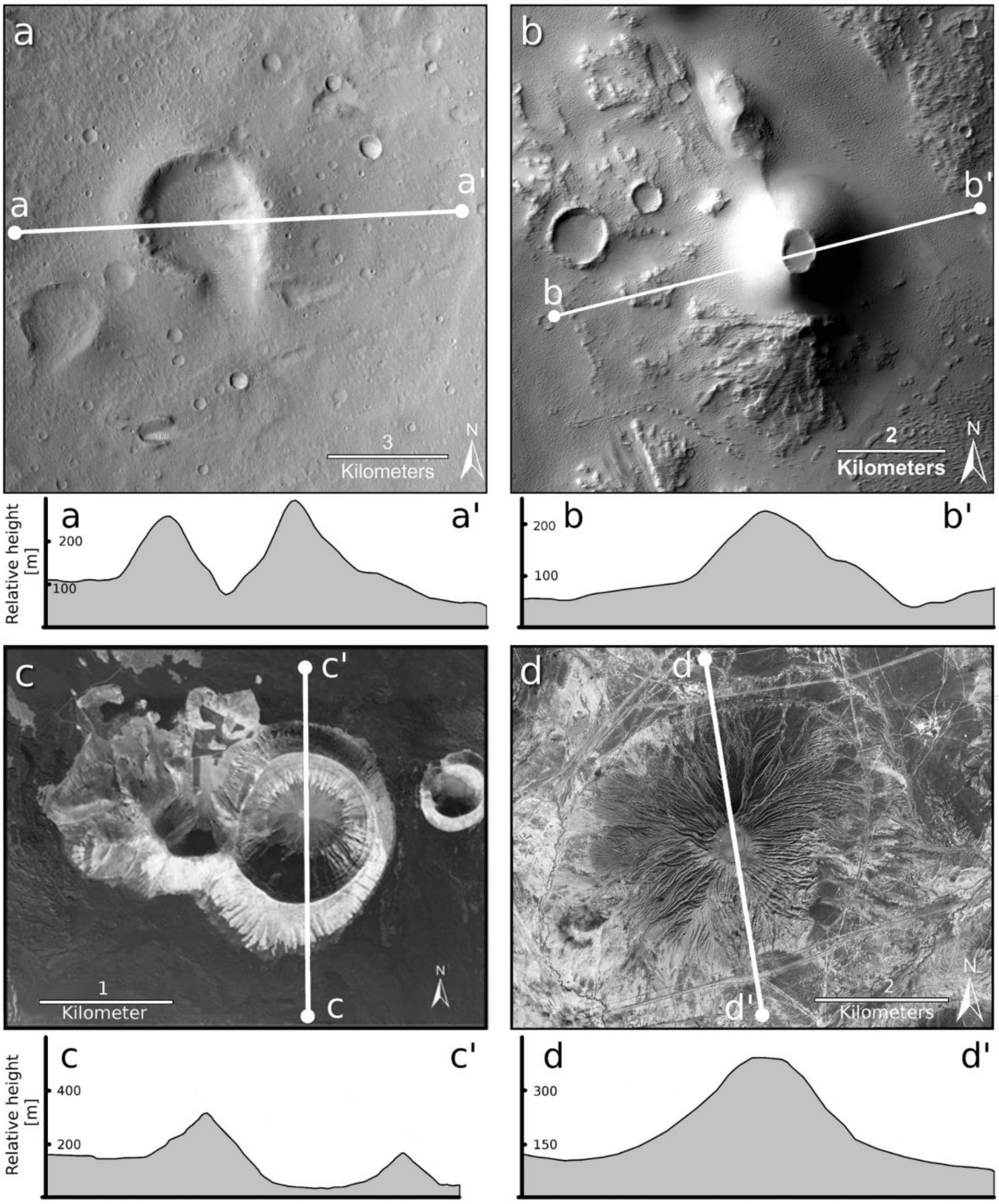

Figure 3.10: Different types of cones with topographic profiles. (a) Investigated pitted cone in the NAC field (detail of CTX image P17_007489_1967_ 16.32°N/102.32°E). (b) Steep-sided cone with associated flow-like structure in the Ulysses Colles scoria cone field in Tharsis, Mars (modified from Brož and Hauber (2012); detail of CTX image P21_009409_1858, 5.69°N/237.05°E). (c) Tuff ring Caldera Blanca, Lanzarote (modified from Kervyn et al. [2012]; Fig. 8d). (d) Mud volcano in Azerbaijan (image: Google Earth; 40.16°N/49.30°E) used by Skinner and Tanaka (2007) as terrestrial analogue for pitted cones in their study. Note the significant difference in cross-sectional shape between the pitted cone in the NAC field (a), displaying a crater with a depth equaling its height, and the Martian scoria cone b). Terrestrial mud volcanoes (d) typically lack a central deep and wide crater. On the other hand, morphological and topographical similarities are obvious between the NAC cone (a) and the terrestrial tuff ring (c).

seems to apply for scoria cones on Earth and Mars. Terrestrial mud volcanoes are different from the NAC both with respect to basal diameter and W_{CR}/W_{CO} ratio. It appears that for both explosive and effusive eruptions, edifices of the same type tend to be larger in diameter on Mars (i.e. shifted to the right in Fig. 3.5). The W_{CR}/W_{CO} ratios, however, seem to be very similar, despite predictions that explosive eruptions may produce larger relative crater sizes on Mars, due to the lower gravity and atmospheric pressure (Wilson and Head, 1994). Instead, the same W_{CR}/W_{CO} ratios on Mars and Earth may suggest that this ratio is perhaps independent of gravity and atmospheric pressure, as assumed by Wood (1979b) and confirmed by measurements of the scoria cone field, Ulysses Colles, on Tharsis (Brož and Hauber, 2012). In an attempt to explain this surprising fact, Wood (1979b) assumed that the higher ejection velocities and the wider dispersal of pyroclasts equally affect crater rims and more distal deposits (W_{CO}).

Importantly, the crater floors of many cones (13 out of 47 measured cones) in the NAC region have elevations at or below the surrounding plains (i.e., the preexisting ground level; see Tab A.1. in the Appendix) (Figs. 3.4b, c, e), and the craters are surrounded by rims up to several dozen meters high. This does not seem to be consistent with the morphometry of terrestrial mud volcanoes. Kholodov (2002) summarized several different types of mud volcanoes on Earth, none of them having similar relief and size as observed with the NAC. For example, mud volcanoes forming a depressed syncline on the Kerch Peninsula in Ukraine have crater levels below the surrounding plains, similar to the NAC pitted cones, but they are lacking cones around vents, high rims surrounding these depressions, and they are surrounded by ring faults. On the other hand, mud volcanoes in Azerbaijan, offered as terrestrial analogs to the NAC by Skinner and Tanaka (2007), display conical shapes with heights of up to several hundred meters, again similar to the NAC, but without deeply excavated craters (for more details see Fig. 2 in Kholodov [2002], or Tab. 3.1). Deep craters situated on top of cones are not a common feature of terrestrial mud volcanoes in Azerbaijan, and it appears that the morphologies of the NAC and the previously suggested analogs in Azerbaijan are inconsistent (see Figs. 3.4 and 3.10).

Another observation that appears to be possibly inconsistent with a mud volcano shape is a low cone with a double or nested crater (Fig. 3.3c). The cone is situated in a cluster of pitted cones and some lobate flows. Based on relative stratigraphy, a similar age as the other cones in this cluster is inferred. This atypical cone is about 3.5 km wide and 60 m high, with clearly recognizable rims of the inner and outer crater in profiles. A double or nested crater morphology was already ascribed to martian rootless cones (Noguchi and Kurita, 2011) as a result of lava/water interaction; however the described possible rootless cones was smaller by on order of magnitude (about 130 m in diameter). On the other hand, similar structures with similar dimensions are known from Earth as a result of repeated phreatomagmatic activity formed by magma/water interaction. A characteristic example is the tuff ring Tagus Cove on Isabela Island (Galápagos archipelago, Ecuador), and another well-known feature with nested circular features in plan view is the maar, Split Butte, in the Snake River Plain, which consists of a tephra ring and the remnants of a lava lake (Womer et al., 1980). It has to be noted, though, that nested craters have also been observed on terrestrial mud volcanoes (e.g., Figs. 6e and f in Skinner and Mazzini [2009]).

The HiRISE observation did not help to differentiate between an igneous versus a mud volcanic origin of the NAC cones, because a thick dust cover hides potentially diagnostic surface textures. In the case of boulders surrounding small impact craters, it is impossible to distinguish if they represent mud breccia or welded volcanic ash and/or volcanic bombs. Despite the fact that mud volcanoes on Earth are mainly formed by fine grained material (Manga and Bonini, 2012), they may be able to carry larger clasts forming mud breccias (Pondrelli et al., 2011).

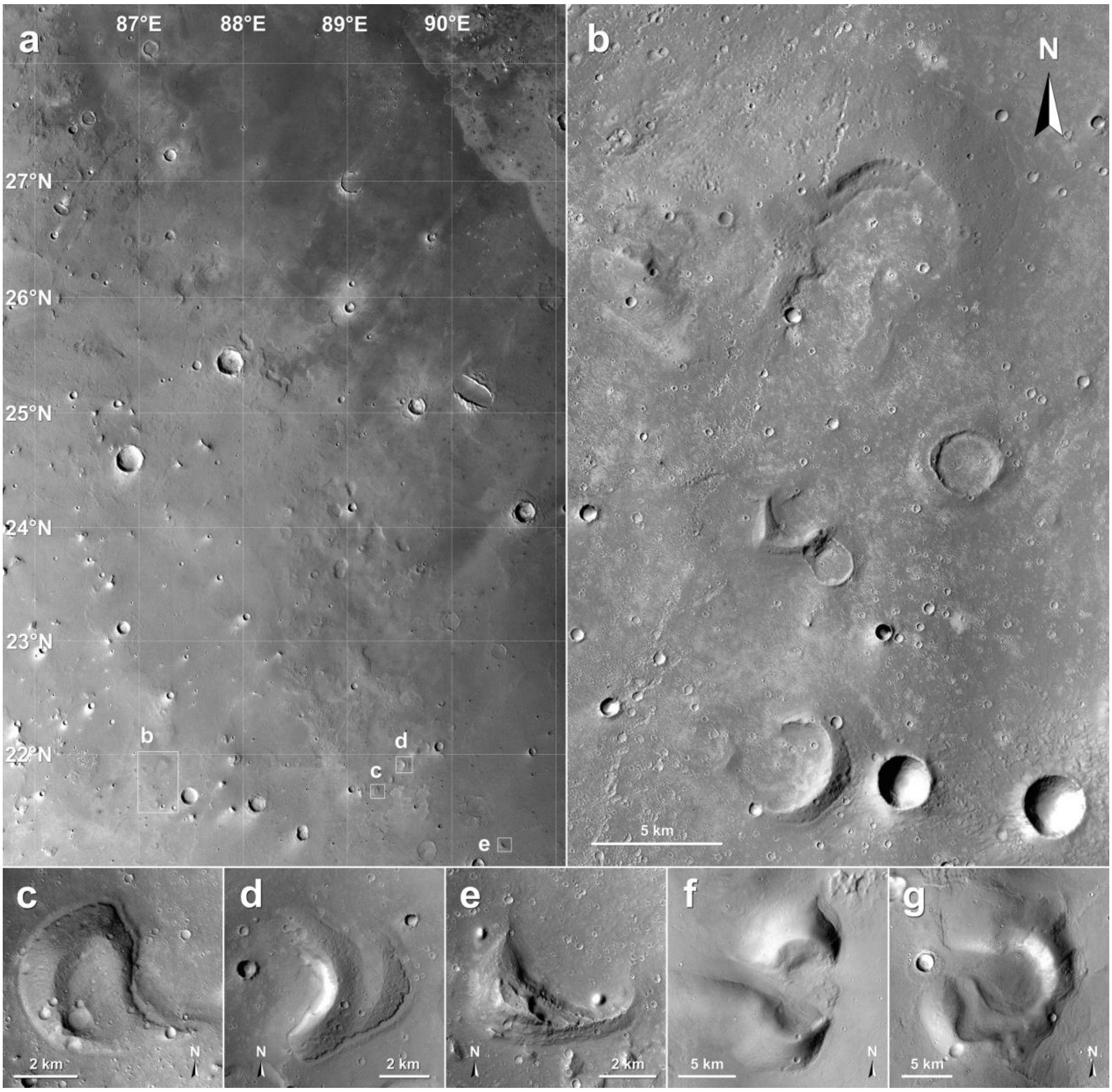

Figure 3.11. Pitted cones in the Arena Colles region. (a) Context image. Note the poor visibility of the cones, which are spread over the entire image. Letters b-e mark locations of panels b-e. HRSC image mosaic (for location see Fig. 3.1). (b) Group of cones with different sizes and rim appearance. While the rim of the cone in the middle right of the image is complete, the rims of all other cones are breached or only partly preserved (CTX image mosaic; see (a) for location). (c) Breached cone (detail of CTX image G09_021572_2026; see (a) for location). (d) Remnant of (breached?) cone (detail of CTX image B20_017392_2009; see (a) for location). (e) Layered cone remnant (detail of CTX image B18_016825_2018; see (a) for location). (f) Breached cone at 31.87°N/82.93°E (mosaic of CTX images G19_025594_2108 and P13_006158_2112). (g) Nested cones centered at 30.77°N/82.94°E (mosaic of CTX images G19_025594_2108 and P13_006158_2112). Note that panels f and g are located outside the area shown in panel a.

We conclude that several morphometric aspects of the available data are more consistent with an igneous volcanic origin than with a mud volcano scenario, without ruling out the latter. In the next sections, we discuss the factors that would have been critical in an igneous volcanic model to explain the formation of the pitted cones and mounds.

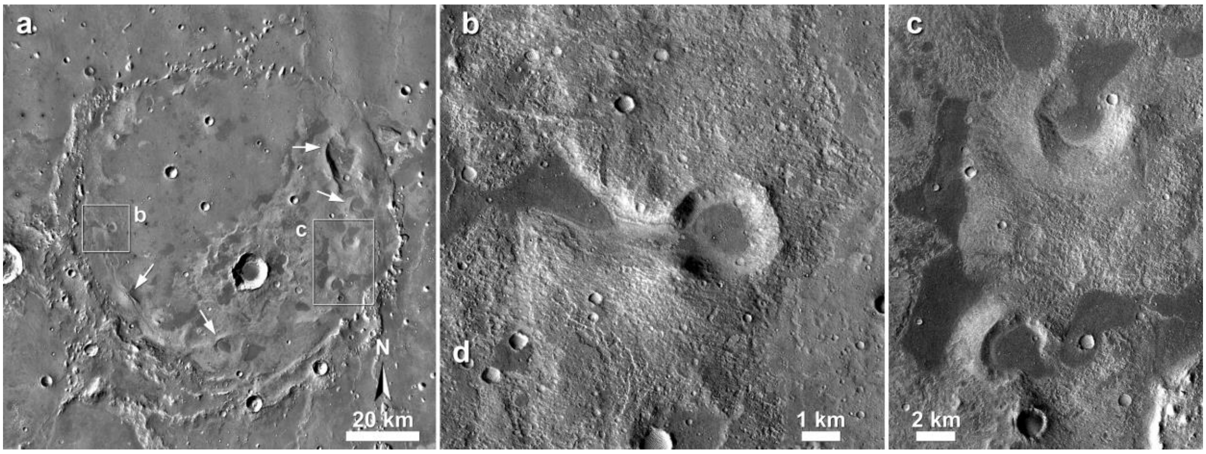

Figure 3.12: Cones of similar morphology in Xanthe Terra. (a) Lederberg crater (center 13.01°N, 314.08°E), a 90 km wide impact crater, is situated at the southern margin of Chryse Planitia at the dichotomy boundary. Along the inner crater rim, a series of small conical positive landforms with deep and wide craters can be observed (CTX image mosaic). (b) and (c) Examples of breached cones with morphology similar to the NAC cones. White arrows in panel (a) point to other examples.

3.5.3. Other regions with morphologically similar landforms

To find out whether the NAC represent a unique class of landforms on Mars we searched for similar landforms in other areas near the dichotomy boundary. A field with cones of identical morphology was identified in the Arena Colles region north of Isidis Planitia (Fig. 3.11). To our knowledge, it has never been mentioned in the literature before. The general context of this field seems to be comparable to that of the NAC, because it is also located on a topographical bench at the margin of the Utopia basin, and at the dichotomy boundary (Fig. 3.1). Since this cone field is similar in morphology and in the geotectonic context, it could also be explained by the scenario of Skinner and Tanaka (2007), in particular by their annular space and basin setting, and, therefore, does not provide additional arguments for one or the other formation hypothesis.

Other similar cones were found in Xanthe Terra, at the southern margin of the ancient impact basin, Chryse (Fig. 3.12). Xanthe Terra is part of the heavily cratered highlands dominated by Noachian terrain (Rotto and Tanaka, 1995). It is surrounded by younger lava plains of Lunae Planum in the west, by Ophir Planum in the south, by chaotic terrain in the east, and by Chryse Planitia in the north. The area of interest is the ~90 km-diameter impact crater, Lederberg, close to the dichotomy boundary and centered at 13.01°N/314.08°E. As the NAC and Arena Colles cone fields, Lederberg lies close to the dichotomy boundary (Scott and Tanaka, 1986) on the southern edge of the ancient impact basin, Chryse (Schultz et al., 1982). In a regional context this area displays evidence of past fluvial (outflow channels, river beds, river deltas etc.), volcanic and glacial activity (Hauber et al., 2009b, 2012; Martínez-Alonso et al., 2011). A wide range of landforms caused by aqueous activity, including rampart craters, offers a plausible prerequisite for hydrovolcanic interactions due to the occurrence of subsurface water ice. Lederberg crater itself is filled with smooth material and hosts several cones with partly breached rims, which are aligned on the floor along its interior wall. These cones do not resemble impact craters, and their floors are at the same level with their surroundings. Based on the morphological similarity of these cones and the NAC cones, we suggest that the cones in Lederberg crater were also formed by a similar genesis, which we interpret to be possibly phreatomagmatic. Since the local tectonic environment of Lederberg crater is different from that of the NAC field, the formation of this type of cones may not require a unique geotectonic setting.

3.5.4. Hydrovolcanism

Hydrovolcanism is a common phenomenon in all environments on Earth where water is mixing with magma (Sheridan and Wohletz, 1983). The type of landforms which occurs depends on whether surges contain superheated steam media (in the case of tuff rings) or condensing steam media (tuff cones) (Sheridan and Wohletz, 1983). Hydrovolcanic landforms are second in abundance on Earth to scoria cones only (Vespermann and Schmincke, 2000), and they represent the most common landforms created by explosive hydromagmatic volcanism (Wohletz and Sheridan, 1983). Phreatomagmatic eruptions can occur with magma of various compositions, both basaltic and more evolved (Wohletz and McQueen, 1984a; 1984b). All prerequisites for phreatomagmatic eruptions are encountered on Mars: (basaltic) volcanism and crustal water/ice, both widely spread around the planet in space and time (Grott et al., 2013; Lasue et al., 2013). Hence, we may reasonably expect that hydrovolcanism operated on Mars. However, direct observations of phreatomagmatic landforms on Mars (especially tuff rings, tuff cones and maars) are sparse and published reports are not very detailed (Wilson and Mouginis-Mark, 2003a; 2003b; Wilson and Head, 2004, Keszthelyi et al., 2010).

Terrestrial tuff rings and tuff cones are generally small (less than 5 km in diameter) monogenetic volcanoes composed of tuff that results from hydrovolcanic (hydro-magmatic) explosions. They display well-developed, relatively large craters (large W_{CR}/W_{CO} ratio), and the crater floors of tuff rings and tuff cones extend down to and even below the level of the preexisting surface level, respectively (Wohletz and Sheridan, 1983; Leach, 2011). Tuff rings have normally low topographic profiles and gentle external slopes ranging from 2° to 15° (Sheridan and Wohletz, 1983), and they are underlain by shallow diatremes (Lorenz, 1986; White and Ross, 2011). On the other hand, tuff cones have high profiles with steep outer slopes (Wohletz and Sheridan, 1983) ranging from 25° to 30° (Sheridan and Wohletz, 1983) without underlying diatremes (White and Ross, 2011). Both classes of tuff edifices have generally asymmetric rims caused by wind moving ash in downwind direction (Farrand et al., 2005), or by a change of vent location and multiple vents with different production rates

(Sheridan and Wohletz, 1983). Maars are volcanic depressions that have typical widths of several hundred meters. They are underlain by deep diatremes and lie below the level of the surrounding unit (Lorenz, 1986).

In general, the observed morphology, shape and size of the pitted cones in our study area are similar to those of terrestrial tuff cones or rings, except for a larger absolute basal diameter. We note, however, that cone morphometry alone is not a reliable indicator for eruptive conditions. The results can be affected by difficulties in determining the correct basal perimeter of the edifice (Grosse et al., 2012), by slope angle variations within a single cone (Kereszturi et al., 2012), by the effects of cone burial by later deposits (Favalli et al., 2009b), and by other factors such as the applied methodology, the local setting, time-dependent eruption conditions, and material properties (Kervyn et al., 2012). Although the clear distinction of the NAC cones from other edifices (Fig. 3.5) appears to be a robust result, we interpret that these features may not all be tuff cones or tuff rings. Instead, it is typical on Earth that volcanic fields are formed by several types of monogenetic volcanoes overlapping each other. Wohletz and Sheridan (1983) noted that a dry environment would contain scoria cones, whereas tuff rings may occur in places with abundant ground water source, and tuff cone formation would be favored by a shallow body of standing water. Moreover, even an individual cone can change its eruption style from an initially phreatomagmatic stage to a final Strombolian activity (Clarke et al., 2009). Because of this variability it is reasonable to expect that some of investigated NAC might represent scoria cones formed by magma degassing, and therefore it would be too simplistic to ascribe all NAC edifices to a single eruption type. More likely, we interpret that the history of NAC formation was diverse and several volcanic processes took place (degassing and water/magma interaction) and overlap each other. In fact, the mounds would represent a more effusive type of eruption if our interpretation is correct. Nevertheless, we suggest that the dominant volcanic process forming the NAC field was hydrovolcanism, producing cones by phreatomagmatic eruptions.

3.5.5. Origin of magmatism

We now explore if there are plausible geodynamic scenarios that would explain the occurrence of igneous volcanism in the study area. The cones occur within an elongated zone of ~1500 km length and 200 km width that is oriented roughly parallel to the highland-lowland scarp. Together with other hypothesized volcanic centres (Lanz et al., 2010; Ghent et al., 2012; de Pablo and Pacifici, 2008; de Pablo and Caprarelli, 2010), this zone would be part of a wide zone of magmatic activity that spans from the Elysium bulge in the east to Isidis Planitia to the west (Fig. 3.1). It has to be noted, however, that alternative interpretations exist for several of these localized volcanic centres (e.g., for the pitted cones in Isidis Planitia), so without further confirmation they only provide weak support for an igneous scenario.

Modeling by McGovern and Litherland (2011) shows that loading stresses due to the magmatic infilling of large (compared to the planetary radius) impact basins can induce at basin margins a favorable combination of extensional membrane stresses and upward-increasing extensional flexural stresses (positive 'tectonic stress gradient'; [Rubin, 1995]). Such conditions can create favorable environments for magma ascent in annular zones around basins that can drive the ascent of magma in dikes directly from mantle melt zones to the surface (McGovern et al., 2011). The annular ring basins inferred by Skinner and Tanaka (2007) would be consistent with such a scenario as well as with the mud volcano hypothesis. Indeed, the studied cones are located within the Utopia-circumferential zones of maximum likelihood of magma ascent (McGovern et al., 2011), and the densest population of cones (in the western part of the study area) is situated near the overlap of this zone and the corresponding zone concentric to the Isidis basin. The location of a newly detected cone field in the Arena Colles region (see below) also fits to the same zone circumferential to Utopia (Fig. 3.1). It appears possible; therefore, that igneous volcanism was focused in the study area by basin-related effects as described by McGovern and Litherland (2011).

Igneous volcanism may also be explained by the location of the NAC along the dichotomy boundary. The bench or boundary plain on which the pitted cones are located lies along a zone of extension that parallels the topographic scarp of the dichotomy boundary between eastern Arabia and Cimmeria Terrae (Watters, 2003) (Fig. 3.1), which also marks the transition of thicker crust in the south to thinner crust in the north (Zuber et al., 2000). Lower-crustal flow from thick crust in the south towards thinner crust in the north may be able to induce extension (favorable for magma ascent) just north of the highland-lowland scarp (Nimmo, 2005). It has also been speculated (cf., Zuber et al., 2000) that thick accumulations of volcanic material could explain the positive Bouguer anomalies along this part of the dichotomy boundary (Neumann et al., 2004). Hence, past volcanism seems to be plausible at the study site, and indeed the relatively high dielectric constant of the substrate at the study area (Mouginot et al., 2012) is consistent with this possibility.

If our interpretation of explosive (hydro)volcanism in the NAC field and in Arena Colles is true, some implications for the global view on martian magmatism may be inferred. The style of volcanism on Mars appears to be diverse and includes hydromagmatism, as we may expect on a volcanically active planet with widespread evidence for water and ice in the subsurface.

The study area containing the NAC field is located west of the light-toned layered Medusae Fossae Formation (MFF), which consists of a material that is either ice-rich or, if dry, has a low density (Watters et al., 2007) and would be consistent with a volcanic airfall deposit (e.g., Bradley et al., 2002). It has been suggested that the large volcano, Apollinaris Patera, might be the source of the dispersed volcanic clasts that build the MFF (Kerber et al., 2012), but the volume of the MFF seems large compared to Apollinaris Patera. The dispersal of pyroclasts from the NAC field in an ESE direction (assuming a speculative dominant WNW wind direction; Fig. 3.1) may have contributed to the deposition of the MFF and would lessen the volume problem.

3.8. Conclusions

1) Pitted cones along the southern margin of Utopia Planitia share morphological similarities to terrestrial tuff cones and tuff rings. A hydrovolcanic origin of these cones is consistent with the observed morphology and the regional geologic setting. Mounds associated with the cones resemble terrestrial lava domes (coulées). Together, we interpreted these landforms as a volcanic field.

2) Another field with identical landforms was newly detected north of Isidis Planitia in the Arena Colles region, also along the margin of Utopia Planitia. Several cones in an impact crater Lederberg in Xanthe Terra share the same morphological characteristics. These new observations of this type of pitted cones suggest that their formation may not require unique tectonic or environmental conditions.

3) While the consistent mud volcano-scenario of (Skinner and Tanaka, 2007) cannot be ruled out, several points used previously against an igneous volcanic origin of these landforms have been reevaluated. The geotectonic setting and the growing evidence for additional volcanic centres in the wider region would be consistent with igneous volcanism. The general lack of obvious structural control is not a conclusive argument, as structural control would be expected for both igneous and mud volcanism. The spatial association with Amenthes Cavi, as postulated by *Skinner and Tanaka* (2007), however, is not explained by an igneous volcanic scenario.

4) If our interpretations are correct, they would add to the morphologic diversity of martian volcanic surface features. To our knowledge, however, the total number of similar landforms on Mars is low. Given that subsurface water was likely widespread in martian history, this prompts the question as to why hydrovolcanic landforms are not observed more frequently. One possible answer is that phreatomagmatic eruptions were indeed more frequent in the past, but much of their traces have now been eroded, and the fields reported here are among the latest to be formed.

5) If mud volcanism is the process of NAC formation, then the process varies from terrestrial mud volcanism in producing morphologically varied forms and warrants further study. More morphometric work is needed for terrestrial mud volcanoes, including mud volcanoes in areas other than Azerbaijan, so that we can more accurately assess the comparison with morphologically similar landforms on Mars.

Acknowledgements

We appreciate the efforts of the instrument teams (MOLA, THEMIS, HRSC, CTX, HiRISE) who acquired and archived the data used in our investigation. Especially, we would like to thank W. Brent Garry for his constructive comments on a previous version of this manuscript, and the HiRISE team which provided new interesting observations on our requests. These data greatly improved our study. Petr Brož was a visiting research student at the Open University, UK, when this research was undertaken. This study was supported by the Grant No. 580313 from the Grant Agency of Charles University in Prague (GAUK) and by the Helmholtz Association through the research alliance 'Planetary Evolution and Life'.

4. Evidence for Amazonian highly viscous lavas in the southern highlands on Mars

Petr Brož[1,2], Ernst Hauber[3], Thomas Platz[4,5] and Matt Balme[5,6]

[1]*Institute of Geophysics ASCR, v.v.i., Prague, Czech Republic*
[2]*Institute of Petrology and Structural Geology, Faculty of Science, Charles University, Prague, Czech Republic*
[3]*Institute of Planetary Research, DLR, Berlin, Germany*
[4]*Institute of Geological Sciences, Freie Universität Berlin, Berlin, Germany*
[5]*Planetary Science Institute, United States*
[6]*CEPSAR, Open University, Milton Keynes, United Kingdom*

Status: Published in Earth and Planetary Science Letters 415,

doi: 10.1016/j.epsl.2015.01.033.

4.0. Abstract

We have identified small-scale volcanic edifices, two cones and three domes with associated flows, within Terra Sirenum, a region situated in the martian southern highlands. Based on thermal, morphological, and morphometrical properties, and the determination of absolute model ages, we conclude that these features were formed by volcanic activity of viscous lavas in the mid-Amazonian epoch, relatively recently in martian history. If our hypothesis is correct, this small volcanic field represents rare evidence of young volcanic activity in the martian highlands in which martian equivalents of terrestrial lava domes and coulées might be present. On Earth, such landforms are usually formed by highly viscous evolved lavas, i.e., andesitic to rhyolitic, for which observational evidence is sparse on Mars. Hence, this field might be one of only a few where martian evolved lavas might be investigated in detail.

4.1. Introduction and background

Volcanism was globally widespread on Mars in the early history of the planet, but became focused with ongoing evolution on two main volcanic provinces in the Tharsis and Elysium regions (Werner, 2009; Robbins et al., 2011; Platz and Michael, 2011; Xiao et al., 2012; Grott et al., 2013). Except for the widespread Hesperian ridged plains (Greeley and Spudis, 1981), and some isolated centres (e.g., Tyrrhenus and Hadriacus Montes (Williams et al., 2009; Robbins et al., 2011), evidence for post-Noachian (<3.7 Ga) volcanism, and in particular for individual volcanic edifices is rare in the martian highlands. It is generally thought that highland volcanism occurred early in Mars' history and stopped not later than ~1 Gyr after planet formation (Williams et al., 2009; Xiao et al., 2012).

The youngest volcanic activity in the Tharsis and Elysium volcanic provinces is characterized by the effusion of low-viscosity basaltic lavas (Vaucher et al., 2009a; Hauber et al., 2011; Platz and Michael, 2011). It was long thought that more evolved (i.e., andesitic to rhyolitic) magma compositions are rare on Mars (Bandfield et al., 2004; Christensen et al., 2005), in contrast to Earth, where these lavas are common (Rogers and Hawkesworth, 2000). More recently, however, based on orbital spectroscopic observations and rover-based in situ measurements, several studies indicate that evolved magmas may have been generated on Mars (Skok et al., 2010; Wray et al., 2013; Stolper et al., 2013; Meslin et al., 2013, Sautter et al., 2014), but there are only few direct observations of kilometer-scale edifices that may be composed of evolved magmas (Rampey et al., 2007, Skok et al., 2010).

On Earth, highly viscous and evolved lavas can produce specific types of small-scale volcanic landforms such as magmatic cryptodomes or extrusive lava domes that are (qualitatively) diagnostic of rheology, and from which composition might be inferred (Fink and Griffiths, 1998). Because of their specific morphology and morphometry, these edifices may be recognized by remote sensing techniques (e.g., Rampey et al., 2007;

Neish et al., 2008). The most promising martian edifices are individual hills in the western Arcadia region which may represent possible crypto- or lava domes (Rampey et al., 2007). Conversely, their spectral absorption characteristics are consistent with the presence of olivine and high-Ca pyroxene, commonly augite, suggesting a basaltic composition, but the possibility that these domes might be more silica-rich (basaltic-andesitic or andesite in composition) was not definitely ruled out (Farrand et al., 2011).

In this study we focus on two cones with associated flow apron features, and three domical structures surrounded by flows, which are all located in the southern highlands. They might represent rare evidences of martian equivalents for terrestrial lava domes and coulées caused by highly viscous (i.e., andesitic to rhyolitic) lavas.

4.2. Data and methods

We used data sets acquired by several cameras on various orbital platforms: Context Camera (CTX; 5–6 m/pixel; Malin et al., 2007), High Resolution Stereo Camera (HRSC; 10-20 m/pixel; Jaumann et al., 2007), High Resolution Imaging Science Experiment (HiRISE; ~30 cm/pixel, McEwen et al., 2007) and THEMIS-IR (day and night; ~100 m/pixel; Christensen et al., 2004). CTX data were processed using the USGS Astrogeology image processing software 'ISIS 3' (Integrated System for Imagers and Spectrometers) and HRSC images using VICAR (Video Imaging Communication And Retrieval) software.

Topographic information was derived from Mars Orbiter Laser Altimeter (MOLA; Zuber et al., 1992; Smith et al., 2001) gridded Digital Elevation Models (DEMs) with 128 pixel/degree resolution (~463 m/pixel) for regional context, and from HRSC DEMs for local scales. HRSC DEMs are interpolated from 3D points with an average intersection error of 12.6 m and most have a regular grid spacing of 50 to 100 m (Scholten et al., 2005;

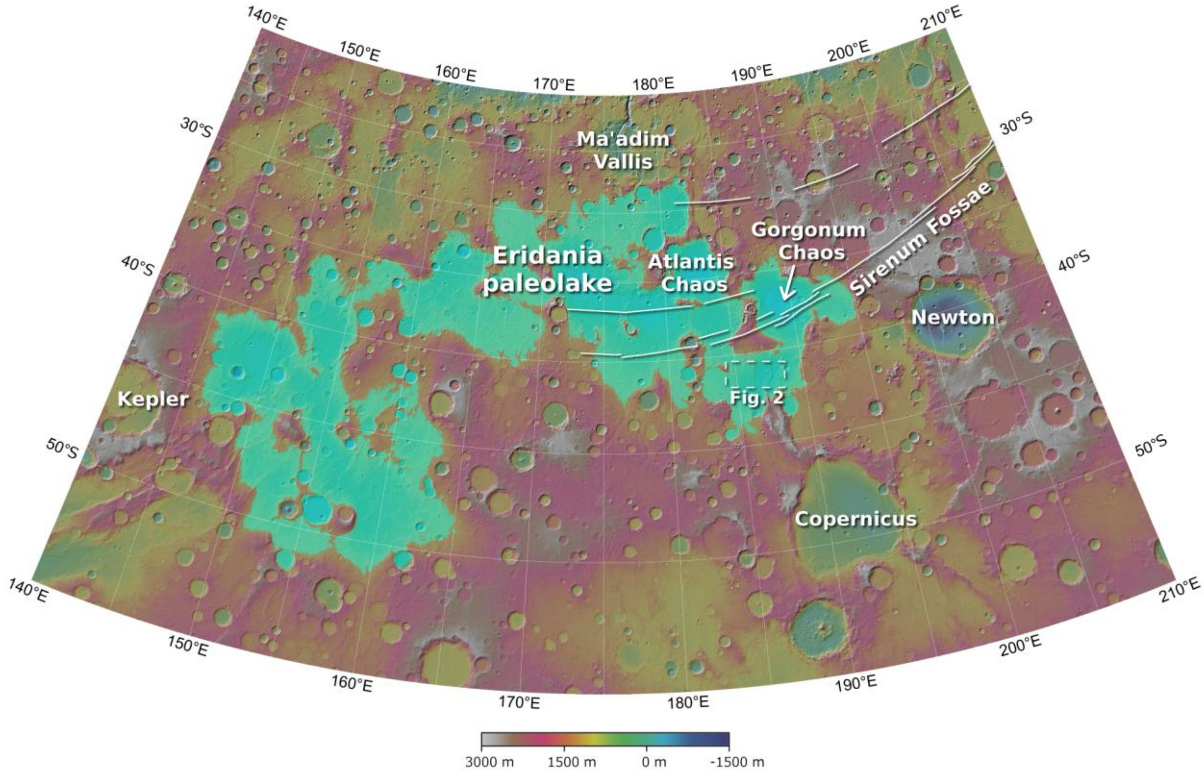

Figure 4.1: Regional map of part of the southern hemisphere on Mars. The cyan colour delineates the extent of the proposed Eridania Lake based on the 1100 m contour. Position of investigated area is marked by dashed box and clearly the area lies inside the proposed borders of the former lake. Base map is MOLA DEM.

Gwinner et al., 2010). For detailed topographical analyses, we also used single shot data from the MOLA PEDR (Precision Experimental Data Record) data which we superposed on CTX images using ESRI ArcGIS 10 software. This software was also used to merge all available datasets. The data were projected in a sinusoidal projection with the central meridian set at 187°E to minimize geometric distortion.

Absolute model ages were determined from crater size–frequency distributions, utilizing the software tool *CraterTools* (Kneissl et al., 2011), which ensures a distortion-free measurement of crater diameters independently from map projection, and the software *Craterstats* (Michael and Neukum, 2010) applying the production function of Ivanov (2001) and the impact-cratering chronology model of Hartmann and Neukum (2001). The mapped crater population was tested for randomness to avoid the inclusion of secondary crater clusters (Michael et al., 2012). Craters were counted on CTX images.

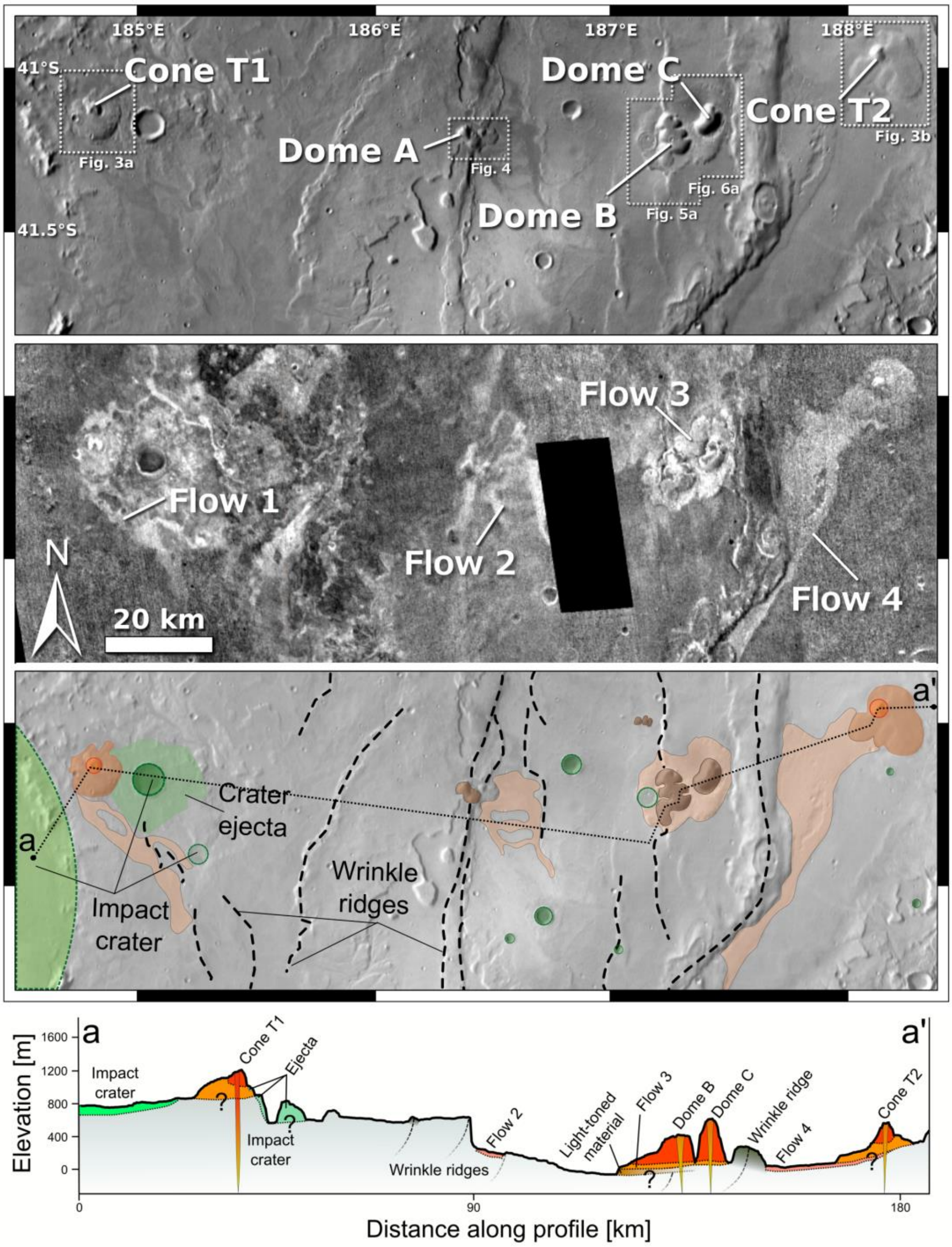

Figure 4.2: THEMIS-IR daytime (upper image), nighttime (middle) and interpretational map of the study area (bottom image). The thermal contrast between the two upper images suggests the presence of flow structures associated with cones and domes. Note the wrinkle ridges crossing the basin. The cross-section shows the stratigraphic relations of the investigated edifices with underlying units. Profile based on MOLA DEM and position marked by dotted line in bottom image.

Table 4.1: List of THEMIS images used in this study.

THEMIS image	Local Solar Time (Max)	Edifice(s)
I06941002	5.565556	Cone T1, Flow 1
I10885002	4.965	Dome A, Flow 2
I14554012	5.926667	Flow 2 and 3
I34557006	3.509167	Dome B, C, Flow 3
I06504011	5.643333	Dome B, C, Flow 3
I06142003	5.623055	Dome B, C, Flow 3
I22828008	5.975555	Flow 4
I06504011	5.643333	Flow 4
I34532006	3.536944	Cone T2

4.3. Regional setting

The study area is located in Terra Sirenum, a highland region which is crossed by approximately E-W-trending Tharsis-radial graben systems propagating from Arsia Mons over a distance of ~3,700 km. These grabens may represent the surface expression of volcanic dykes (Wilson and Head, 2002). Several wrinkle ridges, commonly interpreted as fault-propagation folds (e.g., Mercier et al., 1997; Schultz, 2000), indicate contractional deformation. The study area lies within the borders of the proposed former Eridania paleolake (Irwin et al., 2004; Fig. 4.1), a possible source for the formation of the Ma'adim Vallis outflow channel.

At local scale, the area is found within an unnamed depression (centred 41.40°S, 186.80°E) of unknown origin. Several conical and domical landforms (marked on Fig. 4.2a) are located within an area (~150 km × ~30 km) elongated in E-W direction. Except for one edifice (Cone T1), the remaining edifices are situated inside another, more localized unnamed depression. The margins of this depression are roughly 500 m in elevation above Mars' global datum (MGD). Based on HRSC (High Resolution Stereo Camera) Digital Elevation Models (DEMs), the lowest point (40 m below MGD) is situated close to the southwestern edge (41.35°S, 187.17°E) of Dome B, where a distinctive light-toned scarp is visible.

The depression is cut by several wrinkle ridges with a sinuous trace in plan-view. The wrinkle ridges stand several tens of meters above the surrounding plains, and Domes A and B appear to be superposed on two separate wrinkle ridges. Cone T1 is situated ~850 m above MGD near the edge of a highly eroded, ~110 km diameter impact crater infilled by younger deposits. The edifices are associated with flow landforms as visible in the HRSC and CTX images.

4.4. Results

4.4.1. Thermal properties

Several regions of enhanced relative thermal radiance are visible in the nighttime THEMIS (Thermal Emission Imaging System) infrared images (Fig. 4.2a, b; see Tab. 4.1 for THEMIS image details). The five brightest patches correspond to the locations of the studied small-scale edifices (marked as Cones T1 and T2 and Domes A, B, and C in Fig. 4.2a) and associated flow features (marked as 1, 2, 3, and 4 in Fig. 4.2b). The two conical (Cones T1 and T2), and three dome-shaped edifices (Domes A, B, and C), display steep, lobate margins visible in daytime THEMIS images. Except for Flow 3, the flows are elongated with partially anabranching channels visible in THEMIS day- and night-time images. Flow 3 is different in that it surrounds domes B and C to an approximately constant radius, rather than being elongated. In contrast, Flow 4 is clearly visible on THEMIS night-time images and can be traced for about 50 km in a southern direction. Flow 2 and 4 can be traced to point-like sources, Dome A and Cone T2 respectively, whereas Flow 3 cannot be directly related to either Dome B or Dome C. Flow 1 may also be linked to a point-like source area (Cone T1); but more flows are visible that originate around a ~6 km impact crater (centred at 41.17°S, 185.07°E). The floor of this 6-km diameter crater is characterized by low relative

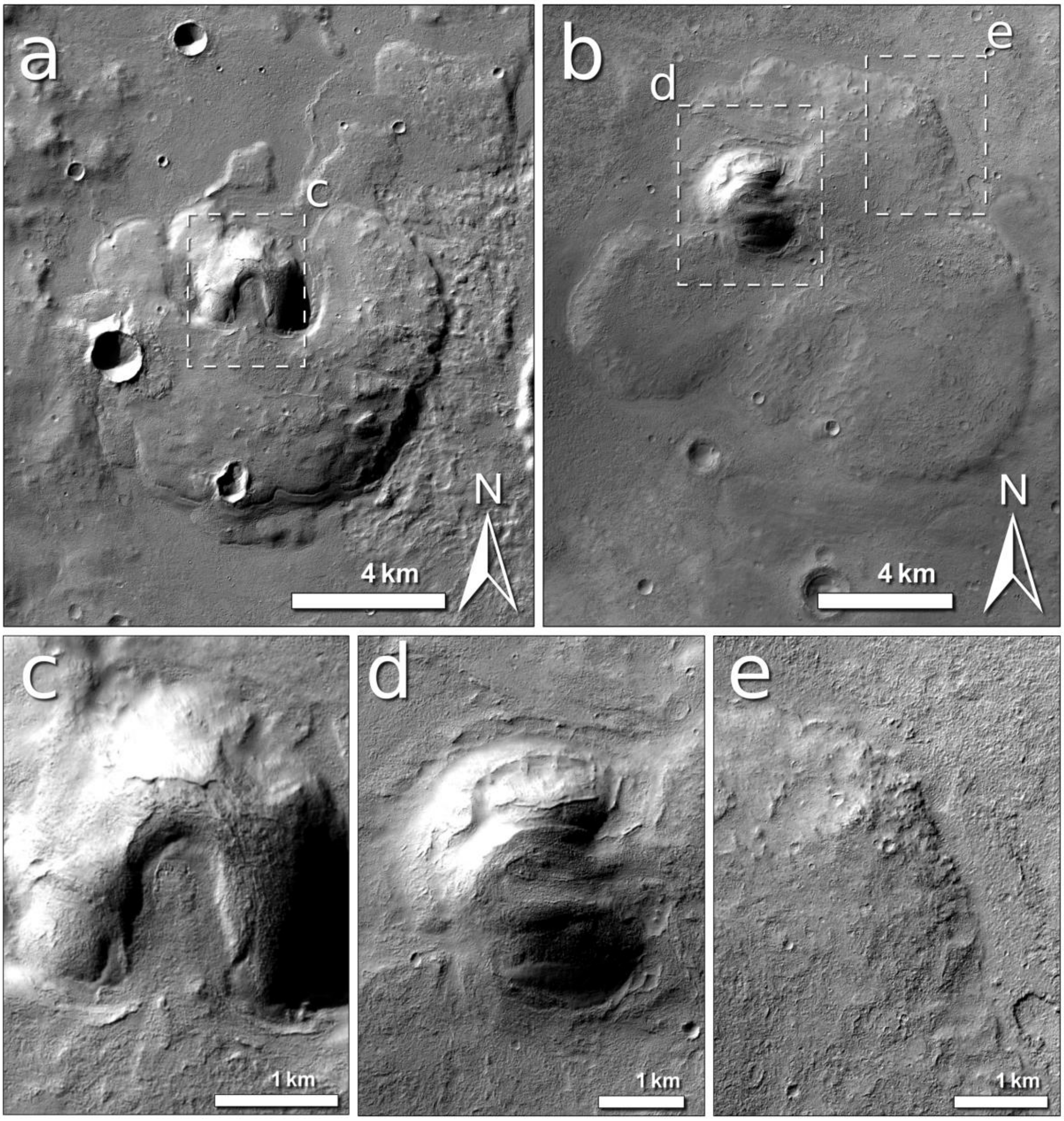

Figure 4.3: Two cones (a,b) with associated flow aprons; note details of cones (c,d) with central vent from flow aprons material erupted to the surface. (e) is showing edge of overlapping flow aprons. See also Fig. 4.2 for position within investigated area. CTX images B18_016835_1386 (a), and mosaic of CTX images B19_016914_1399 and P16_007117_1362 (b), centred 41.15°S, 184.84°E and 41.00°S, 188.15°E, respectively. Image credit NASA/JPL/MSSS.

thermal radiance, as are those of other large impact craters in the study area. The low thermal emission is also visible on the north-facing edge of this crater in contradiction to the domical and conical edifices, where north-facing slopes have higher thermal emission in THEMIS nighttime images.

4.4.2. Morphology

Cones T1 and T2 are shown in Figure 4.2. Both cones are breached to the south and east, respectively (Fig. 4.3a, b), and are associated with flow aprons that partly cover the lower flanks of the cones. The western cone T1 (Fig. 4.3a, 41.13°S, 184.85°E) measures about 3 km in diameter and 230 m in height, based on data acquired through the Mars Orbiter Laser Altimeter (MOLA). A central summit depression is breached towards the south and a small mound from where the flow apron originates is visible (Fig. 4.3c). The flow apron is ~8.5 km wide and spreads as a single, compact unit around the cone, except in the north. The southern edge of the flow apron is relatively steep, as demonstrated by cast shadows and younger talus aprons partly hiding the edge itself. Based on single MOLA shot data, the flow apron is between 100 and 130 m thick and the steepest slopes are ~10° to 11°; however, they can reach up to 20° after the talus is numerically removed by taking values of neighbouring MOLA shots not influenced by talus. The surface of the flow apron is superposed by two small impact craters (with diameters of ~1.3 km and ~0.8 km) without distinctive fluidized ejecta features. The eastern Cone T2 (Fig. 4.3b, 40.945°S, 188.11°E) is similar in size (~3 km in diameter and ~290 m high), but lacks a deep summit depression, although the cone itself is breached towards the east. Its flanks appear partly degraded, especially in the northern part of the cone. No vent sources can be distinguished on the cone flanks. The flow apron extending from the cone is ~12.5 km long in the north-south direction, forming four distinct lobes. Overlapping flow apron margins suggest multiple formation events (Fig. 4.3e). Compared to Cone T1, the flow aprons around Cone T2 do not have such steep margins (between 3° to 5°) and they are morphologically less distinct compared to their surroundings. These flow aprons cover the source of Flow 4 that propagates for ~50 km in a southwestern direction. Flow 4 is between ~1 km and ~8 km wide and between ~30 m and 50 m thick. The flow was impeded to the west by a wrinkle ridge causing flow deflection towards

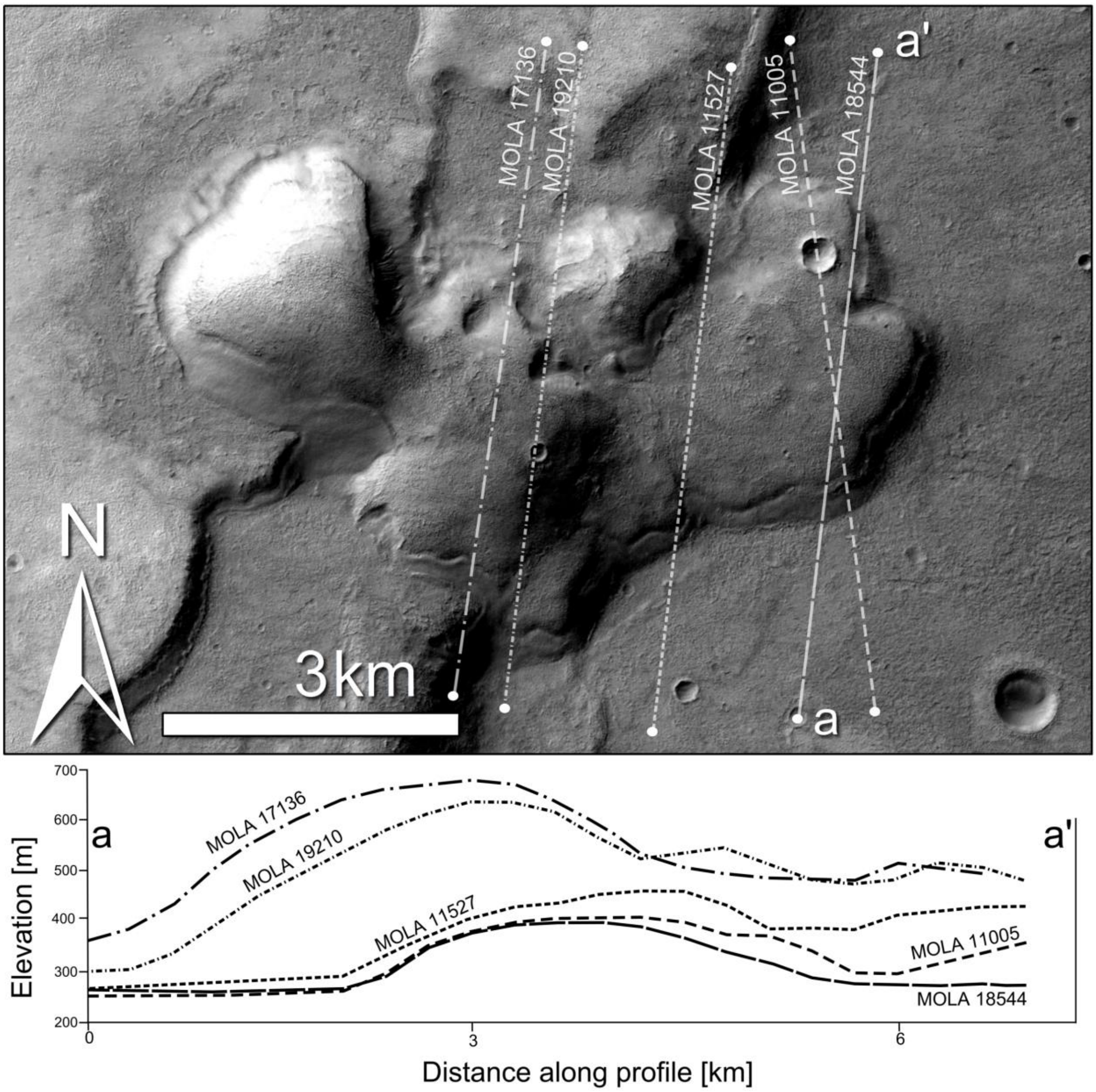

Figure 4.4. Image of Dome A with marked MOLA PEDRs and associated topographic profiles. Part of the Dome A seems to collapse and propagate in eastern direction. See Fig. 4.2 for position within investigated area. Based on CTX image D16_033331_1391, centred 41.21°S, 184.44°E.

the south. The flow margin is relatively rugged with many small-scale lobes and the surface exhibits rough texture partially softened by mantling deposits.

In the central part of the study area, three dome structures are associated with flows (Fig. 4.2a, b). Two of them are covered by CTX and HiRISE images (Domes B and C) whereas Dome A is covered by CTX only. Dome A (Fig. 4.4, 41.20°S, 186.40°E) is

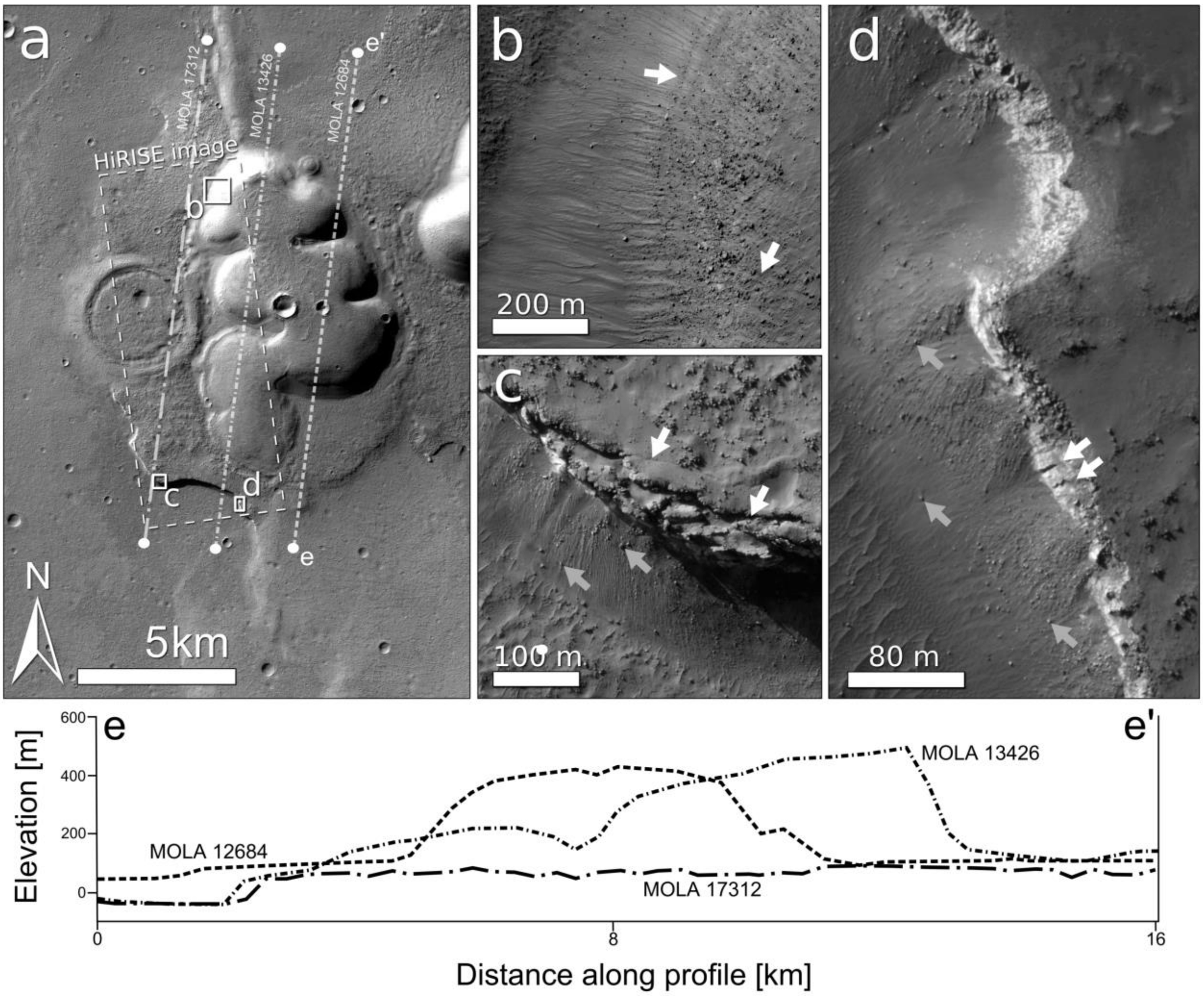

Figure 4.5: Image of Dome B with close up details. (a) Detail of Dome B and surrounding flow and marked position of HiRISE image ESP_033977_1385 with marked positions of MOLA PEDRs and associated topographic profiles. Based on CTX image G19_025696_1389, centred 41.22°S, 187.24°E. (b) Detail of HiRISE image showing the contact between the northwestern edge of the dome and the underlying unit. Large boulders forming dome itself and aeolian deposits at the top of the dome together with modification by gully activities are clearly visible. (c) Detail of the bedrock on which Dome B is superposed on as exposed by a ~80 m high scarp. Pristine fracture morphologies suggest ongoing scarp erosion. Note that the talus is mainly formed by fine-grained material and small amounts of boulders less than ~6 metres large (marked by gray arrows), larger blocks are missing. The tensile fractures parallel to the scarp in the capped unit (marked by white arrows) are similar to fractures associated with rotational block-fall landslides known from Earth. (d) Detail of HiRISE image showing another part of the scarp. Again, no large blocks of fallen rocks are visible and the talus is composed mainly of finer particles and smaller boulders (marked by gray arrows). Two white arrows indicate small grooves, which might have formed by ongoing aeolian erosion. These grooves show that the exposed material is susceptible to erosion. Image credit: NASA/JPL/UofA and NASA/JPL/MSSS.

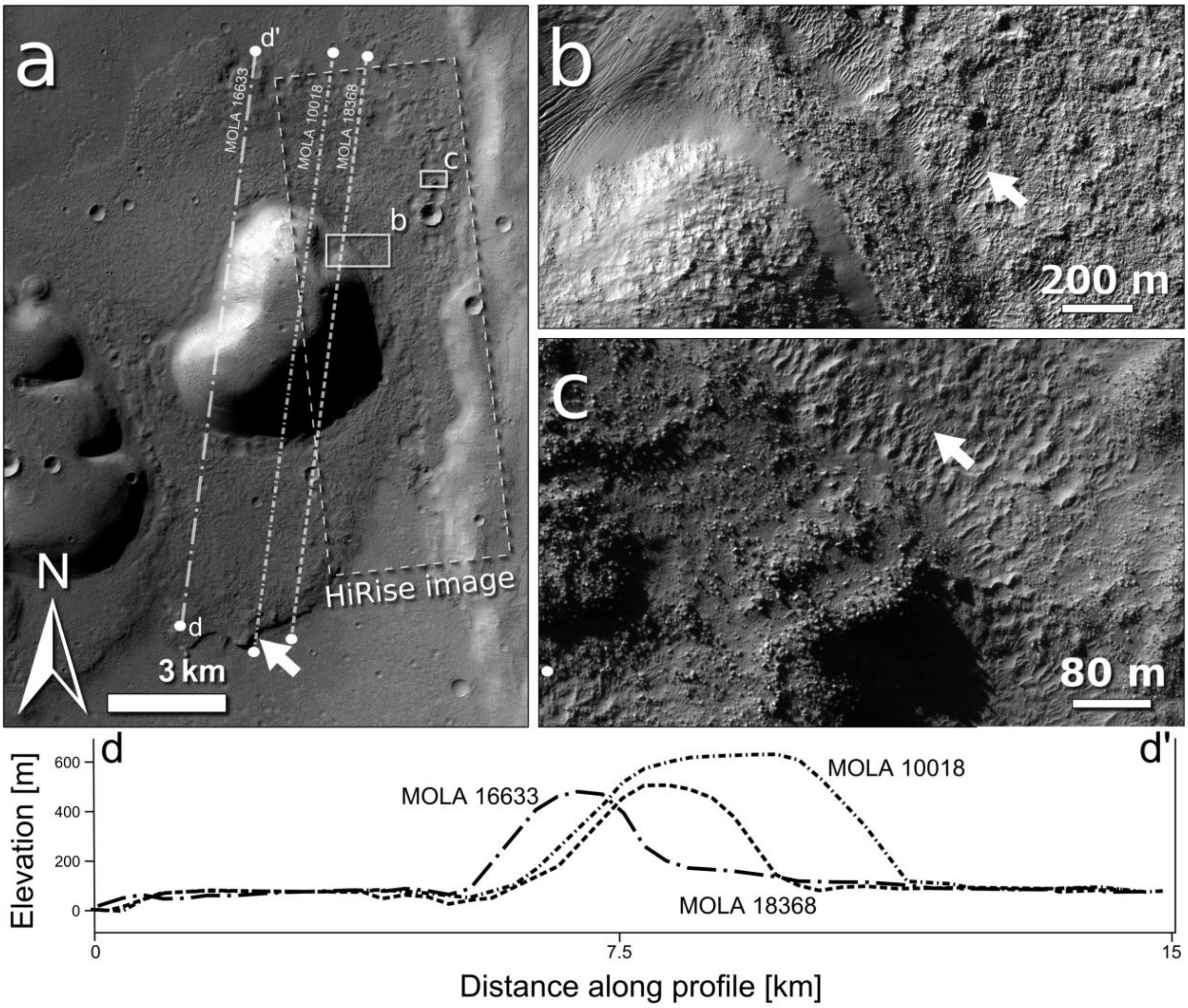

Figure 4.6: Image of Dome C and surrounding flow. (a) The dome edifice (Dome C, see Fig. 4.2 for position) is clearly surrounded by a flow structure that has steep edges, as demonstrated by the shadows on the southern margin. White arrow marks scarp on the edge of Flow 3. Position of MOLA PEDRs marked by lines and HiRISE image ESP_026474_1385 marked by dashed rectangle. Part of CTX image B18_016769_1369, centred 41.15°S, 187.4X°E. (b) Detail of HiRISE image covering part of dome flanks (left part of image b) and flow structure (right part). Note large boulders forming the dome itself and aeolian deposits forming Transverse Aeolian Ridges (marked by white arrow). (c) The edge of the flow structure on the border with surrounding older, flat layer. The margin of the internal flow is formed by large-scale boulders that are partly covered by aeolian material (marked by white arrow). The older unit contains small Transverse Aeolian Ridges (Balme et al., 2008). Image credit NASA/JPL/UofA and NASA/JPL/MSSS.

a ~2.5 km wide mound superposed on a wrinkle ridge. A ~5 km long and over ~300 m high flow apron propagating in the south-eastern direction and appears to be associated with Dome A. The flanks of the flow apron have slope angles between 7° and 11°. The other two domes, marked as Dome B (Fig. 4.5a, 41.19°S, 187.26°E) and Dome C (Fig. 4.6a, 41.16°S, 187.41°E), are ~5 km × 7 km and ~3.5 km × 6 km in size and have maximum heights of 390 m and 530 m, respectively. Their flanks have slopes between 17° and 23°. Topographic data also reveal that the height of both structures decreases towards the south. For example, the highest part of Dome C is located close to its northern edge and is ~170 m higher than the southwestern part. Dome B is superposed on a wrinkle ridge, and the southwestern edge of the dome extends over a short distance to the south along the crest of the wrinkle ridge. The shape of Dome B is more irregular in plan-view compared to Dome C. Dome B exhibits four valleys dividing the dome into four differently-sized portions in plan view.

HiRISE images show that the cones, domes, and associated flow features have bouldery surfaces that are partly covered by younger, fine-grained deposits which infill/occupy the spaces between the exposed boulders. These deposits are less frequent at the steeper edges, where more exposed boulders are seen. The flanks seem to be irregularly layered (Fig. 4.5b, marked by arrows) and contain widely spread shallow gullies in the middle to lower flanks (Fig. 4.5b), which predominantly occur on the western edges. The northern and northeastern part of Dome C are not covered by younger draping material, enabling observations of the contact between flanks and surrounding flow units. The dome seems to be superposed on these units (Fig. 4.6b). Both Domes B and C are surrounded by flow features composed of one or more individual flow units. These flows are superposed on the underlying surrounding unit, which is heavily covered by impact craters in different stages of degradation and covered by a single layer, as demonstrated by the topographic relationship and abrupt transition between the units (e.g., Fig. 4.6c). Also, small ridges and wrinkles forming flow textural patterns are partly visible on the top of both domes (Fig. 4.5a, 4.6a), with inferred flow directions following the local topographic gradient.

The western margin of the flow unit around Dome B is disrupted by a ~3 km impact crater that is almost completely infilled by boulder-rich material. The south-western and southern margins are characterized by light-toned scarps with significant vertical offset (around 80 m at the southern margin of Dome B, based on single MOLA shots). A similar scarp, but with lower vertical offset, is also seen at the southern edge of Dome C (marked by a white arrow on Fig. 4.6a). The scarps show signs of ongoing erosion, as evidenced by talus, falling rocks with boulder trails in the talus, linear to arcuate fractures parallel to the scarp edge (marked by white arrows on Fig. 4.5c), and small grooves (marked by white arrows on Fig. 4.5d). The grain size of talus material at the base of these scarps is too small to be resolved in HiRISE imagery (25cm/pixel), although a small portion of larger boulders is visible (marked by gray arrows on Figs. 4.5c,d). HiRISE images reveal that the surface and margins of the domes and their surrounding flows are composed of boulders up to several meters across (Figs 4.5b and 4.6b,c), and are partly covered by aeolian deposits forming Transverse Aeolian Ridges (e.g., Balme et al., 2008; marked by white arrows on Fig. 4.6b,c). The boulder distribution is spatially random. Several impact craters with diameters of tens to a few hundred meters are superposed on the flow units. The interior floors of the craters also contain boulders of different sizes.

We note that, within the study area, a double-rimmed depression is observed on the top of a wrinkle ridge centred at 41.41°S, 187.64°E. The depression is elongated in a north-south direction and is 7.5 km × 4.5 km in size and contains a 3 km-diameter inner rim. The inner structure is circular in plan-view and exhibits a small central mound. The outer flanks of the depression do not show any evidence of impact ejecta deposits.

Several larger impact craters in the study area have floors filled by re-deposited material. This material originates on the crater flanks and the surface is characterized by flow-like pattern with elongated subparallel grooves and series of small depressions forming knobby terrains in shape corresponding to ‘lineated valley fills’ and/or ‘concentric crater fills’ (Colaprete and Jakosky, 1998).

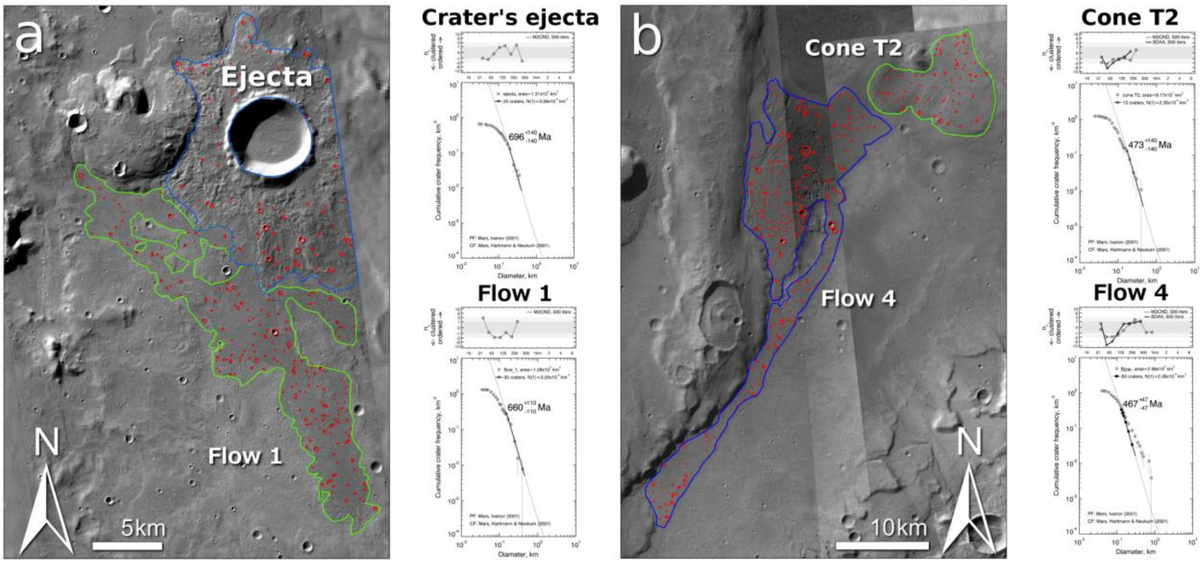

Figure 4.7: Absolute model ages of (a) the crater’s ejecta and Flow 1, and (b) Cone T2, and Flow 4. (a) The cumulative crater size-frequency curves indicate an absolute model age 660±100 Ma for Flow 1 and 700±100 Ma for the crater’s ejecta. (b) The cumulative crater size-frequency curves indicate an absolute model age of 470±100 Ma for Cone T2 and 470±50 Ma for Flow 4. Note the panels above the cumulative crater size-frequency plots represent the randomness analyses (cf. Michael et al., 2012). Background images are CTX images B18_016835_1386 and mosaic of P16_007117_1362, G18_025274_1388 and B18_016769_1369. Image credit NASA/JPL/MSSS.

4.4.3. Ages

The domes and cones do not represent suitable areas for the determination of crater size-frequency distributions (CSFDs) because they are too small in areal extent. Instead, we determined the CSFDs of four units (marked on Fig. 4.7) with known relative stratigraphic relationships (see cross-section in Fig. 4.2). The ejecta blanket from a ~6 km impact crater is partly superposed on the flow apron associated with Cone T1, hence, representing a younger surface than the cone itself and the associated flow apron. From the ejecta material we determined an absolute model age of 700±100Ma. The source of Flow 1 is not exposed but may be covered by the ~1.3 km diameter impact crater on the western margin of the flow apron associated with Cone T1. The formation age of Flow 1 is determined to be 660±100 Ma. The flow apron associated with Cone T2 appears to have formed at 470±100 Ma. Stratigraphically, Flow 4 is older than the apron thereby bracketing the age of volcanic activity. Based on the measured CSFD, Flow 4 formed at about 470±50 Ma.

4.5. Discussion

4.5.1. Infrared images

The investigated edifices and associated flows are brighter in infrared nighttime images relative to the background plains materials. By contrast, the floors of larger craters are darker (Fig. 4.2) than their surroundings. Areas covered with dust, unconsolidated or high-porosity materials cool down quickly after dusk, and hence, appear darker in infrared nighttime images (low thermal inertia), whereas exposed bedrock or boulder surfaces store the heat longer and appear brighter (high thermal inertia; Fergason et al., 2006). HiRISE images of the high relative thermal radiance areas show coarse material including meter-sized boulders (Figs. 4.5, 4.6). Dark areas with low relative thermal radiance in nighttime images are characterized by pitted and irregular terrain with/without a thick dust cover. However, it is noted that significant changes in local slopes can contribute to thermal signature variations (Fergason et al., 2006) due to differential insolation. Therefore, during the day, sunlit slopes accumulate more heat than shady slopes, which might be visible as brighter spots on nighttime THEMIS images as more heat is released. For this reason, the brighter areas on cones and domes may be related to steep flanks, rather than a higher thermal capacity. If the associated flow aprons and flows are taken into account, however, this explanation cannot account for all observed variations in nighttime thermal infrared image brightness, because the flow aprons and flows are brighter than their surroundings despite having similar slopes as the surrounding units. Hence, THEMIS nighttime infrared images suggest

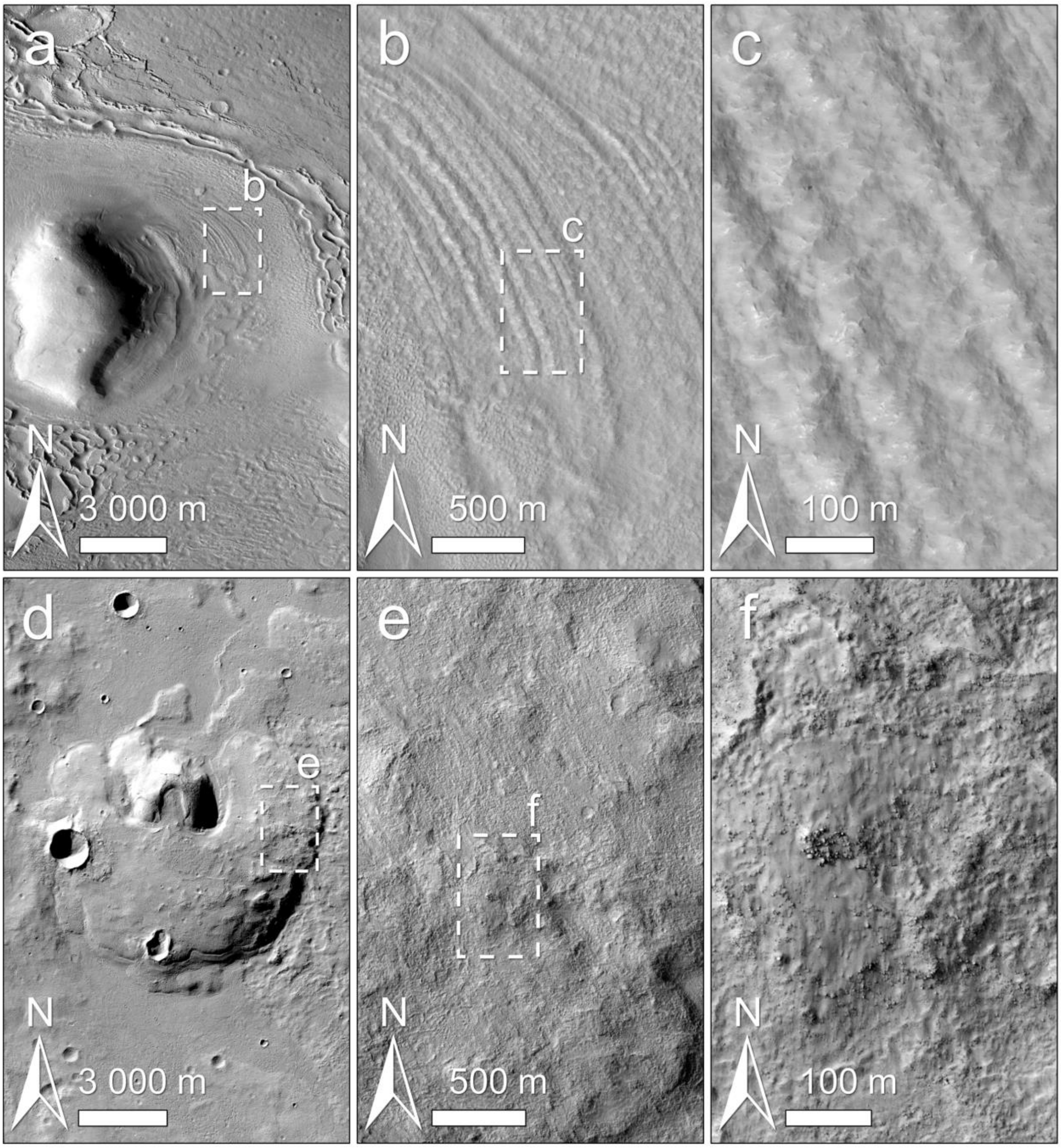

Figure 4.8: Examples of textures of lobate debris aprons at northern latitudes (a-c) and investigated flow aprons associated with Cone T1 (d-f) in various scales. Lobate debris aprons mainly miss significant amount of large boulders (c) which are clearly visible on investigated flow aprons (f) Lobate debris aprons associated with massif in Deuteronilus Mensae (a - part of CTX image D04_028840_2240_XN_44N334W , centred 44.067°N, 25.643°E, b-c based on HiRISE image ESP_037556_2245). (d) The flow apron associated with Cone T1 (d - part of CTX image B18_016835_1386_XI_41S175W, centred 41.13°S, 184.85°E, e-f based on HiRISE image ESP_037511_1385).

that the investigated features are indeed composed of consolidated materials or represent unconsolidated units with high proportions of dense (high thermal inertia) clasts.

4.5.2. Morphology

The domes stand several hundred meters above the surroundings plains and are partially superposed on wrinkle ridges. They exhibit well-preserved shapes and neither the cones nor the domes show much evidence for significant erosion (except a few small gullies), yet the morphological interpretation is not straightforward and depends upon the regional context. The study area is located in the southern mid-latitudes (around 40°S), where glacial and/or periglacial activity has produced a range of ice-related landforms (e.g., Squyres and Carr, 1986; Souness and Hubbard, 2012). For example, Squyres and Carr (1986) suggest that the martian regolith is deformed by quasi-viscous flow due to creep deformation of ice, a process known as 'terrain softening' (Jankowski and Squyres, 1992). A characteristic class of landforms related to this process are lobate debris aprons (Squyres, 1978), which in some ways have similar morphologies to the flow aprons around cones T1 and T2. However, several aspects make it unlikely that cones T1 and T2 are surrounded by lobate debris aprons.

Lobate debris aprons (LDA) are thought to be debris-covered glaciers, consisting of relatively pure ice (Hauber et al., 2008; Holt et al., 2008; Plaut et al., 2009) under a protective cover (Head et al., 2010). They commonly display distinct surface textures (Figs. 4.8a,b,c) that are indicative of subsurface ice and/or degradational processes such as sublimation. Key geomorphic features typically observed on the surfaces of LDA include the initiation of flow lineations in protected alcoves, the coalescence of flow lineations and convex-up topographic profiles (see Levy et al., 2014 and references therein). Possible sublimation-related landforms on lobate debris aprons include fractures and a characteristic pattern of pits and buttes that are interpreted to result from the progressive removal of subsurface ice by sublimation (Mangold, 2003). Chuang and Crown (2005) describe typical morphologies of LDA surfaces, and place them into a degradation sequence progressing from ‘smooth’ to ‘pitted’ to ridge and valley or ‘knobby’. Other surface textures indicative of ice-rich viscous material are the so-called ‘brain terrain’ (Levy et al., 2010) and ring-mold craters, defined as concentric crater forms shaped like a truncated torus and thought to be the result of impacts into relatively pure ice protected by a thin regolith (Kress and Head, 2008).

Neither flow lineations nor ring-mold craters nor possible sublimation landforms can be observed on the surfaces of the lobe-like features around the investigated edifices (Figs. 4.8d, e, f). The progressive degradation morphologies identified by Chuang and Crown (2005) are also not seen. The only property that is consistent with an origin by the viscous flow of ice-rich material is the convex-up cross-sectional shape. Such shape, however, is far from being diagnostic for ice-rich substrate, as it is typical for any plastic deformation. The surface ages of the investigated lobes are inconsistent with an origin as lobate debris aprons: whereas lobate debris aprons are geologically recent landforms and have absolute model ages of typically less than ~500 Ma (e.g., Morgan et al., 2009; Baker et al., 2010; Hartmann and Werner, 2010; Parsons and Holt, 2014; Fassett et al., 2014), the surfaces of the lobes around the edifices in the study area display model ages at the end of this limit or >500 Ma. In addition, impact crater formation on an ice-rich target material would have formed single or multi-layered, lobate rampart ejecta. This is not observed (cf. western crater ejecta on Cone T1 flow apron; Fig. 4.3a). Cones T1 and T2 are breached and flow aprons seem to originate from the centres of craters on the top of the cones. This suggests that material likely extruded from the subsurface through the craters to the surface, rather than originated at alcoves on the flanks of the cones, as it is typical for flowing ice-rich material (Head et al., 2010). A simple comparison between observations and expected characteristics of lobate debris aprons illustrates that an origin of the aprons by the flow of ice-rich material is highly unlikely. Therefore, we exclude in the following the possibility that the lobes consist of an ice-rich substrate covered by a thin layer of regolith.

The inspection of HiRISE images reveals that Cone T2, Domes B and C, and Flows 2 and 3 contain apparently randomly distributed, meter-sized boulders (Fig. 4.5, 4.6). There is no obvious sorting of large boulders, suggesting that the flows are able to carry (and/or form) boulders over their entire length. This homogeneous distribution of boulders is inconsistent with glacial or periglacial processes, where boulders are often aligned or concentrated by flow or into moraines (Boulton, 1978; Arfstrom and Hartmann, 2005) and organized into patterned ground (Washburn, 1956). It is also inconsistent with the formation of gravity-driven rock avalanche deposits where variations in block sizes occur downslope in flow direction (Bulmer et al., 2005; Platz et al., 2012). In contrast, the apparent random distribution of boulders at the surface is consistent with some terrestrial lava flows (Bulmer et al., 2005), whose blocky nature is typically attributed to higher viscosities of the erupted magma.

The southwestern margin of Flow 3 is marked by a ~80 m-high scarp which exposes what appears to be bedrock. The exposed bedrock is relatively light-toned in the stratigraphically lower parts and is capped by a dark layer of massive material topped by boulders (see topographic profile in Fig. 4.2), which we interpret to be a resistant lava carapace. The scarp appears to be undergoing active erosion, as inferred from talus accumulation, rock fall (Fig. 4.5c, d), and occasional sharply-expressed fractures or clefts in the scarp (marked by white arrows on Fig. 4.5d). In addition, well-visible tension fractures with an orientation parallel to the scarp are visible in the cap unit (marked by white arrows on Fig. 4.5c), and are similar to fractures associated with rotational block-fall landslides on Earth. Interestingly, the amount of large boulders released from the scarp by rock fall appears to be limited, as only a few can be observed as part of the talus (marked by gray arrows on Fig. 4.5c, d). This suggests that the exposed light-toned material is less competent and presumably fine-grained, so that the boulders are quickly (in geological terms) broken into smaller pieces or break up upon impact.

Due to a lack of spectroscopic observations with appropriate spatial resolution, we can only speculate about the composition, and hence, the origin of the cliff-forming material and scarp. Two scenarios seem to be plausible: (i) the bedrock might be composed of sedimentary rocks deposited in a lacustrine environment and/or formed by aeolian processes, or (ii), by weakly consolidated tephra (e.g., tuff, scoria, ash) or welded pyroclastic-flow deposits (i.e., ignimbrites) formed by explosive eruptions. Explosive magmatic fragmentation occurs when the pressure in the interconnected bubble-melt network exceeds the load of overlying rocks or through the interaction of ascending magma with surface/subsurface water and/or water ice (cf. phreatomagmatic fragmentation). Both fragmentation processes would cause dispersion and subsequent accumulation and deposition of fragmented material in the close vicinity of the vent. Once the source of fragmentation is depleted, volcanic activity would change in style from explosive into effusive, perhaps causing the formation of a resistant lava unit partly overlying the weaker sedimentary bedrock. However, based on current data, we cannot rule out the possibility that the dark resistant lava unit propagated over sediments of non-volcanic origin. In both scenarios, though, the more resistant dark lava unit protects the easily erodible bright bedrock. The scarp itself might be the result of magma intrusion into shallow sub-crustal levels causing doming of the overlying rocks. Another mechanism might be aeolian erosion removing bright material from the edges of a sedimentary unit partially capped by dark lavas in those areas where the sediments were not protected by the resistant lava unit. Ongoing erosion would then lead to undermining of the more resistant capping unit and scarp formation. Finally, the scarp might have formed as a result of both mutually active processes.

The entire area is covered by thin layer(s) of very fine-grained deposits draping the original surface textures. Such deposits are common on Mars at latitudes between 30° to 60°, where they form 1-10 m thick, ice-rich layers (Mustard et al., 2001). Layers of these very fine-grained deposits are partly missing at the steep edges of the investigated edifices where boulder-rich surfaces are present, again indicating active erosion.

4.5.3. Ages

Our crater counts suggest post-Noachian, probably Middle Amazonian, ages for the formation of the studied landforms; between 0.5 Ga to 0.7 Ga (Fig. 4.7). However, we are aware that smaller surface areas can bias the estimates towards younger ages (Michael and Neukum, 2010) which could introduce inaccuracies into the results. Therefore, we take established ages only in association with relative stratigraphy. Irwin et al. (2004) suggested that the Eridania paleolake was spread over this area during the Late Noachian/Early Hesperian. This conclusion is supported by Tanaka et al. (2014) who dated the unit on which the investigated cones and domes stand as Late Noachian in age. Another hint is recorded by the wrinkle ridges on which Domes A and B are superposed. The ridged plains were dated by Scott and Tanaka (1986) as Hesperian to Amazonian in age and by Greeley and Guest (1987) as Hesperian in age. Wendt et al. (2013) state that the ridged plains cannot have formed earlier than the fields of light-toned knobs filling most of the ancient basins in Terra Cimmeria/Terra Sirenum. These stratigraphic observations suggest that the cones, domes, and flows have to postdate the Early Hesperian Epoch, and are consistent with the notion based on crater statistics that the investigated landforms are mid-Amazonian in age.

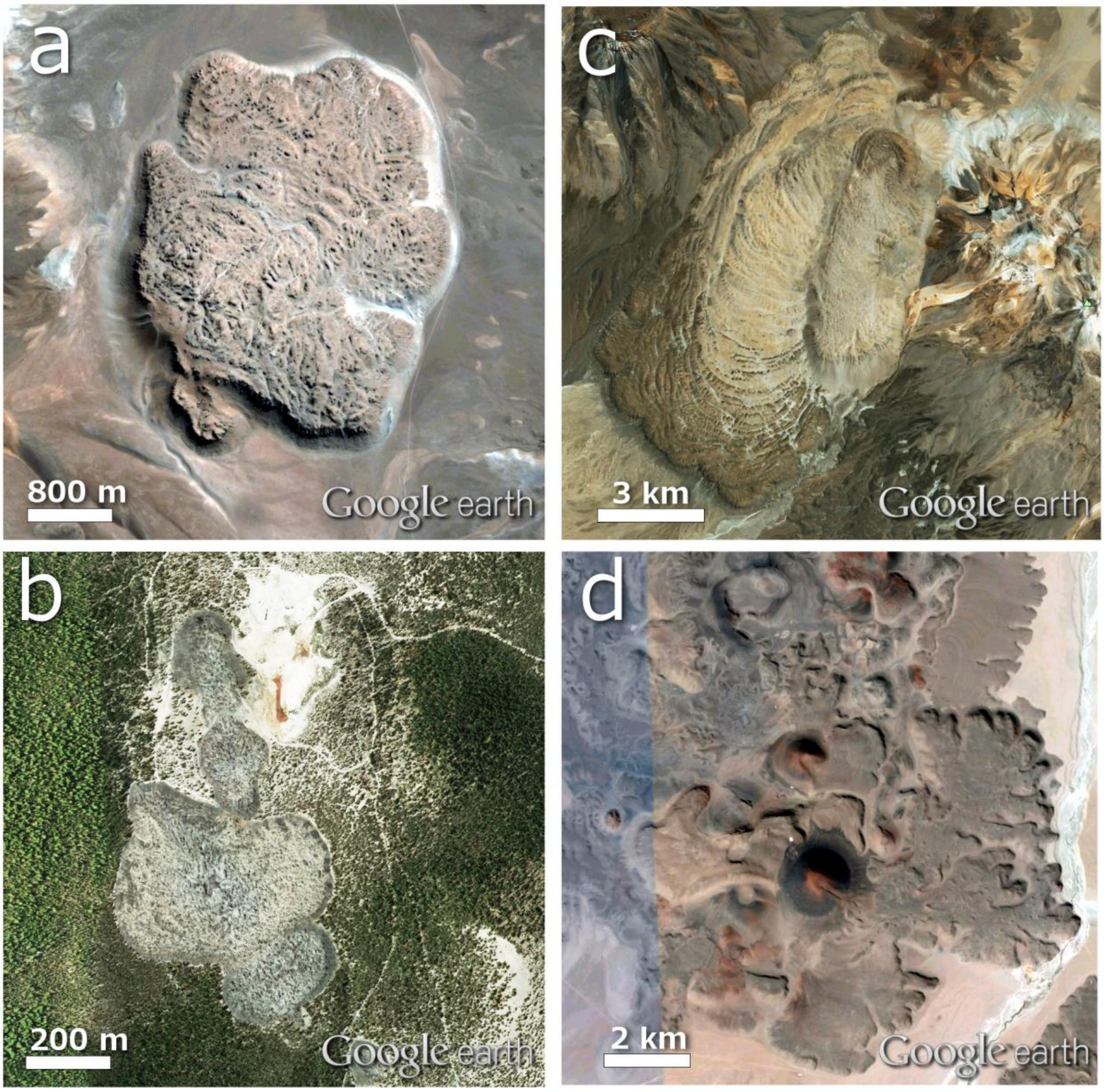

Figure 4.9: Examples of terrestrial lava domes/coulées (a,b,c) and a volcanic cone with associated lava flows (d), which might represent suitable analogues to investigated martian edifices. (a) Chillahuita, large dacitic lava dome in the Chilean Andes (22°8.356'S, 68°1.766'W; image credit: DigitalGlobe 2014) (b) Small lava dome (41°37.2'N, 121°31.5'W) to the North of the rhyolite and dacite obsidian flow known as Glass Mountain, part of Medicine Lake Volcano in California, USA. (c) Chao (22º07'S, 68º09'W, image credit: CNES/Spot Image), 14.5 km long dacitic coulée in Chile. (d) Small basaltic-andesite volcanic cone with outgoing flows situated north of the small village Antofagasta de la Sierra in Argentina (25º53'S, 67º24'W, image credit: Inav/Geosistemas SRL, CNES/Astrium). All images obtained via GoogleEarth™.

4.5.4. Interpretation and implications

Based on the combined morphological and infrared observations, we therefore conclude that volcanism seems to be the most probable explanation for the formation of the edifices and their associated flows. This conclusion is supported by the inspection of OMEGA based (Visible and Infrared Mineralogical Mapping Spectrometer) global maps (Ody et al., 2012), which suggest that exposed boulders atop Domes B and C and Flow 3 have low abundances of olivine and moderate amounts of pyroxene, favoring an origin related to volcanism rather than to water and/or water ice. The morphological similarities to terrestrial lava domes, coulées and obsidian flows (Fig. 4.9) raise the possibility that the studied features represent a suite of volcanic landforms associated with evolved magmas. The cones and associated lava flow aprons are morphologically different to previously observed small volcanic edifices on Mars such as scoria cones (Meresse et al., 2008; Brož and Hauber, 2012) and tuff rings/cones (Brož and Hauber, 2013). Instead, they may represent volcanic cones or collapsed steep-sided domes with associated viscous lava flow aprons which partly embay the cones themselves, a situation that is known from terrestrial coulées such as the 'Chao dacite' (Fig. 4.9c) in the Andes (de Silva et al., 1994). The flow aprons associated with the cones have steep margins (up to 20°), which is in stark contrast to less viscous basaltic flows in Tharsis or Elysium that are typically characterized by low relief and very gentle flank slopes (Hauber et al., 2009). The differences in flow apron thickness compared to flow thickness suggest changes in flow rheology during cone formation and associated flow emplacement, and may be directly linked to differing rates of degassing and/or magma cooling histories. The absence of volcanic craters in association with the investigated edifices also suggests that the dominant style of volcanism was effusive rather than explosive.

The implications of young volcanism in the martian highlands is in agreement with new petrological modeling results. Baratoux et al. (2013) showed that a transition occurred from the Noachian to the Hesperian and Amazonian where in the former primarily low-Ca pyroxene assemblages formed, whereas the latter (i.e., Hesperian and Amazonian periods) are dominated by high-Ca pyroxene occurrences, in accordance with orbital spectroscopic observations. Extrusion of low-volume volcanic materials, which formed the studied edifices, suggests storage of evolved magmas at shallow sub-crustal level(s). Such small magmatic bodies are unlikely to ascend from greater depth or from the crust-mantle boundary. Magmatic differentiation towards more evolved compositions is more likely to occur through multiple stalling and ascending phases, at least as known from terrestrial settings (e.g., Platz et al., 2012). New density constraints of the martian crust (Baratoux et al., 2014), based on martian meteorites, in situ analyses of igneous rocks, and surface element abundances from orbital Gamma-ray spectrometers, reveal higher densities (>3100 kg.m^3) than the conservative values used for crustal thickness modeling (2700 – 3100 kg.m^3). This finding also supports our interpretation that the studied landforms represent volcanic constructs. Higher crustal densities favour the buoyant ascent of even small magmatic bodies and their eruption onto the surface.

4.6. Conclusions

We have identified small-scale volcanic edifices in the southern highlands of Mars that have a relatively young Amazonian age. The steep-sided morphology suggests that highly viscous lava formed them, magma intruding into the crust causing doming and extruding onto the surface or vice versa. If so, volcanic edifices composed of evolved magmas may not only be present in the northern lowlands in Arcadia Planitia (Rampey et al., 2007), but also in the southern highlands, far from any known major volcanic centres. The proposed explanation for cryptodomes in Arcadia Planitia (Farrand et al., 2011), in which magma viscosity increased due to magma degassing and/or a high degree of crystallization, may be also be valid here. Although decompression-induced degassing and/or crystallization changes the magma's composition, it remains open as to how differentiated the magma is that formed these volcanic domes and cones. The extrusion of small-volume differentiated lava onto the surface implies multiple storage levels during magma ascent through a thick, southern highland crust. Our observations and conclusions expand our knowledge about evolved magmas on Mars, which seem to be more widespread than previously thought (Wray et al., 2013; Meslin et al., 2013; Carter and Poulet, 2013; Sautter et al., 2014). Further investigations are required to elucidate the origin of these edifices; they clearly represent ideal candidates for detail spectroscopic observations.

Acknowledgements

We appreciate the efforts of the instrument teams (MOLA, THEMIS, HRSC, CTX, HiRISE) who acquired and archived the data used in our investigation. Especially, we would like to thank W. Brent Garry for his constructive comments on a previous version of this manuscript, and the HiRISE team which provided new interesting observations on our requests. These data greatly improved our study. We would like to also thank to David A. Williams and an anonymous reviewer for their suggestions how to improve our study and to Christophe Sotin for handling the manuscript throughout the editorial process. Petr Brož was a visiting research student at the Open University, UK, when this research was undertaken. This study was supported by the Grant No. 580313 from the Grant Agency of Charles University in Prague (GAUK) and by the Helmholtz Association through the research alliance 'Planetary Evolution and Life'.

5. Shape of scoria cones on Mars: insights from numerical modeling of ballistic pathways

Petr Brož[1,2], *Ondřej Čadek*[3], *Ernst Hauber*[4] *and Angelo Pio Rossi*[5]

[1]*Institute of Geophysics ASCR, v.v.i., Prague, Czech Republic*
[2]*Institute of Petrology and Structural Geology, Faculty of Science, Charles University, Prague, Czech Republic*
[3] *Department of Geophysics, Faculty of Mathematics and Physics, Charles University in Prague, Czech Republic*
[4]*Institute of Planetary Research, DLR, Berlin, Germany*
[5]*Jacobs University Bremen, Bremen, Germany*

Status: Published in Earth and Planetary Science Letters 406,

doi:10.1016/j.epsl.2014.09.002.

5.0. Abstract

Morphological observations of scoria cones on Mars show that their cross-sectional shapes are different from those on Earth. Due to lower gravity and atmospheric pressure on Mars, particles are spread over a larger area than on Earth. Hence, erupted volumes are typically not large enough for the flank slopes to attain the angle of repose, in contrast to Earth where this is common. The distribution of ejected material forming scoria cones on Mars, therefore, is ruled mainly by ballistic distribution and not by redistribution of flank material by avalanching after the static angle of repose is reached. As a consequence, the flank slopes of the Martian scoria cones do not reach the critical angle of repose in spite of a large volume of ejected material. Therefore, the topography of scoria cones on Mars is governed mainly by ballistic distribution of ejected particles and is not influenced by redistribution of flank material by avalanching. The growth of a scoria cone can be studied numerically by tracking the ballistic trajectories and tracing the cumulative deposition of repeatedly ejected particles. We apply this approach to a specific volcanic field, Ulysses

Colles on Mars, and compare our numerical results with observations. The scoria cones in this region are not significantly affected by erosion and their morphological shape still preserves a record of physical conditions at the time of eruption. We demonstrate that the topography of these scoria cones can be rather well (with accuracy of ~10 m) reproduced provided that the ejection velocities are a factor of ~2 larger and the ejected particles are about ten times finer than typical on Earth, corresponding to a mean particle velocity of ~92 m/s and a real particle size of about 4 mm. This finding is in agreement with previous theoretical works that argued for larger magma fragmentation and higher ejection velocities on Mars than on Earth due to lower gravity and different environmental conditions.

5.1. Introduction and background

Until recently, the observational evidence of kilometer-scale edifices produced by explosive volcanic eruptions such as scoria cones, spatter cones, tuff cones and tuff rings on the martian surface was rare due to insufficient image resolution. On the other hand, theoretical predictions of their existence and relative importance had been developed in several studies (Wood, 1979; Dehn and Sheridan, 1990; Wilson and Head, 1994; Fagents and Wilson, 1996; Parfitt and Wilson, 2008). For a given erupted magma volume and volatile content, for example, considerable differences between pyroclastic cones on Earth and on Mars would be expected due to the different surface environment, in particular with respect to gravity and atmospheric pressure (e.g., Wilson and Head, 1994). Recent studies have expanded the known inventory of kilometer-scale volcanic edifices and have determined their morphologies (Bleacher et al., 2007; Keszthelyi et al., 2008; Meresse et al., 2008; Brož and Hauber, 2012, 2013). These studies revealed that scoria cones on Mars differ in morphology from those on Earth and display ~2.6 times larger basal diameters (Brož and Hauber, 2012).

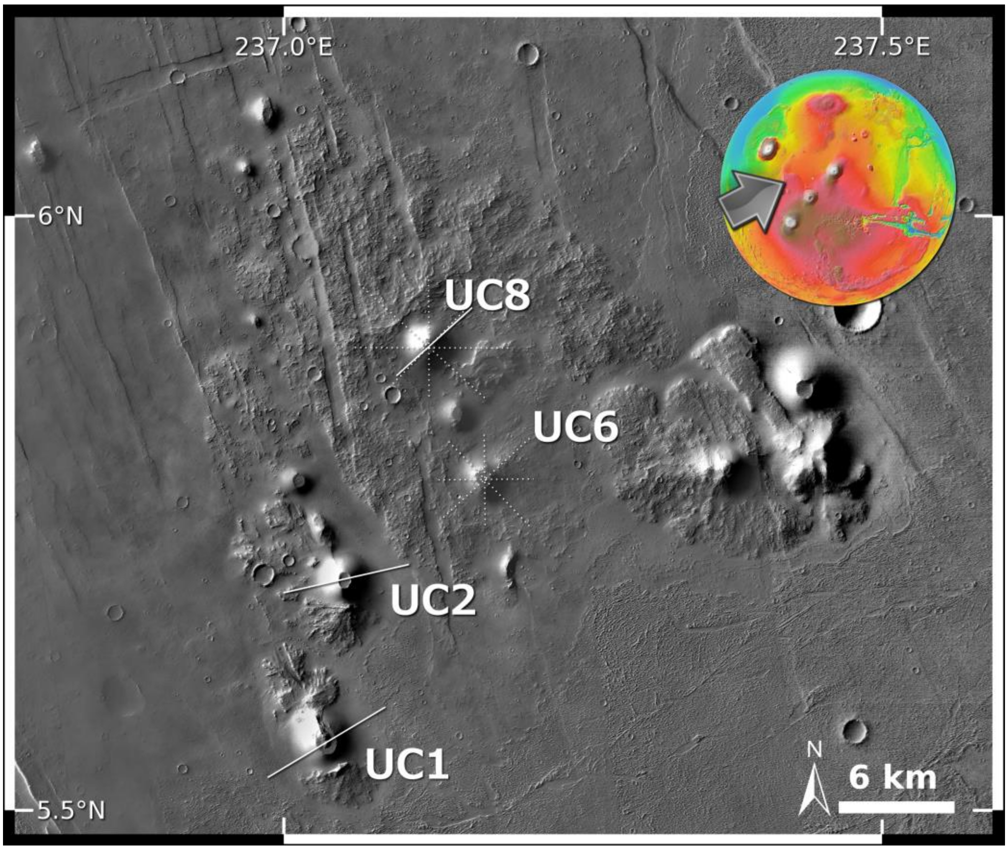

Fig. 5.1: Mosaic of CTX images covering Ulysses Colles in Tharsis on Mars. The field was described as volcanic in origin containing Martian equivalents to terrestrial scoria cones by Brož and Hauber (2012). Marked are cones used in this study with the position of HRSC DEM profiles (continuous lines) and CTX DEM profiles (dashed lines). Centered 5.8°N, 237.1°E, the mosaic of images number: CTX P19 008262 1862, P22 009554 1858 and G11 022582 1863.

Dehn and Sheridan (1990) modeled the shape of scoria cones on different terrestrial bodies (Mars, Earth and Moon) and predicted that, for a given magma volume, basal diameters (W_{CO}) of pyroclastic cones on Mars should be two to three times larger than on Earth. For a given eruption volume, the height (H_{CO}) of cones should be lower on Mars than on Earth because of the lower gravity and the resulting wider dispersal of particles (Wood, 1979). Wilson and Head (1994) estimated that for the same erupted volume the height of cones on Mars should be four times lower than on Earth, and central craters more than five times wider. Dehn and Sheridan (1990) suggest that martian cones should be more than 100 m high and display well-developed central craters. Measurements of cones in the Ulysses Colles region (5.75°N, 237.1°E, Fig. 5.1), a volcanic field on Tharsis, showed that the average W_{CO} of the studied cones is ~2.6 times larger than for typical terrestrial scoria cones (Brož and Hauber, 2012), numerically corresponding with previously predicted values (Dehn and Sheridan, 1990). However, the martian cones are up to 650 m high, clearly contradicting the low heights predicted by Wood (1979b) and Wilson and Head (1994).

Scoria cones consist mainly of tephra particles that are produced via Strombolian eruptions by magma degassing and associated fragmentation (Parfitt and Wilson, 2008). Two main models exist to describe the exact mechanism of fragmentation (Jaupart and Vergniolle, 1989; Parfitt and Wilson, 2008), but both models predict the generation of a wide size range of pyroclasts that are ejected from a vent by explosive eruptions. Depending on particle size, tephra particles are transported away by two main processes. The finer particles are entrained in buoyant convective plumes and are transported far away from the vent by wind transport (Carey and Sparks, 1986; Wilson and Head, 1994; Kerber et al., 2013). The coarser size fractions (> ~1 cm) are mostly ejected on ballistic paths (Saunderson, 2008) close to the vent (Wilson and Head, 1994; Parfitt and Wilson, 2008), where they form a scoria cone. An alternative explanation of scoria cone formation, the jet fallout model, was proposed by Riedel et al. (2003). This model suggests that at least some parts of the cones grow by accumulation of clasts falling from an eruption jet column above the vent. Deposition by jet fallout was observed in situ at some scoria cones (Valentine et al., 2005) as partly contributing factor. Also, at least 50% of the ejected volume might be non-ballistically deposited around the cone as a thin ash blanket (Riedel et al., 2003), which would be hardly observable by remote sensing data in topographic profiles. The distribution of ballistically ejected material depends on particle size and density, initial velocity, the angle of ejection from the vent and the frequency of collisions between particles (Tsunematsu et al., 2014).

The final shape of the cone is controlled by the ballistic range of scoria particles and the total volume of generated scoria. This is only valid, however, until a critical volume of deposited material is reached, after which the cone flank attains the static angle of repose (~30°) and avalanching of tephra takes over as the main process determining the shape of the cone. The later redistribution is dependent on the maximum flank slope angle at which the material

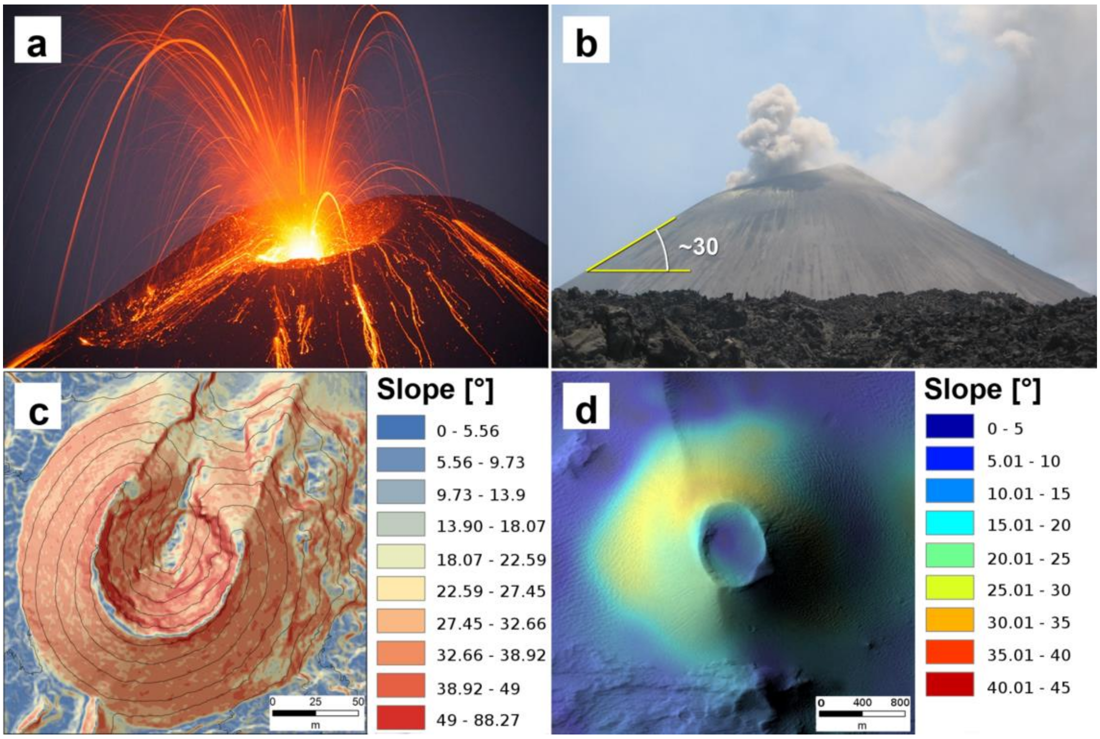

Figure 5.2: (a) Strombolian eruption at Anak Krakatoa, Indonesia in June 2009 (Image: Tom Pfeiffer). Note the ballistic trajectories highlighted in this evening photograph. (b) Scoria cone on Barren Island (Andaman Sea, India). The uniform flank slopes perfectly correspond to the angle of repose (~30°). Image courtesy of Hetu Sheth. (c) Slope map of Puu Kapanaha, a scoria cone at the eastern flank of Mauna Loa, Hawai`i (19.5474°N, 155.4557°W). Slopes were calculated on the basis of an airborne LIDAR-based Digital Elevation Model (DEM) (Hawaii Big Island Lidar Survey, doi: 10.5069/G9DZ067X; data provided by NCALM project, survey date 06/21/2009 - 06/27/2009). A best linear fit to the flank slopes yields 33°. Slopes increase to >40° very close to the summit, probably caused by spatter material that stabilizes the loose scoria particles. The black lines represent the counter lines with interval to be 5 m. (d) Cone UC 2 in the Ulysses Colles volcanic field. Slopes are derived from HRSC DEM. Background image is part of CTX image P22_009554_1858 (5.70°N, 237.04°E).

comes to rest, represented by the dynamic angle of repose (Riedel et al., 2003; Kleinhans et al., 2011). There is a debate whether the angle of repose is gravitationally dependent (Kleinhans et al., 2011) or not (Atwood-Stone and McEwen, 2013), however both studies confirm that the angle of repose for scoria material should be very similar for Earth and Mars.

Observations of martian scoria cones raise the question of why their shapes are so markedly different from scoria cones on Earth. This study focuses on this discrepancy, based on numerical modeling of tephra particle ejection and dispersion around the vent that builds on the work of several authors (e.g., McGetchin et al., 1974; Dehn and Sheridan, 1990; Riedel et al., 2003, Saunderson, 2008; Harris et al., 2012 and references therein). However, the present study adds to our understanding of scoria cone growth on Mars because (i) it point out the significance of larger dispersion of ejected material for the evolution of flank slopes (Fig. 5.2), (ii) compares modeling results with real morphologies of martian scoria cones, which was previously not possible, (iii) refines theoretical predictions about initial conditions in the time of explosive eruptions and (iv) shows predictions of the shape of martian scoria cones for different amounts of ejected material.

5.2. Data and methods

5.2.1. Numerical model

Scoria cones are built by clastic material ejected from the vent along ballistic trajectories. The final shape of the cone is given by the ballistic range of particles, depending mainly on ejection velocity, atmospheric drag and gravity acceleration, and by the subsequent redistribution of the material by avalanches, which occurs when the slope of the cone exceeds the angle of repose. The track of a particle can be reconstructed by numerical modeling (e.g., Riedel et al., 2003; Saunderson, 2006; Harris et al., 2012, and references therein; Tsunematsu et al., 2014). In the present study, we will deliberately construct our physical model of cone growth as simply as possible to minimize the role of speculative parameters which are poorly understood even on Earth, let alone on Mars.

To a first approximation, the deceleration of the ejected particle due to atmospheric drag is given by (e.g., Parfitt and Wilson, 2008):

$$\boldsymbol{a_d} = -\frac{3}{4}\frac{C_d}{d}\frac{\rho_{air}}{\rho_{rock}}\, v\, \boldsymbol{v} \tag{5.1}$$

where $\boldsymbol{v}$ is the particle velocity vector, v is its magnitude, C_d is the drag coefficient, d is the particle size, and ρ_{air} and ρ_{rock} are the density of the air and the particle, respectively. The drag coefficient, C_d, depends on the shape, orientation and roughness of the particle and varies with the Reynolds (*Re*) and Mach (*M*) numbers. For a spherical particle, low *M*, and *Re* between about 300 and 2×10^5, C_d is nearly constant (≈ 0.5; Bird et al., 1960). This range of *Re* corresponds well to recent conditions on Mars, provided that $d \gtrsim 0.01$ m and $v \gtrsim 30$ m/s. The drag coefficients for realistic volcanic fragments are usually between the values for spheres and cubes (Alatorre-Ibargüengoitia and Delgado-Granados, 2006). In this study, we use $C_d = 0.7$. The atmospheric density ρ_{air} of 0.01 kg/m^3 is chosen to correspond to the present-day conditions on Mars and is corrected for the altitude of Ulysses Colles situated ~4.5 km above the martian datum (Brož and Hauber, 2012). The ejected material is assumed to have a uniform density ρ_{rock} of 850 kg/m^3 (Lautze and Houghton, 2005; Harris et al., 2012).

It should be noted that for a given value of velocity *v*, the atmospheric drag is given by a combination of four parameters, C_d, d, ρ_{air} and ρ_{rock}. While parameters C_d and ρ_{rock} are rather well determined and their variations can affect the estimate of atmospheric drag by tens of percent at most, the values of the other two parameters, ρ_{air} and d, are rather uncertain and can vary by orders of magnitude. The particle size on Mars can significantly differ from the values observed on Earth (Wilson and Head, 1994), and the density of air at the time of volcanic activity could be higher than at present. Moreover, there is a trade-off between the two parameters: the ballistic trajectory does not depend on the individual values of ρ_{air} and d, but only on their ratio. That is why, in this study, we keep the values of parameters ρ_{rock}, C_d and ρ_{air} constant and we only vary the particle size and the initial velocity. The results which we present below for the particle size can then be arbitrarily reinterpreted in terms of the other parameters.

In calculating the ballistic trajectories, we neglect the interaction between particles during the ballistic flight (Vanderkluysen et al., 2012; Tsunematsu et al., 2014) and we do not take into account the effect of drag reduction near the vent (Fagents and Wilson, 1993). Both effects are difficult to quantify under martian conditions and are probably of only minor importance. We have investigated the impact of the latter effect numerically and found only a small (<10%) difference between the cases with and without the reduced drag if the radius of the domain where the drag is significantly reduced was smaller than 500 m. This is in agreement with an estimate based on eq. (5) in Fagents and Wilson (1993) if we take into account that the clast range observed in the Ulysses Colles region is ~1500 m or larger.

The statistical distribution of size and initial (ejection) velocity of pyroclastic particles on Mars is not known. Using the data obtained during normal explosions at Stromboli, Harris et al. (2012) showed that these two quantities are only weakly correlated (see their Fig. 10) and questioned the traditional view that the ejection velocity linearly decreases with the square root of the particle size (Steinberg and Babenko, 1978). Harris et al. (2012) suggest that the relationship between these quantities is more complex and involves also other parameters, namely gas density and gas jet velocity, which significantly vary during th volcanic event and thus cannot be used as constant parameters. For simplicity and to avoid over-parameterization, we assume in the present study that the ejection velocity does not depend on the particle diameter and each of the two quantities can be independently described by a log-normal probability distribution,

$$p(x) = const\ exp\ [-\frac{[log_{10}(x) - log_{10}(\mu)]^2}{2\sigma^2}] \tag{5.2}$$

where x is the variable, and $\log_{10}(\mu)$ and σ denote the mean and the standard deviation, respectively. The values of μ and σ are chosen so that the probability functions roughly fit the experimental data obtained for Stromboli by Harris et al. (2012). The mean size of particles is $\mu = 0.04$ m with a standard deviation $\sigma = 0.3$ (cf. Fig. 9a in Harris et al., 2012). The log-normal distribution of ejection velocity is characterized by $\mu = 46$ m/s and $\sigma = 0.2$ (cf. Table 3 in Harris et al., 2012). Only particles with sizes smaller than 0.3 m and ejection velocities between 10-300 m/s are considered. Besides this 'reference model', we also test ejection velocities which are up to three times larger and particle sizes which are up to 100 times smaller than in the reference model. This choice is motivated by the predictions made by Wilson and Head (1994) who argued for larger magma fragmentation due to the lower surface atmospheric pressure. In the result section, the values of ejection velocity and particle size will often be presented in a normalized form, related to the reference model. For example, the normalized velocity of 2 means that the value of μ in eq. (5.2) is chosen to be 92 m/s, thus two times larger than in the reference model. For the statistical distribution of ejection angles, $p(\alpha)$, we consider two set-ups, both showing a Gaussian distribution on a cross-section through the center of the cone,

$$p(\alpha) = const\ exp\ (-\frac{\alpha^2}{2\sigma^2{}_\alpha}) \tag{5.3}$$

but differing with respect to the parameter σ_α. The first set-up with σ_α=15.5º (hereinafter referred to as ECN – 'Ejection Cone – Narrow') roughly corresponds to a normal Strombolian erruption as observed by Gouhier and Donnadieu (2010), while the other set-up (σ_α=31º, denoted by the abbreviation ECW – 'Ejection Cone – Wide') reflects the possibility that dispersion of ejection angles may be wider on terrestrial bodies with low atmospheric pressures than on Earth (Glaze and Bologa, 2000; Wilson and Head, 2007). In both cases, only the ejection angles smaller than 45º are considered.

In calculating the shape of the cone for a given set of model parameters, we assume that each ejected particle is stored at the place where it lands, and its distance from the center of the cone is fully determined by its ballistic trajectory and the current topography of the cone. The vertical coordinate of the ejection point as well as of the spot where the ejected particle hits the surface is gradually modified, in agreement with the growth of the cone. No redistribution by avalanches is considered. The particle ejection stops when the model height reaches the real height of the observed cone at the Ulysses Colles volcanic field. Therefore, the model is not limited by the volume of erupted particles – the volume increases continuously as needed to reach the required height.

The topographic height *h* of the cone at a point at distance *r* from the center can be computed as the total volume of the material stored in annulus with radii $r - \Delta r/2$ and $r + \Delta r/2$ divided by the area *S* of the annulus, $S = 2\pi r\Delta r$. If the particles are approximately spherical, we obtain,

$$h(r) = \frac{c_s}{12r\Delta r} = \frac{const}{r} \sum_i d_i^3 \tag{5.4}$$

where d_i denotes the size of individual particles stored in the annulus. The coefficient c_s characterizes the storage properties of clastic material and generally depends on the shape of particles, their statistical distribution and the total height of the stored material. For simplicity, we assume c_s to be a constant in our study. The total number of particles used in predicting the shape of one cone is ~10^7 and Δr is chosen to be 10 m.

Table 5.1: Key parameters used for modeling of scoria cones on Mars.

Parameter	Earth	Mars	Comment
Drag coefficient	0.5 to 1 with a mean value of ~0.7 for scoria particles	0.7	The average terrestrial value is used due to a lack of in situ data.
Atmospheric density [kg/m^3]	1.2	0.01	Martian value corrected for altitude of 4500 m (position of Ulysses Colles).
Rock density [kg/m^3]	700 to 1000	850	The average terrestrial value is used due to a lack of in situ data (Lautze and Houghton, 2005; Harris et al., 2012).
Gravity [m/s^2]	9.81	3.71	
Initial velocity	log-normal distribution with a peak at 46 m/s	increased by a factor of 1-3	Terrestrial distribution is based on observation by Harris et al. (2012). Due to lower atmospheric density and resulting larger gas expansion, initial ejection velocities are expected higher on Mars than on Earth (Wilson and Head, 1994).
Particles size	log-normal distribution with a peak at 4 cm	decreased by a factor of 1-100	Distribution based on Harris et al. (2012). A higher degree of magma fragmentation is expected on Mars due to the lower atmospheric pressure (Wilson and Head, 1994).
Angle of repose	30°-33°	~30°	Kleinhans et al. (2011), Atwood-Stone and McEwen et al. (2013)
Ejection angles	Narrow ejection cone (see eq. 5.3. for details)	Wide ejection cone (see eq. 5.3. for details)	Gouhier and Donnadieu (2010), Glaze and Bologa (2000), Wilson and Head, (2007)

5.2.2. Topographic data

The topographic profiles of three cones in Ulysses Colles (UC1, UC2 and UC8) were determined from HRSC stereo images (Jaumann et al., 2007) and derived gridded digital elevation models (DEM). HRSC DEM are interpolated from 3D points with an average intersection error of 12.6 m and have a regular grid spacing of 50 to 100 m (Gwinner et al., 2010). In the case of cones UC6 and UC8, additional CTX DEM were used to test the precision of HRSC DEM for kilometer-scale edifices. High-resolution topographic data were based on CTX stereo-derived DEM, which were computed from CTX stereo pairs (Malin et al., 2007) using the methods described, e.g., in Moratto et al. (2010). CTX DEM reach a spatial resolution of ~10 m/pixel and the vertical accuracy of the stereo-derived CTX DEM can be roughly estimated to be around few meters.

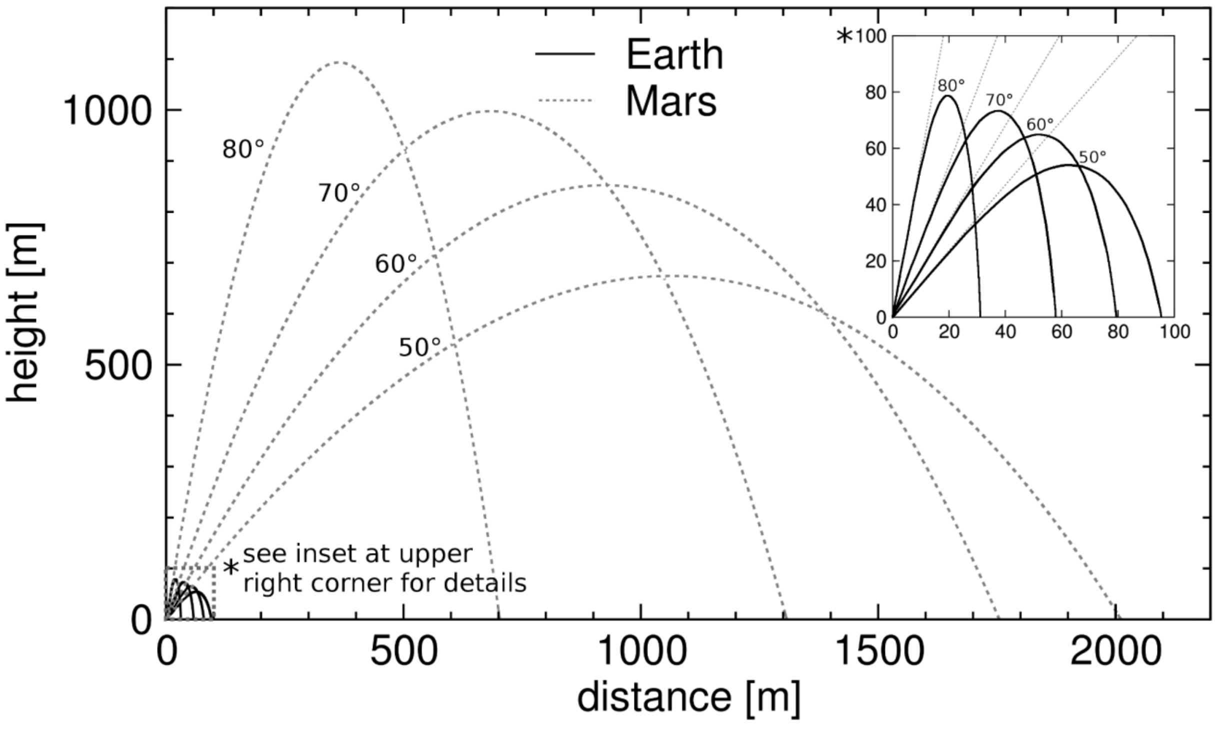

Figure 5.3: Ballistic pathways calculated for 4 cm-diameter particles with a density of 850 kg/m^3, ejected with velocities of 100 m/s at different ejection angles under present Martian (dashed lines) and terrestrial (black lines) environmental conditions (see Tab. 5.1). Note the significant differences in the transport distance between the planets.

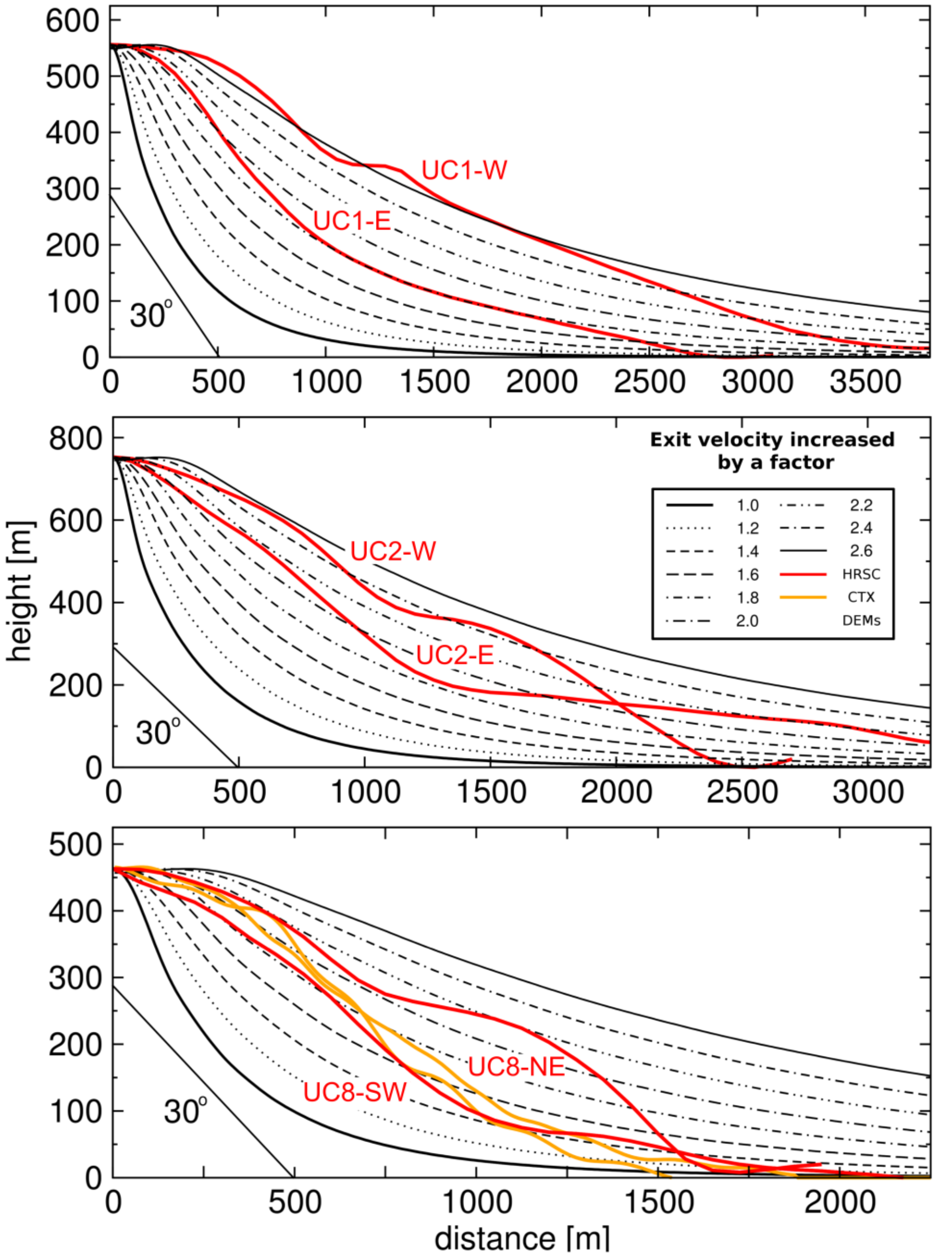

Figure 5.4: Comparison of the observed topographic profiles (HRSC data in red, CTX data in orange) of Martian cones in the Ulysses Colles region (upper panel: cone UC1, middle panel: cone UC2 and lower panel: cone UC 8, see Fig. 5.1 for the position of these cones) with the profiles of the same height computed for different ejection velocities (black lines) in the ECW set-up. If typical Earth-like ejection velocities are used in the current Martian environment (bold solid black line), the resulting shape is inconsistent with the observations. To reproduce the observed shapes, the initial ejection velocities must be increased (dashed lines). The relative (i.e. point-to-point) topographic errors are small as compared to the overall profile shape and are not taken into account. The best fit is obtained for initial velocities that are about two times larger than on Earth, in agreement with the theoretical prediction by Wilson and Head (1994). In all simulations, a particle size distribution (eq. 5.2) with $\mu = 4$ cm is considered.

5.3. Results

A comparison of ballistic curves on Mars and Earth (Fig. 5.3) reveals that the maximum distance of ballistic transport is much larger on Mars than on Earth. While a 4 cm-particle ejected with an initial velocity of 100 m/s travels on Earth less than 100 m from the vent, the same particle reaches a distance of 2 km on Mars, thus about 20 times further. This difference is related to the lower values of atmospheric density and gravitational acceleration on Mars than on Earth (cf. Wood, 1979; Dehn and Sheridan, 1990; Wilson and Head, 1994). The ejected material is dispersed on Mars over a much larger area than on Earth which explains why the scoria cones observed on Mars are so wide, with a mean basal diameter of 1,500 m for cones in Hydraotes Chaos (Meresse et al., 2008) and 2,300 m for cones in Ulysses Colles (Brož and Hauber, 2012). Since the area of particle deposition increases with the square of the ballistic range, the total volume of material needed to build a steep cone with flank slopes reaching the angle of repose would have to be significantly (about two orders of magnitude) larger on Mars than on Earth. Considering this, it is not surprising that the scoria cones on Mars are less steep than on Earth and their slopes remain below the angle of repose (Fig. 5.2).

In Fig. 5.4, we compare the shapes of three scoria cones observed in Ulysses Colles (red and orange lines) with those predicted numerically for the wide ejection cone (ECW), a particle size of 4 cm and different ejection velocity distributions (plotted in black). If the particles are ejected with a similar initial velocity as on Earth (mean velocity of 46 m/s), the resulting cone is steeper and has a smaller W_{CO} than actually observed on Mars. However, if we increase the ejection velocity by a factor of about two (cf. Wilson and Head, 1994; Fagents and Wilson, 1996), we obtain a cone which is similar in shape to the observation and whose slope never exceeds the angle of repose.

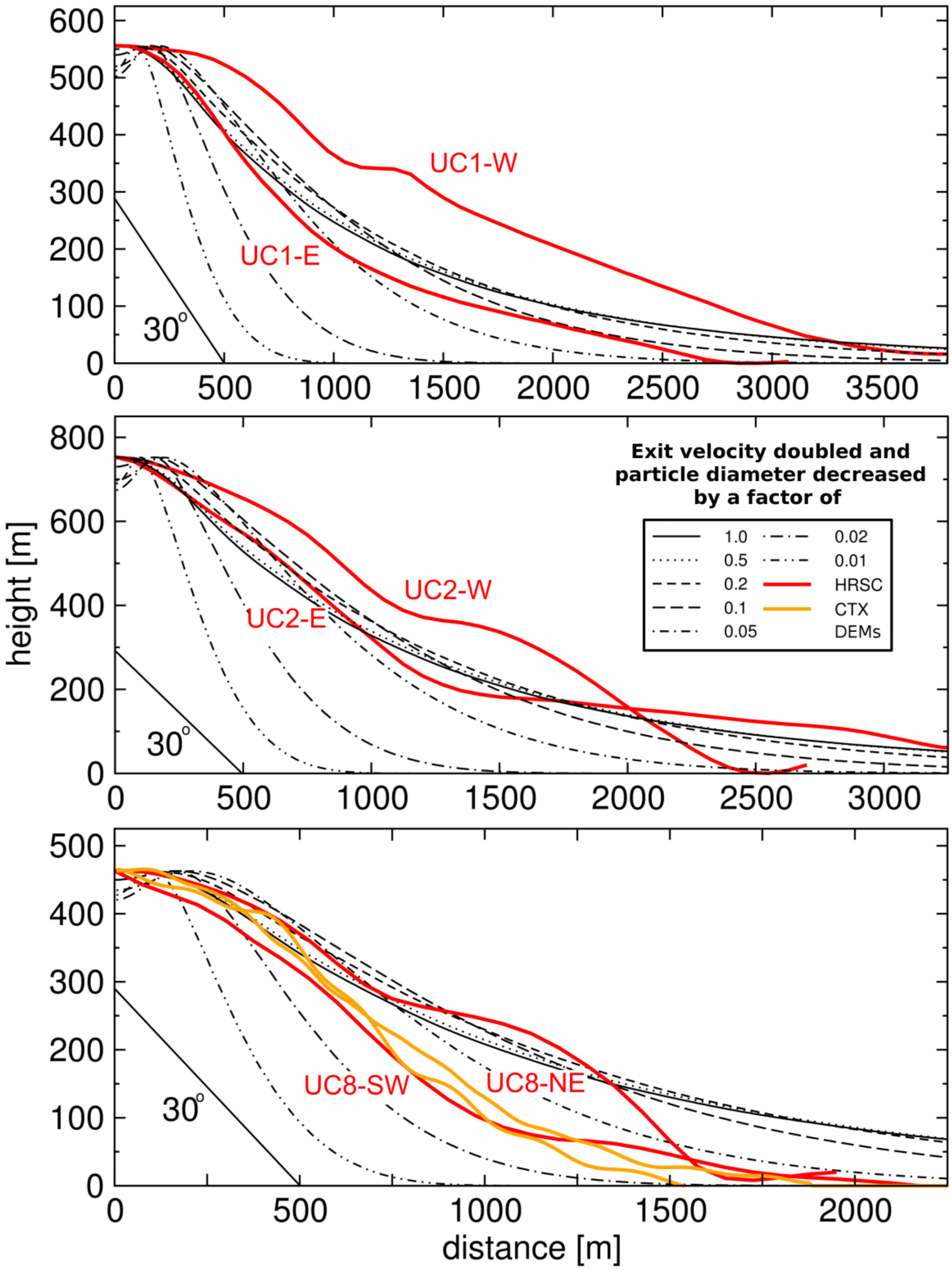

Figure 5.5: The same as in Fig. 5.4 but the model cones (black lines) are computed for two times larger initial velocity than on Earth and various particle-size distributions. The solid black line corresponds to the particle-size distribution as known from Earth while various dashed lines show the cones predicted for particles smaller by a factor of 2, 5, 10, 20, 50, and 100.

The shape of the cone is controlled not only by the initial velocities of ejected particles but also by the distribution of the particle size. In Figure 5.5, we consider an initial velocity which is increased by a factor of two in comparison with the reference model and we test different particle-size distributions in which the particle size is decreased by a factor between 1 and 100. As in Fig. 5.4, the calculation is carried out for the ECW model of ejection angles. When the particles are smaller by a factor of 100, they are deposited in the close vicinity of the vent, forming a cone with slope exceeding 30°. A similar result, though with a somewhat broader W_{CO}, is obtained for particles that are 50 times smaller than in the reference model. Particles that are smaller by a factor of 20, 10 (a factor predicted by Wilson and Head, 1994) and 5, travel further from the vent than finer particles and reach distances which are roughly in agreement with the observation. They are emplaced over a wider area forming a cone where the angle of repose is not reached. A reasonable fit to the observations is also obtained for the particle sizes that are similar as or only slightly (by a factor of 2) smaller than on Earth. However, since the ballistic range of such particles is larger than in the previous case, the agreement between prediction and observation may be deteriorated in the distal zone (see the bottom panel in Fig. 5.5).

The sensitivity of the predicted topographies on particle size and ejection velocity, demonstrated in Figs. 5.4 and 5.5, motivated us to determine those values of these two parameters that yield the best fit of the predicted cone to the observation. We use the standard formulation of the inverse problem, based on the least-squares minimization of the misfit between predicted and observed data,

$$S^2 = \frac{1}{R} \int_0^R \left[h^{obs}(r) - h_{v,d}^{pred}(r)\right]^2 dr \tag{5.5}$$

where h^{obs} is the averaged topography of the cone, $h_{v,d}^{pred}$ is the topography predicted for ejection velocity v and particle size d, both characterized by a log-normal distribution (see

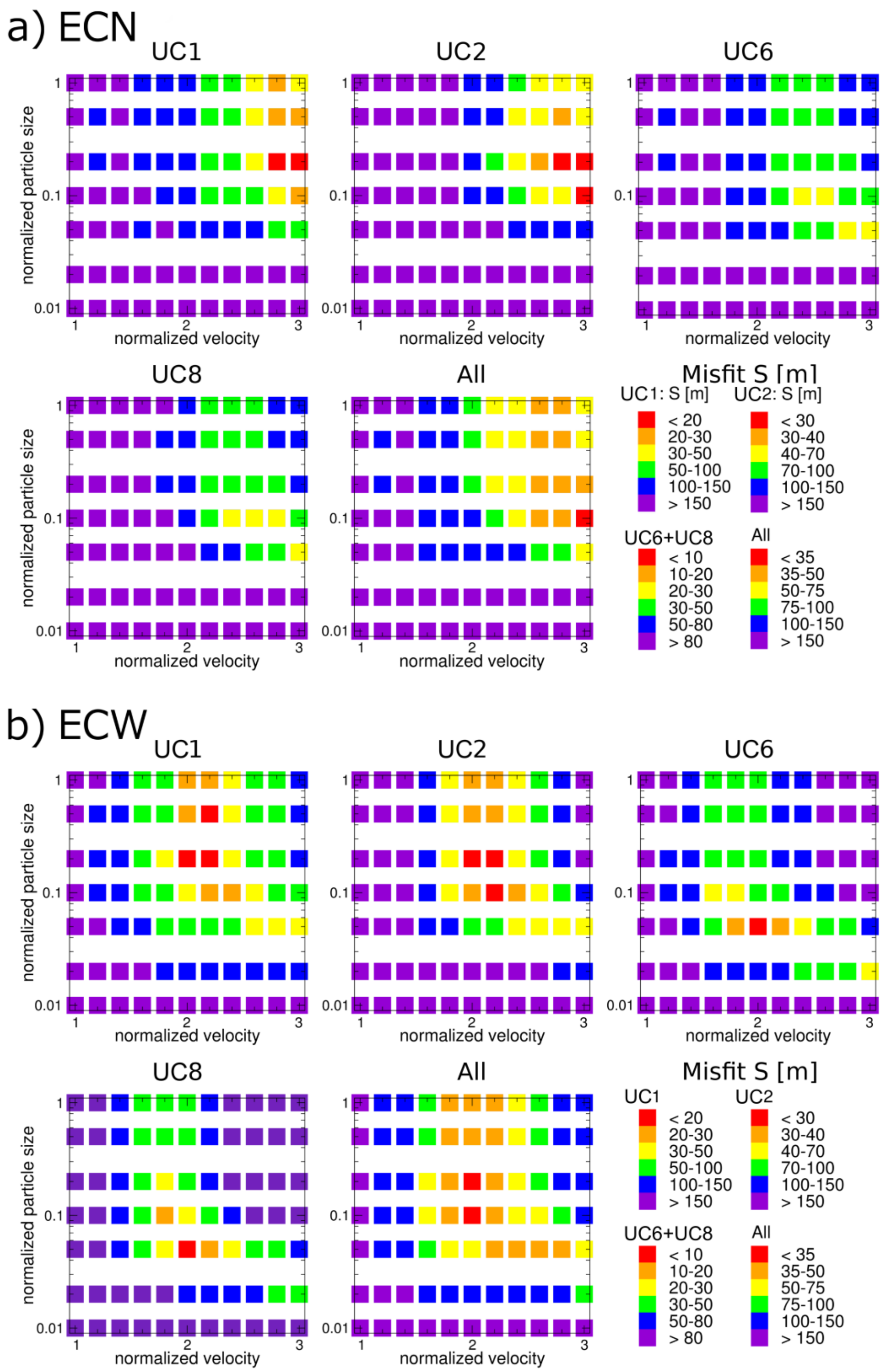

Figure 5.6: Misfit S, eq. (5.5), as a function of normalized ejection velocity and particle size evaluated for ejection angle distributions ECN and ECW. Panel UC1, UC 2, UC 6 and UC 8 show the results obtained for individual scoria cones in Ulysses Colles, panel "All" comprises all available data. The best agreement with observation (red squares) is reached for ejection velocity that is at least 2 larger than on Earth while the best-fitting particle size ranges between 0.05 and 0.5 of the terrestrial value.

section 5.2.1.), and R denotes the horizontal extent of the observed cone. The minimum value of S is found separately for each of scoria cones UC1, UC2, UC6 and UC8 by a systematic exploration of the parameter space. The results of the inversion are shown in Fig. 5.6 where the misfit S is plotted as a function of normalized ejection velocity and particle size separately for the narrow (ECN) and wide (ECW) ejection cone. Note that the agreement between prediction and observation is especially good for cones UC6 and UC8 in the ESW set-up where the best-fitting predicted topography differs from the observed one by less than 10 m in average. In all cases considered, the best fit to observation is found for velocities that are at least about two times larger than on Earth. The optimum value of the normalized particle size ranges between 0.05 (cones UC6 and UC8) and 0.2 (cones UC1 and UC2). When all available data are included (Fig. 5.6, panel 'All'), the preferred value of the normalized particle size is between 0.1 and 0.2, corresponding to a real particle size between 4 and 8 mm. Note that the optimum particle size obtained from the inversion is the same for both ejection angle distributions considered. The choice of parameter σ_α in eq. (5.3) thus only affects the resultant ejection velocities which are larger for the narrow ejection cone.

Figure 5.7 shows the numerical simulation of a gradual growth of a scoria cone until the instant when the slope of the flank exceeds an angle of 30˚. The simulation of the cone on Earth (top panel, calculated for model ECN) is carried out for the reference values of parameters d and v while for Mars (bottom panel, calculated for ECW) the values that best predict the shape of cone UC8 are considered. For the modeled terrestrial cones, the angle of 30˚ is attained after deposition of about 0.00084 km^3 of clastic material when the cone is ~40 m high. In contrast, more than 2.17 km^3 of material, corresponding to a height of about 600 m, are needed for the cone on Mars to reach the angle of repose. Such an amount of material was not available on Mars as indicated by comparison of our model with the observed shape of cone UC8 (plotted in red).

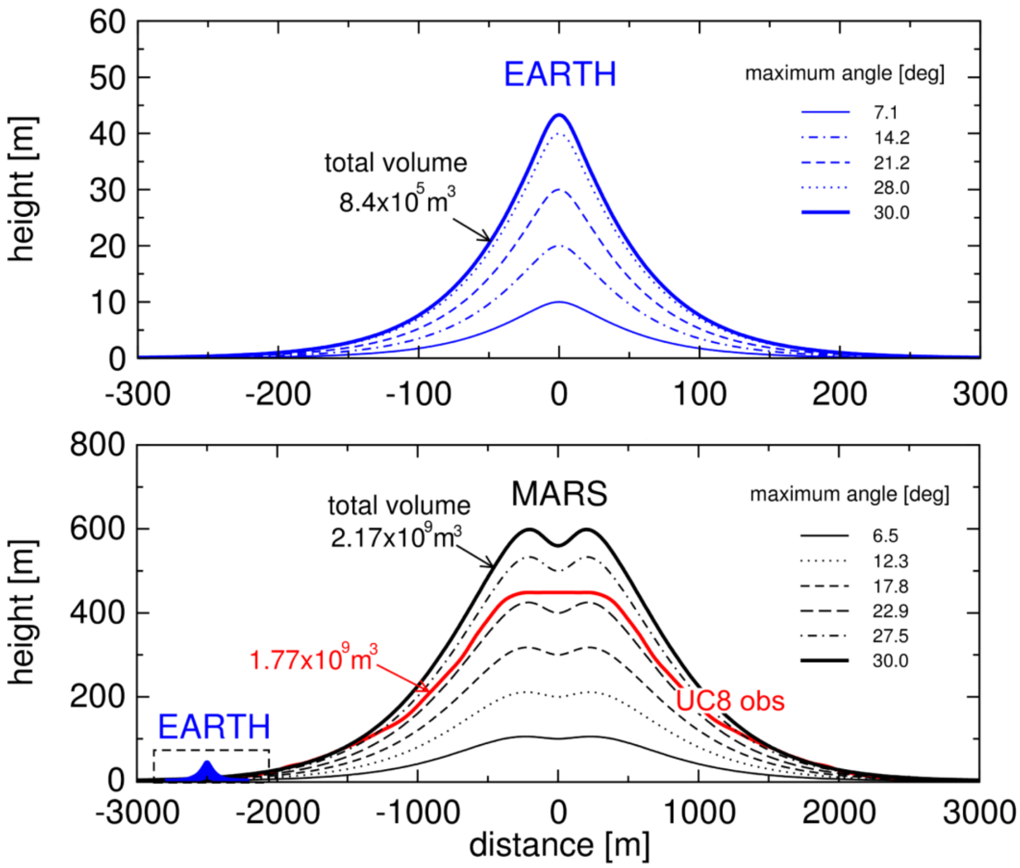

Figure 5.7: Evolution of scoria cones on Earth (top) and Mars (bottom) until the angle of repose (30˚) is reached. The cones are predicted for the reference model and the best-fitting parameters obtained for cone UC8 (Fig. 5.6), respectively. Dashed lines illustrate the gradual growth of the cone. The maximum angle attained for each profile is given in the legend. On Earth, the angle of repose is reached (blue solid line) when the cone is around ~40-m high and its volume is about 8.4×10^5 m^3. The critical height of a cone on Mars (black solid line) is ~600 m, and the angle of repose is reached when the volume of deposited material is about 2.17×10^9 m^3, thus four orders of magnitude larger than typical on Earth. The red profile shows the average topography of scoria cone UC8 based on CTX DEM. Note that the vertical scales are significantly magnified relative to the horizontal scales.

5.4. Discussion

5.4.1. Interpretation of the results

As shown in Fig. 5.3, the area of dispersal increases significantly in martian environmental conditions, and the total volume required to achieve the angle of repose over the entire flank of the cone increases as well. This modeling result explains the different shapes of scoria cones on Mars and Earth. If the typical terrestrial amount of tephra is spread over a wider area on Mars, the resulting cone has a different morphology from that on Earth, simply because there is less material available in the close vicinity of vent. The outcome will be an edifice with gentler flank slopes and a low topographic profile (Fig. 5.7). Therefore, more material needs to be erupted to build a cone with flank slopes that are dominated by avalanching.

If the cones of Ulysses Colles (Brož and Hauber, 2012) and morphologically similar cones in Hydraotes Chaos (0.07°N; 326.19°E; Meresse et al., 2008) represent typical or average-sized pyroclastic cones on Mars, monogenetic explosive volcanism is more voluminous on Mars than on Earth. For example, cone UC2 in Ulysses Colles has a height of ~650 m and basal diameter of 3,200 m with flank slope of ~27.5°, therefore its total volume is around 2.25 km^3 (Brož and Hauber, 2012). This is at least two orders of magnitude more than the average volume of terrestrial scoria cones (0.046 km^3, determined from 986 edifices, data from Pike, 1978 and Hasenaka and Carmichael, 1985). Much more material reached the surface during explosive eruptions and more voluminous scoria cones were created on Mars as compared with Earth. One possible explanation is that the lower acceleration due to gravity on Mars enables the formation and ascent of larger magma bodies into the crust, and also the formation of wider feeder dikes (Wilson and Head, 1994). On the other hand, if the average volume of explosively erupted material on Mars was smaller, and the observed edifices in Ulysses Colles and Hydraotes Chaos have atypically large volumes, smaller scoria cones must have been formed, too. Their identification in remote sensing data may be complicated, either due to degradational processes or due to their low topographic profiles and gently sloping flanks (as visible on Fig. 5.7).

The growth of cones is initially controlled by the ejection velocities and the deposition mechanism of particles, until the amount of material is critical on the flanks and reaches the static angle of repose. If the angle of repose is reached, future growth is controlled by particle avalanching, and the shape of the cone cannot be used for ballistic pathway modeling any more (Riedel et al., 2003). The critical value for tephra composing terrestrial scoria cones was established to be ~26.4° for the case of pristine scoria cones (Porter, 1972; Hooper and Sheridan, 1998), with the slope angle mean maximum reaching 29.7°±4.2° (Hooper and Sheridan, 1998). However, the slope angle of flanks is partly dependent on the sizes of particles (Wood, 1980a) and on the amount of spatter material, especially around the top of a cone (Porter, 1972). Therefore a value of 30° to 33° is often used as a characteristic angle of repose (Riedel et al., 2003). It needs to be emphasized again that these values are valid for pristine scoria cones, and older and eroded cones display lower flank slopes due to material transport and dispersion (Hooper and Sheridan, 1998).

Our study shows that the static angle of repose causing material avalanching is not reached during martian cone growth over the entire length of flanks (Figs. 5.2 and 5.7). Higher angles might be reached locally in the steepest parts close to the top of the cone. This is a common situation on Earth, where the deposition of spatter leads to a steepening of the flank slopes near the vent (Porter, 1972). However, the accumulation of material per unit area in a given time period is a function of the distance from the vent (i.e. proximal deposition rates are higher than distal ones). Such non-uniform deposition rates cause the formation of a small and relatively steeper conical body around the vent (Fig. 5.7). As the eruption continues, more material is deposited and a situation might occur where a small cone near the vent reaches the angle of repose and redeposition of the material by avalanching takes place. On Earth, the ballistically-dominated cone is covered by the newly formed cone dominated by avalanching rather soon, because material is ejected only few dozen meters from the vent (Figs. 5.3 and 5.7, see also McGetchin et al., 1974). On the other hand, this is not the case on Mars because material is spread over a much larger area. Hence, the cone dominated by avalanching does not overlie the entire extent of the ballistically-dominated cone. It has to be noted that such cones dominated by avalanching might develop in the central areas of martian scoria cones, as suggested by the part of profile of the cone UC2 in Fig. 5.4.

Due to a lack of information on flank slopes, it had not previously been recognized that martian scoria cones do not reach the critical angle of repose along their entire length of flanks. The shapes of the cones, therefore, preserve information about explosive eruption processes (initial velocities of ejected particles and their sizes as demonstrated in Fig. 5.6), which can be reconstructed by numerical modeling of ballistic pathways (Fig. 5.4). In turn, if ejection velocities and clast sizes are given or assumed, the distribution of ballistically transported clasts may be used to constrain the atmospheric paleo-pressure at the time of the eruption (Carey and Sparks, 1986, and references therein). The latter approach was applied by Manga et al. (2012) in their study of a volcanic bomb in the Home Plate outcrop in Gusev Crater. The model presented here may also be applied to other terrestrial bodies where results of explosive volcanism were described, for example to volcanic fields containing scoria cones in the Marius Hills on the Moon (Lawrence et al., 2013).

5.4.2. Limitations of the numerical model

As already discussed in section 2.1, our numerical model is deliberately simplified to allow efficient exploration of the parameter space. Before we proceeded to modeling the martian cones we carefully examined the relative importance of individual parameters in our ballistic model. By performing a number of numerical tests (not shown here), we found that the shape of the predicted cone is mainly determined by statistical distributions of ejection angle, initial velocity and particle size. The statistical distribution of ejection angles on Mars is not known. To assess the effect of the ejection angle distribution on the shape of the predicted scoria cone, we consider two models of ejection angles showing a Gaussian distribution. The first one roughly corresponds to the ejection cones observed on the Earth (Gouhier and Donnadieu, 2010) while the other one assumes a two-times wider distribution of ejection angles than on Earth (cf. Glaze and Bologa, 2000; Wilson and Head, 2007). As shown in Fig. 5.6, both these distributions rather well predict the observed shapes of the scoria cones in the Ulysses Colles region and give the same estimates of the particle size. The only difference is that the narrow ejection cone prefers somewhat higher ejection velocities (factor of 2.4-3.0 larger than on Earth) in comparison with the case when the wide ejection cone is considered (factor of ~2).

In our model, the ejection velocity is considered independent of the particle size. Thi choice is motivated by recent findings by Harris et al. (2012), see also discussion in section 2.1, and indirectly justified by our numerical tests which gave unsatisfactory results if the traditional relationship between ejection velocity and particle size (Steinberg and Babenko, 1978) was considered.

We assume that the ejection velocity and particle size have log-normal distributions. The scale parameters (σ in eq. 5.2) of these distributions are estimated from the data published in Harris et al. (2012) and they are not varied in our parametric study. We admit that the value of parameter σ, if significantly changed, can influence the prediction of the cone shape. In contrast, variations of the drag coefficient are of minor importance provided that its value ranges in a similar manner as on Earth. Our numerical tests also suggest that, to a first approximation, we can neglect the effect of drag reduction near the vent, variations of the atmospheric drag along the ballistic path as well as the dependence of the storage coefficient, eq. (5.4), on the local particle-size statistics. The results of our inversion (Fig. 5.6) prefer the models with high ejection velocities where the radius of the drag reduction zone is small in comparison with the horizontal size of the volcano. We note, however, that the drag reduction would be more important for less-energetic explosions that eject particles with small velocities, because the neglected zone would then be a larger fraction of the total clast range.

Another effect which is not considered in our study is the possible interaction between particles during the flight. If collisions between particles are very frequent, the deposition distance cannot be used to estimate the initial parameters of volcanic eruptions (Tsunematsu et al., 2014). Vanderkluysen et al. (2012) observed on Stromboli that only 12% of the analyzed trajectories of particles showed evidence of collisions. If the percentage of the particles affected by collisions were similar on Mars and Earth, and the particles were distributed more or less randomly over a sufficiently large area, then the effect of collisions would be of only minor importance.

Although it is widely assumed that scoria cones are formed by ballistic emplacement of material around the vent (McGetchin et al., 1974; Parfitt and Wilson, 2008), observations suggest that the reality is more complex (Calvari and Pinkerton, 2004; Valentine et al., 2005; Vanderkluysen et al., 2012). Fire fountaining and deposition of material from ash jets can participate in the formation of scoria cones (Riedel et al., 2003; Calvari and Pinkerton, 2004; Valentine et al., 2005). The majority of particles transported by fire fountaining follow ballistic trajectories, because their large size enables decoupling from the motion of the gases (Carey and Bursik, 2000, p. 531), hence their behavior can be predicted by a ballistic emplacement model. The jet deposition is characterized by non-ballistic movement via turbulent currents potentially introducing a degree of uncertainty in our model. On the other hand, the jet deposition is mainly responsible for a thin ash blanket widely extending beyond the cone itself (Riedel et al., 2003) and, therefore, does not significantly affect the resulting cone's topography. The thin ash blanket would be difficult to detect on topographic profiles based on remote sensing data because it smoothly transitions into surrounding plains. In this study, the boundaries of the cones have been determined on the basis of images accompanied by topographic profiles, where a transition to the surrounding plains was visible as a break in slope. Therefore, the investigated scoria cones represent clearly detectable landforms where ballistic emplacement dominates over jet deposition.

Scoria cones on Earth are susceptible to rapid erosion, which changes their morphometric characteristics (Wood, 1980b; Dohrenwend et al., 1986; Hooper and Sheridan, 1998). For example, erosion can decrease the flank slopes of scoria cones with a rate of $0.006°/10^3$ yr (Dohrenwend et al., 1986). On Mars, however, the environmental conditions and consequently, the erosion rates are substantially different. Erosion rates on Mars are extremely low after the end of the Noachian (~3.7 Ga) when liquid water became less abundant on the martian surface. For example, Golombek et al. (2006) estimate that the erosion rates in the Amazonian are as low as 1-10 nm/yr. Since the Ulysses Colles scoria cones are much younger than Noachian-aged and formed sometimes between ~1.5 Ga and ~0.44 Ga (Brož and Hauber, 2012), the cumulative erosion since then should not have significantly affected their shape. In fact, there are no traces of erosion visible on their flanks, e.g., rilles or gullies. Moreover, the Ulysses Colles are mantled by a thick layer of dust, which is further evidence that, least at present, aggradational processes dominate over degradational (erosional) processes in this region. Hence, we consider the possible effect of erosion on the slope angles of the studied scoria cones on Mars to be negligible.

5.5. Conclusions

The flank slopes of scoria cones in the Ulysses Colles region on Mars do not reach the critical angle of repose, in contrast to terrestrial scoria cones. Although the volume of the ejected material is much larger than on Earth, it is not sufficient for the critical angle to be reached since it is dispersed over a much larger area during an explosive eruption. Because the cones on Mars did not reach the angle of repose, their morphological shape still preserves a record of environmental conditions at the time of eruption. This suggests that numerical modeling could be used to examine in more detail the basic physical parameters controlling cone formation and hence refine earlier theoretical predictions. Our results show that to build a scoria cone on Mars as observed, the initial velocity of ejected particles has to be increased by a factor of at least ~2 with respect to the typical velocity on Earth, corresponding to a mean particle velocity of ~92 m/s or higher, and that the particles have to be finer by a factor of 0.1 and 0.2, corresponding to a real particle size of 4 to 8 mm. Our findings thus confirm earlier theoretical predictions by Wilson and Head (1994) and help us to understand the development of scoria cones on Mars. A similar approach might be used on other terrestrial bodies from which small-scale volcanoes of explosive origin were reported.

Acknowledgements

We thank M.G. Kleinhans who kindly provided the data for values of angle of repose, J. L. Grenfell who informed us about dependence of atmospheric pressure on altitude, Matt Balme for helpful discussions, A. Clarke for her constructive comments on a previous version of this manuscript, and an anonymous reviewer for his inspiring suggestions. PB is thankful to Václav Kuna for help to refine the initial idea. Hetu Sheth kindly provided the image shown in Fig. 5.2b, and Tim Jonas helped with LIDAR data to create Fig. 5.2c. This study was supported by the Grant No. 580313 from the Grant Agency of Charles University in Prague (GAUK) and by the Helmholtz Association through the research alliance ‘Planetary Evolution and Life’.

6. Scoria cones on Mars: detailed investigation of morphometry based on HiRISE and CTX DEMs

Petr Brož[1,2], Ondřej Čadek[3], Ernst Hauber[4] and Angelo Pio Rossi[5]

[1]*Institute of Geophysics ASCR, v.v.i., Prague, Czech Republic*
[2]*Institute of Petrology and Structural Geology, Faculty of Science, Charles University, Prague, Czech Republic*
[3] *Department of Geophysics, Faculty of Mathematics and Physics, Charles University in Prague, Czech Republic*
[4]*Institute of Planetary Research, DLR, Berlin, Germany*
[5]*Jacobs University Bremen, Bremen, Germany*

Status: Submitted in June 2015 into Journal of Geophysical Research: Planets

6.0. Abstract

Previous studies have suggested the existence of scoria cones in three regions on Mars: Ulysses Colles, Hydraotes Colles and an unnamed field in Coprates Chasma. So far only the cones in Ulysses Colles have been investigated in more detail, using low and intermediate resolution topographic data. Here we analyze the shapes of volcanic edifices in all three regions (altogether 28 cones) using available HiRISE and CTX DEMs, and estimate the basic physical characteristics of the volcanic eruptions that formed them. Most of the studied cones show larger volumes of ejected material (up to 4.2×10^{9} m^{3}), larger heights (up to 573 m) and smaller average slopes than their terrestrial counterparts. The cones in Hydraotes Colles and Coprates Chasma are in average smaller and steeper than the cones in Ulysses Colles, which is likely to be associated with the difference in topographic elevations causing variations in the atmospheric pressure. The average slopes of Ulysses, Hydraotes and Coprates cones range between 7° and 25°, and the maximum slopes only rarely exceed 30°, which suggests only a minor role of avalanche redistribution. Ballistic analysis of the cones indicates that all of them were formed in a similar way and their shapes are

consistent with an ejection velocity about two times larger and a particle size about twenty times smaller than on the Earth. Our results support the hypothesis that the investigated edifices in all three regions were formed by low energetic volcanic eruptions and hence are equivalent to terrestrial scoria cones. The study provides the basic morphometric characteristics of martian scoria cones which can be used to identify this type of volcanoes elsewhere on Mars and distinguish them from other conical edifices.

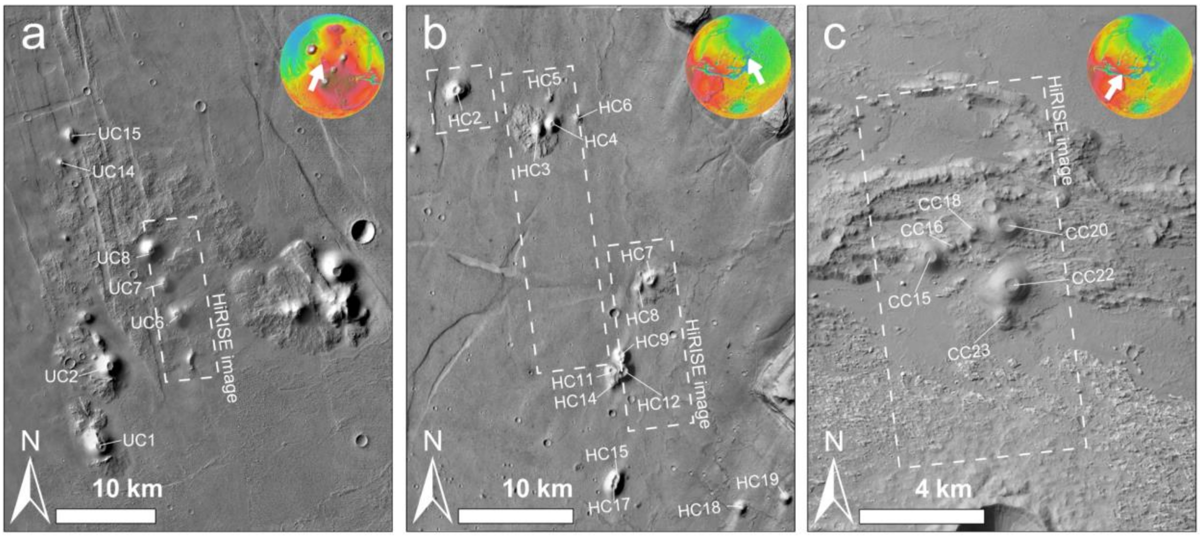

Figure 6.1: Positions of investigated scoria cones in a) Ulysses Colles (UC), b) Hydraotes Colles (HC), and c) an unnamed field in Coprates Chasma (CC). The boundaries of HiRISE images are marked by dashed white lines. Small insets in the upper right show positions of the volcanic fields on global MOLA topography. Panel a) is based on mosaic of CTX images P21_009409_1858_XN_05N122W, G11_022582_1863_XN_06N122W and P19_008262_ 1862_XN_06N123W; HiRISE image PSP_009554_1860 forming stereo-pair with PSP_009409_1860, centered 5.86°N, 237.22°E; panel b) is based on HiRISE images ESP_019269_1805, ESP_021458_1800 and ESP_017634_1800 forming stereo-pairs with ESP_019124_1805, ESP_013177_1800 and ESP_025493_1800 respectively, based on mosaic of CTX images G19_025493_1800_XN_00N033W and G02_019124_1803_XN_00N034W centered 0.03°N, 326.26°E; and panel c) is based on HiRISE image ESP_034131_1670 forming stereo-pair with ESP_033986_1670, based on CTX image D01_027538_1674_XN_12S062W, centered 12.73°S, 297.21°E.

6.1. Introduction

Our knowledge of small-scale explosive volcanic cones on Mars has significantly increased in the recent years owing to a new generation of high resolution images that allow their direct observation (Bleacher et al., 2007; Keszthelyi et al., 2008; Meresse et al., 2008; Lanz et al., 2010; Brož and Hauber, 2012; 2013). Possible martian equivalents of terrestrial scoria cones were reported as parasitic cones on the flanks of large volcanoes (Bleacher et al., 2007; Keszthelyi et al., 2008) or as cone clusters forming volcanic fields (Meresse et al., 2008; Lanz et al., 2010; Brož and Hauber, 2012; Fig. 6.1). Although the interpretation of these edifices as scoria cones is mainly based on their apparent morphological similarity with terrestrial scoria cones, no detailed investigation of their morphometry using high-resolution data has yet been performed to support such a conclusion, with a partial exception for the Hydraotes Colles cone field (Meresse et al., 2008) and the Ulysses Colles cone field (Brož and Hauber, 2012; Brož et al., 2014).

It has been recognized that martian scoria cones differ in size and shape from terrestrial scoria cones (Meresse et al., 2008; Brož and Hauber 2012). Martian scoria cones are usually larger in basal diameter, higher in height and more voluminous by one to two orders of magnitude than their terrestrial counterparts, and have flanks not exhibiting slopes over 30° (e.g., Brož and Hauber, 2012; Kereszturi et al., 2013). This difference can be explained by lower values of gravitational acceleration and atmospheric density on Mars than on Earth, which allow the scoria particles to be ejected further from the vent and deposited across a wider area than in terrestrial conditions (McGetchin et al., 1974; Wood, 1979; Dehn and Sheridan, 1990; Wilson and Head, 1994; Brož et al., 2014). Although martian cones are higher and have larger volumes than on Earth (Brož and Hauber, 2012), the amount of scoria material is typically not sufficient for the critical angle of repose to be attained over the main part of their flanks as it is common on Earth (Riedel et al., 2003). The principal mechanism of scoria cones formation on Mars is thus the ballistic emplacement of ejected particles which accumulate around the vent over time (Brož et al., 2014), rather than a redistribution of particles by avalanching processes typical of terrestrial scoria cones (Riedel et al., 2003).

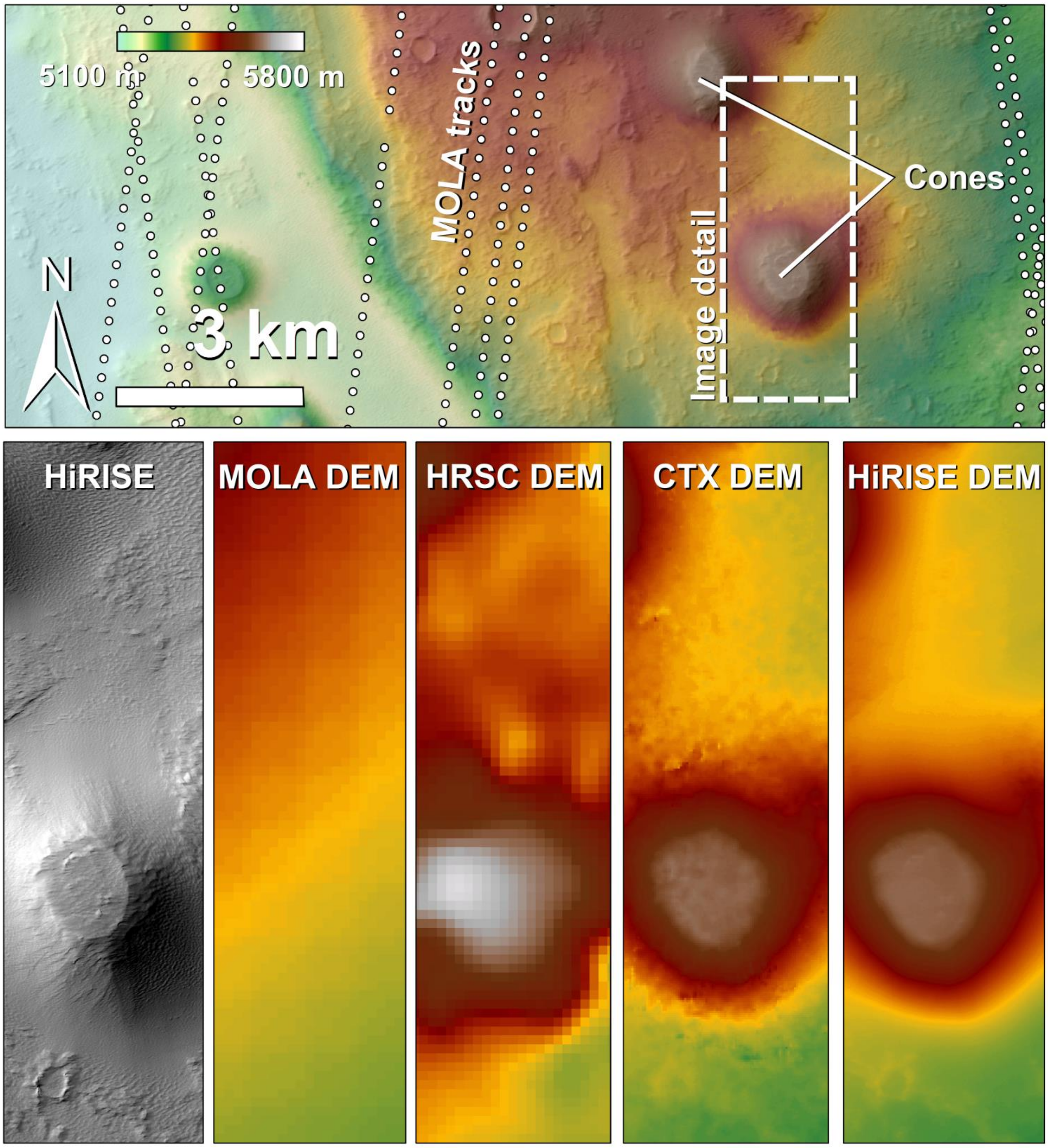

Figure 6.2: Resolution of various DEMs. The top panel shows the regional context around one particular cone (UC6) in the Ulysses Colles region. The MOLA tracks are marked by white dotted lines. The most detailed information is obtained from the HiRSE DEM.

Previous studies dealing with the shape of scoria cones on Mars (Meresse et al., 2008; Brož and Hauber, 2012 and partially Lanz et al., 2010) were based on data obtained through the High Resolution Stereo Camera (HRSC, Jaumann et al., 2007) and the Mars Orbiter Laser Altimeter (MOLA) Precision Experimental Data Records (PEDRs; Zuber et al., 1992; Smith et al., 2001). Both instruments have only a limited horizontal resolution, which is optimal for investigating topographic features of a typical size of tens of kilometers or larger, but insufficient to provide detailed (~100 m - 1 km) information about the small-scale features such as scoria cones (Fig. 6.2). This information is necessary for understanding the variability of the cones and determining their morphometric characteristics. These are required for a quantitative comparison of the cones with similar features on Earth and other martian conical edifices of various origins (e.g., mud volcanoes, pingos, rootless cones etc.; Burr et al., 2009b). In the present study, we use new high-resolution data from the High Resolution Imaging Science Experiment (HiRISE; McEwen et al., 2007) and the Context Camera (CTX; Malin et al., 2007) which enable investigating small edifices in unprecedented detail and analyzing their shapes quantitatively (Fig. 6.2). Such an approach was tested previously by Brož et al. (2014) who investigated the shapes of two martian scoria cones in Ulysses Colles using CTX Digital Elevation Models (DEMs) and one cone by HRSC DEMs.

Using the available high-resolution DEMs based on HiRISE and CTX stereo image pairs, we investigate the shapes of cones within three hypothesized volcanic fields – Ulysses Colles (UC), Hydraotes Colles (HC) and Coprates Chasma (CC) where the existence of scoria cones has been suggested (Meresse et al., 2008; Harrison and Chapman, 2008; Brož and Hauber, 2012). For each field, we first select a representative subset of cones that are well covered by HiRISE and/or CTX data. The topography of each cone is averaged with respect to the central axis, and the resultant axisymmetric structure is then characterized by several morphometric parameters, such as total volume, cone height and width, average and maximum slope etc. By comparing the parameters obtained for individual cones we evaluate the shape variability within each volcanic field and assess the degree of similarity among the fields. Finally, following the approach by Brož et al. (2014), we determine for each cone the ejection velocity and the particle size that best reproduce the observed shape of the cone, and again compare the results within and among the volcanic fields. The joint results of our morphometric analysis and numerical modeling are then discussed from the viewpoint of the formation mechanism of the cones and their volcanic origin.

6.2. Regional setting

The three fields considered in this study contain well-shaped cones of various sizes with only limited signs of modification by erosion. Here, we briefly summarize the basic characteristics of the fields as described in previous studies.

6.2.1. Ulysses Colles

This volcanic field is situated in the Tharsis region at the south-eastern margin of Ulysses Fossae (Fig. 6.1a), a several-hundred-kilometer-long fault system trending mainly in north-south direction and fracturing a window of older crust which survived later resurfacing event(s) by younger lava flows. This field is located at a height of 4.5 km above the martian datum over an area of about 80 × 50 km at the southern edge of Ulysses Fossae and it is formed by (at least) 29 volcanic cones (Brož and Hauber, 2012). The cones are not distributed randomly; there is a cluster of 10 cones at the southern edge of this field. These cones have well-developed truncated shapes and they seem to be well preserved. Three cones may be associated with flow-like features originating at the base and/or at the top of the cones. Unfortunately, only a small part of this field is covered by HiRISE or CTX stereo-pair images suitable for DEM production, hence our investigation of this field is based only on 7 cones.

6.2.2. Hydraotes Colles

The volcanic field is located in the chaotic terrain of Hydraotes Chaos (Fig. 6.1b) on the eastern edge of Xanthe Terra. The terrain lies at the contact of two major outflow channels (Simud and Tiu Vallis) with an inlet channel. The area is partly filled with large mesas separated by narrow valleys and by a basin with a smooth floor located 5 km below the martian datum. Based on HRSC and THEMIS data Meresse et al. (2008) identified about 40 pitted cones of various sizes and shapes inside this basin. The observed cones have been divided into three classes: basin cones, valley cones and small cones. The basin cones represent the largest edifices and are subject of our investigation. These cones are predominantly localized in the southern part of the chaotic terrain over 40 × 30 km large area. They have central craters and often form small sub-clusters separated by 5 km. The individual clusters are composed of cones which often partially overlap and/or are accompanied by flow-like units, interpreted by Meresse et al. (2008) as lava flows. Three clusters and one individual cone are covered by HiRISE stereo-pairs and two other cones are covered by CTX DEMs. This allows us to investigate 15 cones in this field.

6.2.3. Coprates Chasma

The largest field of hypothesized scoria cones is situated in the bottom part of the Coprates Chasma valley (Fig. 6.1c), one of the largest canyons in Valles Marineris, which extends over 1000 km. The cones and mounds are located in a west-eastern direction over an area of 155 × 35 km, 5 km below the martian datum on the floor of Coprates Chasma. Similarly to the cones in HC, the cones in CC sometimes form small clusters containing up to ten edifices, partly overlapping each other. The cones have been briefly mentioned by Harrison and Chapman (2008) as possible volcanic edifices; however, the origin associated with mud volcanism was also discussed and in the end chosen as the most plausible explanation. CTX and HiRISE images recently revealed previously unknown details (Hauber et al., 2015) which seem to be consistent with a volcanic origin. At the time of writing this study, HiRISE stereo-pairs were available only for one cluster of cones. Our investigation focuses on 6 cones within this cluster, which represent only a small sample of this extensive field.

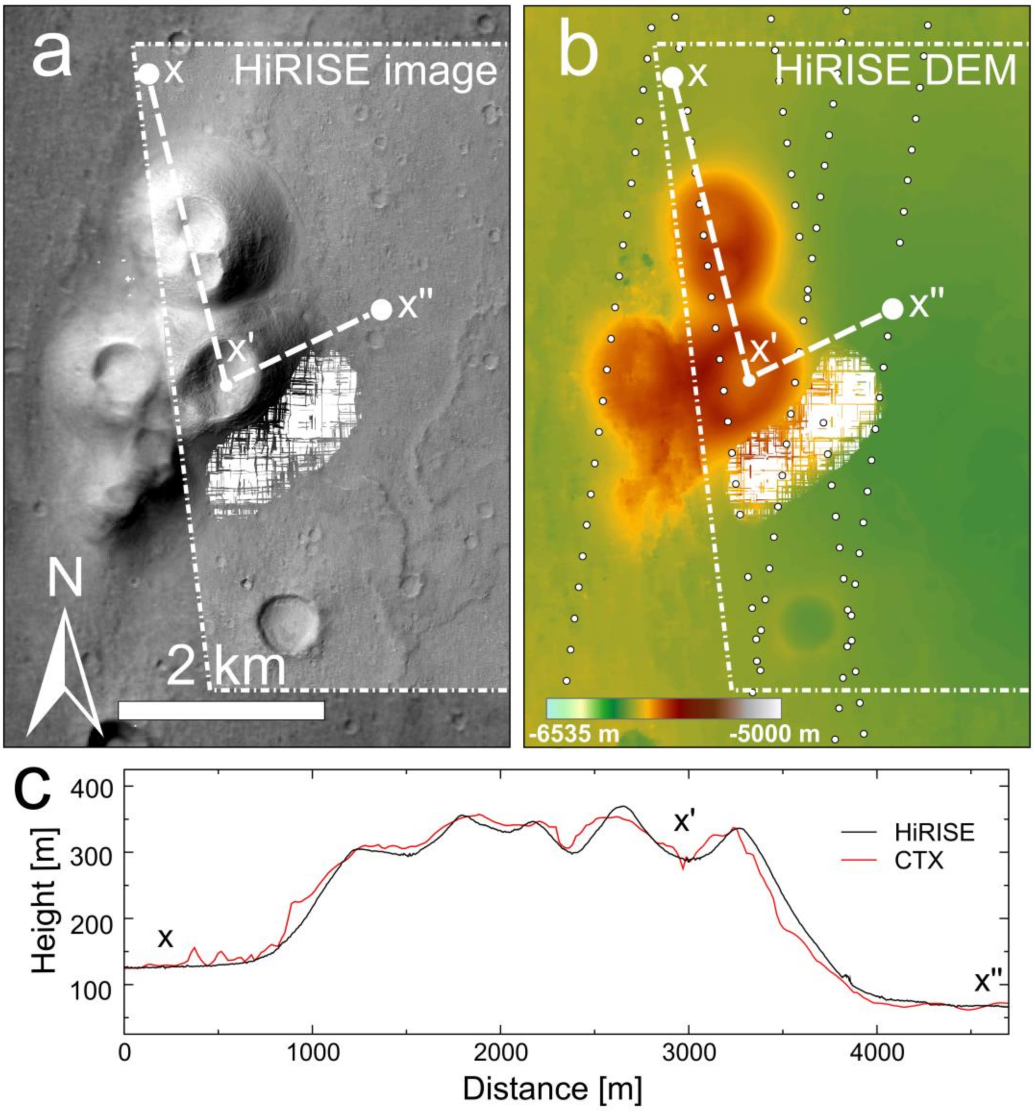

Figure 6.3: Cones HC9-14 as seen by a) the data sets based on HiRISE and CTX stereo-pairs and b) the colored mosaic of DEMs with marked position of MOLA PEDRs. Resultant DEMs contain data gaps (marked in white on both panels) which do not allow the shapes of some cones to be determined along their entire perimeter. The profiles panel c) illustrates the differences between the HiRISE and CTX DEMs data. Position of the profile connecting points x and x'' is shown in panels a and b. Image center is at 0.13°S, 326.25°E.

6.3. Topographic datasets

We used topographic data based on gridded digital elevation models (DEMs) derived from HiRISE (~30 cm/pixel, McEwen et al., 2007) and CTX (5–6 m/pixel; Malin et al., 2007) images. The high-resolution DEMs were computed from HiRISE and CTX stereo pairs using the methods described, e.g., in Moratto et al. (2010). The image data were processed using the USGS Astrogeology image processing software Integrated System for Imagers and Spectrometers (ISIS3). The gridded HiRISE DEMs in UC, HC and CC have ground sampling distances of 0.53 m, 1.48 m and 3.82 m, respectively, while the resolution of CTX DEMs is 17.78 m, and the vertical accuracy of the stereo-derived DEM can be roughly estimated to be approximately a few meters. The elevations of the DEMs are consistent with single shot data from MOLA PEDRs (Garvin et al., 2000). In regions where both kinds of DEMs are available, we use only the HiRISE DEMs since they have a higher resolution than the CTX DEMs and hence provide more realistic shape representation (Fig. 6.3). The spatial resolution of the HiRISE DEMs deteriorates in regions with large amount of missing data (for an example, see Figs. 6.3a,b where the missing data are marked by white color). These data gaps are associated with the process of DEM generation and affect the areas where an insufficient amount of matched points was produced before the interpolation of a DEM surface. The regions affected by too many data gaps were excluded from further analysis. Although the DEMs used in this study are not too noisy (Fig. 3, bottom panel), small high-frequency variations in the topographic signal makes the accurate evaluation of the topographic slope difficult. The usual way to overcome this problem is to perform a spectral analysis of the signal and filter out the high-frequency noise in the spectral domain, or to remove the noise directly in the spatial domain using a moving average or smoothing method. However, we find that neither of these methods works reliably when applied to the topographic data derived from HiRISE and CTX images because we are not able

Table 6.1: Morphometric characteristics of the cones.

ID	W_{CR} [m]	W_{CO} [m]	H_{CO} [m]	Volume [m^3]	Average slope [°]	Maximum slope [°]	HiRISE (H) or CTX (C) DTM	Azimuth* [°]	W_{CR}/W_{CO}	H_{CO}/W_{CO}	Initial speed of ejected particles [m/s]	Size of ejected particles [mm]	Match [m]
							Ulysses Colles						
UC1	934	5210	479	2.50E+09	18	24	C	45-90; 225-300	0.18	0.09	110	2	14.2
UC2	576	7500	573	4.20E+09	16	24	C	105-150; 210-265	0.08	0.08	101	4	12.4
UC6	956	2818	245	6.10E+08	17	21	H	135-225	0.34	0.09	138	1	21.8
UC7	586	2980	238	4.40E+08	14	19	H	60-135	0.20	0.08	120	1	6.5
UC8	800	4558	445	1.70E+09	18	26	H	75-180	0.18	0.10	92	2	9.5
UC14	358	3112	99	1.50E+08	7	10	C	0-360	0.12	0.03	64	2	3.2
UC15	322	2392	155	2.00E+08	12	16	C	0-360	0.13	0.06	92	1	3.0
							Hydraotes Colles						
HC2	572	2994	245	4.60E+08	18	23	H	0-360	0.19	0.08	129	2	12.3
HC3	178	1570	222	1.40E+08	21	26	H	180-260	0.11	0.14	120	1	6.1
HC4	414	2046	243	2.40E+08	22	26	H	315-355	0.20	0.12	83	2	11.0
HC5	210	1364	81	2.40E+07	14	20	H	185-355	0.15	0.06	55	1	1.2
HC6	144	1522	130	5.30E+07	15	24	C	225-90	0.09	0.09	46	2	4.0
HC7	394	2520	211	2.40E+08	18	24	H	270-90	0.16	0.08	83	2	6.6
HC8	46	1570	181	7.90E+07	19	25	H	180-315	0.03	0.12	83	1	5.1
HC9	414	2194	210	2.00E+08	19	24	H	0-90	0.19	0.10	83	2	7.8
HC11	182	1706	182	1.20E+08	18	24	C	225-315	0.11	0.11	129	1	4.5
HC12	534	2370	257	3.20E+08	21	28	H	45-60	0.23	0.11	101	2	13.9
HC14	108	1528	136	5.90E+07	13	24	C	0-360	0.07	0.09	46	5	5.5
HC15	392	1812	202	2.10E+08	20	34	C	330-60	0.22	0.11	83	2	12.4
HC17	286	1980	245	2.60E+08	20	32	C	150-240	0.14	0.12	83	2	10.5
HC18	250	1480	164	1.10E+08	19	29	C	0-360	0.17	0.11	138	1	8.0
HC19	216	1564	174	9.50E+07	22	29	C	0-360	0.14	0.11	101	1	7.3
							Coprates Chasma						
CC15	276	1376	197	1.00E+08	25	not determined	H	340-20; 150-225	0.20	0.14	101	1	8.3
CC16	310	928	75	2.10E+07	17	23	H	315-45	0.33	0.08	55	1	4.2
CC18	124	1040	94	2.20E+07	15	23	H	135-180; 290-350	0.12	0.09	55	1	4.0
CC20	488	1890	165	1.60E+08	19	not determined	H	45-225	0.26	0.09	83	2	11.7
CC22	428	1896	247	2.20E+08	24	not determined	H	270-90	0.23	0.13	83	2	15.5
CC23	90	1796	202	1.20E+08	17	23	H	135-225	0.05	0.11	129	1	10.0

* azimuth is measured clockwise with 0° as north

to distinguish spurious high- and intermediated-frequency signal, arising from image processing, from the real small-scale topographic signal. The problem is obviously complex and its solution would require a better understanding of data errors. Here we simplify the problem by assuming that the studied edifices are axisymmetric. For each cone we define the center of symmetry as the geometrical center of the summit plateau and then we determine the average shape of the cone by averaging the topographic heights along the cross-sections passing through the center of symmetry. The angular step between the neighboring cross-sections is chosen to be 1 degree. This approach significantly reduces the noise in the topographic data and allows each cone to be described by a limited number of parameters (see next section). The parts of the cone with frequent data gaps and those where the axial symmetry is clearly disturbed (e.g., due to a lava flow, an irregularity of the bedrock topography or an overlap with other cone) are excluded from the averaging (see Table 6.1 for the list of sectors which have been considered).

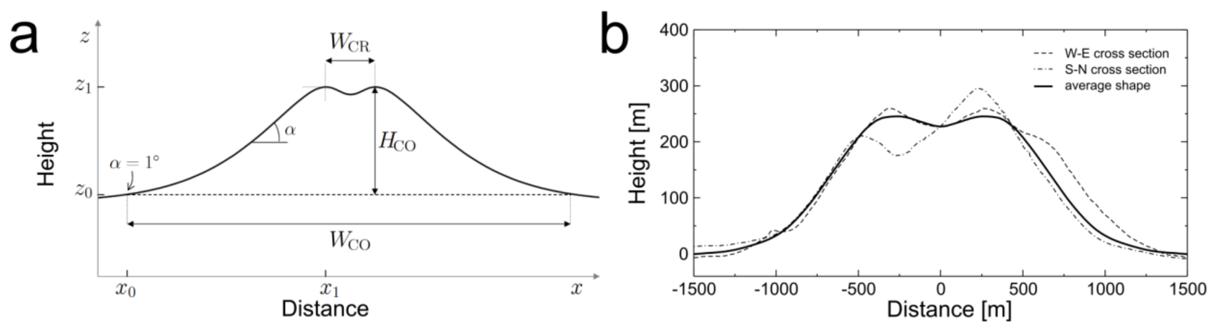

Figure 6.4: a) Morhometric parameters used in this study. b) Comparison of two profiles passing through the center of the cone HC2 (dashed and dashed-dotted lines) with the average shape of the same cone (full line). The profiles are based on HiRISE DEM.

6.4. Morphometric parameters

The morphometric properties of the studied cones are the same that are commonly used for terrestrial scoria cones (Fig. 6.4a, for an overview see Grosse et al., 2012). These parameters are: the width or basal diameter of the cone (W_{CO}), the width of the crater (W_{CR}), the height of the cone (H_{CO}), the flank slope (α), and the volume. To determine these parameters for each cone we first correct for the influence of irregularities and compute the average shape (Fig. 6.4b) as described in section 6.3.

The base level z_0 (marked by the dotted line in Fig. 6.4a), used to determine parameters W_{CO} and H_{CO}, is defined as the horizontal plane passing through the point where the slope of the average topographic profile exceeds one degree. This definition is independent of subjective factors and the results can be easily reproduced. It should be noted, however, that this approach may ignore far-reaching volcanic products hardly detectable on topographic profiles and therefore may affect our volume estimates by reducing the amounts of ejected material. The slope of each cone is described by a function α_z characterizing the dependence of slope α on relative height h,

$$\alpha_z(\mathrm{h}) = 0.1 \int_{\mathrm{h}-0.05}^{\mathrm{h}+0.05} \alpha\,(\mathrm{h}')\mathrm{dh}', where\ \mathrm{h} = \frac{z-z_0}{z_1-z_0}\ ,\ \mathrm{h} \in \langle 0.05, 0.95\rangle \tag{6.1}$$

and by two constant parameters, the average slope $\bar{\alpha}$ and the maximum slope α_M, defined as the average and maximum values of α_z, respectively. Since the slope α is determined by numerical differention of the cone's shape, its accuracy strongly depends on the smoothness of the averaged topography. In the Coprates region, a high density of data gaps around the cones CC15 and CC22 and asymmetry of the cone CC20 do not allow the averaged shape to be reliably differentiated. The slope characteristics of these cones are

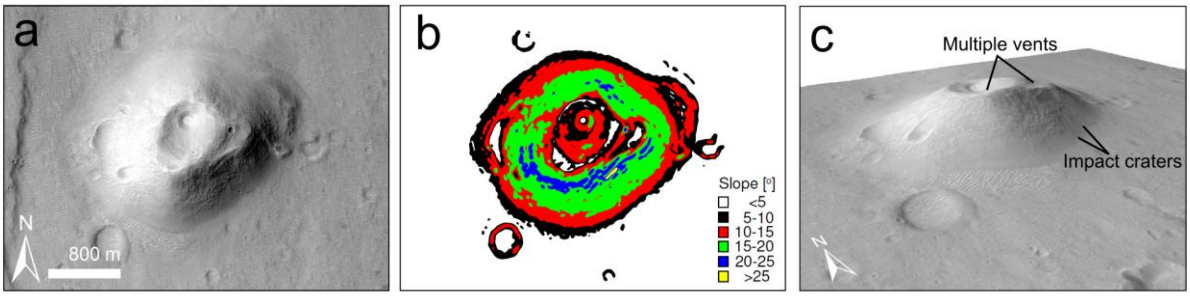

Figure 6.5: a) Cone HC2 on HiRISE image, centered 0.26N, 326.04°E. b) Slope map of the same cone. Note that the slope only rarely exceeds 20°. c) A perspective view.

therefore excluded from further analysis. In contrast, small errors in topographic height only weakly affect the evaluation of the volume and other parameters. The largest error in determining these parameters arises from the definition of the base level z_0 and the violation of the symmetry assumption.

6.5. Results of morphometric analysis

We have processed 8 stereo image pairs (5 HiRISE, 3 CTX) that enable investigating 28 conical structures in the three fields. 17 cones are covered by HiRISE DEMs and 11 by CTX DEMs. In all fields, only a subset of cones is considered since none of the fields is completely covered with stereo data of sufficient quality. As individual cones display morphological heterogeneity causing small variations in shapes, we determine for each cone the average shape (for details, see section 6.3). These small variations may be caused by impact craters, sector collapses, migrations of feeder dikes, increase/decrease in explosivity and partly by erosion. Examples of such variations are shown in Figs. 6.4b and 6.5a-c for the case of a cone in the Hydraotes region. The topographic height on the cone depends not only on the distance from the center but also on azimuth, suggesting variations in particle distribution and deposition over the entire perimeter of the cone – see Fig. 6.4b where topographic profiles

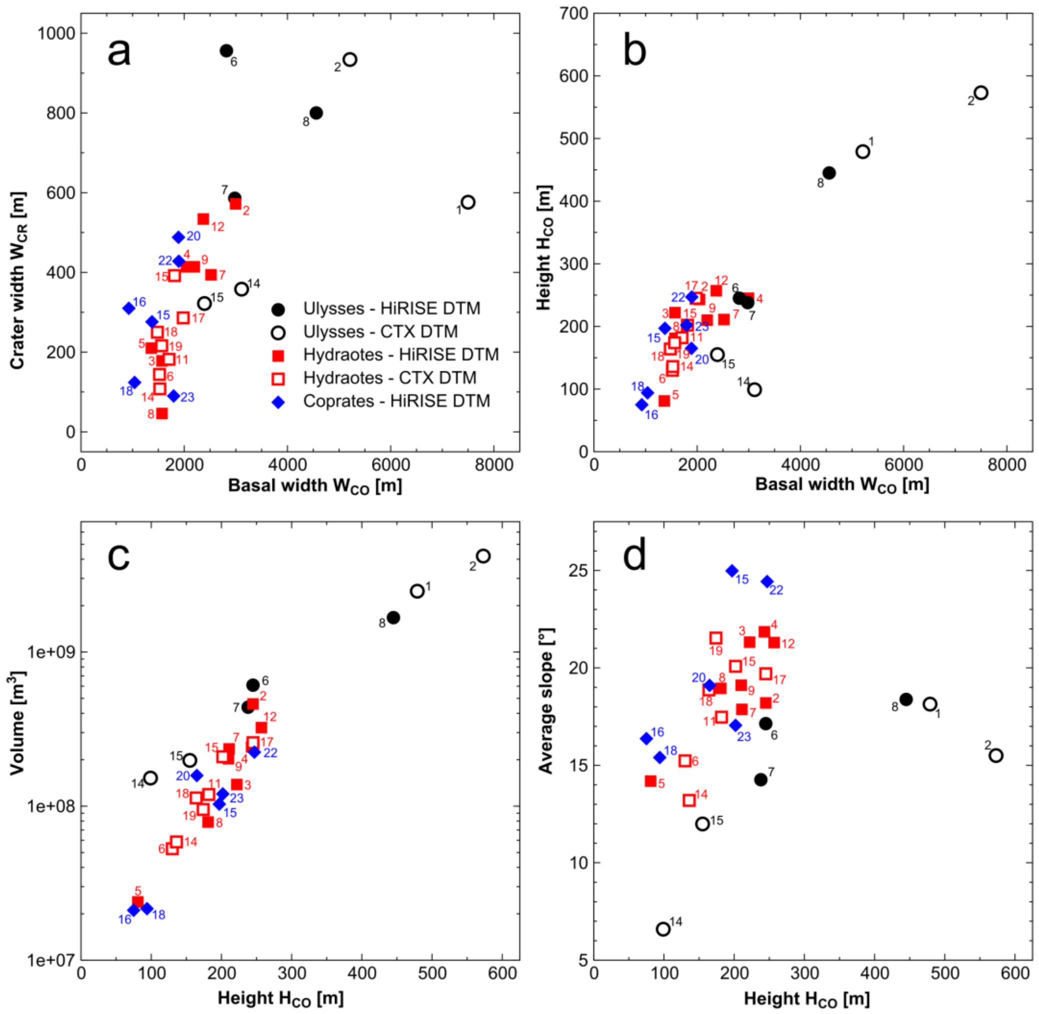

Figure 6.6: Values of morphometric parameters obtained for average shapes of 28 cones considered in this study. Full symbols represent the HiRISE while empty symbols correspond to CTX DEMs. The results obtained for the UC, HC and CC regions are marked in black, red and blue, respectively.

along two cross-sections are compared with the resultant average shape. As obvious from the slope map (Fig. 6.5b), the southern part of the cone is steeper than the northern one, while the western part is affected by sector collapse and/or impact craters (Fig. 6.5c).

The parameters of the cones obtained after averaging are summarized in Table 6.1 and depicted in Fig. 6.6. In general, the sizes of cones vary among the three investigated fields (Fig. 6.6a). The cones in UC have in average the largest mean basal diameter, the widest central crater~~s~~ and also include the highest edifices (Fig. 6.6b) with mean values of 4080 m, 650 m and 320 m, respectively. The cones in HC are mostly smaller than the cones in UC, with mean basal diameter, crater width and cone height of 1880 m, 290 m and 190 m, respectively. The statistically smallest edifices are found in the CC region; but their mean characteristics (W_{CO}=1490 m, W_{CR}=290 m and H_{CO}=160 m) do not differ much from those of the HC cones.

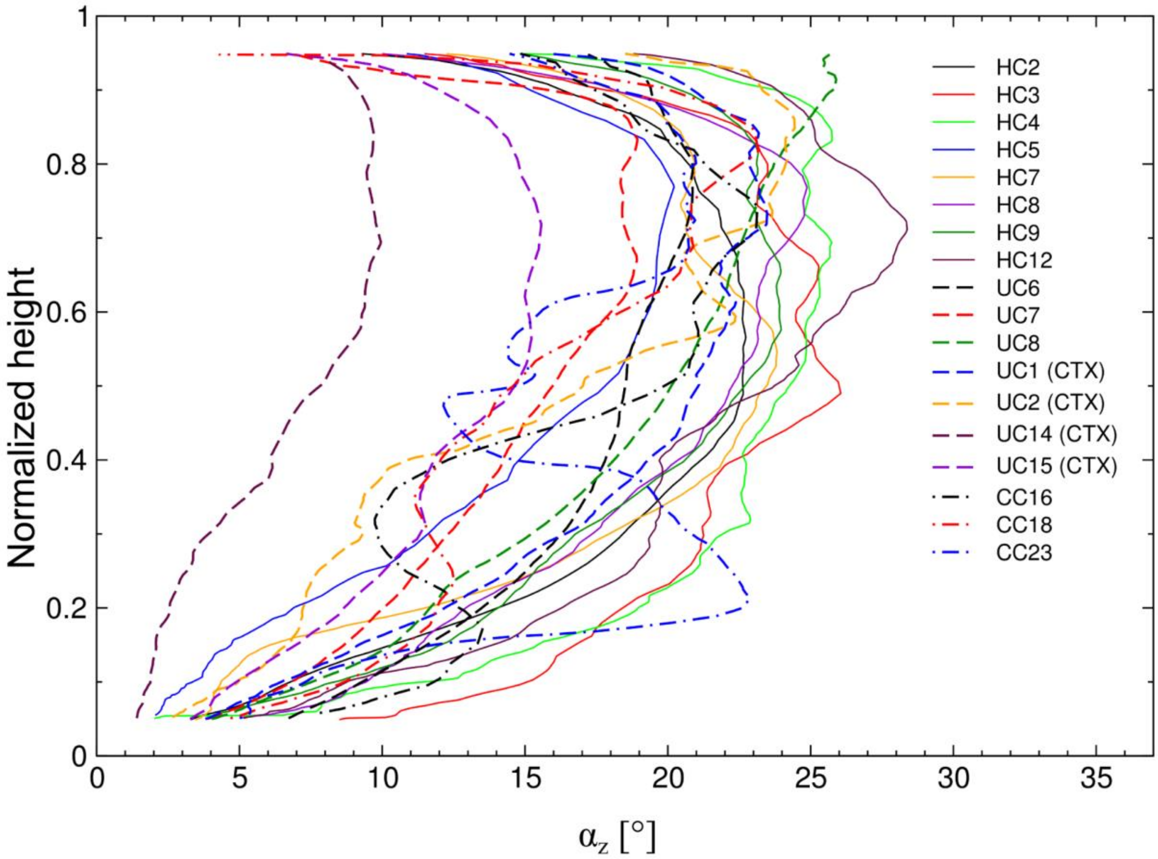

Figure 6.7: Slope α_z, eq. (6.1), as a function of normalized height h, plotted for selected cones in HC (full lines), UC (dashed lines) and CC (dash-dotted lines). The curves are computed from the HiRISE data, unless stated otherwise.

The slopes and volumes of the cones vary significantly from cone to cone and among the fields. As the cones in UC are largest and highest, they include the most voluminous edifices (Fig. 6.6c). However, even the largest cones in this region show smaller average slopes than the steepest edifices in HC and CC (Fig. 6.6d). The average slopes $\bar{\alpha}$ in UC range between 7° and 18° with corresponding cone volumes between 1.5×10^8 m^3 and 4.2×10^9 m^3, while the cones in HC and CC have similar or even larger average slopes (13° – 24°), but their volumes range from 2.1×10^7 m^3 to only 4.6×10^8 m^3 (see also Tab. 6.1).

The slope α_z (eq. 1) is not uniform along the entire length of a cone flank but changes with height (Fig. 6.7). It is lowest at the cone's bottom and increases with height, reaching the maximum for the normalized height between 0.6 and 0.8. Then the slope again decreases as the height approaches the edge of the crater. Note that in all plotted cases (8 cones in HC, 7 cones in UC and 3 cones in CC) the slope is always smaller than the angle of repose (~30°; Kleinhans et al., 2011).

6.5.1. Ballistic emplacement models

To assess the mechanism of cone formation, we used the numerical code developed by Brož et al. (2014) which is able to track the ballistic trajectories and trace the cumulative deposition of repeatedly ejected particles during low-energetic Strombolian eruptions. This code can be used to reconstruct the shapes of ballistically emplaced volcanic edifices (e.g., scoria cones) and hence to confirm or disprove the formation mechanism of investigated cones. Brož et al. (2014) have applied this approach to study three selected cones (UC1, UC2 and UC8) in the UC region. Using log-normal statistical distributions of ejection velocities and particle sizes having the same standard deviations as on the Earth and assuming that the density of air at the time of eruption was the same as today, they found that the shapes of the cones are consistent with a Strombolian origin, provided that the mean ejection velocity was about two times larger and the particle size about ten twenty smaller than on Earth.

Here we repeat the same numerical experiment but using much larger and more accurate topographic datasets. For each of 28 cones considered in this study we determine the mean particle size and the mean ejection velocity that best predict the average shape

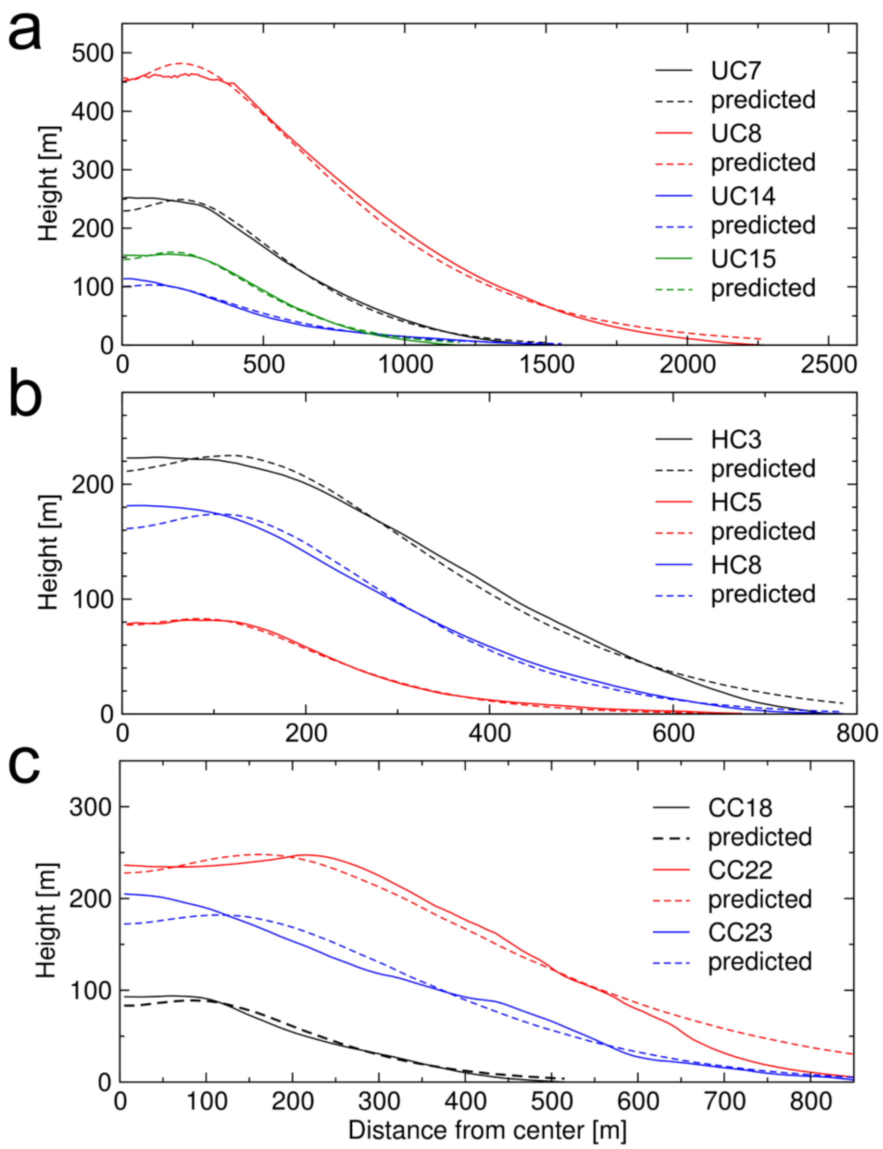

Figure 6.8: Comparison of the average shapes of selected cones in a) UC, b) HC and c) CC (full lines) and the results of numerical ballistic modeling obtained for the same cones (dashed lines). Note that in some cases the model predicts the observed profile with a vertical error smaller than 10 m.

of the cone. We use the same parameters as in Brož et al. (2014), except that we prescribe a higher density of air in HC and CC (0.023 kg/m^3) than in UC (0.010 kg/m^3) and consider only the wide ejection cone (0-45°), which is likely on a terrestrial body with a low atmospheric pressure (Glaze and Baloga, 2000; Wilson and Head, 2007). The large difference in the air density is associated with the different elevation of the fields about 9.5 km. Since the atmospheric drag is proportional to the air density, the ballistic range in HC and CC should be smaller than in UC, and the HC and CC cones should be steeper than their UC counterparts.

The results of our modeling are summarized in Table 6.1 and illustrated in Fig. 6.8 where the observed topographies are compared with our ballistic predictions for several selected cones. Our results suggest that the ballistic model is not only able to reconstruct rather well the cones in all three fields but also that the shapes of most of them can be explained using similar values of ejection velocity and particle size, even though the cones have various sizes and volumes and are located in regions with different air drag. The average vertical difference between the observed and predicted topography is 9 m. The predicted values of the ejection velocities range by a factor of three, from 45 to 135 m/s, but 50% of them lie in the narrow interval between 82 and 102 m/s. The particle size is found between 1 and 2 mm, except two cones where it reaches 4-5 mm. The mean values of the ejection velocity and the particle size for individual fields are, respectively, ~100 m/s and 1.8 mm for UC, 91 m/s and 1.8 mm for HC, and 84 m/s and 1.3 mm for CC. We note that our ballistic inversion is sensitive to the ratio between particle size and air density, but not to the particle size itself. To obtain the particle sizes given above, we had to assume particular values of air density corresponding to the time of eruption. Since the ages of individual cone fields are not known with sufficient accuracy and the evolution of the atmosphere is poorly constrained, we used the current atmospheric density, namely 0.010 kg/m^3 for UC and 0.023 kg/m^3 for HC and CC.

6.6. Discussion

The investigation of the origin of martian surface landforms is complicated by the lack of in-situ data which could provide conclusive evidence of their formation. The available remote sensing data provide only limited insight into the formation of surface features, and they can be usually interpreted in several different ways (e.g., Beven, 1996). This is also the case of the cones in HC and CC for which two different explanations have been suggested: igneous volcanism and mud volcanism (Meresse et al., 2008; Harrison and Chapman, 2008). To distinguish between these two scenarios is difficult since both fields are located in areas where water played or may have played an active role, and both mechanisms may form conical landforms associated with central craters and material flows. However, the existence of the cones in UC may help to solve this problem. Situated in Tharsis, this field is at a location where the existence of mud volcanism is highly unlikely, and an explanation in terms of Strombolian volcanism is more plausible (Brož and Hauber, 2012). The shape similarity (or dissimilarity) between the cones in this region and those in HC and CC may thus provide a key to understanding of how the features in HC and CC were formed.

As already mentioned, the cones in all three investigated fields can be described as conical edifices with a central crater (Fig. 6.1), their slopes seem to be formed by a fine-grained material of smooth texture, and some of them are accompanied by flow-like units with lobate edges and a rough texture. Therefore, it is reasonable to expect that a similar physical mechanism was responsible for their formation. However, when the shapes of the cones are compared quantitatively (section 6.5), the similarity of the fields becomes less obvious. As shown in Fig. 6.6 and Table 6.1, individual cones show variations in sizes, heights, volumes and slopes, and, on the morphometric graphs, they do not form one homogenous cluster with a clear linear trend as common for fresh scoria cones on Earth (Porter, 1972; Wood, 1980). Instead, two clusters may be distinguished: one formed by the cones in HC and CC where the studied objects show a significant overlap in all measured parameters (Fig. 6.6), and the other consisting of the cones in UC following a different trend.

The close agreement in morphometries of the cones in HC and CC supports the concept that the both fields were formed by the same or similar physical mechanism. On the other hand, the morphological differences between the cones in these two fields and those in UC may raise doubts whether the HC and CC cones were formed by the same process as the cones in UC, which are likely of volcanic origin (Brož and Hauber, 2012). The analysis of the cones in terms of ballistic modeling however shows that the difference between UC on one side and HC and CC on the other is only apparent. Despite the obvious morphological differences, the cones in all three fields can be explained by the same ballistic model with the same or similar ejection velocity and particle size distributions. This result suggests that the edifices in the three regions are scoria cones which were formed by the same physical process, though under different atmospheric pressure.

The ballistic model provides a simple explanation of the morphological differences between the cones in UC and those in HC and CC, indicating that these differences are associated with different topographic heights of the sites, rather than with different processes of cones' formation. At present, the atmospheric density in HC and CC is a factor of about 2.3 larger than in UC. Although the fields may have different ages, it is likely that they were formed during the last one billion years (Brož and Hauber, 2012; Hauber et al., 2015) when the atmospheric pressure was already low (Lammer et al., 2013). One can thus assume that the difference in the density of air between the sites at the time of their origin was similar to that at present. The atmospheric drag is linearly proportional to the air density and hence is about 2.3 times smaller in UC than in other two regions. The ballistic range of ejected particles increases as the atmospheric drag decreases (Brož et al., 2014), and the ejected material is thus deposited on a wider area in UC than in HC and CC. For the same volume of ejected material, the cones in HC and CC must be therefore narrower and steeper than those in UC, which is well illustrated in Fig. 6.6. But even in the case of HC and CC, the atmospheric friction is significantly (about 50 times) lower than on Earth so that the ejected material is dispersed over a larger area than under terrestrial conditions (Brož et al., 2014). The dispersion of particles on Mars is further enhanced by low gravity. As a consequence, the slopes angles of the cones are supply-limited and do not reach the angle of repose as it is common for the scoria cones on Earth which explains why the scoria cones on Mars do not morphologically resemble their terrestrial analogues. While the shape of the martian scoria cones is only determined by ballistic emplacement, the shape of the cones on Earth is also influenced by avalanche redistribution of the ejected material occurring after the cone reached the angle of repose (Riedel et al., 2003).

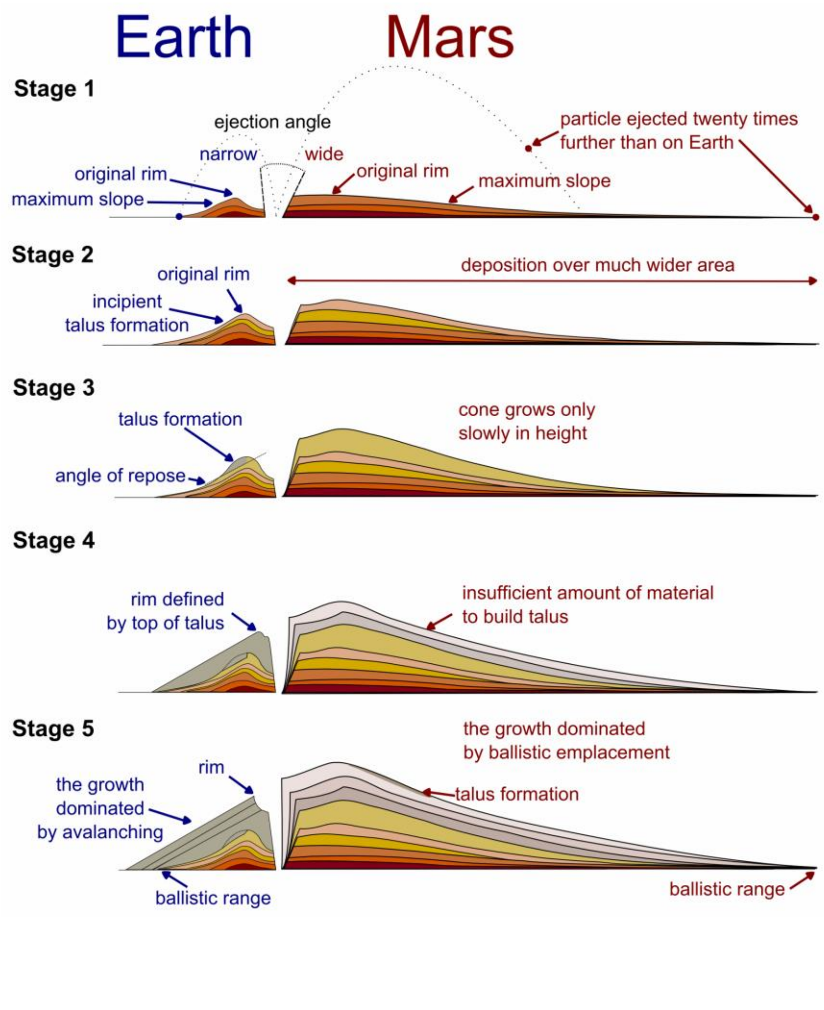

Figure 6.9: A sketch of scoria cone growth on Earth (after McGetchin et al., 1974) and on Mars (based on Brož et al., 2014, and this study).

The differences in evolution of scoria cones on Earth and Mars are illustrated in Fig. 6.9. At the beginning (stages 1 and 2 in Fig. 6.9), both cones grow in a similar manner, gradually increasing the height and the slope angle. Because of the differences in the ballistic range, the ejected particles are deposited on much smaller area on Earth than on Mars and, for the same amount of ejected material, the terrestrial cone is thus steeper than the martian one. Once the angle of repose (~30°) on Earth is reached (stage 3, Fig. 6.9 left), the slope angle stops increasing and it remains stable during the rest of evolution. The further growth is accommodated by an increase of the cone width (McGetchin et al., 1974; Kereszturi and Németh, 2012). To summarize, the evolution of a scoria cone on Earth has two main phases: The first one (stages 1 and 2 in Fig. 6.9) is characterized by a positive correlation between the height and the slope angle and, in first approximation, by a constant basal diameter. In the second phase (stages 3 to 5 in Fig. 6.9), the slope does not change and the correlated parameters are the height and the basal diameter. As a consequence, the terrestrial population of scoria cones can be classified into two main groups. The first group consists of small cones corresponding to the first phase and showing a correlation between the angle of slope and the height due to the ballistic deposition and/or the fallout from turbulent jets (Riedel et al., 2003; Valentine et al., 2005). The second (and much more numerous) group includes the large cones that reached the second phase and show a correlation between the height and the basal diameter due to the avalanching (Bemis et al., 2011). The cones of this group have the same or very similar shapes even though they have different volumes and their basic physical characteristics (ejection velocity, particle size etc.) may vary significantly from cone to cone. Thanks to this self-similarity, scoria cones on Earth can be easily identified, but the physical conditions at the time of eruption (e.g., ejection velocity) can hardly be traced back.

The evolution of scoria cones on Mars is different in that none of the studied cones does reach the second phase. The cones were built by ballistic deposition only and, in spite of large volumes of ejected material, their flank slopes did not attain the angle of repose because the area where the material was deposited was very large. Each scoria cone on Mars thus contains a record of the specific physical conditions at the time of eruption which can be, at least partly, inferred from its shape. This also explains the wide variety of shapes (Fig. 6.6 and 6.7) observed in the three regions studied in this paper.

We find that the volumes of investigated cones are generally larger by one to two orders of magnitude than is typical of terrestrial scoria cones (Fig. 6.6c; Brož et al., 2014). This suggests that monogenetic volcanism on Mars had to be more voluminous in the past than on Earth. Unfortunately, a direct link between the size of cone and the total amount of erupted material is not easy to establish and our estimates of magma volumes are only approximate. On Earth, the size of the scoria cone is a function of the amount of magma erupted to the close vicinity of the vent and does not necessarily correspond to the total amount of magma reaching the surface. This is because a large amount of fine grained material fragmented from magma during the volcanic eruption can be transported by a neutrally buoyant volcanic cloud and deposited far away from the main body of the cone (Bemis et al., 2011). One can expect that some amount of material was also transported away from the immediate vicinity of the martian cones (Brož et al., 2014). Therefore, the measured volumes (Table 6.1 and Fig. 6.6c) may be underestimated as they represent only the material contained in the cone itself. The investigated datasets include only a few edifices higher than 400 m (Fig. 6.6c). Whether the style of monogenic volcanism on Mars in the past is better represented by the small- and intermediate-size volcanoes prevailing in HC and CC rather than the large-size volcanoes in UC is not yet clear.

For each cone we also determine the W_{CR}/W_{CO} and H_{CO}/W_{CO} ratios (Table 6.1 and Fig. 6.6a,b). These two ratios have been widely used in terrestrial and planetary science since they are considered to have a potential to distinguish different landforms (e.g., Wood, 1980, Burr et al., 2009b; Brož and Hauber, 2012; 2013; Noguchi and Kurita, 2015). The average values of these ratios for terrestrial scoria cones are 0.4 and 0.17, respectively (Porter, 1972; Wood, 1980). On Mars, W_{CR}/W_{CO} ranges from 0.05 to 0.34 with the average value being 0.17. The large differences between the values of W_{CR}/W_{CO} may be associated with variations in explosivity caused by a varying amount of released magma gases and/or water, or with different widths of the explosive conduit (Bemis et al., 2011). The H_{CO}/W_{CO} ratio varies from 0.03 to 0.14 with the average value being 0.10. This value is significantly smaller than on Earth which can be accounted for by the differences in formation mechanisms – ballistic deposition on Mars and avalanching on Earth.

6.7. Conclusions

Our study provides a coherent set of morphometric characteristics of 28 conical martian edifices from three regions – Ulysses Colles, Hydraotes Colles and Coprates Chasma. These characteristics are derived from newly available high-resolution DEMs based on HiRISE and CTX stereo-pair images. For each cone we carefully reconstruct its average (axisymmetric) shape and determine the basic morhometric parameters – volume, height, basal width, crater width and slope.

The parameters obtained for the cones in HC and CC show similar distributions which suggests that both fields were created by the same geological process. The cones in UC, which have been interpreted by Brož and Hauber (2012) as scoria cones, form an independent cluster on morphometric graphs and their characteristics differ from those in HC and CC – the cones are more voluminous and have smaller average slope angles than the cones in the other two regions. Using our numerical ballistic model, we show that the difference between the cones in UC and those in HC and CC is only apparent. In spite of obvious morphological differences, the cones in all three fields can be explained by the same ballistic model with the same ejection velocity and particle size distributions. This result suggests that the edifices in all three regions are scoria cones which were formed by the same physical process. The differences in the shape of the cones in UC and those in HC and CC are associated with different elevations of the sites and can be explained by different values of the atmospheric drag. The values of ejection velocity and particle size inferred from the topographic data are in agreement with the theoretical predictions by Wilson and Head (1994) who argued for stronger magma fragmentation and higher ejection velocities on Mars in comparison with the Earth.

Our results support the hypothesis that martian scoria cones differ in shape from the terrestrial cones due to the different mechanism of flank formation (Brož et al., 2014). Because of a long ballistic range, the slopes of scoria cones on Mars never reach the angle of repose and their shapes are fully determined by ballistic deposition – in contrast to the Earth where the subsequent avalanche redistribution plays the dominant role. As a consequence, martian scoria cones show a wide variety of sizes and slope angles, corresponding to different stages of the scoria cone's growth and different volumes of ejected material.

The set of morphological characteristics derived in this study can further be used for comparative studies of other conical edifices on Mars, such as pingos (Burr et al., 2009b), rootless cones (Noguchi and Kurita, 2015), mud volcanoes (Skinner and Mazzini, 2009) or tuff rings and tuff cones (Brož et al., 2013). This set can help to overcome the uncertainties associated with using terrestrial morphometric data which correspond to different environmental conditions and possibly include effects that are not relevant to Mars.

Acknowledgements

This study was supported by the Grant No. 580313 from the Grant Agency of Charles University in Prague (GAUK).

7. Conclusions

This thesis concentrates on small-scale volcanoes on Mars – a comprehensive group of volcanic landforms which have not been a subject of any detailed study. I investigate several conical and domical volcanic edifices on martian surface using available visible-light image and topographic data sets and stereo-pair images (HiRISE, CTX, HRSC; MOLA, HRSC DEM; HiRISE, CTX DEMs). These data permit to determine various morphological and morphometric parameters and compare edifice shapes with possible terrestrial counterparts. As a result, several types of volcanic edifices, namely the scoria cones, tuff rings, tuff cones and lava domes, were discovered on the martian surface.

I have documented the presence of several types of small-scale volcanoes in various regions of Mars: scoria cones in the volcanic field Ulysses Colles situated within Tharsis, tuff cones and tuff rings in the Nephenthes/Amenthes region at the southern edge of the ancient impact basin Utopia, north of Isidis Planitia in the Arena Colles region and within the impact crater Lederberg in Xanthe Terra, and lava domes within an unnamed depression in Terra Sirenum. Additionally, I have confirmed the presence of previously suggested scoria cones in Hydraotes Chaos and supported a hypothesis about the existence of scoria cones on the floor of Coprates Chasma, a part of large canon systems of Valles Marineris, by morphological data. These volcanoes are now interpreted to indicate a globally widespread activity, partly independent and unrelated to the major volcanic provinces Tharsis and Elysium. The age of these volcanoes, constrained by crater counting, is Hesperian or younger, providing additional constraint on much wider time window for the volcanic activity than previously thought, at least regionally and in terms of magma volumes required for the small-scale volcanism.

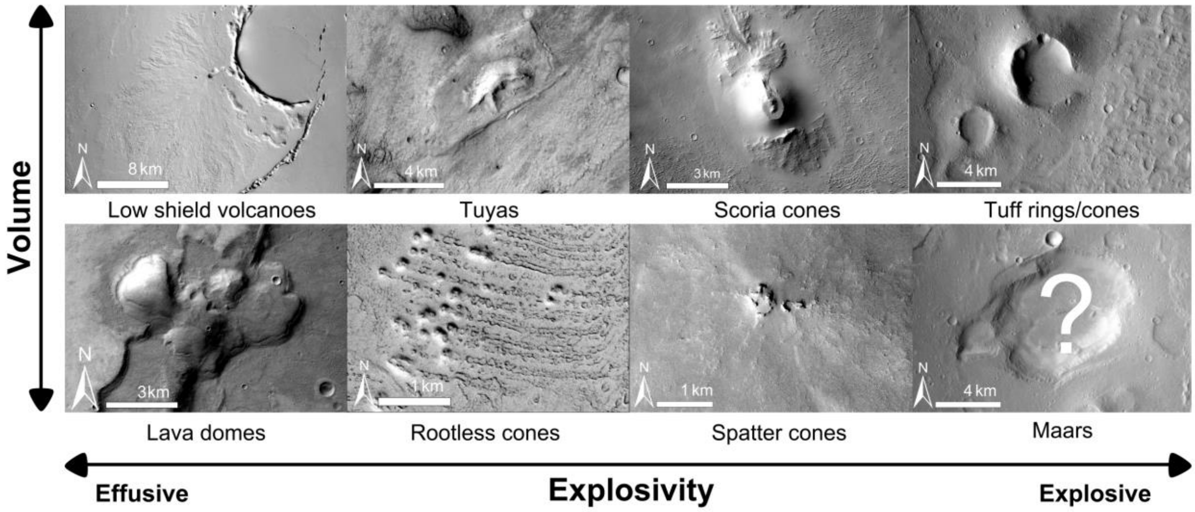

Figure 7.1. Representative examples of different types of small-scale volcanoes present on Mars with the exception of maars – their confirmation has not been clearly confirmed yet. Based on CTX images. Low shield volcanoes: P08_004108_2046_XI_24N110W; tuyas: P19_008430_2212_XN_41N036W; scoria cones: P22_009554_1858_XN_05N122W; tuff rings/cones: P04_002452_1969_XN_16N256W; lava domes: D15_032909_1391_XI_40S173W; rootless cones: B11_014000_2062_XN_26N186W; spatter cones: P11_005216_1726_XN_07S113W; maars: P17_007489_1967_XN_16N257W.

The new morphological and morphometric observations now prove that Mars has been a volcanically rich and diverse body of the Solar system where many styles of small-scale volcanic edifices were created by igneous processes but governed by local physical and environmental factors (Fig. 7.1). This may be illustrated using the example of scoria cones in volcanic field of Ulysses Colles whose formation was likely caused by the presence of a magma enriched by volatiles responsible its fragmentation and the Strombolian eruption style. This volcanic field is superposed on a slightly elevated heavily fractured crust, probably early Hesperian in age, which escaped flooding by younger lava flows associated with effusive plain-style volcanism produced during the youngest large-scale volcanic activity. This spatial configuration thus offers the rare possibility to observe an older martian surface in Tharsis. Furthermore, the presence of scoria cones in Ulysses Colles revealed that volcanism in Tharsis was not exclusively effusive throughout the martian history as it may appear to be today, but it varied in time. In addition, the possible presence of tuff cones and tuff rings in the vicinity of Utopia Basins and at several other localities suggests the presence of (sub)surface water and/or water ice during the time of magma ascent, hence it constrains the paleo-environmental conditions on Mars during the Hesperian epoch. On the other hand, the presence of highly viscous lava domes in the southern highlands suggests that storage of evolved magmas at shallow sub-crustal level(s) may be viable on Mars thus supporting a new, higher density estimate of the martian crust (>3100 kg m^3) proposed by Baratoux et al. (2014).

The morphometry investigations of the small-scale volcanoes demonstrate that scoria cones, tuff rings and tuff cones significantly differ in their shapes from terrestrial analogues. A new numerical model tracks the ballistic trajectories and traces the cumulative deposition of repeatedly ejected particles to predict morphological shapes of scoria cones within Ulysses Colles, Hydraotes Colles and an unnamed field in Coprates Chasma. The observed shapes of the scoria cones in Ulysses Colles have the predicted ejection velocities by a factor of ∼2 higher and the ejected particles have their size ~20 finer than is typical on Earth, corresponding to a mean particle velocity of ∼92 m/s and a particle size of ~2 mm on Mars. These higher ejection velocities combined with lower atmospheric pressure and gravity acceleration cause a wider dispersion of volcanic ejecta. Characteristic eruptive volumes are then not large enough for the flank slopes to reach the angle of repose, in contrast to the Earth where attainment of this limit is common. Overall, the scoria cones on Mars are mainly formed by ballistic distribution rather then by redistribution of flank material by avalanching due to its slope instability.

These above observations and inferences lead to a comprehensive scenario for the growth of the martian scoria cones. Initially, cones on Mars and Earth develop in a comparable manner by gradually increasing the height and the slope angle. Because

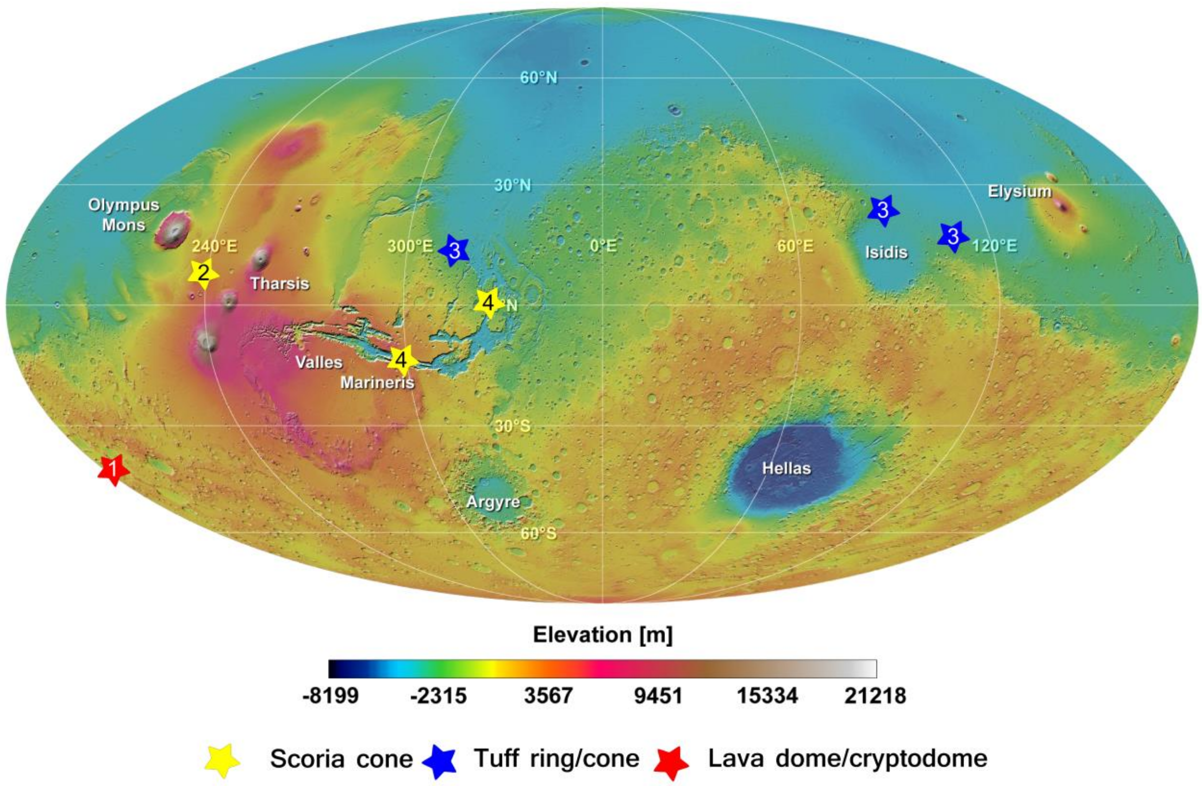

Figure 7.2.: Location of small-scale volcanoes on Mars discovered or confirmed in this thesis, image based on the MOLA DTM data. Numbers refer to: 1 – Brož et al. (2015); 2 – Brož and Hauber (2012); 3 – Brož and Hauber (2013) 4 – Brož et al. (submitted).

of the differences in the ballistic range, ejected particles are deposited on a much smaller area on Earth than on Mars and, for the same volume of ejecta, the terrestrial cone is steeper than the martian one. Once the angle of repose on Earth (~30°) has been reached, the slope inclination remains constant. Continuing growth is accommodated by an increase of the cone width hence terrestrial cones show a correlation between the height and the basal diameter, also due to the avalanching. On the other hand, the martian scoria cones are built by ballistic deposition only and, despite of substantial volumes of ejected material, they never reach the angle of repose because the ejecta is distributed over much greater area. Each scoria cone on Mars thus contains a record of specific physical conditions at the time of eruption which can be, at least partly, reconstructed from its shape. This thesis highlights the significance of environmental setting on physical processes driving the volcanic activity on Mars, and more broadly on other bodies of the Solar system.

8. Outlook and future prospective

Detailed investigation of the small-scale volcanoes on Mars identifies several outstanding questions. It is still unclear how frequent are these volcanoes on the martian surface. They occur at numerous sites suggesting their global distribution (Fig. 7.2), but it is not known whether these volcanoes represent a complementary, perhaps local feature or indicate presence of an important phenomenon that is widespread but perhaps yet overlooked. This thesis shows that these volcanoes may be situated far away from the well-known volcanic provinces hence emphasizing the need to further search for volcanic edifices in the regions where volcanic activity has not been expected.

General shape and size of several types of the small-scale volcanoes present additional, poorly constrained variables. The well-studied volcanic localities with individual types of volcanoes are rather rare and often host only a small number of well-preserved edifices, where detailed morphometric parameters can be determined. For example, lava domes were described from two localities only (Rampey et al., 2006; Brož et al., 2015), scoria cones from eight occurrences, and only three localities covered by high-resolution data (Meresse et al., 2008; Brož and Hauber, 2015; Hauber et al., 2015) contain well-shaped scoria cones (Brož et al., submitted). The scoria cones in these three regions show variations in their volume, size, and shape (*cf.* more voluminous cones of Ulysses Colles or smaller cones of Hydraotes Colles and in Coprates Chasma). Therefore, a 'representative' martian scoria cone has yet to be established. This uncertainty regarding the volumes of the martian scoria cones may be generalized: investigations of the scoria cones (Meresse et al., 2008;

Brož and Hauber, 2012; Brož et al., 2014), low shield volcanoes (Hauber et al., 2009), tuff rings and tuff cones (Brož and Hauber, 2013) suggest that the monogenetic volcanism is more voluminous on Mars than on Earth. However, no quantitative comparison is possible yet and it will have to await discoveries of new edifices of individual types of small-scale volcanoes on the martian surface. Nevertheless, this study provides an extensive dataset of morphometric data that may be used in future research and comparative studies with other conical features such as mud volcanoes on Mars, but also on other terrestrial planets.

The shape of volcanoes depends on the eruptive mechanism and environmental constraints. Hence investigation of the small-scale edifices offers a tool for understanding paleo-environmental conditions in specific regions of Mars. The tuff rings and tuff cones, newly identified (Brož and Hauber, 2013), require presence of subsurface water and/or water ice for their formation hence their existence on the planetary surfaces identifies areas where water ice was or still is stable. Similarly, the size fraction of the ejected particles forming the scoria cones revealed by in-situ investigation provides constraints on levels of atmospheric pressure during the volcanic event. The integrated physical volcanological modeling can thus provide vital insights into the characteristics of the martian surface, which would be difficult to obtain otherwise.

9. References

Alatorre-Ibargüengoitia, M. A., Delgado-Granados, H., 2006. Experimental determination of drag coefficient for volcanic materials: Calibration and application of a model to Popocatépetl volcano (Mexico) ballistic projectiles, Geophysical Research Letters, 33, L11302, doi: 10.1029/2006GL026195.

Anderson, R. C., Dohm, J. M., Golombek, M. P., Haldemann, A. F. C., Franklin, B. J., Tanaka, K. L., Lias, J., Peer, B., 2001. Primary centers and secondary concentrations of tectonic activity through time in the western hemisphere of Mars, Journal of Geophysical Research, 106, 20,563–20,585, doi:10.1029/2000JE001278.

Arfstrom, J., Hartmann, W. K., 2005. Martian flow features, moraine-like ridges, and gullies: Terrestrial analogs and interrelationships, Icarus, 174, 321–335, doi: 10.1016/j.icarus.2005.05.011.

Atwood-Stone, C., McEwen, A. S., 2013. Avalanche Slope Angles in Low Gravity Environments from Active Martian Sand Dunes, Geophysical Research Letters, 40, 2929–2934, doi: 10.1002/grl.50586.

Baker, V. R., 2001. Water and the martian landscape, Nature, 412, 228–236, doi:10.1038/35084172.

Baker, D. M., Head, J. W., Marchant, D. R., 2010. Flow patterns of lobate debris aprons and lineated valley fill north of Ismeniae Fossae, Mars: Evidence for extensive mid-latitude glaciation in the Late Amazonian, Icarus, 207, 186–209, doi: 10.1016/j.icarus.2009.11.017.

Balme, M., Berman, D., Bourke, M. Zimbelman, J., 2008. Transverse Aeolian Ridges (TARs) on Mars, Geomorphology, 101, 703–720, doi: 10.1016/j.geomorph.2008.03.011.

Bandfield, J. L., Hamilton, V. E., Christensen, P. R., McSween, H. Y. Jr., 2004. Identification of quartzofeldspathic materials on Mars, Journal of Geophysical Research, 109 (E10009), doi: 10.1029/2004JE002290.

Baratoux, D., Toplis, M. J., Monnereau, M., Sautter, V., 2013. The petrological expression of early Mars volcanism, Journal of Geophysical Research: Planets, 118, 59–64, doi:10.1029/2012JE004234.

Baratoux, D., Samuel, H., Michaut, C., Toplis, M. J., Monnereau, M., Wieczorek, M., Garcia, R., Kurita, K., 2014. Petrological constraints on the density of the Martian crust, Journal of Geophysical Research: Planets, 119, 1707–1727, doi:10.1002/2014JE004642.

Basaltic Volcanism Study Project, 1981. Basaltic Volcanism on the Terrestrial Planets, Pergamon Press, Inc., New York, 1286.

Bemis, K., Walker, J., Borgia, A., Turrin, B., Neri, M., Swisher, C. III, 2011. The growth and erosion of cinder cones in Guatemala and El Salvador: models and statistics, Journal of Volcanology and Geothermal Research, 201, 39–52, doi: 10.1016/j.jvolgeores.2010.11.007.

Beven, K., 1996. Equifinality and Uncertainty in Geomorphological Modelling. In: The Scientific Nature of Geomorphology, Proc. 27th Binghampton Symp. Geomorphology, B.L. Rhoads and C.E. Thorn (eds.), 289–313, Wiley.

Bird, R. B., Steward, W. E., Lightfood, E. N., 1960. Transport Phenomena, John Wiley and Sons, New York.

Blackburn, E. A., Wilson, L., Sparks, R. S. J., 1976. Mechanisms and dynamics of Strombolian aktivity, Journal of the Geological Society, 132, 429–440, doi: 10.1144/gsjgs.132.4.0429.

Bleacher, J. E., Greeley, R., Williams, D. A., Cave, S. R., Neukum, G., 2007. Trends in effusive style at the Tharsis Montes, Mars, and implications for the development of the Tharsis province, Journal of Geophysical Research, 112 (E09005), doi:10.1029/2006JE002873.

Bleacher, J. E., Glaze, L. S., Greeley, R., Hauber, E., Baloga, S. M., Sakimoto, S. E. H., Williams, D. A., Glotch, T. D., 2009. Spatial and alignment analyses for a field of small volcanic vents south of Pavonis Mons and implications for the Tharsis province, Mars, Journal of Volcanology and Geothermal Research, 185, 96–102, doi: 10.1016/j.jvolgeores.2009.04.008.

Bonali, F. L., Corazzato, C., Tibaldi, A., 2011. Identifying rift zones on Volcanoes: an example from La Réunion Island, Indian Ocean, Bulletin of Volcanology, 73, 347–366, doi: 10.1007/s00445-010-0416-1.

Bonini, M., 2012. Mud volcanoes: Indicators of stress orientation and tectonic controls, Earth-Science Reviews, 115, 121–152, doi: 10.1016/j.earscirev.2012.09.002.

Boulton, G. S., 1978. Boulder shapes and grain size distributions of debris as indicators of transport paths through a glacier and till genesis, Sedimentology, 25, 773–799, doi: 10.1111/j.1365-3091.1978.tb00329.x.

Bradley, B. A., Sakimoto, S. E. H., Frey, H., Zimbelman, J. R., 2002. Medusae Fossae Formation: New perspectives from Mars Global Surveyor, Journal of Geophysical Research, 107, 2–1–2–17, doi: 10.1029/2001JE001537.

Brož, P., Hauber, E., 2012. A unique volcanic field in Tharsis, Mars: Pyroclastic cones as evidence for explosive eruptions, Icarus, 218, 88–99, doi:10.1016/j.icarus.2011.11.030.

Brož, P., Hauber, E., 2013. Hydrovolcanic tuff rings and cones as indicators for phreatomagmatic explosive eruptions on Mars, Journal of Geophysical Research: Planets, 118, 1656–1675, doi: 10.1002/jgre.20120.

Brož. P. Čadek, O., Hauber, E., Rossi, A. P., 2014. Shape of scoria cones on Mars: insights from numerical modeling of ballistic pathways, Earth and Planetary Science Letters, 406, 14–23, doi: 10.1016/j.epsl.2014.09.002.

Brož, P., Hauber, E., Platz, T., Balme, M., 2015. Evidence for Amazonian highly viscous lavas in southern highlands on Mars, Earth and Planetary Science Letters, 415, 200–212, doi: 10.1016/j.epsl.2015.01.033.

Brož. P., Čadek, O., Hauber, E., Rossi, A. P., submitted. Scoria cones on Mars: detailed investigation of morphometry based on HiRISE and CTX DEMs, Journal of Geophysical Research: Planets.

Buisson, C., Merle, O., 2002. Experiments on internal strain in lava dome cross sections, Bulletin of Volcanology, 64, 363–371, doi: 10.1007/s00445-002-0213-6.

Bulmer, M. H., Glaze, L. S., Anderson, S., Shocky, K. M., 2005. Distinguishing between primary and secondary emplacement events of blocky volcanic deposits using rock size distributions, Journal of Geophysical Research, 110 (B01201), doi:10.1029/2003JB002841.

Burr, D. M., Bruno, B. C., Lanagan, P. D., Glaze, L. S., Jaeger, W. L., Soare, R. J., Wan Bun Tseung, J.-M., Skinner, J. A., Baloga, S. M., 2009a. Mesoscale raised rim depressions (MRRDs) on Earth: A review of the characteristics, processes, and spatial distributions of analogs for Mars, Planetary and Space Science, 57, 579–596, doi: 10.1016/j.pss.2008.11.011.

Burr, D. M., Tanaka, K. L., Yoshikawa, K., 2009b. Pingos on Earth and Mars, Planetary and Space Science, 57, 541–555, doi: 10.1016/j.pss.2008.11.003.

Byrne, S., et al., 2009. Distribution of Mid-Latitude Ground Ice on Mars from New Impact Craters, Science, 325, 1674–1676, doi: 10.1126/science.1175307.

Calvari, S., Pinkerton, H., 2004. Birth, growth and morphologic evolution of the 'Laghetto' cinder cone during the 2001 Etna eruption, Journal of Volcanology and Geothermal Research, 132, 225–239, doi:10.1016/S0377-0273(03)00347-0.

Carey, S., Sparks, R. S. J., 1986. Quantitative models of the fallout and dispersal of tephra from volcanic eruption columns, Bulletin of Volcanology, 48, 109–125, doi: 10.1007/BF01046546.

Carey, S., Bursik, M., 2000. Volcanic plumes, in: Sigurdsson, H. (Ed.), Encyclopedia of Volcanoes, Academic Press, San Diego, California, 527–544.

Carn, S. A., 2000. The Lamongan volcanic field, East Java, Indonesia: physical volcanology, historic activity and hazards, Journal of Volcanology and Geothermal Research, 95, 81–108, doi: 10.1016/S0377-0273(99)00114-6.

Carr, M. H., Greeley, R., Blasius, K. R., Guest, J. E., Murray, J. B., 1977. Some Martian volcanic features as viewed from the Viking Orbiters, Journal of Geophysical Research, 82, 3985–4015, doi: 10.1029/JS082i028p03985.

Carr, M. H., Head, J. W., 2010. Geologic history of Mars, Earth and Planetary Science Letters, 185–203, doi:10.1016/j.epsl.2009.06.042.

Carruthers, M. W., McGill, G. W., 1998. Evidence for igneous activity and implications for the origin of a fretted channel in southern Ismenius Lacus, Mars, Journal of Geophysical Research, 103, 31,433–31,443, doi: 10.1029/98JE02494.

Carter, J., Poulet, F., 2013. Ancient plutonic processes on Mars inferred from the detection of possible anorthositic terrains, Nature Geoscience, 6, 1008–1012, doi:10.1038/ngeo1995.

Cashman, K. V., Sturtevant, B., Papale, P., Navon, O. 2000. Magmatic Fragmentation, in: Sigurdsson, H. (Ed.), Encyclopedia of Volcanoes, Academic Press, San Diego, California, 421–430.

Cebriá, J. M., Martín-Escorza, C., López-Ruiz, J., Morán-Zenteno, D. J., Martiny, B. M., 2011. Numerical recognition of alignments in monogenetic volcanic areas: Examples from the Michoacán-Guanajuato Volcanic Field in Mexico and Calatrava in Spain, Journal of Volcanology and Geothermal Research, 201, 73–82, doi: 10.1016/j.jvolgeores.2010.07.01.

Cattermole, P., 1986. Linear volcanic features at Alba Patera, Mars-probable spatter ridges, Journal of Geophysical Research, 91, 159–165, doi: 10.1029/JB091iB13p0E159.

Clark, P. J., Evans, F. C., 1954. Distance to nearest neighbour as a measure of spatial relationships in populations, Ecology, 35, 445–453, doi: 10.2307/1931034.

Clarke, H., Troll, V. R., Carracedo, J. C., 2009. Phreatomagmatic to Strombolian eruptive activity of basaltic cinder cones: Montaña Los Erales, Tenerife, Canary Islands, Journal of Volcanology and Geothermal Research, 180, 225–245, doi: 10.1016/j.jvolgeores.2008.11.014.

Colaprete, A., Jakosky, B. M., 1998. Ice flow and rock glaciers on Mars, Journal of Geophysical Research, 103, 5897–5909, doi: 10.1029/97JE03371.

Connor, C. B., 1990. Cinder cone clustering in the TransMexican Volcanic Belt: Implications for structural and petrologic models, Journal of Geophysical Research, 95, 19,395–19,405, doi: 10.1029/JB095iB12p19395.

Connor, C. B., Conway, F. M., 2000. Basaltic Volcanic Fields, in: Sigurdsson, H. (Ed.), Encyclopedia of Volcanoes, Academic Press, San Diego, California, 331–343.

Corazzato, C., Tibaldi, A., 2006. Fracture control on type, morphology and distribution of parasitic volcanic cones: An example from Mt. Etna, Italy, Journal of Volcanology and Geothermal Research, 158, 177–194, doi: 10.1016/j.jvolgeores.2006.04.018.

Crater Analysis Techniques Working Group, 1979. Standard techniques for presentation and analysis of crater size-frequency data, Icarus, 37, 467–474, doi: 10.1016/0019-1035(79)90009-5.

Crown, D. A., Greeley, R., 1993. Volcanic geology of Hadriaca Patera and the eastern Hellas region of Mars, Journal of Geophysical Research, 98, 3431–3451, doi: 10.1029/92JE02804.

de Pablo, M. A., Pacifici, A., 2008. Geomorphological evidence of water level changes in Nepenthes Mensae, Mars, Icarus, 196, 667–671, doi:10.1016/j.icarus.2008.04.005.

de Pablo, M. A., Caprarelli, G., 2010. Possible Subglacial Volcanoes in Nepenthes Mensae, Eastern Hemisphere, Mars, LPSC, 41st Lunar and Planetary Institute Science Conference, #1584 (abstract).

de Silva, S., Self, P., Francis, P. W., Drake, R. E., Ramirez, R. C., 1994. Effusive silicic volcanism in the Central Andes: the Chao dacite and other young lavas of the Altiplano-Puna Volcanic Complex, Journal of Geophysical Research, 99 (B9), 17,805–17,825, doi: 10.1029/94JB00652.

Dehn, J., Sheridan, M. F., 1990. Cinder cones on the Earth, Moon, Mars, and Venus: A computer model, 21st Lunar and Planetary Institute Science Conference, #270 (abstract).

Dohrenwend, J. C., Wells, S. G., Turrin, B. D., 1986. Degradation of Quaternary cinder cones in the Cima volcanic field, Mojave Desert, California, Geological Society of America Bulletin, 97, 421–427, doi: 10.1130/0016-7606(1986)97<421:DOQCCI>2.0.CO;2.

Edgett, K. S., 1990. Possible cinder cones near the summit of Pavonis Mons, Mars. 21st Lunar and Planetary Institute Science Conference, 311–312 (abstract).

Ennis, M. E., Schmidt, M. E., McCoy, T., Farrand, W., Cabrol, N., 2007. Hydorvolcano on Mars? A comparison of Home Plate, Gusev Crater and Zuni Salt Lake Maar, New Mexico, 38th Lunar and Planetary Institute Science Conference, #1966 (abstract).

Erkeling, G., Hiesinger, H., Reiss, D., Hielscher, FJ., Ivanov, M. A., 2011. The stratigraphy of the Amenthes region, Mars: Time limits for the formation of fluvial, volcanic and tectonic landforms, Icarus, 215, 128–152, doi: 10.1016/j.icarus.2011.06.041.

Erkeling, G., Reiss, D., Hiesinger, H., Carter, J., Ivanov, M. A., Hauber, E., Jaumann, R., 2012. Valleys, paleolakes and possible shorelines at the Libya Montes/Isidis boundary: Implications for the hydrologic evolution of Mars, Icarus, 219, 393–413, doi: 10.1016/j.icarus.2012.03.012.

Fagents, S. A., Wilson, L., 1993. Explosive volcanic eruptions—VII. The ranges of pyroclasts ejected in transient volcanic explosions, Geophysical Journal International, 113(2), 359–370, doi:10.1111/j.1365-246X.1993.tb00892.x.

Fagents, S. A., Wilson, L., 1996. Numerical modeling of ejecta dispersal from transient volcanic explosions on Mars, Icarus, 123, 284–295, doi: 10.1006/icar.1996.0158.

Fagents, S. A., Thordarson, T., 2007. Rootless volcanic cones in Iceland and on Mars. In: Chapman, M. (Ed.), The Geology of Mars, Cambridge University Press, Cambridge, 151–177.

Farr, T. G., et al., 2007. The Shuttle Radar Topography Mission, Reviews of Geophysics, 45, RG2004, doi:10.1029/2005RG000183.

Farrand, W. H., Gaddis, L. R., Keszthelyi, L., 2005. Pitted cones and domes on Mars: Observations in Acidalia Planitia and Cydonia Mensae using MOC, THEMIS, and TES data, Journal of Geophysical Research, 110 (E5), doi:10.1029/2004JE002297.E05005.

Farrand, W. H., Lane, M. D., Edwards, B. R., Yingst, R. A., 2011. Spectral evidence of volcanic cryptodomes on the northern plains of Mars, Icarus, 211 (1), 139–156, doi: 10.1016/j.icarus.2010.09.006.

Fassett, C. I., Head, J. W., 2008. The timing of martian valley network activity: constraints from buffered crater counting, Icarus, 195, 61–89, doi: 10.1016/j.icarus.2007.12.009.

Fassett, C. I., Levy, J. S., Head, J. W., Dickson, J. L., 2014. Long-lived Glaciation in the Northern Mid-Latitudes of Mars: New Constraints on Timing, 45th Lunar and Planetary Institute Science Conference, #1494 (abstract).

Favalli, M., Mazzarini, F., Pareschi, M. T., Boschi, E., 2009a. Topographic control on lava flow paths at Mt. Etna (Italy): Implications for hazard assessment, Journal of Geophysical Research, 114 (F01019), doi: 10.1029/2007JF000918.

Favalli, M, Karátson, D., Mazzarini, F., Pareschi, M. T., Boschi, E., 2009b. Morphometry of scoria cones located on a volcano flank: A case study from Mt. Etna (Italy), based on high-resolution LiDAR data, Journal of Volcanology and Geothermal Research, 186, 320–330, doi: 10.1016/j.jvolgeores.2009.07.011.

Feldman, W. C., et al., 2004. Global distribution of near-surface hydrogen on Mars, Journal of Geophysical Research, 109 (E09006), doi:10.1029/2003JE002160.

Fergason, R. L., Christensen, P. R., Kieffer, H. H., 2006. High-resolution thermal inertia derivation from THEMIS: Thermal model and applications, Journal of Geophysical Research, 111, E12004, doi:10.1029/2006JE002735.

Fink, J. H., Griffiths, R. W., 1998. Morphology, eruption rates, and rheology of lava domes: Insights from laboratory models, Journal of Geophysical Research-Solid Earth, 103 (B1), 527–545, doi: 10.1029/97JB02838.

Fink, J. H., Anderson, S. W., 2000. Lava domes and coulees, in: Sigurdsson, H. (Ed.), Encyclopedia of Volcanoes, Academic Press, San Diego, California, 307–319.

Francis, P. W., Wood, C. A., 1982. Absence of silicic volcanism on Mars - Implications for crustal composition and volatile abundance, Journal of Geophysical Research, 87, 9881–9889, doi: 10.1029/JB087iB12p09881.

Frey, H., Jarosewich, M., 1982. Subkilometer Martian volcanoes - Properties and possible terrestrial analogs, Journal of Geophysical Research, 87, 9867–9879, doi: 10.1029/JB087iB12p09867.

Garvin, J. B., Sakimoto, S. E. H., Frawley, J. J., Schnetzler, C. C., 2000. North polar region craterforms on Mars: Geometric characteristics from the Mars Orbiter Laser Altimeter, Icarus, 144, 329–352, doi: 10.1006/icar.1999.6298.

Ghent, R. R., Anderson, S. W., Pithawala, T. M., 2012. The formation of small cones in Isidis Planitia, Mars through mobilization of pyroclastic surge deposits, Icarus, 217, 169–183, doi: 10.1016/j.icarus.2011.10.018.

Gilichinsky, M., Melnikov, D., Melekestsev, I., Zaretskaya, N., Inbar, M., 2010. Morphometric measurements of cinder cones from digital elevation models of Tolbachik volcanic field, central Kamchatka, Canadian Journal of Remote Sensing, 36, 287–300, doi: 10.5589/m10-049.

Glaze, L. S., Baloga, S. M., 2000. Stochastic-ballistic eruption plumes on Io, Journal of Geophysical Research: Planets, 105, 17579–17588, doi: 10.1029/1999JE001235.

Golombek, M. P., et al., 2006. Erosion rates at the Mars Exploration Rover landing sites and long-term climate change on Mars, Journal of Geophysical Research, 111 (E12S10), doi: 10.1029/2006JE002754.

Google Inc., 2011, Google Earth (Version 6.1.0.5001, software). Available from http://www.google.com/earth.

Gouhier, M., Donnadieu, F., 2010. The geometry of Strombolian explosions: insights from Doppler radar measurements, Geophysical Journal International, 183, 1376–1391, doi: 10.1111/j.1365-246X.2010.04829.x.

Greeley, R., 1973. Mariner 9 photographs of small volcanic structures on Mars, Geology, 1, 175–180, doi: 10.1130/0091-7613(1973)1<175:MPOSVS>2.0.CO;2.

Greeley, R., 1982. The Snake River Plains, Idaho: representative of a new category of volcanism, Journal of Geophysical Research, 87, 2705–2712, doi: 10.1029/JB087iB04p02705.

Greeley, R., Theilig, E., 1978. Small Volcanic Constructs in the Chryse Planitia Region of Mars. NASA TM-79729, 202 pp.

Greeley, R., Spudis, P. D., 1981. Volcanism on Mars, Reviews of Geophysics and Space Physics, 19, 13–41, doi: 10.1029/RG019i001p00013.

Greeley, R., Guest, J. E., 1987. Geological Map of the Eastern Equatorial Region of Mars I-1802-B. U.S. Geological Survey, Flagstaff, AZ, USA.

Greeley, R., Crown, D. A., 1990. Volcanic geology of Tyrrhena Patera, Mars, Journal of Geophysical Research, 95, 7133–7149, doi: 10.1029/JB095iB05p07133.

Gregg, T. K. P., Williams, S. N., 1996. Explosive mafic volcanoes on Mars and Earth: Deep magma sources and rapid rise rate, Icarus, 122, 397-405, doi: 10.1006/icar.1996.0132.

Gregg, T. K. P., Farley, M. A., 2006. Mafic pyroclastic flows at Tyrrhena Patera, Mars: Constraints from observations and models, Journal of Volcanology and Geothermal Research, 155, 81–89, doi: 10.1016/j.jvolgeores.2006.02.008.

Grosse, P., van Wyk de Vries, B., Euillades, P.A., Kervyn, M., Petrinovic, I., 2012. Systematic morphometric characterization of volcanic edifices using digital elevation models, Geomorphology, 136, 114–131, doi:10.1016/j.geomorph.2011.06.001.

Grott, M., Baratoux, D., Hauber, E., Sautter, V., Mustard, J., Gasnault, O., Ruff, S. W., Karato, S.-I., Debaille, V., Knapmeyer, M., Sohl, F., Van Hoolst, T., Breuer, D., Morschhauser, A., Toplis, M. J., 2013. Long-Term Evolution of the Martian Crust-Mantle System, Space Science Reviews, 174, 49–111, doi:10.1007/s11214-012-9948-3.

Guth, P. L., 2006. Geomorphometry from SRTM: Comparison to NED, PE&RS, 72, 269–277, doi: 10.14358/PERS.72.3.269.

Gwinner, K., Scholten, F., Preusker, F., Elgner, S., Roatsch, T., Spiegel, M., Schmidt, R., Oberst, J., Jaumann, R., Heipke, C., 2010. Topography of Mars from global mapping by HRSC high-resolution digital terrain 2 models and orthoimages: Characteristics and performance, Earth and Planetary Science Letters, 294, 506–519, doi:10.1016/j.epsl.2009.11.007.

Hale, H. J., Bourgouin, L., Mühlhaus, H.-B., 2007. Using the level-set method to model endogenous lava dome growth, Journal of Geophysical Research, 112 (B3), doi: 10.1029/2006JB004445.

Hamilton, C. W., Fagents, S. A., Thordarson, T., 2011. Lava-ground ice interactions in Elysium Planitia, Mars: Geomorphological and geospatial analysis of the Tartarus Colles cone groups, Journal of Geophysical Research, 116 (E03004), doi: 10.1029/2010JE003657.

Harris, A. J. L, Ripepe, M., Hughes, E. A., 2012. Detailed analysis of particle launch velocities, size distributions and gas densities during normal explosions at Stromboli, Journal of Volcanology and Geothermal Research, 231–232, 109–131 doi:10.1016/j.jvolgeores.2012.02.012.

Harrison, K. P, Chapman, M. G., 2008. Evidence for ponding and catastrophic floods in central Valles Marineris, Mars, Icarus, 198, 351–364, doi: 10.1016/j.icarus.2008.08.003.

Hartmann, W. K., Neukum, G., 2001. Cratering chronology and the evolution of Mars, Space Science Reviews, 96, 165–194, doi: 10.1023/A:1011945222010.

Hartmann, W. K., Werner, S. C., 2010. Martian Cratering 10. Progress in use of crater counts to interpret geological processes: Examples from two debris aprons, Earth and Planetary Science Letters, 294, 230–237, doi: 10.1016/j.epsl.2009.10.001.

Hasenaka, T., Carmichael, I. S. E., 1985a. A compilation of location, size, and geomorphological parameters of volcanoes of the Michoacán-Guanajuato volcanic field, Central Mexico, Geofísica Internacional, 24–4, 577–607.

Hasenaka, T., Carmichael, I. S. E., 1985b. The cinder cones of Michoacán–Guanajuato, central Mexico: their age, volume and distribution, and magma discharge rate, Journal of Volcanology and Geothermal Research, 25, 104–124, doi: 10.1016/0377-0273(85)90007-1.

Hauber, E., van Gasselt, S., Chapman, M. G., Neukum, G., 2008. Geomorphic evidence for former lobate debris aprons at low latitudes on Mars: Indicators of the Martian paleoclimate, Journal of Geophysical Research, 113 (E02007), doi:10.1029/2007JE002897.

Hauber, E., Bleacher, J., Gwinner, K., Williams, D., Greeley, R., 2009a. The topography and morphology of low shields and associated landforms of plains volcanism in the Tharsis region of Mars, Journal of Volcanology and Geothermal Research, 185, 69–95, doi: 10.1016/j.jvolgeores.2009.04.015.

Hauber, E., Gwinner, K., Kleinhans, M., Reiss, D., Di Achille, G., Ori, G.-G., Scholten, F., Marinangeli, L., Jaumann, R., Neukum, G., 2009b. Sedimentary deposits in Xanthe Terra: Implications for the ancient climate on Mars, Planetary and Space Science, 57, 944–957, doi: 10.1016/j.pss.2008.06.009.

Hauber, E., Brož, P., Jagert, F. Jodłowski, P., Platz, T., 2011. Very recent and wide-spread basaltic volcanism on Mars, Geophysical Research Letters, 28, L10201, doi:10.1029/2011GL047310.

Hauber, E., Platz, T., Kleinhans, M., Le Deit, L., Carbonneau, P., De Haas, T., Marra, W. Reiss, D., 2012. Old or Not So Old: That is the Question for Deltas and Fans in Xanthe Terra, Mars, Third Conference on Early Mars, #7078 (abstract).

Hauber, E., Brož, P., Rossi, A. P., Michael, G., 2015. A Field of Small Pitted Cones on the Floor of Coprates Chasma, Mars: Volcanism Inside Valles Marineris?, 46th Lunar and Planetary Institute Science Conference, #1476 (abstract).

Head, J. W., Wilson, L., 1989. Basaltic pyroclastic eruptions: influence of gas release patterns and volume fluxes on fountain structure, and the formation of cinder cones, spatter cones, rootless flows, lava ponds and lava flows, Journal of Volcanology and Geothermal Research, 37, 261–271, doi: 10.1016/0377-0273(89)90083-8.

Head, J. W., Crumpler, L. S., Aubele, J. C., Guest, J. E., Saunders, R. S., 1992. Venus volcanism - Classification of volcanic features and structures, associations, and global distribution from Magellan data, Journal of Geophysical Research, 97, 13,153–13,197, doi: 10.1029/92JE01273.

Head, J. W., Kreslavsky, M. A., Pratt, S., 2002. Northern lowlands of Mars: Evidence for widespread volcanic flooding and tectonic deformation in the Hesperian Period, Journal of Geophysical Research, 107 (E1), doi:10.1029/2000JE001445.

Head, J. W., Marchant, D. R., Shean, D. R., Fassett, C. I., Wilson, L., 2005. Interrelated glacial, volcanic and hydrologic processes on the Tharsis Montes, Olympus Mons and Hecates Tholus, Mars, Eos Transactions American Geophysical Union, 86 (52). P23B-0191. ISSN 0096-3941.

Head, J. W., Marchant, D. R., Dickson, J. L., Kress, A. M., Baker, D. M., 2010. Northern mid-latitude glaciation in the Late Amazonian period of Mars: Criteria for the recognition of debris-covered glacier and valley glacier landsystem deposits, Earth and Planetary Science Letters, 294 (3-4), 306–320, doi:10.1016/j.epsl.2009.06.041.

Hodges, C. A., 1979. Some lesser volcanic provinces on Mars. Reports of Planetary Geology Program, 1978–1979, NASA TM-80339, Washington, D.C., 247–249.

Hodges, C. A., 1980. The domes and associated flow lobes in Arcadia Planitia, Mars, in Reports of the planetary geology program, 1979-1980: Technical Memorandum 81776, edited by P. Wirth, R. Greeley and R. E. D'Alli, 184–186, US National Aeronautics and Space Administration.

Hodges, C. A., Moore, H. J., 1979. The subglacial birth of Olympus Mons and its aureoles, Journal of Geophysical Research, 84, 8061–8074, doi 10.1029/JB084iB14p0806.

Hodges, C. A., Moore, H. J., 1994. Atlas of volcanic features on Mars. U. S. Geol. Survey Professional Paper 1534, U. S. Govt. Printing Office, Washington DC, 194 pp.

Holt, J. W., Safaeinili, A., Plaut, J. J., Head, J. W., Phillips, R. J., Seu, R., Kempf, S. D., Choudhary, P., Young, D. A., Putzig, N. E., 2008. Radar sounding evidence for buried glaciers in the southern mid-latitudes of Mars, Science, 322, 1235–1238, doi: 10.1126/science.1164246.

Hooper, D. M., Sheridan, M. F., 1998. Computer-simulation models of scoria cone degradation, Journal of Volcanology and Geothermal Research, 83, 241–267, doi: 10.1016/S0377-0273(98)00031-6.

Hynek, B. M., Phillips, R. J., Arvidson, R. E., 2003. Explosive volcanism in the Tharsis region: Global evidence in the Martian geologic record, Journal of Geophysical Research, 108 (E9), doi: 10.1029/2003JE002062.

Chapman, M. G., 2002. Layered, massive and thin sediments on Mars: possible Late Noachian to Late Amazonian tephra? In: Smellie, J. L., Chapman, M. G. (Eds.), Volcano-Ice Interaction on Earth and Mars, Geological Society, 273-293, doi: 10.1144/GSL.SP.2002.202.01.14.

Christensen, P. R. et al., 2004. The Thermal Emission Imaging System (THEMIS) for the Mars 2001 Odyssey Mission, Space Science Reviews, 110, 85–130, doi: 10.1023/B:SPAC.0000021008.16305.94.

Christensen, P. R., et al., 2005. Evidence for magmatic evolution and diversity on Mars from infrared observations, Nature, 436, 504–509, doi: 10.1038/nature03639.

Chuang, F. C, and Crown, D. A., 2005. Surface characteristics and degradational history of debris aprons in the Tempe Terra/Mareotis fossae region of Mars, Icarus, 179 (1), 24–42, doi:10.1016/j.icarus.2005.05.014.

Inbar, M., Risso, C., 2001. A morphological and morphometric analysis of a high density cinder cone volcanic field — Payun Matru, south-central Andes, Argentina. Zeitschrift für Geomorphologie, 45, 321–343, doi: 10.1016/j.jvolgeores.2010.07.013.

Inbar, M., Gilichinsky, M., Melekestsev, I., Melnikov, D., Zaretskaya, N., 2011. Morphometric and morphological development of Holocene cinder cones: A field and remote sensing study in the Tolbachik volcanic field, Kamchatka, Journal of Volcanology and Geothermal Research, 201, 301–311, doi: 10.1016/j.jvolgeores.2010.07.013.

Irwin III, R. P., Howard, A.D., Maxwell, T. A., 2004. Geomorphology of Ma'adim Vallis, Mars, and associated paleolake basins, Journal of Geophysical Research, 109 (E12), doi: 10.1029/2004JE002287.

Ivanov, M. A., 2001. Mars/Moon Cratering Rate Ratio Estimates, Space Science Reviews, 96, 87–104, doi: 10.1023/A:1011941121102.

Ivanov, M. A., Hiesinger, H., Erkeling, G., Hielscher, F. J., Reiss, D., 2012. Major episodes of geologic history of Isidis Planitia on Mars, Icarus, 218, 24–46, doi: 10.1016/j.icarus.2011.11.029.

Jankowski, D. G., Squyres, S. W., 1992. The topography of impact craters in 'softened' terrain on Mars, Icarus, 100, 26–39, doi: 10.1016/0019-1035(92)90015-Y.

Jarvis, A., Reuter, H. I., Nelson, A., Guevara, E., 2008. Hole-filled SRTM for the globe Version 4, available from the CGIAR-CSI SRTM 90m Database (http://www.cgiar-csi.org/data/elevation/item/45-srtm-90m-digital-elevation-database-v41).

Jaumann, R., et al., 2007. The high-resolution stereo camera (HRSC) experiment on Mars Express: Instrument aspects and experiment conduct from interplanetary cruise through the nominal mission, Planetary and Space Science, 55, 928–952, doi: 10.1016/j.pss.2006.12.003.

Jaupart, C., Vergniolle, S., 1988. Laboratory models of Hawaiian and Strombolian eruptions, Nature, 331, 58–60, doi:10.1038/331058a0.

Jaupart, C., Vergniolle, S., 1989. The generation and collapse of a foam layer at the roof of a basaltic magma chamber, Journal of Fluid Mechanics., 203, 347–380, doi: 10.1017/S0022112089001497.

Kendall, J.-M., Stuart, G. W., Ebinger, C. J., Bastow, I. D., Keir, D., 2005. Magma-assisted rifting in Ethiopia, Nature, 433, 146–148, doi:10.1038/nature03161.

Kerber, L., Head, J. W., Madeleine, J. B., Wilson, L., Forget, F., 2010. The distribution of ash from ancient explosive volcanoes on Mars, 41st Lunar and Planetary Institute Science Conference, #1006 (abstract).

Kerber, L., Head, J. W., Madeleine, J.-B., Forget, F., Wilson, L., 2012. The dispersal of pyroclasts from ancient explosive volcanoes on Mars: Implications for the friable layered deposits, Icarus, 219, 358–381, doi: 10.1016/j.icarus.2012.03.016.

Kerber, L., Forget, F., Madeleine, J.-B., Wordsworth, R., Head, J. W., Wilson, L., 2013. The effect of atmospheric pressure on the dispersal of pyroclasts from martian volcanoes, Icarus, 223, 149–156, doi:10.1016/j.icarus.2012.11.037.

Kereszturi, G., Németh, K., 2012. Monogenetic basaltic volcanoes: genetic classification, growth, geomorphology and degradation. In: Németh, K. (Ed.), Updates in Volcanology — New Advances in Understanding Volcanic Systems. ISBN: 978-953-51-0915-0, 3–88, doi: 10.5772/51387.

Kereszturi, G., Jordan, G., Németh, K., Doniz-Paez, J. F., 2012. Syn-eruptive morphometric variability of monogenetic scoria cones, Bulletin of Volcanology, 74 (9), 2171–2185, doi: 10.1007/s00445-012-0658-1.

Kereszturi, G., Geyer, A., Martí, J., Németh, K., Dóniz-Páez, F. J., 2013. Evaluation of morphometry-based dating of monogenetic volcanoes—a case study from Bandas del Sur, Tenerife (Canary Islands), Bulletin of Volcanology, 75:734, doi 10.1007/s00445-013-0734-1.

Kervyn, M., Kervyn, F., Goossens, R., Rowland, S. K., Ernst, G. G. J., 2007. Mapping volcanic terrain using high-resolution and 3D satellite remote sensing, In: Teeuw, R. M. (ed.) Mapping Hazardous Terrain using Remote Sensing, 283, 5–30, doi: 10.1144/SP283.2.

Kervyn, M., Ernst, G. G. J., Goossens, P., Jacobs, P., 2008. Mapping volcano topography with remote sensing: ASTER vs. SRTM, International Journal of Remote Sensing, 29 (22), 6515–6538, doi: 10.1080/01431160802167949.

Kervyn, M., Ernst, G. G. J., Carracedo, J.-C., Jacobs, P., 2012. Geomorphometric variability of “monogenetic” volcanic cones: evidence from Mauna Kea, Lanzarote and experimental cones, Geomorphology, 136, 59–75, doi:10.1016/j.geomorph.2011.04.009.

Keszthelyi, L., Jaeger, W., McEwen, A., Tornabene, L., Beyer, R.A., Dundas, C., Milazzo, M., 2008. High Resolution Imaging Science Experiment (HiRISE) images of volcanic terrains from the first 6 months of the Mars Reconnaissance Orbiter primary science phase, Journal of Geophysical Research, 113, E04005. doi:10.1029/ 2007JE002968.

Keszthelyi, L. P., Jaeger, W. L., Dundas, C. M., Martínez-Alonso, S., McEwen, A. S., Milazzo, M. P., 2010. Hydrovolcanic features on Mars: Preliminary observations from the first Mars year of HiRISE imaging, Icarus, 205, 211–229, doi: 10.1016/j.icarus.2009.08.020.

Kholodov, V. N., 2002. Mud volcanoes: distribution regularities and genesis (Communication 2. geological–geochemical peculiarities and formation model), Lithology and Mineral Resources, 37, 293–310, doi: 10.1023/A:1019955921606.

Kienzle, S., 2004. The effect of DEM raster resolution on first order, second order and compound terrain derivatives, Transactions GIS, 8, 83–111, doi: 10.1111/j.1467-9671.2004.00169.x.

Kleinhans, M. G., Markies, H., de Vet, S. J., in 't Veld, A. C., Postema, F. N., 2011. Static and dynamic angles of repose in loose granular materials under reduced gravity, Journal of Geophysical Research, 116 (E11004), doi:10.1029/2011JE003865.

Kneissl, T., van Gasselt, S., Neukum, G., 2011. Map-projection-independent crater size-frequency determination in GIS environments – new software tool for ArcGIS, Planetary and Space Science, 59, 1243–1254, doi: 10.1016/j.pss.2010.03.015.

Konrad, J.-M., Ayad, R., 1987. An idealized framework for the analysis of cohesive soils undergoing desiccation, Canadian Geotechnical Journal, 34 (4), 477–488, doi: 10.1139/t97-015.

Kress, A. M., Head, J. W., 2008. Ring-mold craters in lineated valley fill and lobate debris aprons on Mars: Evidence for subsurface glacial ice, Geophysical Research Letters, 35, L23206, doi: 10.1029/2008GL035501.

Lammer, H., et al., 2013. Outgassing history and escape of the Martian atmosphere and water inventory, Space Science Reviews, 174 (1–4), 113–154, doi: 10.1007/s11214-012-9943-8.

Lanagan, P. D., McEwen, A. S., Keszthelyi, L. P., Thordarson, T., 2001. Rootless cones on Mars indicating the presence of shallow equatorial ground ice in recent times, Geophysical Research Letters, 28, 2365–2368, doi: 10.1029/2001GL012932.

Lanz, J. K., Saric, M. B., 2009. Cone fields in SW Elysium Planitia: Hydrothermal venting on Mars? Journal of Geophysical Research, 114. doi:10.1029/2008JE003209.

Lanz, J. K., Wagner, R., Wolf, U., Kröchert, J., Neukum, G., 2010. Rift zone volcanism and associated cinder cone field in Utopia Planitia, Mars, Journal of Geophysical Research, 115 (E12019), doi:10.1029/2010JE003578.

Lasue, J., Mangold, N., Hauber, E., Clifford, S., Feldman, W., Gasnault, O., Grima, C., Maurice, S., Mousis, O., 2013. Quantitative Assessments of the Martian Hydrosphere, Space Science Reviews, 174, 155–212, doi: 10.1007/s11214-012-9946-5.

Lautze, N. C., Houghton, B. F., 2005. Physical mingling of magma and complex eruption dynamics in the shallow conduit at Stromboli volcano, Italy, Geology 33 (5), 425–428, doi: 10.1130/G21325.1.

Lawrence, S. J., et al., 2013. LRO observations of morphology and surface roughness of volcanic cones and lobate lava flows in the Marius Hills, Journal of Geophysical Research: Planets, 118, 615–634, doi:10.1002/jgre.20060.

Leach, J. H. J., 2011. The Tuff Rings of South East Australia and the Surficial Deposits of Mars: A Cautionary Tale, 42nd Lunar and Planetary Science Conference, #1020 (abstract).

Levy, J., Head, J. W., Marchant, D. R., 2010. Concentric crater fill in the northern mid-latitudes of Mars: Formation processes and relationships to similar landforms of glacial origin, Icarus, 209 (2), 390–404, doi:10.1016/j.icarus.2010.03.036.

Levy, J., Fassett, C. I., Head, J. W., Schwartz, C., Watters, J. L., 2014. Sequestered glacial ice contribution to the global martian water budget: Geometric constraints on the volume of remnant, midlatitude debris-covered glaciers, Journal of Geophysical Research, 119, 2188–2196, doi: 10.1002/2014JE004685.

Lorenz, V., 1986. On the growth of maars and diatremes and its relevance to the formation of tuff rings, Bulletin of Volcanology, 48, 265–274 doi:10.1007/BF01081755.

Lorenz, V., 1987. Phreatomagmatism and its relevance, Chemical Geology, 62, 149–156, doi: 10.1016/0009-2541(87)90066-0.

Lutz, T. M., 1986. An analysis of the orientations of large-scale crustal structures: a statistical approach based on areal distributions of pointlike features, Journal of Geophysical Research, 91 (B1), 421–434, doi: 10.1029/JB091iB01p00421.

Lutz, T. M., Gutmann, J. T., 1995. An improved method for determining and characterizing alignments of point-like features and its implications for the Pinacate volcanic field, Sonoran, Mexico, Journal of Geophysical Research, 100 (B9), 17,659–17,670, doi: 10.1029/95JB01058.

Malin, M. C., 1977. Comparison of volcanic features of Elysium (Mars) and Tibesti (Earth), Geological Society of America Bulletin, 88, 908–919, doi: 10.1130/0016-7606(1977)88<908:COVFOE>2.0.CO;2.

Malin, M. C., et al., 2007. Context camera investigation on board the Mars Reconnaissance Orbiter, Journal of Geophysical Research, 112 (E05S04), doi: 10.1029/2006JE002808.

Mandt, K. E., de Silva, S. L., Zimbelman, J. R., Crown, D. A., 2008. Origin of the Medusae Fossae Formation, Mars: Insights from a synoptic approach, Journal of Geophysical Research, 113 (E12011), doi: 10.1029/2008JE003076.

Manga, M., Bonini, M., 2012. Large historical eruptions at subaerial mud volcanoes, Italy, Natural Hazards and Earth System Sciences, 12, 3377–3386, doi: 10.5194/nhess-12-3377-2012.

Manga, M., Patel, A., Dufek, J., Kite, E. S., 2012. Wet surface and dense atmosphere on early Mars suggested by the bomb sag at Home Plate, Mars, Geophysical Research Letters, 39, L01202, doi:10.1029/2011GL050192.

Mangold, N., 2003. Geomorphic analysis of lobate debris aprons on Mars at Mars Orbiter Camera scale: Evidence for ice sublimation initiated by fractures, Journal of Geophysical Research, 108 (E4), doi: 10.1029/2002JE001885.

Martínez-Alonso, S., Mellon, M. T., Banks, M. E., Keszthelyi, L. P., McEwen, A. S., The HiRISE Team, 2011. Evidence of volcanic and glacial activity in Chryse and Acidalia Planitiae, Mars, Icarus, 212, 597–621, doi:10.1016/j.icarus.2011.01.004.

McCauley, J. F., Carr, M. H. et al. 1972. Preliminary Mariner-9 report on the geology of Mars, Icarus, 17, 289–327, doi: 10.1016/0019-1035(72)90003-6.

McEwen, A. S., et al., 2007. Mars Reconnaissance Orbiter's High Resolution Imaging Science Experiment (HiRISE), Journal of Geophysical Research, 112 (E05S02), doi: 10.1029/2005JE002605.

McGetchin, T. R., Settle, M., Chouet, B. A., 1974. Cinder cone growth modelled after North East crater, Mt Etna, Sicily, Journal of Geophysical Research, 79, 3257–3272, doi: 10.1029/JB079i023p03257.

McGill, G. E., 1989. Buried topography of Utopia, Mars: Persistence of a giant impact depression, Journal of Geophysical Research, 94, 2753–2759, doi: 10.1029/JB094iB03p02753.

McGovern, P. J., Litherland, M. M., 2011. Lithospheric stress and basaltic magma ascent on the Moon, with implications for large volcanic provinces and edifices, Lunar and Planetary Institute Science Conference, #2587 (abstract).

McGovern, P. J., Powell, K., Kramer, G. Y., Litherland, M., 2011. Stress-enhanced magma ascent at the margins of large impact basins in the solar system, AGU Fall Meeting 2011, #P31E-1736 (abstract).

McKnight, S. B., Williams S. N., 1997. Old cinder cone or young composite volcano? The nature of Cerro Negro, Nicaragua, Geology, 25, 339–342, doi: 10.1130/0091-7613(1997)025<0339:OCCOYC>2.3.CO;2.

Mercier, E., Outtani, F., De Lamotte, D. F., 1997. Late-stage evolution of fault-propagation folds: principles and example, Journal of Structural Geology, 19, 185–193, doi: 10.1016/S0191-8141(96)00081-8.

Meresse, S., Costard, F., Mangold, N., Masson, P., Neukum, G., the HRSC Co-I Team, 2008. Formation and evolution of the chaotic terrains by subsidence and magmatism: Hydraotes Chaos, Mars, Icarus, 194, 487–500, doi: 10.1016/j.icarus.2007.10.023.

Meslin, P.-Y., et al., 2013. Soil diversity and hydration as observed by ChemCam at Gale Crater, Mars, Science, 341 (6153), doi:10.1126/science.1238670.

Michael, G. G., Neukum, G., 2010. Planetary surface dating from crater size–frequency distribution measurements: Partial resurfacing events and statistical age uncertainty. Earth and Planetary Science Letters, 294, 223–229, doi:10.1016/j.epsl.2009.12.041.

Michael, G. G., Platz, T., Kneissl, T., Schmedemann, N., 2012. Planetary surface dating from crater size-frequency distribution measurements: a quantitative test of spatial randomness, Icarus, 218, 169–177, doi:10.1016/j.icarus.2011.11.033.

Mitchell, K. L., Wilson, L., 2001. Explosive volcanic eruptions on Mars: Misconceptions and new insights, 32nd Lunar and Planetary Institute Science Conference, #1190 (abstract).

Moore, H. J., Plaut, J. J., Schenk, P. M., Head, J. W., 1992. An unusual volcano on Venus, Journal of Geophysical Research, 97, 13,479–13,493, doi: 10.1029/92JE00957.

Moratto, Z. M., Broxton, M. J., Beyer, R. A., Lundy, M., Husmann K., 2010. Ames Stereo Pipeline, NASA's Open Source Automated Stereogrammetry Software, 41st Lunar and Planetary Institute Science Conference, #2364 (abstract).

Morgan, G. A., Head, J. W., Marchant, D. R., 2009. Lineated valley fill (LVF) and lobate debris aprons (LDA) in the Deuteronilus Mensae northern dichotomy boundary region, Mars: Constraints on the extent, age and episodicity of Amazonian glacial events, Icarus, 202, 22–38, doi: 10.1016/j.icarus.2009.02.017.

Morrissey, M. M., Zimanowski, B., Wohletz, K., 1999. Phreatomagmatic Fragmentation, in: Sigurdsson, H. (Ed.), Encyclopedia of Volcanoes, Academic Press, San Diego, California, 431–445.

Mouginis-Mark, P. J., Christensen, P. R. 2005. New observations of volcanic features on Mars from THEMIS instrument, Journal of Geophysical Research, 110 (E08007), doi: 10.1029/2005JE002421.

Mouginis-Mark, P. J., Wilson, L., Zuber, M. T., 1992. The Physical Volcanology of Mars. In: Kieffer, H. H., Jakosky, B. M., Snyder, C. W., Matthews, M. S. (Eds.), Mars, Univ. of Arizona Press, Tucson, 424–452.

Mouginot, J., Pommerol, A., Beck, P., Kofman, W., Clifford, S. M., 2012. Dielectric map of the Martian northern hemisphere and the nature of plain filling materials, Geophysical Research Letters, 39, L02202, doi:10.1029/2011GL050286.

Mueller, K., Golombek, M., 2004. Compressional structures on Mars, Annual Review of Earth and Planetary Sciences, 32, 435–464, doi: 10.1146/annurev.earth.32.101802.120553.

Mustard, J. F., Cooper, C. D., Rifkin, M. K., 2001. Evidence for recent climate change on Mars from the identification of youthful near-surface ground ice, Nature, 412, 411–414, doi: 10.1038/35086515.

Nakamura, K., 1977. Volcanoes as possible indicators of tectonic stress orientation – principle and proposal, Journal of Volcanology and Geothermal Research, 2, 1–16, doi: 10.1016/0377-0273(77)90012-9.

Neish, C. D., Lorenz, R. D., Kirk, R. L., 2008. Radar topography of domes on planetary surfaces, Icarus, 196, 552–564, doi:10.1016/j.icarus.2008.03.013.

Neumann, G. A., Zuber, M. T., Wieczorek, M. A., McGovern, P. J., Lemoine, F. G., Smith, D. E., 2004. Crustal structure of Mars from gravity and topography, Journal of Geophysical Research, 109, E08002, doi:10.1029/2004JE002262.

Nimmo, F., 2005. Tectonic consequences of Martian dichotomy modification by lower-crustal flow and erosion, Geology, 3(7), 533– 536, doi: 0.1130/G21342.1.

Noguchi, R., Kurita, K., 2011. Double cone structure in Central Elysium Planitia, Mars, EPSC-DPS Joint Meeting 2011, EPSC-DPS2011-415-1 (abstract).

Noguchi, R., Kurita, K., 2015. Unique characteristics of cones in Central Elysium Planitia, Mars, Planetary and Space Science, 111, 44–54, doi:10.1016/j.pss.2015.03.007.

Ody, A., Poulet, F., Langevin, Y., Bibring, J.-P., Bellucci, G., Altieri, F., Gondet, B., Vincendon, M., Carter, J., Manaud, N., 2012. Global maps of anhydrous minerals at the surface of Mars from OMEGA/MEx, Journal of Geophysical Research: Planets, 117 (E11), doi:10.1029/2012JE004117.

Ollier, C. D., 1967. Maars - their characteristics, varieties and definition, Bulletin of Volcanology, 31, 45-73, doi: 10.1007/BF02597005.

Parfitt, E. A., Wilson, L., 1995. Explosive volcanic eruptions-IX. The transition between Hawaiian-style lava fountaining and Strombolian explosive aktivity, Geophysical Journal International, 121, 226–232, doi: 10.1111/j.1365-246X.1995.tb03523.x.

Parfitt, E. A., 2004. A discussion of the mechanisms of explosive basaltic eruptions, Journal of Volcanology and Geothermal Research, 134, 77–107, doi: 10.1016/j.jvolgeores.2004.01.002.

Parfitt, E. A., Wilson, L., 2008. Fundamentals of Physical Volcanology, Blackwell, Oxford, 256 pp.

Parsons, R. A., and Holt, J. W., 2014. Determining the Age and Physical Properties of Martian Lobate Debris Aprons Using High-Resolution Topography, SHARAD Observations, and Numerical Ice Flow Modeling: A Case Study at Euripus Mons, 45th Lunar and Planetary Institute Science Conference, #1484 (abstract).

Phillips, R. J., et al., 2011. Massive CO2 ice deposits sequestered in the south polar layered deposits of Mars, Science, 332, 838–841, doi: 10.1126/science.1203091.

Pike, R. J., 1978. Volcanoes on the inner planets: Some preliminary comparisons of gross topography. Proc. Lunar Sci. Conf. IX, 3239–3273 (abstract).

Pioli, L., Azzopardi, B. J., Cashman, K. V., 2009. Controls on the explosivity of scoria cone eruptions: Magma segregation at conduit junctions, Journal of Volcanology and Geothermal Research, 186, 407–415, doi: 10.1016/j.jvolgeores.2009.07.014.

Platz, T., Michael, G. G., 2011. Eruption history of the Elysium Volcanic Province, Mars. Earth and Planetary Science Letters, 312, 140–151, doi:10.1016/j.epsl.2011.10.001.

Platz, T., Cronin, S. J., Procter, J. N., Neall, V. E., Foley, S. F., 2012. Non-explosive, dome-forming eruptions at Mt. Taranaki, New Zealand, Geomorphology (Special Issue: Volcano Geomorphology: landforms, processes and hazards), 136, 15–30, doi:10.1016/j.geomorph.2011.06.016).

Platz, T., Massironi, M., Byrne, P. K., Hiesinger, H., 2015. Volcanism and Tectonism Across the Inner Solar System. Geological Society, London, Special Publications, 401, 1–56, doi: 10.1144/SP401.22.

Plaut, J. J., Safaeinili, A., Holt, J. W., Phillips, R. J., Head, J. W., Seu, R., Putzig, N. E., Frigeri, A., 2009. Radar evidence for ice in lobate debris aprons in the mid-northern latitudes of Mars, Geophysical Research Letters, 36(2), L02203, doi:10.1029/2008GL036379.

Plescia, J. B., 1990. Recent flood lavas in the Elysium region of Mars, Icarus, 88, 465–490, doi: 10.1016/0019-1035(90)90095-Q.

Plescia, J. B., 1994. Geology of the small Tharsis volcanoes: Jovis Tholus, Ulysses Patera, Biblis Patera, Mars. Icarus, 111, 246–269, doi: 10.1006/icar.1994.1144.

Plescia, J. B., 2003. Cerberus Fossae, Elysium, Mars: a source for lava and water, Icarus, 164, 79–95, doi: 10.1016/S0019-1035(03)00139-8.

Plescia, J. B., 2004. Morphometric properties of Martian volcanoes. Journal of Geophysical Research, 109, E03003, doi: 10.1029/2002JE002031.

Pondrelli, M., Rossi, A. P., Ori, G. G., van Gasselt, S., Praeg, D., Ceramicola, S., 2011. Mud volcanoes in the geologic record of Mars: The case of Firsoff Crater, Earth and Planetary Science Letters, 304, 511–519, doi:10.1016/j.epsl.2011.02.027.

Porter, S. C., 1972. Distribution, morphology, and size frequency of cinder cones on Mauna Kea Volcano, Hawaii, Geological Society of America Bulletin, 83, 3607–3612, doi: 10.1130/0016-.

Rampey, M. L., Milam, K. A., McSween, H. Y., Moersch, J. E., Christensen, P. R., 2007, Identity and emplacement of domical structures in the western Arcadia Planitia, Mars. Journal of Geophysical Research, 112, E06011, doi: 10.1029/2006JE002750.

Rice, J. W., et al., 2006. Origin of Home Plate, Columbia Hills, Mars: hydrovolcanic hypothesis. Eos, Trans. – Am. Geophys. Union 87, P41B-1274 (abstract).

Riedel, C., Ernst, G. G. J., Riley, M., 2003. Controls on the growth and geometry of pyroclastic constructs, Journal of Volcanology and Geothermal Research, 127, 121–152, doi: 10.1016/S0377-0273(03)00196-3.

Richardson, J. A., Bleacher, J. E., Glaze, L. S., 2013. The volcanic history of Syria Planum, Mars, Journal of Volcanology and Geothermal Research, 252, 1–13, doi: 10.1016/j.jvolgeores.2012.11.007.

Robbins, S. J., Di Achille, G., B. Hynek, M., 2011. The volcanic history of Mars: High-resolution crater-based studies of the calderas of 20 volcanoes, Icarus, 211, 1179–1203, doi:10.1016/j.icarus.2010.11.012.

Roberts, K. S., Davies, R. J., Stewart, S. A., Tingay, M., 2011. Structural control on mud volcano vent distributions: example from Azerbaijan and Lusi, east Java, J. Geol. Soc. London, 168, 1013–1030, doi:10.1144/0016-76492010-158, 2011.

Rodriguez, S. R., Morales-Barrera, W., Layer, P., González-Mercado, E., 2010. A quaternary monogenetic volcanic field in the Xalapa region, eastern Trans-Mexican volcanic belt: Geology, distribution and morphology of the volcanic vents, Journal of Volcanology and Geothermal Research, 197, 149–166, doi: 10.1016/j.jvolgeores.2009.08.003.

Rogers, N., and Hawkesworth, C., 2000. Composition of magmas, in: Sigurdsson, H. (Ed.), Encyclopedia of Volcanoes, Academic Press, San Diego, California, 307–320.

Roggensack, K., Hervig, R. L., McKnight, S. B., Williams, S. N., 1997. Explosive basaltic volcanism from Cerro Negro volcano: Influence of volatiles on eruptive style, Science, 277, 1639–1642, doi: 10.1126/science.277.5332.1639.

Rooney, T., Bastow, I. D., Keir, D., 2011. Insights into extensional processes during magma assisted rifting: Evidence from aligned scoria cones and maars, Journal of Volcanology and Geothermal Research, 201, 83–96, doi: 10.1016/j.jvolgeores.2010.07.019.

Rotto, S., Tanaka, K. L., 1995. Geologic/geomorphic map of the Chryse Planitia region of Mars: US Geological Survey Misc. Invest. Series Map I-2441, scale 1:5,000,000.

Rubin, A. M., 1995. Propagation of magma-filled cracks, Annual Review of Earth and Planetary Sciences, 23, 287–336, doi: 10.1146/annurev.ea.23.050195.001443.

Saunderson, H. C., 2008. Equations of motion and ballistic paths of volcanic ejecta, Computational Geosciences, 34, 802–814, doi: 10.1016/j.cageo.2007.10.004.

Sautter, V. et al., 2014. Igneous mineralogy at Bradbury Rise: The first ChemCam campaign at Gale crater, Journal of Geophysical Research: Planets, 119, 30–46, doi :10.1002/2013JE004472.

Scott, D. H., Tanaka, K. L., 1986. Geologic map of the western equatorial region of Mars. U.S. Geological Survey Miscellaneous lnvestigation Series Map I-1802-A, scale 1:15,000,000.

Scott, D. H., Dohm, J. M., 1990. Faults and ridges - Historical development in Tempe Terra and Ulysses Patera regions of Mars, 20th Lunar and Planetary Institute Science Conference, 503–513 (abstract).

Settle, M., 1979. The structure and emplacement of cinder cone fields, American Journal of Science, 279, 1089–1107, doi: 10.2475/ajs.279.10.1089.

Sheridan, M. F., Wohletz, K. H., 1983. Hydrovolcanism: basic considerations and review, Journal of Volcanology and Geothermal Research, 17, 1–29, doi: 10.1016/0377-0273(83)90060-4.

Schmidt, M. E., et al., 2006. Geochemical evidence for the volcanic origin of Home Plate in the inner basin of the Columbia Hills, Gusev Crater. Eos, Trans. – Am. Geophys. Union 87 (52), #P44A-07 (abstract).

Scholten, F., Gwinner, K., Roatsch, T., Matz, K.-D., Wählisch, M., Giese, B., Oberst, J., Jaumann, R., Neukum, G., the HRSC Co-Investigator Team, 2005. Mars Express HRSC Data Processing - Methods and Operational Aspects, PE&RS, 71, 1143–1152.

Schultz, P. H., Schultz, R. A., Rogers, J., 1982. The structure and evolution of ancient impact basins on Mars, Journal of Geophysical Research, 87, 9803–9820, doi: 10.1029/JB087iB12p09803.

Schultz, R. A., Frey, H., 1990. A new survey of multiring impact basins on Mars, Journal of Geophysical Research, 95, 14,175–14,189, doi: 10.1029/JB095iB09p14175.

Schultz, R. A., 2000. Localization of bedding plane slip and backthrust faults above blind thrust faults: Keys to wrinkle ridge structure, Journal of Geophysical Research, 105, 12,035–12,052, doi: 10.1029/1999JE001212.

Skinner, J. A., Tanaka, K. L., 2007. Evidence for and implications of sedimentary diapirism and mud volcanism in the southern Utopia highland-lowland boundary plain, Mars, Icarus, 186, 41–59, doi: 10.1016/j.icarus.2006.08.013.

Skinner, J. A., Mazzini, A., 2009. Martian mud volcanism: Terrestrial analogs and implications for formational scenarios, Marine and Petroleum Geology, 26(9), 1866–1878, doi:10.1016/j.marpetgeo.2009.02.006.

Skok, J. R., Mustard, J. F., Ehlmann, B. L., Milliken, R. E., Murchie, S. L., 2010. Silica deposits in the Nili Patera caldera on the Syrtis Major volcanic complex on Mars, Nature Geoscience, 3, 838–841, doi:10.1038/ngeo990.

Smith, D. E. et al., 2001. Mars Orbiter Laser Altimeter: Experiment summary after the first year of global mapping of Mars, Journal of Geophysical Research, 106 (E10), 23,689–23,722, doi: 10.1029/2000JE001364.

Smith, P. H., et al., 2009. H2O at the Phoenix landing site, Science, 325, 58–61, doi: 10.1126/science.1172339.

Souness, C., Hubbard, B., 2012. Mid-latitude glaciation on Mars, Progress in Physical Geography, 36(2), doi: 10.1177/0309133312436570.

Spudis, P. D., 1993. The Geology of Multi-Ring Impact Basins, Cambridge Univ. Press, Cambridge, UK, 263 pages.

Squyres, S. W., 1978. Martian fretted terrain: flow of erosional debris, Icarus, 34, 600–613, doi: 10.1016/0019-1035(78)90048-9.

Squyres, S. W., Carr, M. H., 1986. Geomorphic evidence for the distribution of ground ice on Mars, Science, 231(4735), 249–252, doi: 10.1126/science.231.4735.249.

Squyres, S. W. et al., 2008. Pyroclastic activity at Home Plate in Gusev Crater, Mars, Science, 316, 738–742, doi: 10.1126/science.1139045.

Steinberg, G. S., Babenko, J. L., 1978. Gas velocity and density determination by filming gas discharges, Journal of Volcanology and Geothermal Research 3, 89–98.

Stolper, E. M. et al., 2013. The Petrochemistry of Jake_M: A Martian Mugearite, Science, 341, doi: 10.1126/science.1239463.

Tanaka, K. L., Skinner, J. A., Hare, T. M., Joyal, T., Wenker, A., 2003a. Resurfacing history of the northern plains of Mars based on geologic mapping of Mars Global Surveyor data, Journal of Geophysical Research, 108 (E4), doi:10.1029/2002JE001908.

Tanaka, K. L., Carr, M. H., Skinner, J. A., Gilmore, M. S., Hare, T. M., 2003b. Geology of the MER 2003 'Elysium' candidate landing site in southeastern Utopia Planitia, Mars, Journal of Geophysical Research, 108, 8079, 20-1–20-19, doi:10.1029/2003JE002054.

Tanaka, K. L., Skinner, J. A., Hare, T. M., 2005. Geologic map of the northern plains of Mars, scale 1:15,000,000, U.S. Geol. Surv. Sci. Invest., Map 2888, http://pubs.usgs.gov/sim/2005/2888.

Tanaka, K. L., Skinner, J. A., Jr., Dohm, J.M., Irwin, R.P., III, Kolb, E.J., Fortezzo, C.M., Platz, T., Michael, G.G., Hare, T.M, 2014. Geologic Map of Mars. U.S. Geological Survey Scientific Investigations Map SIM 3292, 1:20,000,000.

Tibaldi, A., 1995. Morphology of pyroclastic cones and tectonics, Journal of Geophysical Research, 100, 24,521–24,535, doi: 10.1029/95JB02250.

Tibaldi, A., 2005. Volcanism in compressional tectonic settings: Is it possible? Geophysical Research Letters, 32, L06309, doi:10.1029/2004GL021798.

Tsunematsu, K., Chopard, B., Falcone, J.-L., Bonadonna, C., 2014. A numerical model of ballistic transport with collisions in a volcanic setting, Computers & Geosciences, 63, 62-69, 10.1016/j.cageo.2013.10.016.

Valentine, G. A., Gregg, T. K. P., 2008. Continental basaltic volcanoes - processes and problems, Journal of Volcanology and Geothermal Research, 177, 857–873, doi: 10.1016/j.jvolgeores.2008.01.050.

Valentine, G. A., Kier, D., Perry, F. V., Heiken, G., 2005. Scoria cone construction mechanisms, Lathrop Wells volcano, southern Nevada, USA, Geology, 33, 629–632, doi: 10.1130/G21459AR.1.

Vanderkluysen, L., Harris, A. J. L., Kelfoun, K., Bonadonna, C., Ripepe, M., 2012. Bombs behaving badly: unexpected trajectories and cooling of volcanic projectiles, Bulletin of Volcanology, 74(8), 1849–1858, doi: 10.1007/s00445-012-0635-8.

Vaucher, J., Baratoux, D., Mangold, N., Pinet, P., Kurita, K., Grégoire, M., 2009a. The volcanic history of central Elysium Planitia: Implications for Martian magmatism, Icarus, 204, 418–442, doi:10.1016/j.icarus.2009.06.032.

Vaucher, J., Baratoux, D., Toplis, M. J., Pinet, P., Mangold, N., Kurita, K., 2009b. The morphologies of volcanic landforms at Central Elysium Planitia: Evidence for recent and fluid lavas on Mars, Icarus, 200, 39–51, doi: 10.1016/j.icarus.2008.11.005.

Vergniolle, S., Mangan, M., 2000. Hawaiian and Strombolian eruptions, in: Sigurdsson, H. (Ed.), Encyclopedia of Volcanoes, Academic Press, San Diego, California, 447–461.

Vespermann, D., Schmincke, H.-U., 2000. Scoria cones and tuff rings, in: Sigurdsson, H. (Ed.), Encyclopedia of Volcanoes, Academic Press, San Diego, California, 683–694.

Vincendon, M., Forget, F., Mustard, J., 2010. Water ice at low to midlatitudes on Mars, Journal of Geophysical Research, 115, E10001, doi:10.1029/2010JE003584.

Wadge, G., Cross, A., 1988. Quantitative methods for detecting aligned points: an application to the volcanic vents of the Michoacan–Guanajuato volcanic field, Mexico, Geology, 16, 815–818, doi: 10.1130/0091-7613(1988)016<0815:QMFDAP>2.3.CO;2.

Washburn, A. L., 1956. Classification of patterned ground and review of suggested origins, Geological Society of America Bulletin, 67(7), 823–865, doi: 10.1177/0309133312438909.

Watters, T. R., 2003. Lithospheric flexure and the origin of the dichotomy boundary on Mars, Geology, 31, 271-274, doi: 10.1130/0091-7613(2003)031<0271:LFATOO>2.0.CO;2.

Watters, T. R., et al., 2007. Radar sounding of the Medusae Fossae Formation Mars: equatorial ice or dry, low-density deposits? Science, 318, 1125–1128, doi: 10.1126/science.1148112.

Wendt, L., Bishop, J., Neukum, G., 2013. Knob fields in the Terra Cimmeria/Terra Sirenum region of Mars: Stratigraphy, mineralogy and morphology, Icarus, 225, 200–215, doi: 10.1016/j.icarus.2013.03.020.

Werner, S. C., 2009. The global martian volcanic evolutionary history, Icarus, 201, 44–68, doi: 10.1016/j.icarus.2008.12.019.

White, J. D. L., Ross, P. S., 2011. Maar-diatreme volcanoes: A review, Journal of Volcanology and Geothermal Research, 201, 1–29, doi:10.1016/j.jvolgeores.2011.01.010.

Williams, D. A., Greeley, R., Zuschneid, W., Werner, S. C., Neukum, G., Crown, D. A., Gregg, T. K. P., Gwinner, K., Raitala, J., 2007. Hadriaca Patera: Insights into its volcanic history from Mars Express High Resolution Stereo Camera, Journal of Geophysical Research, 112, E10004, doi: 10.1029/2007JE002924.

Williams, D. A., Greeley, R., Werner, S. C., Michael, G., Crown, D. A., Neukum, G., Raitala, J., 2008. Tyrrhena Patera: Geologic history derived from Mars Express High Resolution Stereo Camera, Journal of Geophysical Research, 113, E11005, doi: 10.1029/2008JE003104.

Williams, D. A., Greeley, R., Fergason, R. L., Kuzmin, R., McCord, T. B., Combe, J.-P., Head III, J. W., Xiao, L., Manfredi, L., Poulet, F., Pinet, P., Baratoux, D., Plaut, J. J., Raitala, J., Neukum, G., the HRSC Co-Investigator Team, 2009. The Circum-Hellas Volcanic Province, Mars: Overview, Planetary and Space Science, 57, 895–916, doi: 10.1016/j.pss.2008.08.010.

Wilson, L., 1980. Relationships between pressure, volatile content and ejecta velocity in three types of volcanic explosion, Journal of Volcanology and Geothermal Research, 8, 297–313, doi: 10.1016/0377-0273(80)90110-9.

Wilson, L., Head, J. W., 1981. Ascent and eruption of basaltic magma on the Earth and Moon, Journal of Geophysical Research, 86, 2971–3001, doi: 10.1029/JB086iB04p02971.

Wilson, L., Head, J. W., 1994. Review and analysis of volcanic eruption theory and relationships to observed landforms, Reviews of Geophysics, 32, 221–263. doi:10.1029/94RG01113.

Wilson, L., Head, J. W., 2002. Tharsis-radial graben systems as the surface manifestation of plume-related dike intrusion complexes: Models and implications, Journal of Geophysical Research, 107, 1-1–1-24, doi: 10.1029/2001JE001593.

Wilson, L., Head, J. W., 2004. Evidence for a massive phreatomagmatic eruption in the initial stages of formation of the Mangala Valles outflow channel, Mars, Geophysical Research Letters, 31, L15701, doi:10.1029/2004GL020322.

Wilson, L., Head, J. W., 2007. Explosive volcanic eruptions on Mars: tephra and accretionary lapilli formation, dispersal and recognition in the geological record, Journal of Volcanology and Geothermal Research, 163, 83–97, doi: 10.1016/j.jvolgeores.2007.03.007.

Wilson, L., Mouginis-Mark, P. J., 2003a. Phreatomagmatic explosive origin of Hrad Vallis, Mars, Journal of Geophysical Research, 108(E8), 5082, doi:10.1029/2002JE001927.

Wilson, L., Mouginis-Mark, P. J., 2003b. Phreato-magmatic dike-cryosphere interactions as the origin of small ridges north of Olympus Mons, Mars, Icarus, 165, 242–252, doi: 10.1016/S0019-1035(03)00197-0.

Wohletz, K. H., Sheridan, M. F., 1983. Hydrovolcanic explosions II. Evolution of basaltic tuff rings and tuff cones, American Journal of Science, 283, 385–413, doi: 10.2475/ajs.283.5.385.

Wohletz, K. H. McQueen, R. G., 1984a. Volcanic and stratospheric dust-like particles produced by experimental water-melt interactions, Geology, 12, 591–594, doi: 10.1130/0091-7613(1984)12<591:VASDPP>2.0.CO;2.

Wohletz, K. H., McQueen, R. G., 1984b. Experimental studies of hydromagmatic volcanism. In: Geophysics Study Committee: Studies in Geophysics: Explosive volcanism: Inception. evolution, and hazards, National Academy Press., Washington 158-169.

Womer, M. B., Greeley, R., King, J. S., 1980. The geology of Split Butte – a maar of the south central Snake River Plain, Idaho, Bulletin of Volcanology, 43, 453–472, doi: 10.1007/BF02597685.

Wood, C. A., 1979a. Monogenetic volcanoes of the terrestrial planets. 20th Lunar and Planetary Institute Science Conference, 2815–2840.

Wood, C. A., 1979b. Cinder cones on Earth, Moon and Mars, 10th Lunar and Planetary Institute Science Conference, 1370–1372 (abstract).

Wood, C. A., 1980a. Morphometric evolution of cinder cones, Journal of Volcanology and Geothermal Research, 7, 387–413, doi: 10.1016/0377-0273(80)90040-2.

Wood, C. A., 1980b. Morphometric analysis of cinder cone degradation, Journal of Volcanology and Geothermal Research, 8, 137–160, doi: 10.1016/0377-0273(80)90101-8.

Wray, J. J., Hansen, S. T., Dufek, J., Swayze, G. A., Murchie, S. L., Seelos, F. P., Skok, J. R., Irwin, R. P., Ghiorso, M. S., 2013. Prolonged magmatic activity on Mars inferred from the detection of felsic rocks, Nature Geoscience, 6, 1013–1017, doi: 10.1038/NGEO1994.

Wright, R., Garbeil, H., Baloga, S. M., Mouginis-Mark, P, J., 2006. An assessment of shuttle radar topography mission digital elevation data for studies of volcano morphology, Remote Sensing of Environment, 105, 41–53, doi: 10.1016/j.rse.2006.06.002.

Xiao, L., Huang, J., Christensen, P. R., Greeley, R., Williamsm D. A., Zhao, J., He, Q., 2012. Ancient volcanism and its implication for thermal evolution of Mars, Earth and Planetary Science Letters, 323, 9–18, doi: 10.1016/j.epsl.2012.01.027.

Zimbelman, J. R., 2000. Volcanism on Mars, in: Sigurdsson, H. (Ed.), Encyclopedia of Volcanoes, Academic Press, San Diego, California, 771–783.

Zuber, M. T., Smith, D. E., Solomon, S. C., Muhleman, D. O., Head, J. W., Garvin, J. B., Abshire, J. B., Bufton, J. L., 1992. The Mars Observer Laser Altimeter investigation, Journal of Geophysical Research, 97, 7781–7797, doi:10.1029/92JE00341.

Zuber, M. T., Solomon, S. C., Phillips, R. J., Smith, D. E., Tyler, G. L., Aharonson, O., Balmino, G., Banerdt, W. B., Head, J. W., Lemoine, F. G., McGovern, P. J., Neumann, G. A., Rowlands, D. D., Zhong, S., 2000. Internal structure and early thermal evolution of Mars from Mars Global Surveyor topography and gravity, Science, 287, 1788–1793, doi: 10.1126/science.287.5459.1788.

10. Appendix

Table A.1. All measured values of investigated volcanic cones.

ID	Location	W_{CO} [m]	W_{CR} [m]	H_{CO} [m]	Depth of crater [m]	W_{CR}/W_{CO}	H_{CO}/W_{CR}	H_{CO}/W_{CO}
A10	16.36°N 99.18°E	11,562	3582	-	-	0.310	-	-
A11	16.39°N 99.00°E	8560	2944	-	-	0.344	-	-
A12	16.76°N 99.14°E	14,967	4649	-	-	0.311	-	-
A14	16.76°N 98.70°E	8250	3138	-	-	0.380	-	-
A17	17.00°N 98.46°E	5958	3348	-	-	0.562	-	-
A18	17.03°N 98.8°E	7207	3588	-	-	0.498	-	-
A20	17.27°N 99.10°E	5347	2418	-	-	0.452	-	-
B2	17.27°N 101.41°E	7600	3890	121	50	0.512	0.0311	0.0159
B3	17.30°N 101.53°E	6750	4781	47	68	0.708	0.0098	0.0070
B4	17.33°N 101.62°E	15,562	3563	122	72	0.229	0.0342	0.0078
B5	17.51°N 101.65°E	8730	4108	-	-	0.471	-	-
B7	17.35°N 101.8°E	5888	1222	31	74	0.208	0.0254	0.0053
B8	17.46°N 101.88°E	9860	4816	-	-	0.488	-	-
B10	17.55°N 102.24°E	5650	2453	-	-	0.434	-	-
B13	17.58°N 102.52°E	14,727	5762	-	-	0.391	-	-
B14	17.35°N 102.22°E	3391	1826	13	39	0.538	0.0071	0.0038
B15	17.28°N 102.18°E	5690	2687	176	92	0.472	0.0655	0.0309
B16	17.22°N 102.35°E	6799	3393	111	82	0.499	0.0327	0.0163
B17	17.19°N 102.28°E	9844	3918	57	98	0.398	0.0146	0.0058
B18	17.16°N 102.25°E,	6750	2637	166	76	0.391	0.0630	0.0246
B19	17.07°N 102.17°E	11,811	3095	92	74	0.262	0.0297	0.0078
B20	16.93°N 102.18°E	14,170	4734	105	84	0.334	0.0222	0.0074
B22	17.11°N 102.5°E	4175	1595	-	66	0.382	-	-
B23	17.05°N 102.51°E	6333	3520	150	64	0.556	0.0426	0.0237
B30	17.17°N 102.79°E	5835	2411	-	-	0.413	-	-
B32	17.00°N 102.88°E	7928	3243	-	-	0.409	-	-
B34	17.04°N 103.00°E	5600	2191	-	-	0.391	-	-
B35	17.10°N 103.07°E	8599	4089	-	-	0.476	-	-
B36	16.48°N 102.29°E	10,958	4494	130	107	0.410	0.0289	0.0119
B37	16.39°N 102.14°E	11,827	3879	89	87	0.328	0.0229	0.0075
B38	16.25°N 102.26°E	3565	1906	45	40	0.535	0.0236	0.0126
B39	16.30°N 102.32°E	7675	3185	227	203	0.415	0.0713	0.0296

ID	Location	W_{CO} [m]	W_{CR} [m]	H_{CO} [m]	Depth of crater [m]	W_{CR}/W_{CO}	H_{CO}/W_{CR}	H_{CO}/W_{CO}
B40	16.66°N 103.15°E	3678	1263	-	-	0.343	-	-
B42	16.41°N 103.34°E	7001	2607	-	-	0.372	-	-
B47	17.59°N 103.44°E	6941	3241	-	-	0.467	-	-
B48	17.41°N 103.58°E	8890	4804	-	-	0.540	-	-
B53	16.55°N 103.86°E	10,068	2585	-	-	0.257	-	-
B56	16.62°N 104.14°E	7261	2778	189	115	0.383	0.0680	0.0260
B57	16.68°N 104.13°E	13,543	3258	222	67	0.241	0.0681	0.0164
B59	17.34°N 104.13°E	7007	2030	124	67	0.290	0.0611	0.0177
B60	17.18°N 104.14°E	9487	1785	168	39	0.188	0.0941	0.0177
B61	17.30°N 104.27°E	6182	2917	96	32	0.472	0.0329	0.0155
B62	17.39°N 104.34°E	4220	2345	43	48	0.556	0.0183	0.0102
B63	17.40°N 104.38°E	7468	3127	108	63	0.419	0.0345	0.0145
B64	17.26°N 104.45°E	6962	2512	38	78	0.361	0.0151	0.0055
B65	16.97°N 104.56°E	8618	2978	89	60	0.346	0.0299	0.0103
B66	17.42°N 104.65°E	3179	1917	112	122	0.603	0.0584	0.0352
B68	17.91°N 104.68°E	7644	2679	-	-	0.350	-	-
B69	17.28°N 105.34°E	11,025	5503	-	-	0.499	-	-
B70	17.20°N 105.59°E	7384	3105	-	-	0.421	-	-
B72	17.41°N 105.83°E	5574	2435	-	-	0.437	-	-
B73	17.28°N 105.81°E	8499	3245	-	-	0.382	-	-
B74	17.12°N 106.18°E	8751	3617	-	-	0.413	-	-
C1	17.29°N 106.72°E	4179	2712	87	27	0.649	0.0321	0.0208
C4	17.26°N 106.76°E	7162	2900	35	80	0.405	0.0121	0.0049
C5	17.15°N 106.76°E	3556	1349	132	60	0.379	0.0979	0.0371
C6	17.02°N 106.76°E	4375	1577	101	56	0.360	0.0641	0.0231
C7	17.07°N 106.89°E	5256	2443	63	-	0.465	0.0258	0.0120
C8	16.99°N 106.95°E	4813	1949	126	90	0.405	0.0647	0.0262
C9	16.99°N 107.04°E	4750	1628	64	51	0.343	0.0393	0.0135
C10	16.99°N 107.17°E	6531	3049	62	41	0.467	0.0203	0.0095
C12	16.95°N 107.47°E	-	-	78	-	-	-	-
C14	16.91°N 107.02°E	3758	2030	65	73	0.540	0.0320	0.0173
C15	16.86°N 107.06°E	11,588	3733	71	36	0.322	0.0190	0.0061
C16	16.79°N 107.21°E	4012	2234	73	25	0.557	0.0327	0.0182
C19	16.84°N 106.77°E	13,905	5437	110	60	0.391	0.0202	0.0079

ID	Location	W_{CO} [m]	W_{CR} [m]	H_{CO} [m]	Depth of crater [m]	W_{CR}/W_{CO}	H_{CO}/W_{CR}	H_{CO}/W_{CO}
C20	16.76°N 106.73°E	7201	2842	84	105	0.395	0.0296	0.0117
C21	16.68°N 106.69°E	7745	2087	87	72	0.269	0.0417	0.0112
C22	16.56°N 106.6°E	13,674	5296	104	108	0.387	0.0196	0.0076
C23	16.53°N 106.75°E	8778	3323	67	55	0.379	0.0202	0.0076
C24	16.49°N 106.83°E	15,879	3953	274	144	0.249	0.0693	0.0173
C25	16.23°N 107.02°E	17,535	4764	372	207	0.272	0.0781	0.0212
C26	16.43°N 107.25°E	10,188	3431	237	-	0.337	0.0691	0.0233
C27	16.35°N 107.32°E	7273	3522	185	137	0.484	0.0525	0.0254
C28	16.21°N 107.34°E	9757	3453	171	129	0.354	0.0495	0.0175
C29	16.14°N 107.21°E	12,259	4560	189	124	0.372	0.0415	0.0154
C30	16.11°N 107.28°E	7652	3286	82	152	0.429	0.0250	0.0107
C31	16.00°N 107.33°E	5294	1976	120	36	0.373	0.0607	0.0227
D6	16.27°N 110.06°E	8750	3754	-	-	0.429	-	-
D8	16.27°N 110.66°E	10,077	3992	-	-	0.396	-	-
D9	16.29°N 111.31°E	5097	2227	-	-	0.437	-	-
D10	16.74°N 112.25°E	3903	2148	-	-	0.550	-	-
D14	16.03°N 112.86°E	5820	2637	-	-	0.453	-	-
D15	16.28°N 113.06°E	6636	3432	-	-	0.517	-	-
D20	12.98°N 114.49°E	7141	3665	164	137	0.513	0.0448	0.0230
D21	12.83°N 114.61°E	5550	3450	91	65	0.622	0.0264	0.0164
E3	13.02°N 117.81°E	7833	3193	-	-	0.408	-	-
E6	13.16°N 118.02°E	8542	3831	-	-	0.448	-	-
E10	13.49°N 118.46°E	2929	1233	-	-	0.421	-	-
E12	13.23°N 118.54°E	5512	2385	-	-	0.433	-	-
E14	12.61°N 118.47°E	4575	2649	-	-	0.579	-	-
E15	12.67°N 118.66°E	4571	2281	-	-	0.499	-	-
E18	12.37°N 118.48°E	6779	2937	-	-	0.433	-	-